Geogrid Reinforced Earth versus Piles for The Foundation of Bridges

In the name of Allah, the most gracious, the most merciful Praise be to Allah and prayer and peace be upon the Prophet Mohammed and his posterity the good, the virtuous I introduce this book in your hands as a contributions from me in enriching cognitive side to researchers in the field of geotechnical engineering... hoping that the researchers find a useful information in the use of geogrids in the construction of bridges

-B.Sc. degree from the University of Kufa / Civil Engineering Department / 1998. -M.Sc. degree from the University of Technology / Department of Building and Construction Engineering/ Geotechnical Engineering / 2001. -Ph.D. from Al-Nahrain University / Civil Engineering Department / 2015. -Member in Iraqi Engineers Association.

NOOR PUBLISHING

978-3-330-84590-9

Geogrid Versus Piles

Sheer Ali, Al-Omari, Khaled

NOOR PUBLISHING

Tawfek Sheer Ali

Raid Al-Omari

Zeyad Khaled

Geogrid Reinforced Earth versus Piles for The Foundation of Bridges

Geogrid versus Piles

Tawfek Sheer Ali
Raid Al-Omari
Zeyad Khaled

Geogrid Reinforced Earth versus Piles for The Foundation of Bridges

Tawfek Sheer Ali
Raid Al-Omari
Zeyad Khaled

Geogrid Reinforced Earth versus Piles for The Foundation of Bridges

Geogrid versus Piles

Noor Publishing

Impressum / Imprint
Bibliografische Information der Deutschen Nationalbibliothek: Die Deutsche Nationalbibliothek verzeichnet diese Publikation in der Deutschen Nationalbibliografie; detaillierte bibliografische Daten sind im Internet über http://dnb.d-nb.de abrufbar.
Alle in diesem Buch genannten Marken und Produktnamen unterliegen warenzeichen-, marken- oder patentrechtlichem Schutz bzw. sind Warenzeichen oder eingetragene Warenzeichen der jeweiligen Inhaber. Die Wiedergabe von Marken, Produktnamen, Gebrauchsnamen, Handelsnamen, Warenbezeichnungen u.s.w. in diesem Werk berechtigt auch ohne besondere Kennzeichnung nicht zu der Annahme, dass solche Namen im Sinne der Warenzeichen- und Markenschutzgesetzgebung als frei zu betrachten wären und daher von jedermann benutzt werden dürften.

Bibliographic information published by the Deutsche Nationalbibliothek: The Deutsche Nationalbibliothek lists this publication in the Deutsche Nationalbibliografie; detailed bibliographic data are available in the Internet at http://dnb.d-nb.de.
Any brand names and product names mentioned in this book are subject to trademark, brand or patent protection and are trademarks or registered trademarks of their respective holders. The use of brand names, product names, common names, trade names, product descriptions etc. even without a particular marking in this work is in no way to be construed to mean that such names may be regarded as unrestricted in respect of trademark and brand protection legislation and could thus be used by anyone.

Coverbild / Cover image: www.ingimage.com

Verlag / Publisher:
Noor Publishing
ist ein Imprint der / is a trademark of
OmniScriptum GmbH & Co. KG
Bahnhofstraße 28, 66111 Saarbrücken, Deutschland / Germany
Email: info@omniscriptum.com

Herstellung: siehe letzte Seite /
Printed at: see last page
ISBN: 978-3-330-84590-9

Zugl. / Approved by: Baghdad, Al-Nahrain University, 2015

Copyright © Tawfek Sheer Ali, Raid Al-Omari, Zeyad Khaled
Copyright © 2017 OmniScriptum GmbH & Co. KG
Alle Rechte vorbehalten. / All rights reserved. Saarbrücken 2017

Republic of Iraq

Ministry of Higher Education and Scientific Research

Al-Nahrain University/College of Engineering

Department of Civil Engineering

GEOGRID REINFORCED EARTH VERSUS PILES FOR THE FOUNDATIONS OF INTERCHANGE BRIDGES

by

TAWFEK AAMIR JAWAD SHEER ALI

B.Sc. (Civil Engineering, 1998)

M.Sc. (Geotechnical Engineering, 2001)

Rijab **1436**

April **2015**

ABSTRACT

Geogrids represent a rapidly growing segment within the field of geosynthetics. Rather than being a woven, nonwoven or knitted textile fabric, geogrids are polymers formed into a very open grid-like configuration having large apertures between individual ribs in the transverse and longitudinal directions.

The present research aims at studying the ability and feasibility of using geogrids instead of piles in the footings of interchange bridges resting on sandy soil as well as studying the behavior of geogrids under strip and rectangular footings.

A series of laboratory tests are carried out to compare the bearing capacity of unreinforced sand with that reinforced using Netlon CE121 and Tensar SS2 geogrids as well as measuring the strain and elongation occurring in the ribs of geogrids. TML strain gauges and compatible accessories are used for this purpose.

Tests are also carried out on piled strip and piled rectangular footings. Plane strain pile model is used in the case of strip footing and three square piles model are used in the case of rectangular footing. The end bearing and skin friction are experimentally estimated and the load sharing between the base of footings and the piles are also determined.

It is found that the use of geogrids to reinforce the sand under strip footings yields a higher bearing capacity than the case of unreinforced sand by a bearing capacity ratio (BCR) of (1.88) and (2.5) for Netlon CE121 and Tensar SS2 types of geogrids respectively. In addition, the use of geogrids under rectangular footings yields a higher (BCR) of (2.35) and (2.9) for Netlon CE121 and Tensar SS2 as well. The test have also revealed that the rib strain and elongation decrease gradually when the depth of the grid layer and the distance from the centerline of the footing increase. The strain and elongation in the geogrid ribs have been significantly reduced at a depth equal to the width of footing (B) and at a horizontal distance of about (3.6B) from the centerline of the footing.

In the case of using plane strain pile model with strip footings, it is found that the contributions of resistance are (75.6%) for end bearing and (24.4%) for skin friction. The contributions of resistance became (73%) for end bearing and (27%) for skin friction when using square piles with rectangular footings. This is because the scale of pile model length is smaller than the scale of pile end. It is also found that the sharing of loads is (66.2%) for

piles and (33.8%) for base in the strip footing, while for rectangular footing the sharing is (75%) for piles and (25%) for the footing base.

The experimental results of bearing capacity and piles capacity are also analyzed using the PLAXIS software. Good agreement between experimental and numerical results is found.

In addition, an economic study using MATLAB package is carried out. Optimization technique is used to formulate a case study in order to investigate the feasibility of using geogrids instead of piles in the foundations of interchange bridges. The results ensure that geogrids save up to (54%) of the construction cost within the limits of the adopted loads and the properties of in situ sandy soil put into consideration.

List of Contents

Contents	Page
Abstract	I
List of Contents	III
Notations	VII
List of Tables	XI
List of Figures	XII
Chapter One: Introduction	
1.1 General	1
1.2 Environmental Benefits of Geosynthetics	3
1.3 Economic Importance of Geosynthetics	3
1.4 Piled-Raft System	3
1.5 Purpose and Scope of the Study	4
1.6 Layout of the Thesis	5
Chapter Two: Literature Review	
2.1 Introduction	6
2.2 Classification of Soil Reinforcement Systems and Interaction Mechanisms	7
2.3 Previous Experimental Work in Soil Reinforcement Field	10
2.4 Methods of Analysis	29
2.5 Plane strain FEM-Model for Piled Rafts	30
2.6 Previous Work on Piled-Raft Foundation	32
2.7 Summary	39
Chapter Three: Experimental Work and Materials	
3.1 Introduction	41
3.2 Test Apparatus	41
3.2.1 Sand Container	41
3.2.2 Footing and Piles Models	42
3.2.3 Loading Frame	44
3.2.4 Density Control System	45
3.3 Electronic Universal Testing Machine	45
3.4 Soil Properties	48
3.5 Soil Preparation	50
3.6 Triaxial Testing of In-situ Soil	50

3.7 Strain Gauge Technique	54
3.7.1 General Description	54
3.7.2 Strain Gauge Measurements	56
3.8 Datatronic 128-Channel Automatic Data Acquisition System	60
3.9 Displacement Measurements	61
3.10 Geogrids Types and Properties	61
3.11 Research Program and Procedure	65
Chapter Four: : Presentation and Discussion of Experimental Results	
4.1 Introduction	70
4.2 Unreinforced Soil Model Tests	70
4.3 Reinforced Sand Model Tests	72
4.4 Effect of Footing Type	74
4.5 Geogrid Strain and Elongation Measurements	78
4.6 Calibration Methods	78
4.7 Strains in Tensar SS2	82
4.7.1 Strip Footing	82
4.7.2 Rectangular Footing	92
4.8 Model Tests of Plane Strain Piles	101
4.8.1 Capacity of Plane Strain Piles under Strip Footing (Piled-Strip System)	101
4.8.2 Skin and End Bearing Piles Capacity	103
4.8.3 End Bearing Piles Capacity	103
4.8.4 Piled-Strip System Capacity Components	105
4.9 Model Tests of Piled-Rectangular Footing	107
4.9.1 Full Capacity	107
4.9.2 Skin and End Bearing Piles Capacity	110
4.9.3 End Bearing Piles Capacity	110
4.9.4 Piled-Rectangular System Capacity Components	111
Chapter Five: Comparison between Numerical Results and Experimental Results	
5.1 Introduction	114
5.2 Theoretical Results	114
5.2.1 Bearing Capacity	114
5.2.1.1 Strip Footing	115
5.2.1.2 Rectangular Footing	116

5.2.2 Piles capacity	117
5.2.2.1 Plane Strain Piles	117
5.2.2.2 Rectangular Piles	119
5.3 Numerical Investigation	120
5.3.1 3D PLAXIS Software	120
5.3.1.1 The Input Program	120
5.3.1.2 Starting the Program	121
5.4 Strip Footing Modeling and Results	121
5.4.1 Unreinforced Soil	121
5.4.2 Reinforced Soil Using Netlon CE121 Geogrid	129
5.4.3 Reinforced Soil Using Tensar SS2 Geogrid	131
5.5 Rectangular Footing Modeling and Results	133
5.5.1 Unreinforced Soil	133
5.5.2 Reinforced Soil Using Netlon CE121 Geogrid	134
5.5.3 Reinforced Soil Using Tensar SS2 Geogrid	136
5.6 Plane Strain Piles under Strip Footing (Piled-Strip) Modeling and Results	137
5.6.1 Piled-Strip System	137
5.6.2 Skin and Bearing Only	139
5.6.3 End Bearing Only	139
5.7 Piles under Rectangular Footing (Piled-Rectangular) Modeling and Results	141
5.7.1 Piled-Rectangular System	141
5.7.2 Skin and End Bearing only	142
5.7.3 End Bearing Only	142
5.8 Load Sharing Between Piles and Footing	145
5.8.1 Load Sharing Between Piles and Footing From Experimental	146
5.8.2 Load Sharing Between Piles and Footing From PLAXIS	147
5.9 Summary of Results	147
5.10 Extrapolation of Results to Field Condition	148
Chapter Six: Economic Study	
6.1 Introduction	152
6.2 Calculations of Loads	153
6.3 Problem Statement	153
6.3.1 Objective Function of the Reinforced Soil Case	153

6.3.2 Constraints of the Reinforced Soil Case	155
6.3.3 The Objective Function of the Piles Case	158
6.3.4 Constraints of the Piles Case	159
6.4 Discussion	162
6.5 Parametric Study	163
6.6 Summary	164
Chapter Seven: Conclusions and Recommendation	
7.1 Conclusions from Experimental Work	169
7.1.1 Unreinforced and Reinforced Sand Model	169
7.1.2 The Geogrid Straining Mechanism	169
7.1.3 Piled-Footings Systems	170
7.2 Comparisons of Experimental, Theoretical and Numerical Results	170
7.2.1 Bearing Capacity of Footings	171
7.2.2 Piled-Footings System	172
7.3 Load Sharing Between Piles and Footing From Experimental and PLAXIS	172
7.4 Economic Study	172
7.5 Recommendations for Future Work	173
References	174
APPENDIX A: Typical Design Adopted as Case Study	-
APPENDIX B: Figures of PLAXIS and MATLAB	-
APPENDIX C: Papers	-

Notations

Abbreviations

MSE	Mechanically Stabilized Earth
GRS	Geosynthetic reinforced soil
LVDTs	Linear variable displacement transducers
ASTM	American Society for Testing and Materials
K30	Subgrade reaction coefficient
BCR_u	Ultimate bearing capacity ratio
BCR	Bearing capacity ratio
FEA	Finite element analysis
FEM	Finite element method
UU	Unconsolidated undrained triaxial compression tests
HDPE	High Density Polyethylene
PET	Polyester (PET) geogrids
ML	Monotonic loading
EA_{psp}	Normal stiffness for plain strain pile
EA_p	Normal stiffness for one pile
CPRF	Combined piled raft foundation
MSEW	Mechanically stabilized earth wall
CBR	California Bearing ratio
MD	Machine direction
XMD	Cross machine direction
FHWA	Federal Highway Administration

Symbols

k_s	Modulus of subgrade reaction
T	Apertures of the geogrid mesh
D_{60}	Particle diameter in mm that 60% of sand is finer
D_{50}	Particle diameter in mm that 50% of sand is finer
D_{30}	Particle diameter in mm that 30% of sand is finer
D_{10}	Particle diameter in mm that 50% of sand is finer
C_u	Coefficient of uniformity

C_c	Coefficient of curvature
e	Eccentricity
σ_1	Major principal stress
σ_3	Minor principal stress
$\Delta\sigma_3$	Enhanced confining stress
σ_1/σ_3	Principal stress ratio
ΔH	Vertical spacing of reinforcement
N, n	Number of layers
γ	Unit weight of soil
u	Depth below the footing of the first layer of reinforcement
D_f, d_f	Surface model footing
B	Footing width
L	Length of footing, length of strain gauge
s	Settlement
d/B	Horizontal distance of strain gauge/width of footing
h/B	Vertical distance of strain gauge/width of footing
D	Diameter of circular footing
L_p	Raft length in plane
E	Modulus of elasticity
w	Weight of raft foundation
A_s	Shaft area per unit depth
α_{ar}	Area ratio
R	Strength reduction factor
FS	Factor of safety
SP	Uniformly graded sand
b	Width size of square sheet of reinforcement
A	Cross-sectional area of strain gauge
ρ	Resistivity of the material
ε_α	Axial strain
ε_3	Minor principal strain
μ	Poisson's ratio
F	Gauge factor
So_3	Sulfate content

T.S.S	Total soluble salts content
G_s	Specific gravity of sand
γ_{dmin}	Minimum density of sand
γ_{dmax}	Maximum density of sand
γ_{dused}	Density used in test
e_{max}	Maximum void ratio
e_{min}	Minimum void ratio
e_{used}	void ratio used during test
n_{used}	Porosity used during test
$Ø_{used}$	angle of internal friction used during test
$R_{D\ used}$	Relative density used during test
O.M.C	Optimum moisture content
m_c	Moisture content
M	Load per inch/strain
l_w	Longitudinal rib width
t_w	Transverse rib width
s/B	Relative settlement
h	Distance between reinforcement layers
q_{ult}	Ultimate bearing capacity for the unreinforced
c	Cohesion of soil
Nc, Nq and	Terzaghi bearing capacity factors
δ	Reading of dial gauge (displacement).
h	Height of cross section of steel square bar
Δl	Elongation in the rib
d	Distance of gauge from footing center
σ	Applied stress on the material
$Ø_{Ps}$	Angle of internal friction due to plain strain
$Ø_{tr}$	Angle of internal friction due to triaxial
q_a	Allowable bearing capacity
Ø	Angle of internal friction of soil
γ_b	Submerged unit weight of soil
B	Width of footing
L	Length of footing

IQD	Iraqi dinar
nl	Number of geogrids layers (as written in MATLAB program)
cg	Cost of geogrids IQD/m^2
sz	Stress zone in two sides of footing
ef	Expansion factor for excavation and filling (for field purposes)
ce	Cost of excavation IQD/m^3
cw	Cost of working IQD/m^2
cf	Cost of filling and compaction IQD/m^3
k_s	Modulus of subgrade reaction
cwp	Cost of work of piles
ccp	Cost of concrete
cwp	Cost of work
cs	Cost of steel reinforcement
Pp	Total load on footing
np	Number of piles
Dp	Pile diameter
Lp	Pile length

List of Tables

Table	Title	Page
2-1	Interaction mechanisms and predominant reinforcement forces for different reinforced soil systems, (Pedley 1990)	9
3-1	The physical and chemical properties of the sand	49
3-2	The properties of the strain gauge coating material ***SB*** tape	58
3-3	The properties of the strain gauge adhesive	59
3-4	The typical properties of Netlon CE121 geogrid, (after Fakhraldin, 2013)	63
3-5	Typical properties of Tensar SS2, (after Fakhraldin, 2013)	64
4-1	Horizontal distances of the strain gauge from the center line of strip footing	83
4-2	Horizontal distances of the strain gauge from the center line of rectangular footing	93
5-1	The properties of soil and the properties of the model of footing	124
5-2	The properties of geogrids modeled in PLAXIS	132
5-3	The results of sharing between piles and footings	148
5-4	Summary of results	151
6-1	Inputs and outputs of cost optimization analyses of the reinforced soil case	158
6-2	Inputs and outputs of cost optimization analyses of piles case	163
A-1	Part of contracting tender of case study	A-8

List of Figures

Figure	Title	Page
1-1	Applications of Reinforced Earth as Retaining wall and Abutments (Reinforced Earth Company, 2011)	2
2-1	Types of geosynthetics (Available on Wikipedia, 2014)	8
2-2	Mechanisms of soil reinforcement interaction: (a) friction (b) bearing, (Pedley 1990)	9
2-3	Variation of peak stress ratio with dimensionless factor T/D50, (Al-Omari et al., 1987)	11
2-4	Relation between stress and settlement, (after Al-Sinaidi and Ali, 2006)	14
2-5	Configuration of 3D reinforcing elements: (a) single-sided and (b) double-sided, (after Zhang et al., 2006)	14
2-6	Pressure-settlement curves for model footing tests on unreinforced sand with different shape footing. (after Chen, 2007)	16
2-7	Pressure-settlement curves for model footing tests with four layers of BX6100. (after Chen, 2007)	16
2-8	Strain distribution along the center line of BX6100 geogrid (B×L: 152mm×254 mm). (after Chen, 2007)	17
2-9	Strain distribution along the center line of BX6100 geogrid placed at a depth of 152 mm. (after Chen, 2007)	18
2-10	Vertical stress distribution along the center line of footing at a depth of 254 mm for five layers of different types of reinforcement (B×L: 152 mm×254mm). (after Chen, 2007)	19
2-11	Load–settlement curves for unreinforced and geogrid-reinforced fine sand and coarse sand, (after Phanikumar et al., 2009)	22
2-12	Schematic diagram of the test set-up	25
2-13	Typical diagram defining various geometric parameters	27
2-14	Geometry of the geocell reinforced foundation bed	28
2-15	Typical diagram defining various geometric parameters	31
2-16	Axisymmetric finite element model of piled raft foundation, (after Hooper, 1973)	33
2-17	Finite element model FEM of piled raft system, ,(after Yu Bao, 2003)	37
2-18	Load-settlement curve of piled raft and pile,(after Yu Bao, 2003)	37
2-19	Load-settlement curve of piled raft and raft, (after Yu Bao, 2003)	38
3-1	Sand container used in the experimental study (100 cm length × 50 cm width × 60 cm depth)	42
3-2	Strip footing (49 cm length × 13.5 cm width), rectangular footing (23 cm length × 6 cm width), and loading blades	43
3-3	Models of piles	44
3-4	The loading frame	45
3-5	The density control system, (*After Fakhraldin, 2013*)	46
3-6	Electronic Universal Testing Machine	47
3-7	Grain size distribution of soil	48

3-8	Density calibration curves	51
3-9	Stress system in Triaxial test	52
3-10	Triaxial friction angle-porosity relationship	53
3-11	Triaxial test equipment	54
3-12	Definition of strain**,** TML strain gauges manual	55
3-13	Strain gauge configuration, TML strain gauges manual	56
3-14	Strain gauge circuit**,** TML strain gauges manual	57
3-15	TML strain gauges, ***SB*** tape, and compatible adhesive type ***CN***	59
3-16	The Datatronic 128-Channel Automatic Data Acquisition System	61
3-17	Types of used geogrids, (a) Netlon CE121 (b) Tensar SS2	62
3-18	Flow chart of the experimental testing program	69
4-1	Model of strip and rectangular footing on unreinforced soil	71
4-2	Bearing pressure versus relative settlement for strip and rectangular footings resting on unreinforced soil	72
4-3	Geometry and top plan of the geogrid and strip footing model	73
4-4	Geometry and top plan of the geogrid and rectangular footing model	74
4-5	Model with strip and rectangular footing on soil with geogrid	75
4-6	Bearing pressure versus relative settlement for two types of footings using Netlon CE121	76
4-7	Bearing pressure versus relative settlement for two types of footings using Tensar SS2	76
4-8	Bearing pressure versus relative settlement for strip footing with and without geogrid	77
4-9	Bearing pressure versus relative settlement for rectangular footing with and without geogrid	77
4-10	The calibration of strain occurring in the rib using the first method of calibration	81
4-11	The calibration of strain occurring in the rib using the second method of calibration	81
4-12	The calibration of strain occurring in the rib using the two method of calibration	82
4-13	(a) pasting operation. (b) The distribution of strain gauges in the strip footing	84
4-14	Strain measurements in Tensar SS2 geogrid for strip footing	85
4-15	The relationship between strain in ribs of first geogrid layer (Tensar SS2) and applied stress on reinforced sand using strip footing	86
4-16	The relationship between elongation in ribs of first geogrid layer (Tensar SS2) and applied stress on reinforced sand using strip footing	86
4-17	The relationship between strain in ribs of second geogrid layer (Tensar SS2) and applied stress on reinforced sand using strip footing	87
4-18	The relationship between elongation in ribs of second geogrid layer (Tensar SS2) and applied stress on reinforced sand using strip footing	87
4-19	The relationship between strain in ribs of third geogrid layer (Tensar SS2)	88

	and applied stress on reinforced sand using strip footing	
4-20	The relationship between elongation in ribs of third geogrid layer (Tensar SS2) and applied stress on reinforced sand using strip footing	88
4-21	The relationship between strain and (relative distance, distance) from the centerline of footing	90
4-22	The relationship between elongation and (relative distance, distance) from the centerline of footing	90
4-23	The relationship between strain and (relative depth, depth) below the base of strip footing	91
4-24	The relationship between strain and (relative depth, depth) below the base of strip footing	91
4-25	The distribution of strain gauges in the rectangular footing test	92
4-26	Strain measurements in Tensar SS2 geogrid for rectangular footing	93
4-27	The relationship between strain in ribs of first geogrid layer (Tensar SS2) and applied stress on reinforced sand using rectangular footing	95
4-28	The relationship between elongation in ribs of first geogrid layer (Tensar SS2) and applied stress on reinforced sand using rectangular footing	95
4-29	The relationship between strain in ribs of second geogrid layer (Tensar SS2) and applied stress on reinforced sand using rectangular footing	96
4-30	The relationship between elongation in ribs of second geogrid layer (Tensar SS2) and applied stress on reinforced sand using rectangular footing	96
4-31	The relationship between strain in ribs of third geogrid layer (Tensar SS2) and applied stress on reinforced sand using rectangular footing footing	97
4-32	The relationship between elongation in ribs of third geogrid layer (Tensar SS2) and applied stress on reinforced sand using rectangular footing	97
4-33	The relationship between strain and (relative distance, distance) from the centerline of rectangular footing	99
4-34	Relationship between elongation and (relative distance, distance) from the centerline of rectangular footing	99
4-35	Relationship between strain and (relative depth, depth) below the base of rectangular footing	100
4-36	Relationship between elongation and (relative depth, depth) below the base of rectangular footing	100
4-37	Plane strain piles model test under strip footing, (piled-strip)	101
4-38	Load-Settlement relationship for piled-strip system	102
4-39	Comparison between the results of loading the strip footing with geogrid, without geogrid and the piled-strip system	103
4-40	Details of skin friction and end bearing for piled-strip model test	104
4-41	Load-Settlement relationship for skin and end bearing only	104
4-42	Details of end bearing piled-strip model test	105
4-43	Load-Settlement relationship for end bearing only	106
4-44	Details of skin friction and end bearing for piled-strip	107
4-45	Rectangular piles model test	108
4-46	Load-Settlement relationship for piles under rectangular footing	109
4-47	Comparison between the results of loading the rectangular footing with	109

	geogrid, without geogrid and with piles	
4-48	Details of skin friction and end bearing for rectangular piles model test	110
4-49	Load-Settlement relationship for skin and end bearing only of rectangular piles	111
4-50	Details of end bearing of rectangular piles model test	112
4-51	Details of end bearing only for piles under rectangular footing	113
4-52	Details of skin friction and end bearing for piles under rectangular footing	113
5-1	Bearing capacity factor N_q for piles, (FHWA, 2006a)	119
5-2	Bearing pressure versus relative settlement for strip footing resting on unreinforced sand	129
5-3	Borehole of the strip footing with Netlon CE121 geogrid case	130
5-4	Bearing pressure versus relative settlement for strip footing with Netlon CE121 geogrid	130
5-5	Borehole of the strip footing with Tensar SS2 geogrid case	131
5-6	Bearing pressure versus relative settlement for strip footing with Tensar SS2 geogrid	132
5-7	The geometry of the rectangular footing case on sand alone	133
5-8	Bearing pressure versus relative settlement for rectangular footing resting on sand alone	134
5-9	Borehole of the rectangular footing using Netlon CE121 geogrid case	135
5-10	Bearing pressure versus relative settlement for rectangular footing with Netlon CE121 geogrid	135
5-11	Borehole of the rectangular footing with Tensar SS2 geogrid case	136
5-12	Bearing pressure versus relative settlement for rectangular footing on soil reinforced using Tensar SS2 geogrid	137
5-13	Final geometry of the piled-strip system	138
5-14	Load-Settlement relationship for pled-strip system	138
5-15	(a) 3D finite element mesh (b) Total displacement	139
5-16	Load-Settlement relationship of skin and end bearing only for piled-strip system	140
5-17	Option of elimination of skin friction of pile in PLAXIS	140
5-18	Load-Settlement relationship of end bearing only for piled-strip system	141
5-19	Final geometry of the piled-rectangular system	142
5-20	Load-Settlement relationship for piled-rectangular system	143
5-21	Final geometry of the rectangular piles without footing	143
5-22	Load-Settlement relationship of skin and end bearing only for piled-rectangular system	144
5-23	Option of elimination skin friction of pile in PLAXIS	144
5-24	Load-Settlement relationship of end bearing only for piled-rectangular system	145
5-25	Load sharing between piles and raft, (after Hooper, 1973)	146
6-1	One design unit for the sake of cost comparison	154
6-2	Chart for estimating bearing capacity factor N'q (FHWA, 2006).	161
6-3	Relationship between Øº and cost for Netlon CE121 geogrid	165
6-4	Relationship between Øº and cost for Tensar SS2 geogrid	165
6-5	Relationship between Øº and cost for piles	166
6-6	Relationship between load and cost for Ø = 20º	166

6-7	Relationship between load and cost for Ø = 25º	167
6-8	Relationship between load and cost for Ø = 30º	167
6-9	Relationship between load and cost for Ø = 35º	168
6-10	Relationship between load and cost for Ø = 40º	168
A-1	Location of the Nothern Garage interchange bridge in Al-Najaf city	A-1
A-2	Plan of grade separation of bridge	A-2
A-3	Row of piers and piles	A-3
A-4	Section of piled-strip system of bridge	A-4
A-5	Section in site soil of project	A-5
A-6	Cross section of bridge	A-9
B-1	Main window of the input program (Model mode)	B-1
B-2	Project and dimensions tabs sheet of the general settings window	B-2
B-3	Work-planes window	B-3
B-4	Final geometry of the strip footing case	B-3
B-5	Final geometry of the strip footing case	B-4
B-6	2D finite element mesh of the geometry	B-4
B-7	Generated 3D mesh in the output window	B-5
B-8	The calculations toolbar	B-5
B-9	The phases window with the general tab sheet	B-6
B-10	The parameters tab sheet of the phases window	B-6
B-11	Setting the magnitude of load for phases	B-7
B-12	The calculations information window	B-7
B-13	Samples of Outputs	B-8
B-14	Formulation and running the optimization of reinforced soil case in MATLAB	B-9
B-15	Formulation and running the optimization of piles in MATLAB	B-10

CHAPTER ONE

INTRODUCTION

1.1 General

The Iraqis have used soil since ancient times in architecture and buildings using multiple methods vary depending on the nature of the building and its function. Therefore either the use of soil free or mixed with other materials as a reinforcement such as straw or in the different form of a substance called milk either be used for the entire structure or parts.

In many construction projects such as roads, railways, and bridges, the underlying soil may have low bearing capacity, high compressibility, high susceptibility to differential settlement and low shear strength. In order to avoid foundation damage, the soil must be improved to ensure the required stability. In the construction of bridges, piles are commonly used to transfer the high loads applied from the main girders to the soil. Piles are usually costly and need more time and effort. To minimize the construction cost, the use of a suitable type of geosynthetics, called geogrids, instead of piles is investigated.

Geosynthetics has been widely used as reinforcing materials in many geotechnical engineering applications, such as Mechanically Stabilized Earth (MSE) walls, slopes, embankments, pavements, and reinforced soil foundations. Since its invention in 1963, the reinforced earth technique has been quickly accepted on a worldwide basis as an economical and efficient solution and has been extensively used since then, in retaining walls and bridge abutments, highways, expressways and railroads lines as well as for other structures as industrial, civil, defense and water works projects. Figure 1.1 shows some applications of these techniques (Reinforced Earth Company, 2011). Structures were constructed in (32) countries and there are presently several specifications issued by state institutes on this technique (e.g., Germany, United States). Worldwide demand for geosynthetics is projected to rise (5.3%) annually to (4.7) billion square meters in 2013. China, India, Russia and other countries with large-scale infrastructure developments have planned, and are evolving environmental protection regulations. Building construction codes are expected to register the strongest advances, (Oyegbile, 2011).

Geosynthetics materials are especially useful in an environment of increasing land scarcity, awareness of seismic hazards, and stringent environmental regulations. Geosyntheticly Reinforced Soil (GRS) is a term used to describe a particular type of internally supported soil mass (Alex et al., 2009).

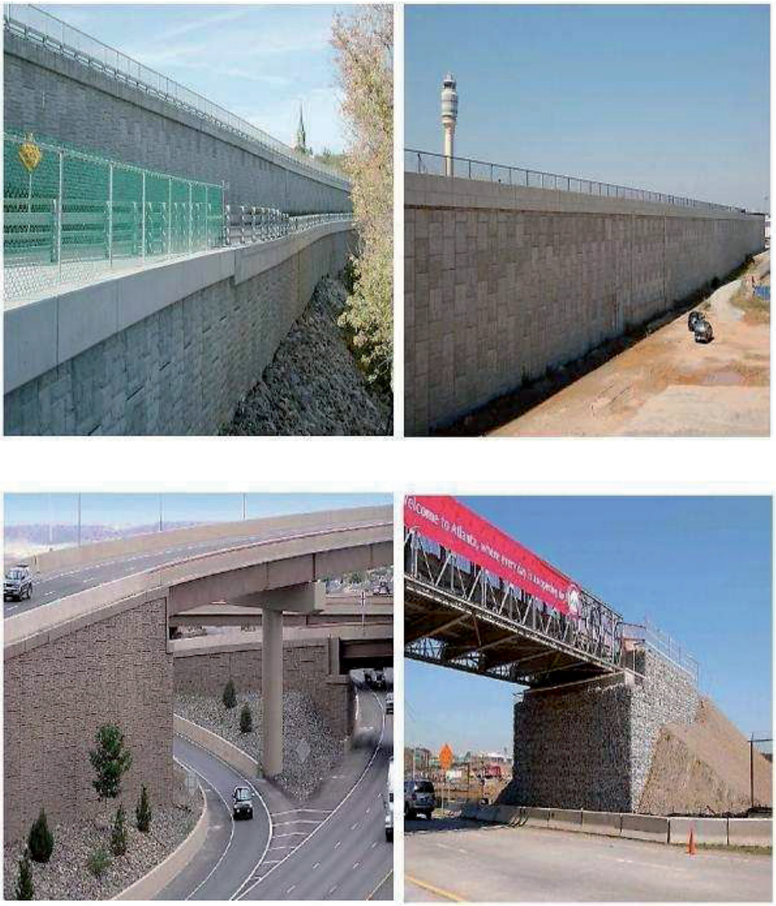

Figure 1-1 Some applications of Mechanically Stabilized Earth walls (Reinforced Earth Company, 2011)

1.2 Environmental Benefits of Geosynthetics

The main environmental benefits of using geosynthetics in the construction works can be summarized as, (Reinforced Earth Company, 2011):

i. Civil engineering structures need to have long term durability to prevent potential ecological disasters (floods, draughts, earthquakes, global warming). Geosynthetics provide such long lasting solutions with minimum cost.
ii. Geo-techs are difficult or impossible to degrade. However, in view of their inert nature they can be disposed of without the danger of contamination.
iii. Geosynthetics assist the environment by acting as a containing barrier for toxic materials.
iv. The envisaged functional lifetime of geosynthetics is extremely long, in many cases over 100 years.
v. Geosynthetics provide sealing and capping of pollution due to chemicals released after road and rail accidents into groundwater areas.

1.3 Economical Benefits of Geosynthetics

The economic benefits of using geosynthetics can be listed as follows, (Reinforced Earth Company, 2011):

i. Commonly accepted as durable, long lasting and environmentally safe solutions to problems geotechnical engineering projects.
ii. The cost of geosynthetics applied usually between 3 to 5 percent of the total cost of projects.
iii. For a number of projects, savings of 30 percent in total project costs have been reported.
iv. In roadways minimize the regular repair and maintenance costs directly.
v. Prevent accidents, increase efficiency of structures, minimize pollution, and leads to efficient use of natural resources.

1.4 Piled-Raft System

In the conventional approach of piled foundations design, all loads are supposed to be transferred to the piles and the contact pressure between the cap and the soil is neglected. In the last few decades, geotechnical engineers started to take this contact pressure into account, where the raft and the piles interact to transfer loads to the ground in a system called piled raft foundation (Ryltenius, 2011).

Piled raft foundation is a combination of both raft and piles also known as pile-enhanced raft. An increasing number of structures are constructed using a piled raft foundation due to its underlying soft ground that low bearing capacity and excessive settlement especially in coastal areas, where piled raft is essential (Naeini and Hosseinzade, 2014). Piled raft foundations provide an economical option for circumstances where the performance of the raft alone does not satisfy design requirements. Many studies on piled-raft design have been carried out by researchers all over the world. The design of piled-raft system basically involves examining the bearing capacity of the supporting sub-soil and the permissible allowable total and differential settlements.

1.5 Purpose and Scope of the Study

The construction of interchange bridges in Iraq witnessed a wide evolution within the last few years. Piled-strip footings are used to resist the load of each row of piers in all interchange bridges in Iraq. The construction of piles almost required special equipment and high quality workmanship as well as high construction cost. Thus, one of the main objectives of this research is to study the ability of using geogrids instead of piles in the foundations of interchange bridges. Laboratory tests are conducted using Netlon CE121 and Tensar SS2 to study the improvement in bearing capacity of sandy soil taken from a bridge construction site in Al-Najaf city called Northern Garage. Results are compared with piled-strip and piled-rectangular footings.

Since strains occurring in the geogrid ribs are vital to understand the mechanism of the reinforcing action and to assess the need of high quality geogrids, therefore strains occurring in Tensar SS2 geogrid ribs using strip and rectangular footings measured during the performance of bearing capacity tests using high quality strain gauges, compatible glue, compatible surface and an imported acquisition system besides well controlled calibration methods. The bearing capacity and strain mechanism tests yielded information on the effect of footing type and distribution of strain in geogrid ribs under the footing.

Many laboratory tests are conducted using plane strain pile model and three rectangular section piles. Plane strain pile model is used with a strip footing to investigate the piled-strip system, end bearing and skin friction capacities. While square piles are used with a rectangular footing. Sharing of piles and footings is investigated also and presented.

An economic study of using geogrids instead of piles in the foundation of interchange bridges is conducted within the limits of applied loads and soil bearing capacity prevailing in most of highway projects in Iraq. Optimization technique is used to estimate the cost of construction of both types of footings (reinforced soil and piles). Comparison between the two cases is adopted to decide whether the use of geogrids is more economic than the use of piles within the range of applied loads. The cost of construction is determined according to prevailing local prices at the time of the study.

1.6 Layout of the Thesis

This thesis is divided into seven chapters. The following is a brief summary of the contents of each chapter.

Chapter One: presents a brief introduction to geosynthetics, environmental benefits of geosynthetics, economic importance of geosynthetics, piled-raft system and the purpose and scope of the study.

Chapter Two: presents a brief review on theory of bearing capacity of soil, design of piles, failure mechanisms in reinforced soil, previous experimental, analytical and numerical research carried out on reinforced sand using geosynthetic and the piled-footing system.

Chapter Three: deals with the experimental program, test apparatus, chemical and physical properties of the sand and triaxial testing of the prepared sand to determine the relation between porosity and angle of internal friction.

Chapter Four: covers presentation, analysis and discussion of the model test results.

Chapter Five: presents a mathematical model for strip and rectangular footings resting on reinforced sand using the finite element computer program PLAXIS 3D foundation and illustrates the results obtained from past theoretical equations and finite element program. This chapter also deals with the comparisons carried out between experimental, theoretical and numerical results.

Chapter Six: Is concerned with an economical study using optimization technique to investigate the feasibility of using geogrids in the foundation of interchange bridges.

Chapter Seven: Summarizes the main conclusions of this research, and some recommendations for future research in the same area of knowledge.

CHAPTER TWO

LITERATURE REVIEW

2.1 Introduction

The term *reinforced soil* describes any soil mass which has had its shear strength improved by combining it with resisting elements; these resisting elements, or reinforcement may take the form of bars, strips, tubes, grid or sheets. Reinforcement can be used as either a permanent component of a reinforced soil structure or simply to provide a temporary increase in soil shear strength to allow the construction of an adjacent structure. The observed increase in soil shear strength of a reinforced soil is always a direct result of relative soil-reinforcement displacement, (Pedley, 1990). Soil reinforcement is the main field of activity of the Reinforced Earth Companies, combining both the geotechnical and structural engineering disciplines. The technique is based on the formation of a composite material through the association of compacted frictional fill and linear soil reinforcement. The soil reinforcement may be either metallic (like the high adherence galvanised steel strips) or synthetic (like the high tenacity polyester-based GeoStrap strips). The resistance and stability of the composite structure provide significant load-bearing capacity. The ease and speed of construction are significant advantages in reducing overall cost. The durability of the materials used is well documented and the safety of the structures unrivalled. The technology provides solutions to complex cases and often proves to be the best answer to circumstances such as restricted right-of-way, unstable natural slopes, marginal foundation conditions and large settlements. The variety of facings can meet all architectural requirements, (Reinforced Earth Company, 2011).

A pile bridge is a structure that uses foundations consisting of long poles (referred to as piles), which are made of wood, concrete or steel and which are hammered into the soft soils beneath the bridge until the end of the pile reaches a hard layer of compacted soil or rock. Piles in such cases are hammered to a depth where the grip or friction of the pile and the soil surrounding it will support the load of the bridge deck. Piles can be also installed in predrilled holes. Piles that are driven into place are generally considered to be low

displacement or high displacement depending on the amount of soil that must be pushed out of the way as the pile is driven. Examples of low displacement piles are steel H-sections and open-ended steel pipe piles that do not form a soil plug at the end. Examples of high-displacement piles are solid section piles, such as round timber piles or square precast concrete piles, and steel pipe piles with a closed end, (Bowles, 1996).

Geosynthetics are the generally polymeric products used to solve civil engineering problems. This includes eight main product categories: geotextiles, geogrids, geonets, geomembranes, geosynthetic clay liners, geofoam, geocells and geocomposites. The polymeric nature of the products makes them suitable for use in the ground where high levels of durability are required. Properly formulated, however, they can also be used in exposed applications. Geosynthetics are available in a wide range of forms and materials, each to suit a slightly different end use. These products have a wide range of applications and are currently used in many civil, geotechnical, transportation, geoenvironmental, hydraulic, and private development applications including roads, airfields, railroads, embankments, retaining structures, reservoirs, canals, dams, erosion control, sediment control, landfill liners, landfill covers, mining, aquaculture and agriculture. Figure 2-1 shows many types of geosynthetics overall the world, (Available on Wikipedia, 2014).

2.2 Classification of Soil Reinforcement Systems and Interaction Mechanisms

The systems of soil reinforcement can be divided into two major categories: *in-situ and constructed*. The former category covers techniques where the reinforcement is placed into virgin soil to form a reinforced soil structure; this includes the techniques of soil nailing and soil doweling. The latter category describes techniques where the reinforcement is placed at the same time as an imported and remolded soil. Such techniques are often referred to as bottom up processes, as they involve the placement of a fill and include structures such as reinforced soil embankments and bridge abutments (Pedley, 1990).

The reinforcement used for in-situ structures is usually linear owing to the method of installation, whereas reinforcement used for the constructed category can be much more varied in form and often consists of strips, mats or grid.

Figure 2-1 Types of geosynthetics (Available on Wikipedia, 2014)

Typical applications of in-situ and constructed reinforced soil are given in Fig. 2-2, (Pedley, 1990). There are two modes of interaction between soil and reinforcement: *reinforcement bearing* leading to bending moments and shear forces, and *reinforcement friction* leading to axial tension or compression. The relative soil-reinforcement stiffness and strength, and the soil deformation occurring in the structures have a large influence on the magnitude of the induced reinforcement forces. Figure 2-2 and table 2-1 illustrate the mechanism of bearing and friction for different soil-reinforcement systems. Table 2-1 shows that whilst of the reinforcement systems exhibit both bearing and frictional interaction mechanisms it is only for soil doweling that shear force is the major reinforcement force; all of the other techniques rely predominantly on axial tension.

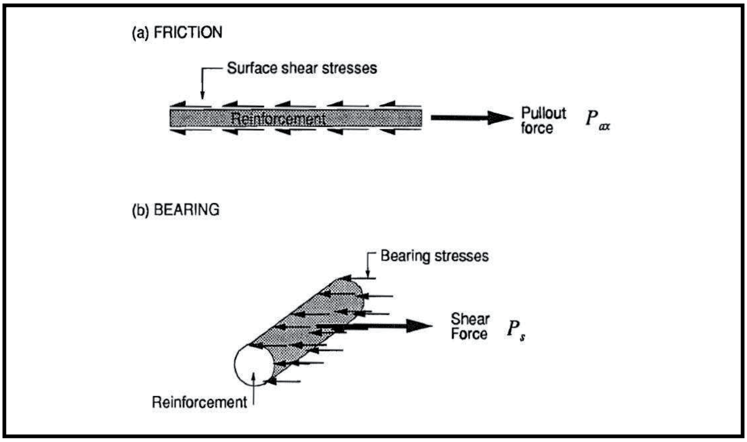

Figure 2-2 Mechanisms of soil reinforcement interaction: (a) friction (b) bearing**,** (Pedley, 1990)

Table 2-1 Interaction mechanisms and predominant reinforcement forces for different reinforced soil systems, (Pedley, 1990)

SYSTEM	INTERACTION MECHANISM		MAJOR REINFORCEMENT FORCE	
	Bearing	Friction	Tension	Shear
Soil Nailing (in-situ)				
Soil Dowelling (in-situ)				
Constructed Walls & Embankments				
Embankments with membrane reinforcement				

2.3 Previous Works in Soil Reinforcement Field

Fannin (1986) studied the mechanisms by which a geogrid acts to reinforce a granular layer over soft clay with reference to trafficking of unpaved roads. Both model and full scale tests performed. Model tests were carried out for monotonic and cyclic loading of a dual footing on to a layer of granular material that was compacted over a consolidated kaolin sample. The tests were made in conditions of plane strain at a quarter scale, and included a scaled geogrid at the base of the granular layer. Measurements of footing load, displacements and photographic observations through a Perspex front face to the test box were used to identify the reinforcing actions of the geogrid. The results for both reinforced and unreinforced layers analyzed using a virtual work procedure. Load tests were also made on footing plates at full scale, involving a similar compacted granular layers over prepared London clay and including a high strength polymer geogrid.

Al-Omari et al. (1987) used perforated steel discs and the plastic geomesh Netlon CE121 as reinforcing materials to investigate the relation of interlocking mechanism to the aperture size (T) of the geogrid mesh. Triaxial compression tests on 100 mm diameter sand samples was conducted. Perforations were performed with constant diameter systemically into each steel disc. The ratio of the aperture size of the steel mesh to the grain size of the sand D_{50} was varied in the test but the area of holes to the area of solid was kept constant in each disc. The conclusion of the study is summarized through the following points as the strength enhancement in mesh reinforced sand depends on the mechanism of interlocking which is in turn affected by the ratio of aperture size to particle diameter. The peak stress ratio (σ_1/σ_3) of mesh reinforced sand increases to a maximum at $T/D_{50} \approx 13.5$ and then drops beyond this value as shown in Fig. 2-3. The use of plastic mesh with the appropriate stiffness and the appropriate aperture size makes the strength of the sand approximately independent of the sand density.

Palmeira (1987) used an apparatus able to contain $1 m^3$ sample of sand in order to perform large scale tests to investigate soil-reinforcement interaction by means of direct shear and pull-out tests. Plastic and metal sheet and grid reinforcements were used in conjunction with sand. The vertical stress and the shear strain development in the central region of the sample were increased with reinforcement. The behavior of the reinforced sample was

found to depend on the type and form of the reinforcement as well as its mechanical properties. The results recorded that interference between grid bearing members is the main factor conditioning the pull-out resistance of grid reinforcement and that maximum bearing pressure exhibited by bearing member depends on the ratio of the member diameter to the mean particles size.

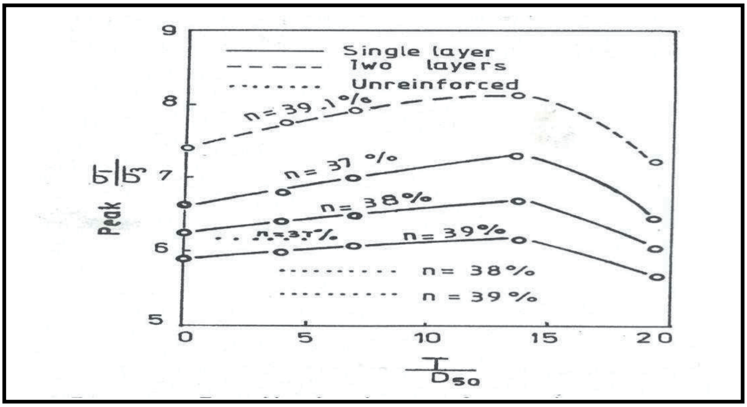

Figure 2-3 Variation of peak stress ratio with dimensionless factor T/D_{50}, (Al-Omari et al., 1987)

Al-Omari et al. (1988) studied the dilatancy characteristics and failure mechanism of geogrid reinforced sand. The sand used was from the western part of Iraq, Karbala specifically. The grain size distribution gave particle size ranging from 0.425 to 1.18 mm with uniformity coefficient of 1.69. A series of triaxial tests were carried out in the saturated condition using a relative density of 73%. It was concluded that the failure mechanism in reinforced sand may be classified in two types: the first is under-reinforced failure which follows the minimum energy option as described by Rowe for plain sand. The sand stretches the reinforcement during dilation and eventually the conventional slip plane develops and yields the reinforcements. The effect of reinforcement may be considered as an enhanced confining stress, $\Delta\sigma_3$, and then the dilatancy characteristic of under reinforced sand becomes similar to that of plain sand and they can be approached using the conventional theories. The second is over-reinforced failure characterized by the

rupture of sand reinforcement bond and the post peak bulging between layers, an option which the conventional dilatancy theories were not made for. An equation was presented for estimating the position of the critical stage which separates between these failures.

Pedley (1990) used a large scale direct shear apparatus able to contain a cubic soil sample of side 1m. the study included the benefit of reinforcement on shear and bending by varying the reinforcement cross section, reinforcement orientation, method of installation and the relative soil-reinforcement stiffness and strength. A well graded uniform quartz sand was used in the tests. The reinforcement was typically mild steel circular bar. A mathematical model for predicting the shear force available from reinforcement in soil was developed. The conclusion was that the reinforcement used in shear is much less efficient than that used in axial tension and the displacements required to mobilize the available reinforcement shear force are much greater than those required for axial force.

Al-Omari et al. (1995) performed a large number of conventional triaxial tests on 100 mm diameter samples of dry sand reinforced using several layers of polymer geogrids. The sand used was sorted out from the Karbala sand deposits located at the western part of Iraq. The material of reinforcement was a polymer geogrid with aperture size of 6 mm by 8 mm. The grid stiffness has been calculated from tests data of load-strain relationships given by the manufacturer based on the strain at 50% maximum load. The study revealed that the density of sand reinforced using plastic grids does not significantly influence the strength as well as the use of multiple layers of medium stiffness reinforcement is generally more efficient than smaller number of high stiffness layers and the limiting stiffness for the reinforcement increases as the spacing between the layers of reinforcement decreases.

Shin and Das (2000) conducted small-scale laboratory model tests on a strip foundation supported by sand reinforced with multiple layers of geogrid. Tests were conducted under surface foundation conditions and on foundations at various depths; the foundation depths were limited to less than the width of the foundation. Based on the results, for a given thickness of the reinforcement zone, the bearing capacity ratio increases when the depth of the foundation is greater than zero.

Al-Sinaidi and Ali (2006) conducted model tests on footing resting on soil with and without multi-layers of geogrid at different depths below the surface. The paper also discusses the mechanisms of this system using a large-scale model footing for case studies in which geogrid-reinforced soil footing were used for a schools project in Saudi Arabia. That site has a very soft silty clay/clayey silt soil, and the large-scale plate loading test was conducted according to the procedure of ASTM D1194. The study presented the successful application in the use of geogrid-reinforcement. The field observations proved that the geogrid-reinforced system creates an enhancement in the very soft/soft soils and minimizes the differential settlement. It is very important to list the conclusions of the study to know the importance of the use of geogrid as it were found in the study. These conclusions are:

1- The graph of load versus settlement of unreinforced ‘natural’ soil indicated failure of the soil at a settlement of 27.75 mm at a stress equal 0.6 kg/cm^2, (Fig. 2-4).

2- Improvement in bearing capacity of reinforced soil over that of unreinforced soil was observed for all five reinforcing layers.

3- The load settlement curves for the reinforced soil test continued to rise beyond the failure point of unreinforced ‘natural’ soil at a settlement of 27.75 mm. This indicated the contribution of reinforcement to resisting bearing pressure.

4- Reinforced soil is better than natural soil by 7 times and better than stone column by 1.75 times.

Zhang et al. (2006) presented a new concept of soil reinforced with three dimensional reinforcing elements. Experimental program included a set of triaxial compression tests to study the effects of various parameters, including reinforcement configuration (horizontal, 3D, single-sided or double-sided reinforcements), reinforcement materials and confining pressures, on the behavior of reinforced sand. A summary of these test parameters as follows:

1-Different configurations of 3D reinforcements are as shown in Fig. 2-5, and triaxial tests included seven cases.

2-Two types of materials for reinforcements: galvanized iron sheet and hard plastic sheet.

3-Four confining pressures (50, 100, 150 and 200 kPa).

Uniform, clean, quartz beach sand from shores of Fujian Province in China was used. The reinforcements used in the tests were galvanized iron sheet with a thickness of 0.12mm and hard plastic sheet with a thickness of 1.0 mm. The experimental results showed that (3D) reinforcement not only gives an apparent cohesion to the soil (sand), but it also increases the angle of internal friction significantly, especially with double-sided (3D) reinforcing elements. Different configurations of (3D) reinforcing elements are discussed and compared. The strength of sand reinforced with (3D) inclusions increases with increasing height of the vertical reinforcements. For samples with the same height of vertical reinforcement, double-sided vertical reinforcements will result in greater increase in strength of reinforced sand than single-sided ones.

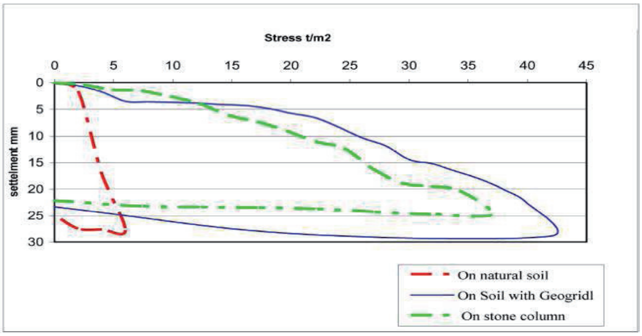

Figure 2-4 Relation between stress and settlement, (after Al-Sinaidi and Ali, 2006)

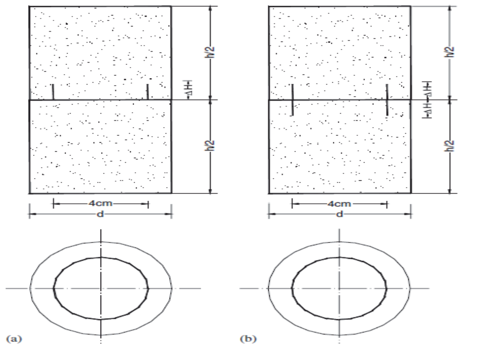

Figure 2-5 Configuration of 3D reinforcing elements: (a) single-sided and (b) double-sided, (after Zhang et al., 2006)

Chen (2007) investigated the potential benefits of using the reinforcement to improve the bearing capacity and reduce the settlement using square and rectangular footings. The results showed that the inclusion of reinforcement can significantly improve the soil bearing capacity and reduce the footing settlement. The geogrids with higher tensile modulus performed better than geogrids with lower tensile modulus. The strain developed along the reinforcement was directly related to the settlement. He claimed that the inclusion of reinforcement can redistribute the applied load to a wider area, thus minimizing stress concentration and achieving a more uniform stress distribution. Two laboratory model tests were conducted to evaluate the strain distribution along the geogrids. One model test was for a square footing with dimensions of 152 mm × 152 mm (B×L), while the other model test was for a rectangular footing with dimensions of 152 mm × 254 mm (B×L). The geogrids with instrumentation were placed at the top and bottom layers (at depths of 51 mm and 203 mm, respectively). The distribution of strains along the centerline of the BX6100 geogrid was measured at different settlement ratios (s/B) of the rectangular footing. Insignificant strain measured in the geogrid beyond its effective length of 4.0~6.0B indicated that the geogrid past this length provided a negligible reinforcement effect. A bearing capacity formula with the contribution of reinforcements to an increase in bearing capacity was then developed for the reinforced soil foundation. However, on scrutiny of the results many shortcomings and unreliable measurement have been diagnosed, some of these non-rational results are:

- The ultimate bearing capacity obtained for sand alone (without reinforcement), using square and rectangular footings is about 3500 and 3400 kPa, respectively as shown in Fig. 2-6. However, for these footing sizes, the rational values may be less than one tenth of that measured.
- The ultimate bearing capacity obtained for reinforced sand using four reinforcement layers and a square footing is 5600 kPa, while for the rectangular footing it is 4600 kPa, as shown in Fig. 2-7. Again, an experienced researcher would realize that such numbers are on the order of ten times the expected values. It is worth to mentioning that such stress values exceed the crushing stress of sand particles and cause a significant reduction in the angle of internal friction and hence the bearing capacity. Al-Omari (1984) used a sophisticated experimental system to squeeze a sand layer between a 0.12 m strip footing and a rigid rough stratum. The sand layer

thicknesses below the footing base and the footing embedment were both half the footing width. However, the measured bearing capacity using different independent load cells was only 320 kN/m^2. At the footing center and the stratum center, the stress approached 540 kN/m^2 and grains crushing was noticed.

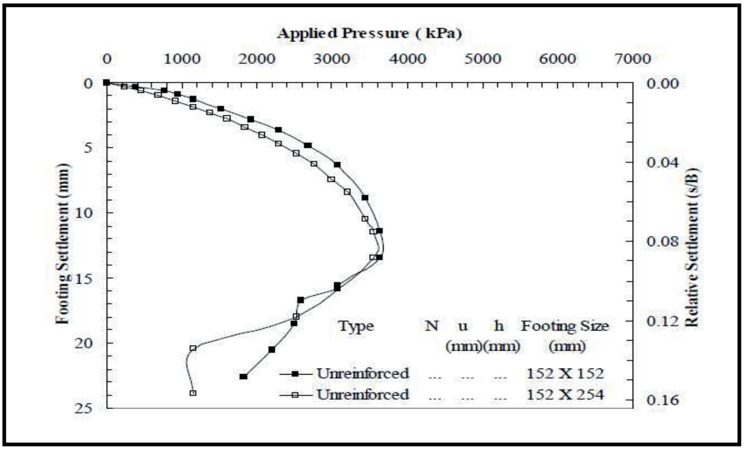

Figure 2-6 Pressure-settlement curves for model footing tests on unreinforced sand with different shape footing. (after Chen, 2007)

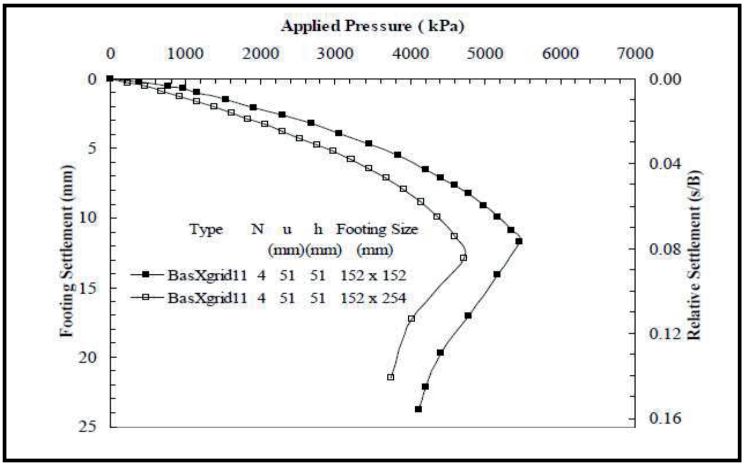

Figure 2-7 Pressure-settlement curves for model footing tests with four layers of BX6100. (after Chen, 2007)

- The maximum values of geogrid strains are unreasonably high. The stress is equal to the modulus of elasticity multiplied by strain, the value of modulus of elasticity for BX6100 geogrid is on the order of 0.19 GPa, while the strain values from Fig 2-9a reach 0.02, then the stress applied is equal to 3800 kPa for only a single rib within the volume of sand. If integrating such rib stresses around the volume of stressed sand, an imaginary value for the footing bearing stress will appear which is even beyond the exaggerated stress given in the stress-settlement relations.
- The appearance of negative strains, as in Figs. 2-8 and 2-9 may be explained as the occurrence of compression in the ribs which is quite questionable, especially when it reaches 0.5%.

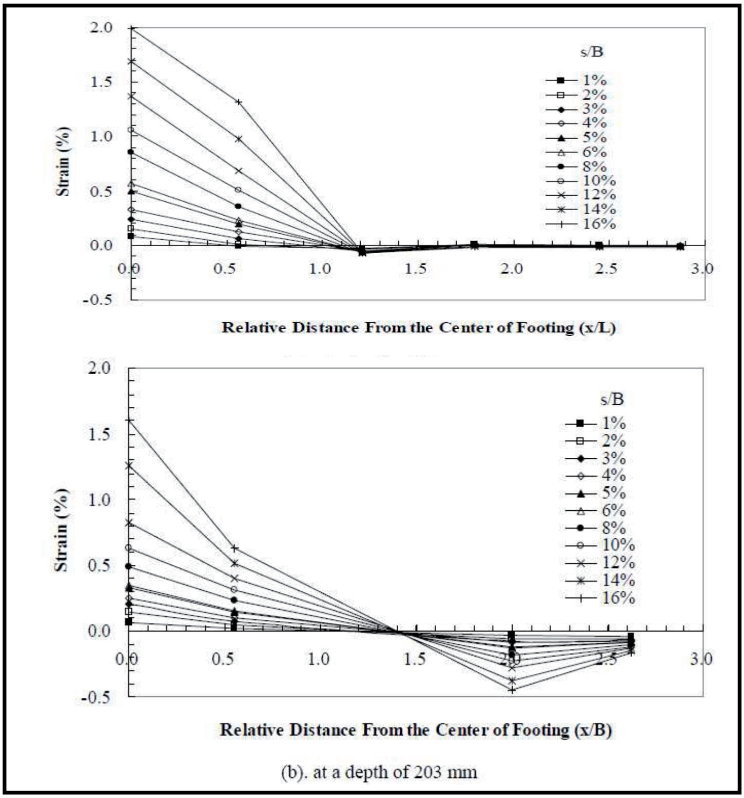

Figure 2-8 Strain distribution along the center line of BX6100 geogrid (B×L: 152 mm×254 mm). (after Chen, 2007)

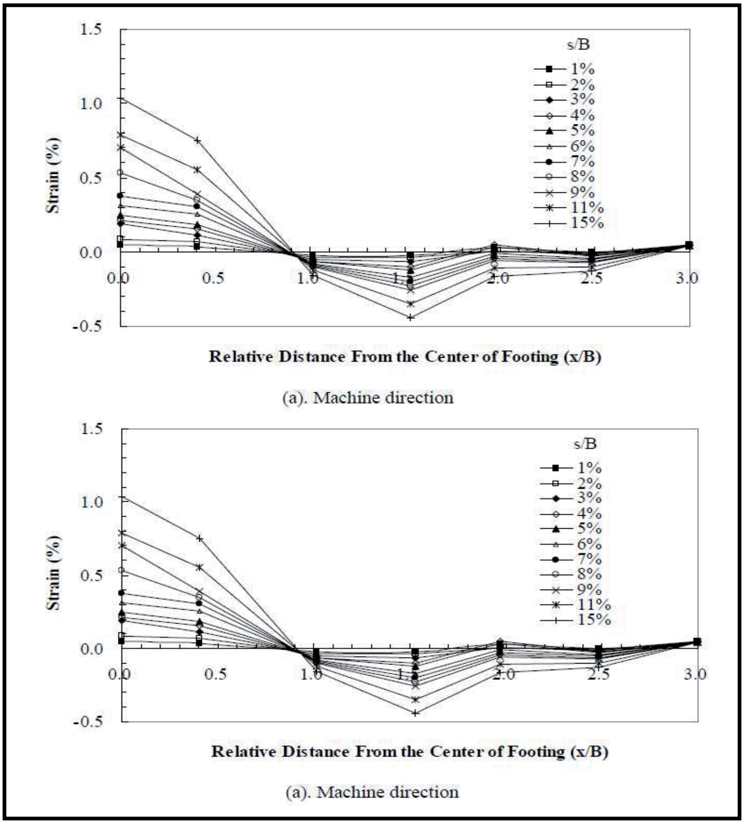

Figure 2-9 Strain distribution along the center line of BX6100 geogrid placed at a depth of 152 mm. (after Chen, 2007)

- The claim that the inclusion of reinforcement can redistribute the applied load to a wider area is not expected since the geogrid philosophy is to restrict the lateral displacement of sand particles. Furthermore, most of the results of pressure distribution given in his thesis do not support his own conclusions, as shown in Fig. 2-10.

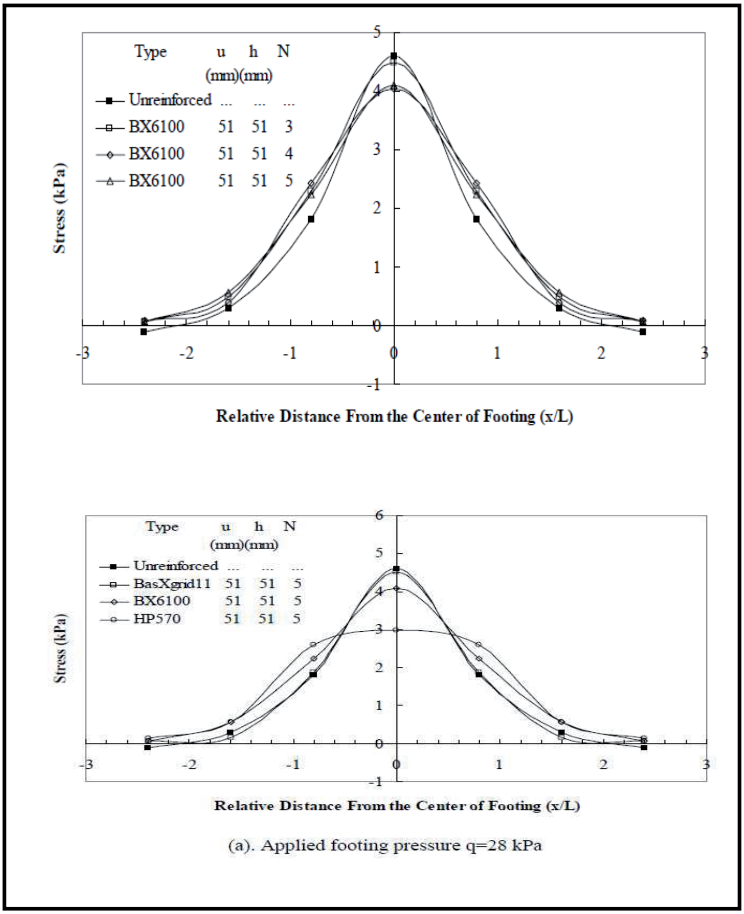

Figure 2-10 Vertical stress distribution along the center line of footing at a depth of 254 mm for five layers of different types of reinforcement (B×L: 152 mm×254mm). (after Chen, 2007)

Shinde and Mandal (2007) presented several experiments to realize the deformation behavior of reinforced soil retaining wall with limited fill zones subjected to vertical surcharge strip loading. Test set-up along with all the instrumentations is developed to perform the experiments. Panel displacements and strain distribution along geogrid layers

are observed using linear variable displacement transducers (LVDTs) and a load cell is also installed to record the amount of loading applied to the rigid plate. The load or displacement path generation and the data acquisition from all measurement devices were recorded via a personal computer and an analogue–digital interface. Effectiveness of the reinforced soil wall was also evaluated using a geogrid material. Finite element analysis using software PLAXIS version 8 was carried out. Panel displacement is found to depend on location of strip load. Displacements and stresses can be reduced greatly by fully utilizing the geogrids in an efficient manner. Strain along geogrids also increases with increase in surcharge pressure. Strain distribution along geogrid layers depend on location of strip load. The finite element results are in good agreement with experimental studies.

Zhou and Wen (2008) placed one or two layers of geosynthetic materials in a sand cushion to create composite layers with improved bearing capacity over a soft-soil foundation. The results of four tests to examine the improvement of the bearing capacity have been reported. The results indicate that with the provision of a geocell-reinforced sand cushion, there is a substantial reduction in settlement of the underlying soft soil. The subgrade reaction coefficient K30 is improved by 3000%, and the deformation is reduced by 44%.

Maubeuge et al. (2008) presented the use of geosynthetics in the construction of roads over soft soils. The effect of the dynamics occurring from the traffic load was discussed. The study concentrated on the design of roads (reinforcement of the base course) with geogrids and introduced criteria for geogrid specifications. Guidelines for geogrid properties discussed and various test trials and field performance data presented. The following conclusions are drawn:

1- Different geogrid types on the market have variably proven their efficiency against solutions without geogrids and demonstrated that geogrids allow a reduction in base course thickness and thus achieving the required stability.
2- Due to different geogrid types manufacturers, designers and/or specifiers have developed various specifications around product types, some not reflecting to the application at all, e. g. junction strength/efficiency requirement.

3- The tensile strength and the modulus need to be compared under realistic site conditions which in the case of a base course reinforcement should be at strains under 2 %.
4- The pullout performance, the resistance to installation damage as well as the aperture stability (torsional stability) reflect more to application related conditions and are therefore more useful to describe the requirements of the geogrid.
5- Finally true test trials under site specific conditions show how geogrids perform and allow a further judgment on the performance of geogrids in base courses

Haripal et al. (2008) presented laboratory model test results for the ultimate bearing capacity of a strip foundation supported by multi-layered geogrid (biaxial-1100)-reinforced sand. The model foundation used for study was 80 mm× 360 mm. It was made of mild steel plate with a thickness of 25 mm. The bottom of the model foundation was made rough by coating it with glue and then rolling it over sand. Bearing capacity tests were conducted in a box of dimension 1.0 m (length) × 0.365 m (width) × 0.6 m (depth). The number of layers of geogrid was varied from 2 to 5. The vertical spacing of the subsequent geogrid layers and the depth of the first geogrid layer were varied. The results of study reveal that:

1- To arrive at the same value of BCR_u, d/B ratio increases as h/B increases keeping u/B constant, which indicates that higher spacing of geogrid has no significant effect on BCR_u.
2- At limited level of settlement (less than ultimate level), the reinforcing effect of geogrid is less as compared to the ultimate level of settlement.
3- The reinforcing effect is more economical, if the first geogrid layer is placed at 0.35B from the base of the footing and the successive layer is placed at 0.25B.
4- The theoretical relationship for ultimate bearing capacity developed by Huang and Menq (1997) provides comparable results with experimental observations.

Phanikumar et al. (2009) presented a series of laboratory plate load tests performed on geogrid reinforced sand beds. Fine, medium and coarse sands were used as test sand beds. Circular geogrids of diameter 120 mm were used as reinforcement layers. The data obtained covered the improvement in load–settlement response as shown in Fig. 2-11. The

test sand beds were compacted to a relative density of 50%. A surface footing plate of diameter 60 mm was used as the shallow foundation. They include that:

1- The geogrid-reinforced sand beds result in improved load–settlement behavior.
2- Increasing number of geogrids (n) improves the behavior further. Compressive load response further is improved with decreasing u and s. of different configurations of geogrid reinforcement, n =3 result in the best load–settlement behavior.
3- LIR increases with D_{10} for all configurations of reinforcement. The increase in LIR with number of geogrids (n) was highest in the case of coarse sand followed by fine sand and medium sand. The interlocking effect was highest in the case of coarse sand as indicated by the variation of compressive load required for a settlement of 0.5 mm with $d_{aperture}/d_{max}$, *where (LIR= Load for a given settlement in geogrid_reinforced case/Load for a given settlement in unreinforced case)*.

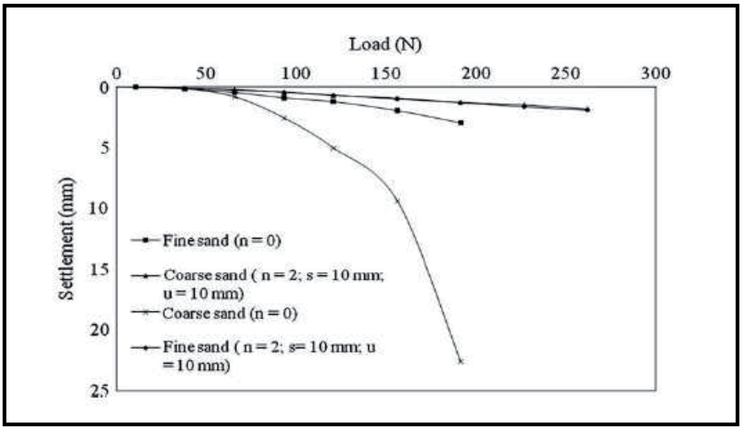

Figure 2-11 Load–settlement curves for unreinforced and geogrid-reinforced fine sand and coarse sand, (after Phanikumar et al., 2009)

Alamshahi and Hataf (2009) performed a series of numerical and model tests to evaluate the bearing capacity of a strip footing resting on georeinforced sand slopes. The study aimed at determining the effect of geogrid reinforcements and its location on the ultimate bearing capacity and settlement characteristics of such footings. Based on this study, the following conclusions are drawn:

1- The provision of a reinforcement layer at an appropriate location in the body of fill slopes has resulted in a significant increase in the bearing capacity of footings.
2- The optimum embedment depth and vertical spacing of the reinforcement layer which resulted in the maximum ultimate bearing capacity of the geogrid-reinforced slope were about 0.75 times the width of the footing. The optimum number of reinforcements is 2.
3- The results clearly show that the effect of the ordinary geogrid on improving the soil bearing capacity is less than that of the grid-anchor. This is because of the presence of anchors in grid anchor reinforcement which provides higher pullout strength. On the other hand, the intrinsic merit of grid-anchor comes about by their anchorage strength or pullout resistance, which can far exceed the direct shear strength.
4- A medium agreement between the experimental and numerical results in general trend of behavior and the critical values of the geogrid parameters an observed. In all cases, the BCR calculated from the FEA for prototype scale appears to be smaller than that obtained from the model slope results. The differences between experimental and numerical results maybe because of the soil parameters and the model (Mohr– Coulomb), used in the numerical analysis. So it is advisable to use a more appropriate model (e.g. a hardening model) in the case.

El Sawwaf (2009) presented an experimental and numerical study of the behavior of an eccentrically loaded strip footing resting on geosynthetic reinforced sand. The experimental model tests were conducted in a test box, having inside dimensions of 1.00 m, 0.50 m in plan and 0.50 m in depth. The tank was made from steel with the front wall made of 20-mm thick glass. A numerical study on a plane strain prototype footing was performed using finite element analysis. Test results indicate that the footing performance could be appreciably improved by the inclusion of layers of geogrid leading to an economic design of the footing. The efficiency of the sand-geogrid system is dependent on the load eccentricity ratio and reinforcement parameters. A close agreement between the experimental and numerical trend lines is observed. Based on the numerical and experimental results, critical values of the geogrid parameters for maximum reinforcing effect are established.

Kumar and Llamparuthi (2009) examined the results of plane strain model tests carried out on strip footings placed on both reinforced and unreinforced sand slopes with a view to study the influence of geogrid reinforcement and slope angle on bearing capacity. The study was carried out for 3 different slope angles and three different edge distances. It was shown that load-settlement behavior and bearing capacity can be improved by inclusion of geosynthetic reinforcement under the footing. The bearing capacity decreases with increase in slope angle and decrease in edge distance both in reinforced and un-reinforced slopes. The effectiveness of geosynthetic reinforcement in improving the bearing capacity is attributed to stiffness, location and length of reinforcement. A numerical study was carried out using Plaxis FEM code and compared with the model test results. The mechanism of footing behavior on sloped ground was brought out and load-settlement response obtained from the FEM is compared reasonably with the model test results.

Latha and Somwanshi (2009) presented the results from laboratory model tests and numerical simulations on square footings resting on reinforced sand beds. The primary objective of the study was to compare the relative performance of different forms of reinforcement (i.e. geocell, planar layers and randomly distributed mesh elements) in improving the bearing capacity and reducing deformations of square footing, using exactly the same quantity of reinforcement. According to the Unified Soil Classification System, the soil is classified as poorly graded sand (SP). The friction angle of the sand at 70% relative density (Dr), as determined from standard Unconsolidated Untrained (UU) triaxial compression tests on dry sand sample, was found to be 44º. The diagram of the test set-up is shown in Fig. 2-12. They concluded that the Geocell reinforcement is the most advantageous form of soil reinforcement technique of those investigated, provided there is no rupture of the material during loading. From the numerical results, they suggested that the geocell layer improve the bearing capacity by transferring the footing load to deeper soil layers and thus reduces the stresses and strains underneath the footing and completely arrests the surface heave adjacent to the footing.

Lovisa et al. (2010) investigated experimentally the degree of improvement generated by prestressing the geosynthetic layer for several embedment depths of a footing resting on a reinforced sand bed. Laboratory physical model tests and finite element analyses were

conducted to study the behavior of prestressed geotextile-reinforced sand bed supporting a loaded circular footing. The addition of prestress to the geotextile reinforcement results in significant improvement to the settlement response and the load-bearing capacity of the foundation. For a surface footing, the load-carrying capacity at 5 mm settlement for the prestressed case (with prestress equal to 2% of the allowable tensile strength of the geotextile) is approximately double that of the geotextile reinforced sand without prestress. The beneficial effects of the prestressed geotextile configuration were evident for greater footing depths, in comparison with unreinforced and reinforced (without prestress) counterparts. Experimental and numerical results were also used to validate a few empirical relationships, which are commonly used for solving soil-structure interaction problems. The results obtained from finite element analysis using the program, PLAXIS are generally in reasonable agreement with experimental results.

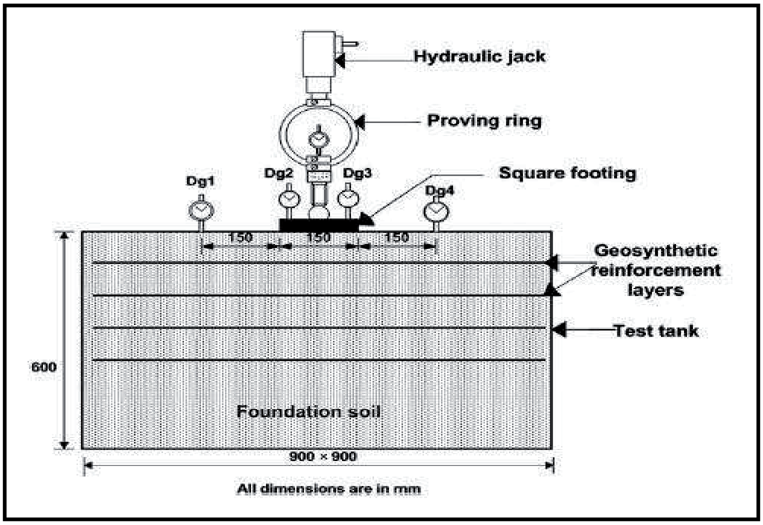

Figure 2-12 Schematic diagram of the test set-up

Mohammed and Ilamparuthi (2010) studied the behavior of strip and square footings on sand bed with and without reinforcement. Ultimate bearing capacity was found to increase, even with single layer reinforcement for both footings. The effectiveness of geosynthetic

reinforcement in improving the bearing capacity was attributed to location and width of the reinforcement in the case of single layer reinforcement whereas in multilayer reinforcement, both spacing and total depth of reinforcement played significant role apart from location and width of reinforcement. The effect of number of reinforcing layers (N), width of reinforcement (b), and depth of first layer of reinforcement (u) and spacing between the reinforcements (h), on the improvement of bearing capacity of footing on reinforced sand bed was investigated. Details of the geometric parameters used in the study are shown in Fig. 2-13.

The important conclusions drawn are:

1- Inclusion of reinforcement in sand beneath the footing enhanced its bearing capacity, which is independent of shape of foundation. The maximum increase in ultimate bearing capacity was found to be 245% and 264% for strip and square footings respectively when sand bed is reinforced with three layers within a depth equal to the width of footing. In this thesis the bearing capacity improvement for the strip footing reaches to 188% for Netlon CE121 and 250% for Tensar SS2 geogrids respectively.
2- Provision of first layer of reinforcement at a depth beyond the width of footing is not effective in improving the bearing capacity.
3- The contribution towards increasing in the bearing capacity of strip footing is found to increase with width ratio of reinforcement and the increase is insignificant if width ratio (b/B) of reinforcement is more than 7.5. Thus the critical width ratio of reinforcement in medium dense sand for strip footing is 7.5. In case of square footing the reinforcement width ratio of 6 is critical value and increase in the width ratio of reinforcement beyond 6 does not contribute to additional increase in the bearing capacity of square footing.
4- The shape factor for square shape model foundation tested on reinforced sand bed were found to vary between 0.74 and 0.88. The shape factor values obtained from the model test are in good agreement with the shape factor value of 0.8 reported for square footing in IS 6403-1981 for unreinforced condition.

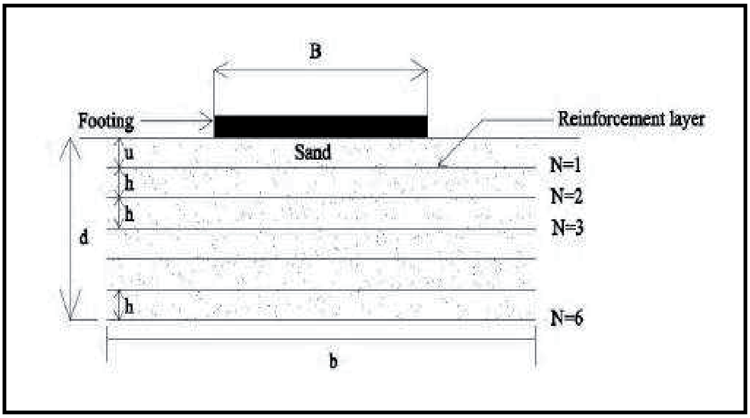

Figure 2-13 Typical diagram defining various geometric parameters

Tafreshi and Dawson (2010) used laboratory model tests to compare the potential benefits of reinforcing foundation sand with geocell and with planar forms of geotextile reinforcement that had the same basic characteristics. Benefits were assessed in terms of increased bearing capacity and decreased settlement of a strip footing subjected to a monotonically increasing load. The geometry of the test configurations for both the geocell is shown in Fig. 2-14. The quantified comparisons were carried out over a range of settlement less than 12% of the footing width. The various parameters studied in this testing program include the reinforcement width, the number of planar layers and the height of the geocell below the footing base. The results reveal that the efficiency of reinforcement is decreased by increasing the number of the planar reinforcement layers, the height of the geocell reinforcement and the reinforcement width. For the same mass of geotextile material used in the tests at the settlement level of 4%, the maximum improvement in bearing capacity (IF) and percentage reduction in footing settlement (PRS) were obtained as 2.73 and 63% with the provision of geocell, respectively, while these values are compared with 1.88 and 47% for the equivalent planar reinforcement. The results indicate that, for the same quantity of geotextile material, the geocell reinforcement system behaves much stiffer and carries greater loading and settles less than does the equivalent planar reinforcement system.

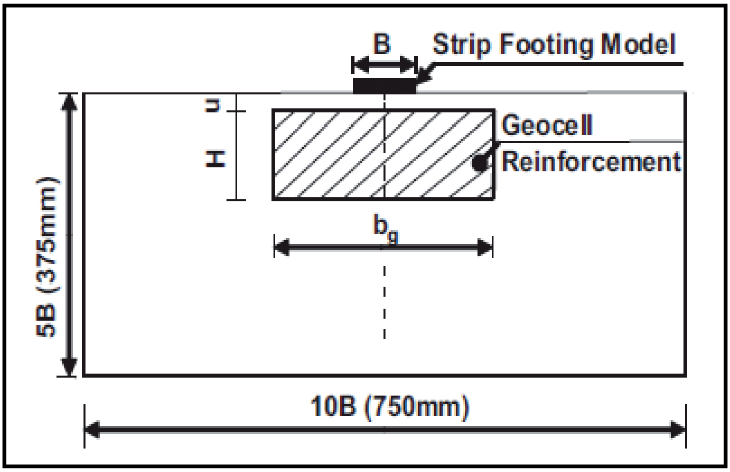

Figure 2-14 Geometry of the geocell reinforced foundation bed

Kongkitkul et al. (2012) performed a series of special tensile loading tests in which both tensile loading history and temperature surrounding test specimens were precisely controlled on Polypropylene (PP), High-Density Polyethylene (HDPE) and Polyester (PET) geogrids. The results from continuous monotonic loading (ML) tests until rupture at different temperatures show that the intrinsic load - strain property of these polymer geogrids is significantly affected by temperature. Both tensile rupture strength and stiffness of these geogrids decrease significantly with an increase in the temperature. Small-strain amplitude unload/reload cycles were applied after a certain period of sustained loading during otherwise ML to determine the elastic stiffness of geogrids. The test results showed that the small-strain stiffness increases with an increase in the tensile load level at a fixed temperature, while it decreases with an increase in the temperature at a fixed load level. These behaviors are modeled by a set of mathematical expressions.

Fakhraldin (2013) studied the potential benefits of using the geogrids to improve the bearing capacity and reduce the settlement of shallow foundations, he measured the

properties of some geogrids and the straining mechanism occurring in the geogrid layers during loading. Three models of footing were used, strip, circular and square. Twelve types of geogrids were used manufactured in various countries. The straining mechanism and elongations occurring in the ribs of geogrids embedded in sand during bearing capacity tests have been investigated. A finite element program Plaxis-3D foundation has been used to analyze the results of reinforced and unreinforced sandy soil using three types of footings and five types of geogrids. The main concluded results are:

1- The geogrids Tensar SS2 and Netlon CE121 have tensile strength and elastic modulus higher than that of other geogrids made by different manufactures.
2- The bearing capacity increases up to about 271, 278 and 336% for strip, circular and square footings respectively, and the settlement decreases about 261, 322 and 380% for strip, circular and square footings respectively.
3- The effect of the horizontal distance from center line of footing and the vertical depth underneath footing base is very significant on the strains and elongations occurring in the geogrid ribs.
4- The strain and elongation of rib decrease along the horizontal direction away from center of footing and also decrease in the downward direction underneath footing base.
5- The strains and elongations occur in geogrid Tensar SS2 using strip footing have vanished in the fifth layer at depth 135 mm which is equivalent to 1B. When using circular footing the strains and elongations in the first layer die out at distance 180mm from footing center in x-direction which is equivalent to 1.44D, while they die out at 154mm from footing center in y-direction which is equivalent to 1.23D because of the anisotropy of Tensar SS2 properties. The strain vanished in the fifth layer in both directions for all gauges. When using square footing the strains in the first layer vanish at distances 140 and 126mm from footing center which are equivalent to 1.4B and 1.26B in x and y directions respectively. The strains vanished in the fourth layer in both directions for all gauges.

2.4 Analysis Methods of Piled-Footing System

Several methods for analyses of piled raft foundation have been developed in the last decades, which all more or less take the pile-raft interaction into account. (Poulos 2001)

has evaluated several of the methods and divided them in three broad categories; simplified calculation methods, approximate computer-based methods and more rigorous computer-based methods.

The simplified calculation methods are empirical methods with numerous simplifications, mostly concerning the soil profile and the load condition, e.g. Poulos-Davids-Randolph method. The approximate computer-based methods include various strips on spring and raft on spring methods, where the raft is modeled as a strip respective a plate, and the soil and the piles are modeled with springs with varying stiffness, e.g. using the Winkler hypothesis. The more rigorous computer-based methods consist of different numerical methods.

Ryltenius (2011) focused on the more rigorous computer-based methods, and four different models are examined; a full 3D FEM model and three plane strain models, all by using programs developed by Plaxis, i.e. Plaxis 3D Foundation and Plaxis 2D, respectively. The first plane strain method is described. The two other plane strain models are analogous to this first plane strain model but they model the interaction between the piles and the soil in a different manner. These two alternative methods are described by and called AM1 and AM2.

2.5 Plane Strain FEM-Model for Piled Rafts

The main problem when modeling a piled raft with a plane strain model is the transition from three to two dimensions, i.e. to express a three dimensional problem in a two dimensional model. To do this the “out off”-plane rows of piles are simplified as wall elements, called plane strain piles (illustrated in Fig. 2-15), Ryltenius (2011).

The wall element is defined per meter; the normal stiffness, bending stiffness and weight for the piles in the “out off”-plane row of piles are therefore “smeared” per meter

$$EA_{psp} = EA_p \frac{n_{\text{P-row-i}}}{L_P} \qquad \text{...2-1}$$

where

EA_{psp} = *Normal stiffness for plain strain pile*

EA_p = *Normal stiffness for one pile*

$n_{\text{P-row-i}}$ = *Number of piles in row i*

L_P = *Raft length in plane*

Analogously, the bending stiffness is inputted as

$$EI_{psp} = EI_p \frac{n_{\text{P-row-i}}}{L_P} \qquad \text{...2-2}$$

and the weight

$$w_{psp} = w_p \frac{n_{\text{P-row-i}}}{L_P} \qquad \text{...2-3}$$

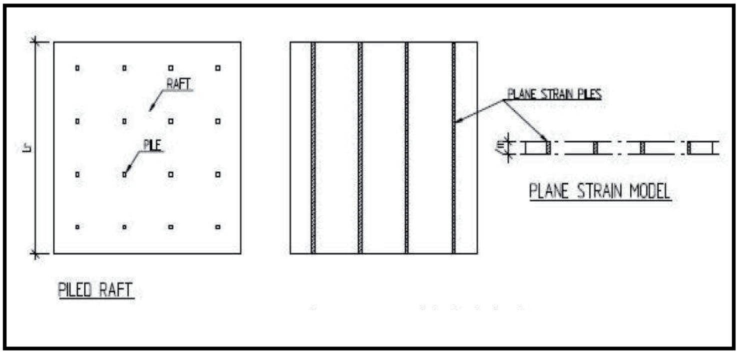

Figure 2-15 Plane strain model of piled rafts, (after Ryltenius, 2011)

The change in cross section when introducing the plane strain piles involves a change in periphery area, which will affect the important shaft resistance and an equivalent shaft resistance is therefore introduced. Since a plane strain pile has a periphery defined by its two sides, the shaft resistance is modified to (Prakoso and Kulhawy, 2001);

$$f_{shaft,eq} = \frac{n_{\text{P-row-i}} A_s f_{shaft}}{2L_P} = \alpha_{ar} f_{shaft} \qquad \text{...2-4}$$

where

A_s = *Shaft area per unit depth*

α_{ar} = *Area ratio*

2.6 Previous Works in Piled-Footing Field

Hooper (1973) examined the behavior of piled raft foundation supporting a tower block in central London as shown in Fig. 2-16. The study was made on the building constructed on piled raft foundation of area 618 m^2 with 51 bored concrete piles of length 25 m and diameter 0.91 m. During several years, the field measurements were taken. The analysis was carried out assuming uniformly distributed load on the raft. The instruments used for measurement of pile load, contact pressure and settlement were pile load cell, earth pressure cell and level. The average settlement of the building measured was 18 mm. Based on the field measurements the estimated proportions of load taken by piles and the raft at the end of construction were 60 % and 40 %. It was found that the long term effect of consolidation is to increase the load carried by piles and to decrease raft contact pressure.

Hain and Lee (1978) developed an analysis to predict the behavior of a raft-pile foundation system. The analysis considers the system as flexible elastic plate supported on a group of compressible friction piles, and the supporting soil is represented as an elastic homogeneous or nonhomogeneous material. In the analysis, they suggested that the behavior of the piled raft would depend on the relative flexibility of the raft and the relative stiffness of the pile to the soil. Four different interactions between the piles, raft and soil were introduced and thoroughly considered in the analysis. In addition, a 'load cut-off' procedure was introduced to account for the development of the ultimate load capacities of the piles.

Kuwabara (1989) described a boundary element analysis based on elastic theory to examine the behavior of a piled raft foundation in a homogeneous elastic soil mass. In the analysis, the raft was assumed to be rigid but compressibility of piles was considered. The raft was discretized into a series of rectangular elements and the pile was discretized into a series of shaft and base elements.

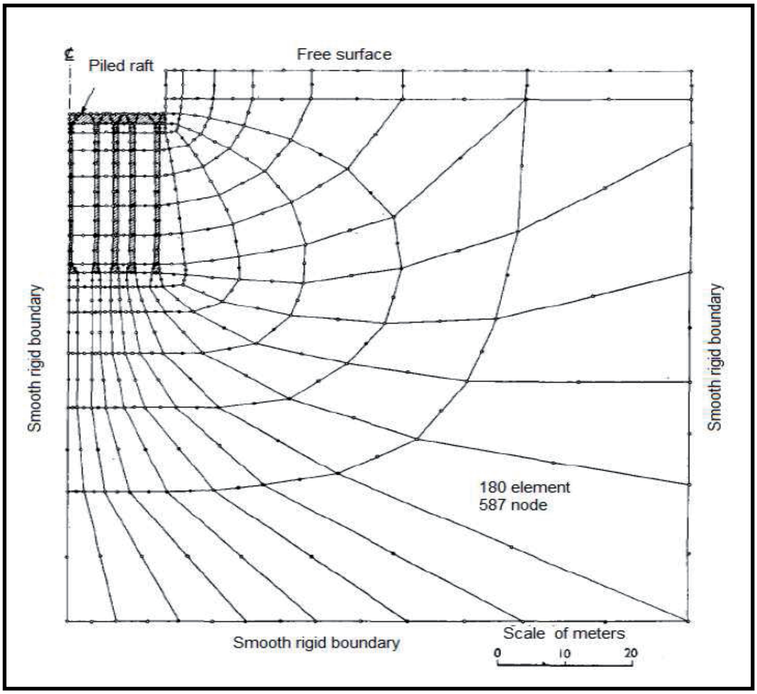

Figure 2-16 Axisymmetric finite element model of piled raft foundation, (after Hooper, 1973)

Liu and Novak (1991) employed the finite element method to examine the behavior of a raft supported by a single pile at the center. In the analysis, the cap was assumed to be circular and to contact the soil perfectly. Nine node isoparametric elements were used to model the cap; the pile and the near field soil medium were modeled by finite elements whereas the far-field soil medium is modeled by mapped infinite elements. The pile was assumed to be linearly elastic and the soil was assumed to be either elastic or elastic perfectly plastic. A weak zone is introduced around the pile to approximately account for slip between the soil and the pile. Numerical results show that this approach is quite efficient and versatile for various soil–structure interaction problems.

Yamashita et al. (1994) analyzed a five story building on piled raft foundation of size 24m × 23m with 20 piles of length 16 m and diameter 0.75 m. The results of field observations during construction and analytical study of the same building have been compared. At the time of completion of the building, the settlement measured was 10 to 20 mm and the load shared by piles was 49 %. Analytical simulation of the settlement behavior of the building is presented taking into account the interaction between piles, soil and raft, which are compared favorably with the field observation.

Gandhi and Maharaj (1996) analyzed a piled raft foundation under uniformly distributed loads using finite element method. The soil is considered to be linearly elastic, isotropic and homogeneous. The raft, pile and soil have been idealized by eight node brick elements. Parametric studies have been carried out by varying the pile length, soil modulus, raft thickness and pile spacing. Design charts have been produced to achieve 50 % load sharing between pile and raft for optimum design.

Maharaj, (1996) carried out linear and nonlinear three dimensional finite element analysis of piled raft foundation using ANSYS Finite Element Software. The infinite pile forest models, strip of piled raft foundation and piled raft foundation with group of piles were the three analyzed models. Both linear and nonlinear analyses have been done for first and the third model while linear elastic analysis has been done for the second model. The material non-linearity of soil has been modeled using Drucker-Prager yield criteria. The raft, pile and soil have been discretized as eight node brick finite elements. Design charts have been produced for load sharing between pile and raft from the infinite pile forest model. The application of design charts for field problems has also been discussed. Load-settlement curves have been produced based on a three-dimensional nonlinear finite element analysis for a single pile, pile group, raft and piled raft foundation. Also, the axial load distributions in piles, contact stress distribution below raft and development of contact stress with settlement have been reported.

Poulos (2001) studied the settlement of Messeturm tower; the building has a basement with two underground floors, 58.8 m square in plan, and a 60-storey core shaft (41 m× 41 m in plan) up to height of 210 m. The estimated total load of the building is 1880 MN. At the site of the Messeturm building there are gravels and sands with a thickness of 8 m, followed by Frankfurt Clay to a depth of more than 100 m below the ground surface. In

order to reduce settlements and tilt, the foundation system comprised a base slab or raft supported and stabilized against tilt by 64 large diameter bored piles. The raft is founded at a depth of 14 m below the ground surface on the Frankfurt Clay, and is 9 m below the groundwater table. The thickness of the raft decreases from 6.0 m at the center to 3.0 m at the edges. The bored piles have a diameter of 1.3 m and are arranged in three concentric circles below the raft. The distance between piles varies from 3.5 to 6 pile diameters. The pile length varies from 26.9 m for the 28 piles in the outer circle to 30.9 m for the 20 piles in the middle circle, and to 34.9 m for the 16 piles in the inner circle. Calculated range of settlement is 150-200 mm using different methods presented and good agreement with measured settlement is obtained.

Small and Zhang (2002) presented a new method of analysis of piled raft foundations in contact with the soil surface. The soil was divided into multiple horizontal layers depending on the accuracy of solution required and each layer may have different material properties. The raft was modeled as a thin plate and the piles as elastic beams. Finite layer theory was employed to analyze the layered soil while finite element theory was used to analyze the raft and piles. Comparisons of forces in piles, moments in the raft and piles and displacement in a 9-pile raft subjected to either vertical loading or horizontal loading show that the present solutions agree closely with those provided by the finite element method. The conclusions demonstrated that the method was capable of producing results for pile groups with general type loadings and can be used to analyze a raft either clear of the ground surface or in contact with the ground. It can also be used for problems where the soil modulus varies with depth or from layer to layer. Furthermore, the method has the advantage that the data are easy to prepare and does not involve creating large meshes as would be required for finite element solutions.

Liang et al., (2003) extended the concept of piled raft to a new type of foundation named composite piled raft. In the system of composite piled raft, the short piles made of flexible materials are used to strengthen the shallow soft soil, while the long piles made of relatively rigid materials are used to reduce the settlements and the cushion beneath the raft was used to redistribute and adjust the stress ratio of piles to subsoil. Finite element method (via ANSYS program) was applied to study the behavior of this new type of

foundation subjected to vertical load. The validity of the numerical results was examined through a seven-story building observed in situ.

Yu Bao (2003) presented a three-dimensional nonlinear analysis of vertically loaded piled raft. Because of the property of the infinite boundary of foundation soil, FEM is subject to great limitation to simulate the semi-infinite medium. Therefore, in the analysis of pile-soil interaction problems, it was necessary to adopted the infinite element to simulate displacement boundary conditions of the limitless boundary of the foundation soil. Besides, the mechanic property of the interface between pile and soil is special, which not only can transfer a certain amount of shear force, but also can slide. Therefore, it is important to employ the interface element to simulate the frictional behavior between pile and soil in the numerical analysis. Hence, if the finite element, the infinite element and the interface element are coupled, the numerical model can well simulate the geometrical and the mechanical behavior of the pile-soil interaction. Figure. 2-17 shows the FEM of piled raft system according to the study. Figures 2-18 and 2-19 show the results obtained from the study. The main conclusions are that the interface between piles and soil can not only transfer shear stress and normal stress, but also it can slide and detach. Therefore, interface element should be adopted to simulate the linkage between pile and soil as well as that the finite element, infinite element and interface element are coupled, the numerical model can well simulate the complicated pile-soil system.

Nakai et al. (2004) investigated the effect of the connection condition between piles and a raft on the dynamic characteristics of a structure supported by a piled raft foundation. In this regard, a series of dynamic centrifuge model tests have been conducted, followed by a parameter survey based on the finite element analysis. It was found that, although the effect of the pile head connection condition on the response characteristics of a superstructure is fairly small when compared to the type of the foundation, it does affect the load bearing characteristics of piles even when piles are not connected to the raft foundation.

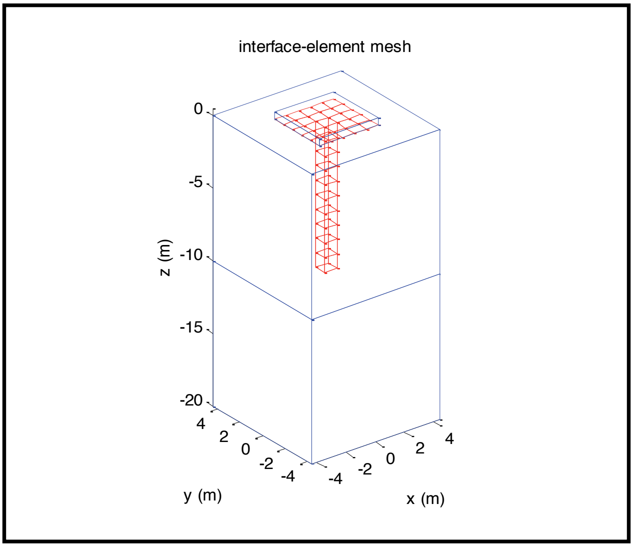

Figure 2-17 Finite element model FEM of piled raft system, ,(after Yu Bao, 2003)

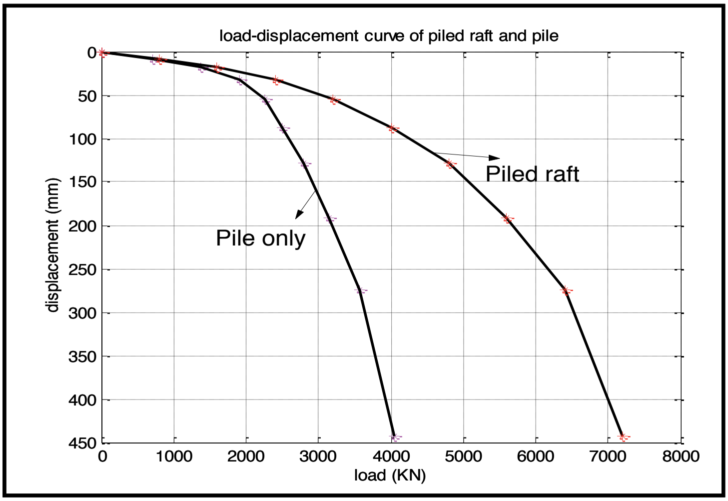

Figure 2-18 Load-settlement curve of piled raft and pile,(after Yu Bao, 2003)

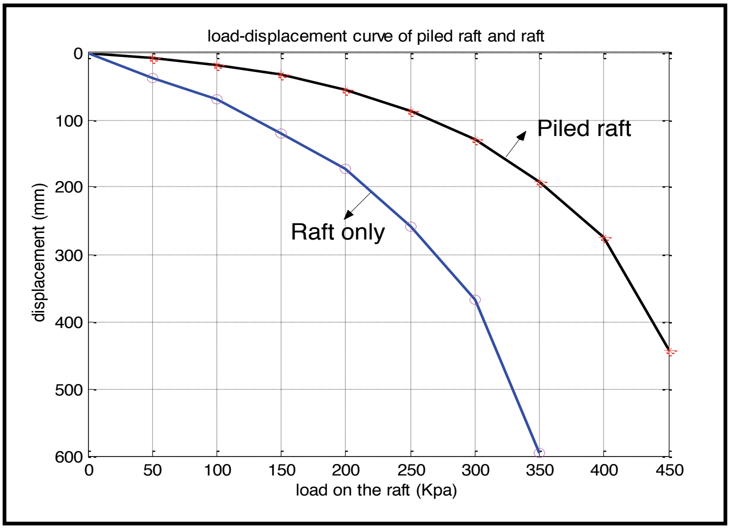

Figure 2-19 Load-settlement curve of piled raft and raft, (after Yu Bao, 2003)

Al-Ani (2008) made an analysis of the combined piled raft foundation (CPRF). It is assumed that the soil under the raft will sustain some of the load, hence establishing the CPRF concept. The case study was modeled by STAAD PRO computer package. Two types of spring (pile and soil) at their nodes were used to represent the raft into finite plate element. The bilinear model was assumed for the original design as a piled foundation and tri- linear model for the proposed CPRF. It was concluded that in the CPRF analysis, the system is considered "safe" from the point of view of traditional factor of safety (FS > 1.5) while it is considered "unsafe" from the reliability based design approach. It was also noted that piles sustained most of the applied load on the CPRF but in different proportion depending on the change in the input parameters.

Sinha (2013) developed analytical models capable of predicting the settlement of each individual pile in the group under the raft. Accordingly, the differential settlement within the pile raft can be estimated. Three independent models were developed to perform; first,

the load sharing model that estimates the load components of the raft and the pile group in the system, the second model was to estimate the maximum settlement of the top of the raft and the third model was to estimate the differential settlement among the pile-raft-foundation. Parametric studies were performed to observe the influence of raft and pile geometry (e.g length, size, spacing of pile and thickness of raft) on the foundation bearing behavior. The raft bearing contribution and its top deflection pattern under various loading and pile-raft configuration were also investigated. The multiple regression analysis technique, using statistical software MINITAB, along with the theory of solid mechanics was used to develop the analytical models for load sharing, maximum and differential settlement. On the basis of parametric study, the results concluded show that, pile raft increases the load resistance about 40% even that of individual pile group or mat foundation, Pile spacing or more than 7D is ineffective in increasing load resistance, and at smaller pile spacing, piles take the greater portion of the load and at larger pile spacing; the major load portion is carried by the raft.

2.7 Summary of Past Research

This chapter reviewed the available literature on the use of geogrids in reinforced soil and the use of piled-footing system. Previous studies investigated the improvement in bearing capacity and settlement of soil using geogrids. The main factors affect the improvement in bearing capacity were the number of geogrid layers, the depth of first layer of geogrid under footing and the type of geogrid. Other studies studied the mechanisms by which a geogrid acts to reinforce a granular layer over soft soil with reference to trafficking of unpaved roads. Also the benefit of reinforcement on shear and bending by varying the reinforcement cross section, reinforcement orientation, method of installation and the relative soil-reinforcement stiffness and strength is studied by many researchers. Other researchers presented several experiments to realize the deformation behavior of reinforced soil retaining wall with limited fill zones subjected to vertical surcharge strip loading.

Results of previous studies on soil reinforced with geogrids showed that the reinforced to unreinforced bearing capacity ratio (BCR) may exceed 2.4 for strip and rectangular footings when soil is reinforced with three to five layers within a depth equal to

the width of footing. The strain distribution along geogrid layers depend on location of load and geogrid layers.

The previous studies on piled-footing system carried out linear and nonlinear three dimensional finite element analysis of piled-raft system using a boundary element analysis based on elastic theory to examine the behavior of a piled raft foundation in a homogeneous elastic soil mass. Other studies conducted field measurements of settlement of piled-raft system. The concept of piled raft as a new type of foundation named composite piled raft is extended by other researchers. In the system of composite piled raft, the short piles made of flexible materials are used to strengthen the shallow soft soil, while the long piles made of relatively rigid materials are used to reduce the settlements and the cushion beneath the raft was used to redistribute and adjust the stress ratio of piles to subsoil. The sharing between piles and footing is studied also.

Main conclusions of previous studies in piled-footing system show that the interface between piles and soil can not only transfer shear stress and normal stress, but also it can slide and detach. Therefore, interface element should be adopted to simulate the linkage between pile and soil. The estimated proportions of load taken by piles and the raft at the end of construction were 60 % and 40 % respectively and the long term effect of consolidation is to increase the load carried by piles and to decrease raft contact pressure.

In this thesis, the comparison between the improvement in the ultimate capacity of soil using geogrid and piles is presented experimentally and theoretically. The economic study is carried out also to study the ability of using the geogrid in the construction of interchange bridges resting on sandy soil which is a topic not covered in previous studies.

CHAPTER THREE

EXPERIMENTAL WORK AND MATERIALS

3.1 Introduction

The experimental work in this research demands many requirements should be used to achieve the goals. Most of the experimental work was carried out in the played postgraduate studies laboratory in Kufa University at the College of Engineering. The loading system has a very important role in this work. Chemical and physical properties and the strength characteristics of the used soil even determined by conducting the appropriate tests. To satisfy one of main goal of this research, the soil used was taken from one of the sites of interchange bridges in Al-Najaf city called as Northern Garage. The region of this interchange bridge on Al-Najaf city map is shown in Fig. A-1 in appendix A. The experimental work consists of model box, models of footings and piles, density controlled system, computer controlled electronic universal testing machine, strain gauges amplifier and datatronic 128-channel automatic data acquisition system.

3.2 Test Apparatus

3.2.1 Sand Container

The sand container was manufactured by Fakhraldin (2013) to contain the soil using inside dimensions of 1 m long, 0.5 m width and 0.6 m depth. The box consists of three steel side frames and the fourth one is of glass, a steel base frame which are connected to each other by bolting and welding to form the box frames of the model as shown in Fig. 3-1. The long side frames and the base are enclosed by steel channel sections of 3 inches width. One of the side frames (1×0.6 m) is made of 3mm thick steel plates and stiffened horizontally using two 2.5 inches channel sections of 6 mm in thickness. The base is made of steel plate of 3 mm thick and stiffened using a grid of solid steel, square 0.5×0.5

inch elements, the distance between each two elements is 100 mm c/c. The two side frames (0.5×0.6 m) are made of 3 mm thick steel plates and the bottom supplied by 3 inches channel sections, 6 mm in thickness. The other (1×0.6 m) side is formed from hardened glass plate of 10 mm thickness. The glass plates supported vertically from outside using two 2.5 inches channel sections. Hard plastic strips were placed between the glass plate and the channels to prevent the lateral deflection in the glass during the test.

Figure 3-1 Sand container used in the experimental study (100 cm length × 50 cm width × 60 cm depth)

3.2.2 Footing and Piles Models

To achieve the goals of the research, two types of footing and two types of pile models were as follows:

1- **Strip footing:** This model of footing was manufactured to represent the pile cap of the bridge foundation which was enclose the piles under the columns load. The model was made of steel plates welded to transform the load using two v-shaped grooves to house the knife – edge loading blades. To achieve a plane strain

condition the dimensions of footing are chosen to have 0.49 m length, 0.135 m width, and 0.2 m height. The footing base is made of a 10 mm thick rigid steel plate as shown in Fig. 3-2.

2- **Rectangular footing:** The footing base is made of 10 mm thick steel plate with 0.23 m in length and 0.06 m in width. One v-shaped groove is made to transform the load using the blades as shown in Fig. 3-2.

3- **Plane strain piles model:** To achieve the plane strain conditions of piles footing, the steel frame with the dimensions of 0.48 m length, 0.4 m depth, and 0.03 m thickness is enfolded by 1 mm aluminum plate. Abrasive papers were glued to give the required roughness to simulate the piles in site, see (Fig. 3-3).

4- **Rectangular piles model:** They are three closed end square section piles represented by square section steel pipes of 2 mm thickness, 3 cm width, and 40 cm length (Fig. 3-3).

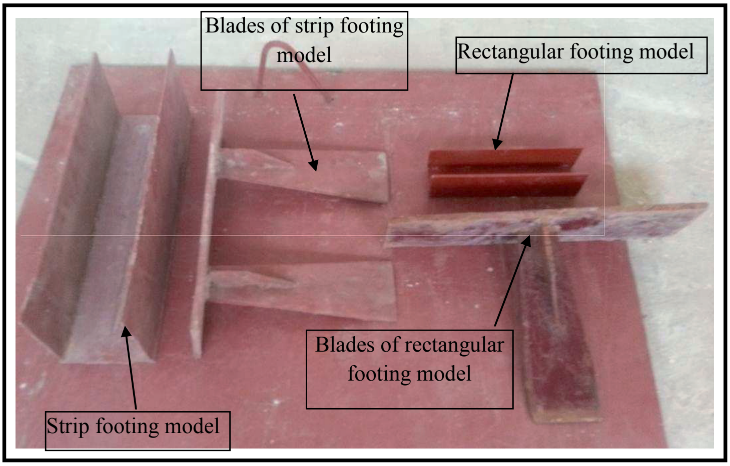

Figure 3-2 Strip footing (49 cm length × 13.5 cm width), rectangular footing (23 cm length × 6 cm width), and loading blades

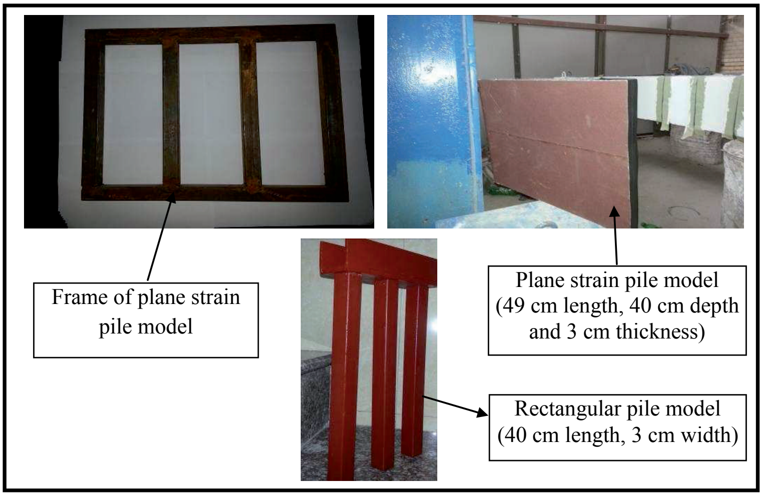

Figure 3-3 Models of piles

3.2.3 Loading Frame

Figure 3-4 shows the loading frame which is used to perform the laboratory tests. The frame is available in the Laboratory of Higher Studies in the College of Engineering / Kufa University. The testing assembly involves many accessories with the frame. Figure 3-4 shows this system and the accessories. The capacity of frame is 2000 kN, the rate of applying load varies from 0 to 100 mm/hr. A hydraulic jack is driven up using a powerful electrical motor. The box can be lifted and positioned within the frame using a hydraulic mechanical crane. The load is applied to the footing using steel blades depending on the type of footing, one blade for rectangular footing and two blades for strip footing. The length of blades is 27.6 cm. This type of blades were used in a similar model (Al-Omari, 1984). When the jack is switched on, the box rises up against the blades. The applied load is recorded and the two 50 mm capacity dial gauges begin to present the vertical displacement. The applied load for each 1 mm displacement was recorded. The load cell was calibrated by the Central Organization for Standardization and Quality Control.

Figure 3-4 The loading frame

3.2.4 Density Control System

To achieve the required relative density of 70% or more, a density control system was used. The system which was prepared by Fakhraldin (2013) consists of a steel mesh with openings of size 4 mm to achieve a uniform fall of soil when the gate of 700 × 700 mm wooden hopper is opened. The hopper moves horizontally on a steel frame which consists of two inverted channel sections (1.5 inches) welded together using two solid circular sections 0.5 inch as shown in Fig. 3-5.

3.3 Electronic Universal Testing Machine

The machine is designed for tension, bend, compression and mechanical property test of metal and nonmetal. It is suitable for use in science and research institutes, colleges and universities, quality inspection center, and commodity inspection (Fig. 3-6).

Figure 3-5 The density control system, (after Fakhraldin, 2013)

The machine performs three functions: applying load, measuring load, as well as recording and processing. The load frame and attachments of construct frame is apply load. The AC servo motor and AC servo system and deceleration system under working bench of load frame construct driving system. Shijin controller and PC and printer construct control and data processing and printing system.

The load frame consists of two pilot columns, upper crosshead, lower crosshead and working table. Governing speed system is installed under working bench. AC servo motor via syngear belt deceleration system drives ball lead-screw couple to rotate. Ball lead screw drives medium crosshead to make tension attachment move up and down so as to realize loading and unloading of specimen. The construction ensures that load frame has enough rigidity, mean whilst, realize high efficient, smooth, steady transmission. Mechanism for eliminating clearance between lead screw and nut raises transmission accuracy of whole machine.

Figure 3-6 Electronic Universal Testing Machine

The load test realizes closed-loop control, crosshead displacement and specimen deformation. The machine has testing progress control mode intelligent setting specialist system. User may set controls mode in each stage of testing progress and test processing according to user self-requirement. PC control system, that's, auto setting corresponding controls calculation method. Progress of testing can automatically be controlled according to the mode set by user.

The testing of load realizes screen display, crosshead displacement, deformation of specimen, and test curve, meanwhile the computer saves and file operational function of test conditions and test results. A controls test processing, alteration of traveling speed of cross heed, and input of parameters. Operations can be performed by mouse, being easy to use.

The data processing conforms to GB228-87 Test Method for Metal Tension and GB/T7314-1987 Metal compression test method in addition to many kinds of standards like GB, ISO, ASTM, DIN etc. Handled results and test curves can not only be printed, but also can be stored on software and operated in network in form of ASCII so as to be easy for later processing of test results. Full process recording curve and reappearance of test data make user handle test data freely by person – machine dialogue mode (for example,

inputting arbitrary value of arbitrary one of testing load, stress deformation, strain, and non-rate tensile length in arbitrary points all may obtain results of other items). It has program-controlled amplifier which makes testing machine realize auto zero adjustment auto-calibration, auto-switching, and the identification of zero point and indicating value among every class, being easy to use, and improving the reliability of machine.

3.4 Soil Properties

The soil used in the research was taken from the site of a highway interchange bridge at intersection of northern garage in Al-Najaf City. This type of soil is the most common soil in Najaf according to many site investigation reports.

About 3 m^3 of the soil was air dried. Sieve analysis was carried out and the grain size distribution according to ASTM (D422-2007) is shown in Fig. 3-7. The soil is classified as ***SP*** type (***Poorly graded sand***) according to the Unified Soil Classification. ASTM (D4253-2007) and ASTM (D4254-2007) are used to determine the maximum and minimum dry unit weight. The chemical properties were performed according to British Standard (BS 812: Part: 1988) and ICS: 91.100.15 71.080.01 19.020 (manual 895/2003). Table 3-1 shows the chemical and physical properties of the soil.

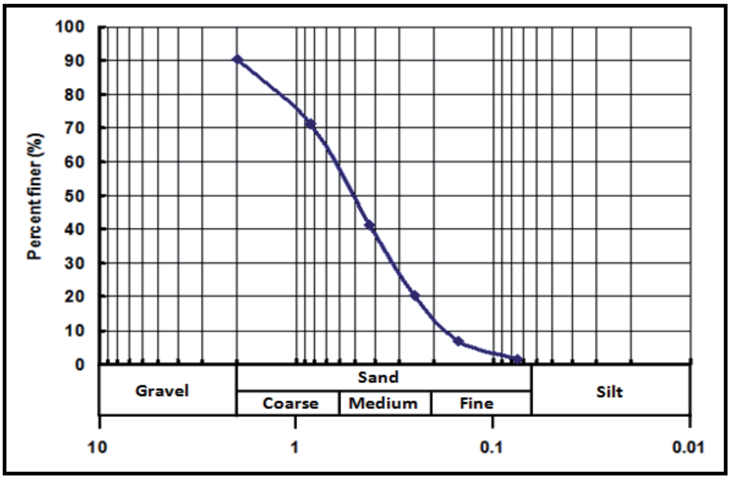

Figure 3-7 Grain size distribution of soil

Table 3-1 The physical and chemical properties of the sand

The Chemical Properties	
SO_3	**0.53%**
T.S.S	**0.73%**
Gypsum content	**1.15%**
The physical properties	
G_s	**2.62**
γ_{dmin} **e_{max}**	**13.8 kN/m^3** **0.863**
γ_{dmax} **e_{min}**	**18.2 kN/m^3** **0.41**
γ_{dused}	**16.7 kN/m^3**
e_{used}	**0.539**
n_{used}	**0.35**
$Ø_{used}$	**40^o**
$R_{D\ used}$	**71.8%**
O.M.C	**9.8%**
D_{60} **D_{50}** **D_{30}** **D_{10}**	**0.65 mm** **0.52 mm** **0.33 mm** **0.18 mm**
C_u	**3.6**
C_c	**0.93**
Natural m_c	**5.3%**

3.5 Soil Preparation

In sand, the relative density is the main parameter to achieve reliable results throughout the tests, the soil sample should simulate the soil in the site. The relative density is a good parameter gives that. Many researchers have used this technique *(Al-Jebouri (1986), Salih (1989), Sulaiman (1991), Jawad (2009), and others).* The dry density, void ratio and relative density vary with the height of drop. Six cylindrical density pot were placed under the hopper to collect the sand. The inside dimensions of the pots are 80 mm in height and 80 mm in diameter, the arrangement of pots inside the box is shown in Fig. 3-1. A pot diameter larger than 3 inches was chosen to satisfy the requirements specified by *Kolbuszewski (1948)* for free fall method. The weight of every empty pot was measured using a sensitive balance and the volume of pots was accurately determined by measuring the weight required to fill each pot. After the deposition of sand, the pots were carefully collected and the excess sand leveled off using a straight-edge tool. The pots were then individually weighed. With the known value of the specific gravity, the porosity can be calculated. The calibration was performed twice for the second and third layer of sand deposit before starting the test. A height of drop of 800 mm was chosen which gave a placing density of 16.7 kN/m^3, which corresponds to a void ratio, porosity and relative density of e = 0.539, n = 0.35 and R_D=71.8 % respectively, Fig. 3-8.

3.6 Triaxial Testing of In-situ Soil

Triaxial Test is the most widely used shear strength test and is suitable for all types of soil. The test has the advantages that drainage conditions can be controlled, enabling saturated soils of low permeability to be consolidated, if required, as part of the test procedure, and pore water pressure measurements can be made. A cylindrical specimen, generally having a length/diameter ratio of 2, is used in the test and is stressed under conditions of axial symmetry in the manner shown in Fig 3.9, ***(Craig, 2004)***.

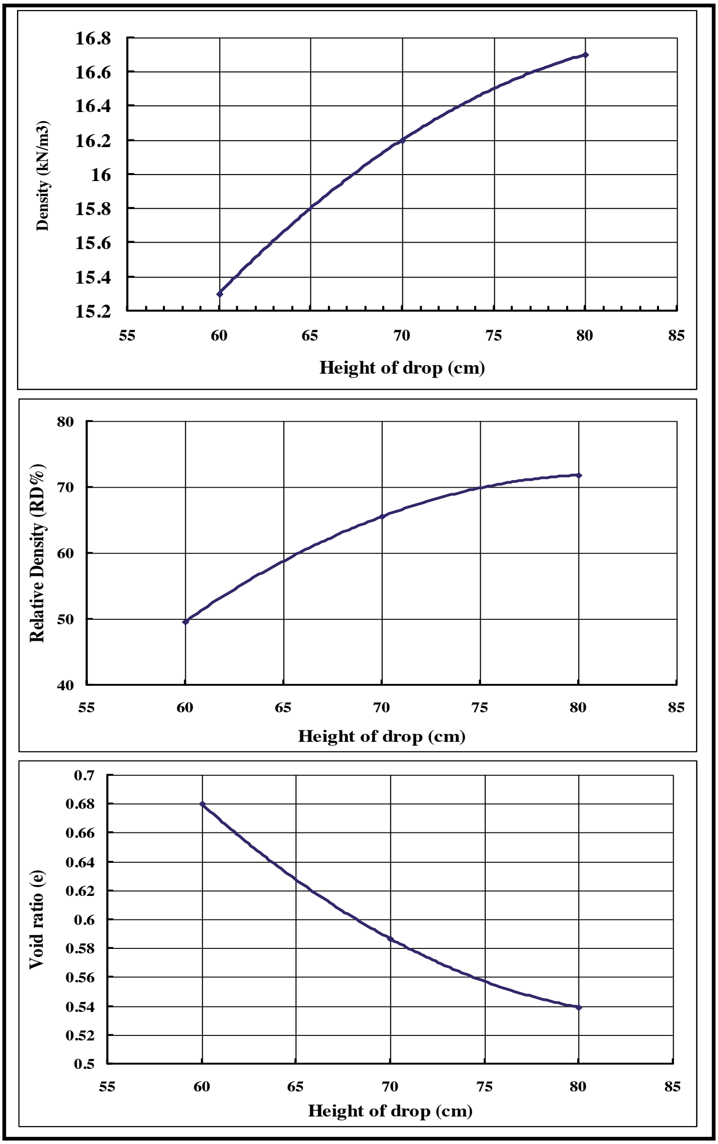

Figure 3-8 Density calibration curves

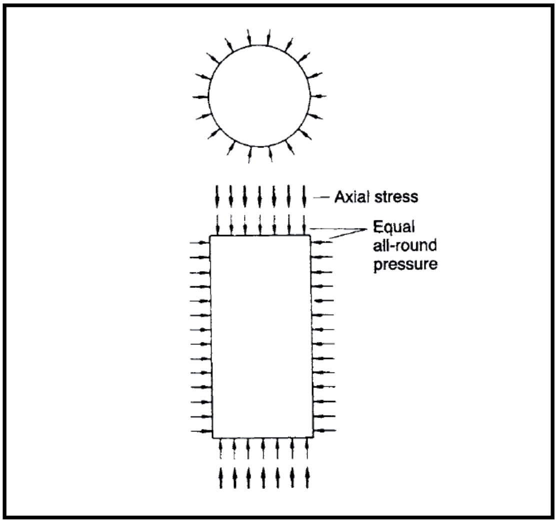

Figure 3-9 Stress system in Triaxial test

Triaxial tests were conducted to determine, the Ø-n relationship. Six tests were performed on dry in-situ soil samples. The size of sample was 38 mm and 76 mm in diameter and height respectively.

Five compacted layers were needed to achieve very dense samples. Small manual suction was applied to the sample through a vacuum before releasing the mold. The sample length and diameter were accurately measured using digital height measuring vernier. The end of a rubber tube was connected to the drain tap of the testing chamber while the other end was connected to a volume measuring burette. Volume change was recorded using the twin-burette volume change unit which consists of two 100 ml burettes graduated at 0.2 ml intervals *(Head, 1984)*. The value of the minor principal stress was 149.5 kN/m^2 for all tests.

Membrane thickness correction for evaluating the sample volume is neglected. The correction for rubber membrane strength is very small and may be ignored *(Al-Omari, 1984)*.

The Ø-n relationship of the sand at the beginning of the bearing capacity tests can be seen in Fig. 3-10. The best mathematical fit for the six points joined by curve was found to be a straight line (R^2 = 90.56%) with the equation:

Ø = 44.373 - 0.1246 × n

From Table 3-1, for **n = 35 %** which is to be used in the model tests, the value of **Ø** is:

Ø = 44.373 - 0.1246 × 35 ≈ 40°.

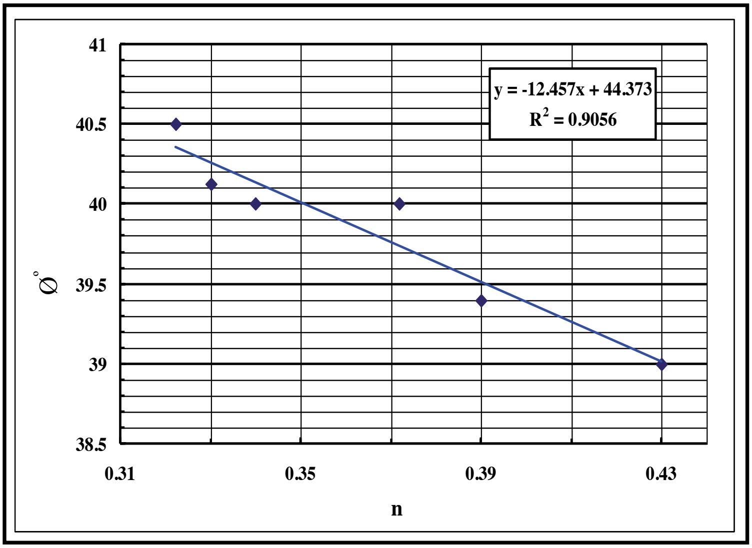

Figure 3-10 Triaxial friction angle-porosity relationship

Figure 3-11 shows the Triaxial test equipment which is supplied to the laboratory of soil mechanics at the College of Engineering in Kufa University in 2014 with the soil specimen shown at the end of the test.

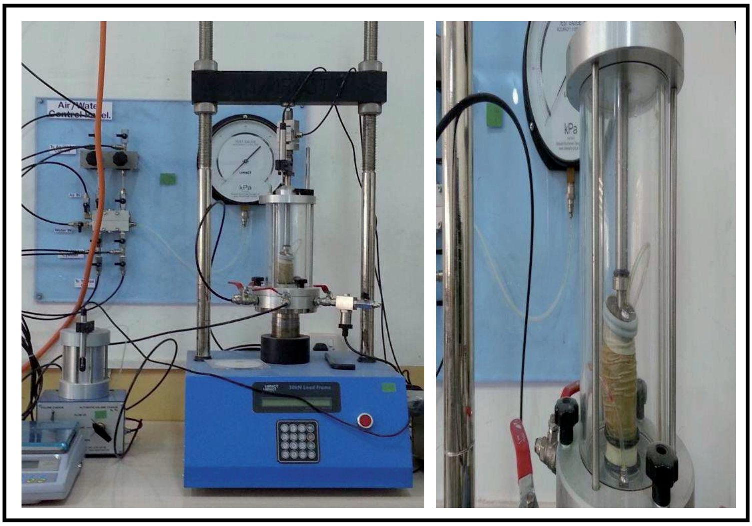

Figure 3-11 Triaxial test equipment

3.7 Strain Gauge Technique

3.7.1 General Description

One of the aims of this research is to investigate the value of progressive strain during load application. The strain is an important parameter to understand the sand-grid interaction. To achieve this aim, the strain gauges were used in the geogrid experimental work.

Strain gauges are used for physical force measurements in mechanical, marine aircraft and civil engineering as well as the fields of architecture, automobiles, and medical science. Strain is an indicator of the magnitude and behavior of stresses or loads. Strain gauges are easy to use and offer a high degree of accuracy and stability. They generally have a simple construction consisting of a fine electric resistance wire or photo-etched metallic resistance foil, together with an electrical insulation base and a set of gauge leads.

When a material is stretched (or compressed), the force used generates a corresponding stress inside this material. This stress in turn generates a proportional tensile strain (or compressive strain) which deforms the material by $L+\Delta L$ or $L-\Delta L$, where L is the original length of the material and the ratio of $\Delta L/L$ is called ***strain*** (Fig 3-12).

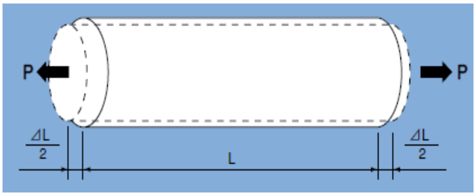

Figure 3-12 Definition of strain**,** (TML strain gauges manual)

External force applied to a ferritic material generates physical deformation and electrical resistance change of the material. In case that such material is stacked onto test specimen via electrical insulation, the material produces a change of electrical resistance corresponding to the deformation. ***Strain gauges*** consist electrical resistance material and measure proportional strains to the resistance changes.

A strain gauge is constructed by bonding a fine electric resistance wire or photographically etched metallic resistance foil to an electrical insulation base using an appropriate bonding materials, and attaching gauge leads. The strain gauge configuration is explained in Fig. 3-13.

Strain gauges are provided with many convenient features, but they also have limitations. Each strain gauge has its limitation in terms of temperature, fatigue, the amount of strain, and the measurement environment. These limitations must be examined before a strain gauge is used. The strain gauge featuring can be summarized as follows:

1- Simple construction with a small mass and volume so as not to interfere with the stresses on the specimen.

2- Short distance between measuring points for localized evaluation.

3- Good frequency response for tracking rapid fluctuations in stress.

4- Simultaneous measurement of multiple points and remote measurements.

5- Electrical output for easy data processing.

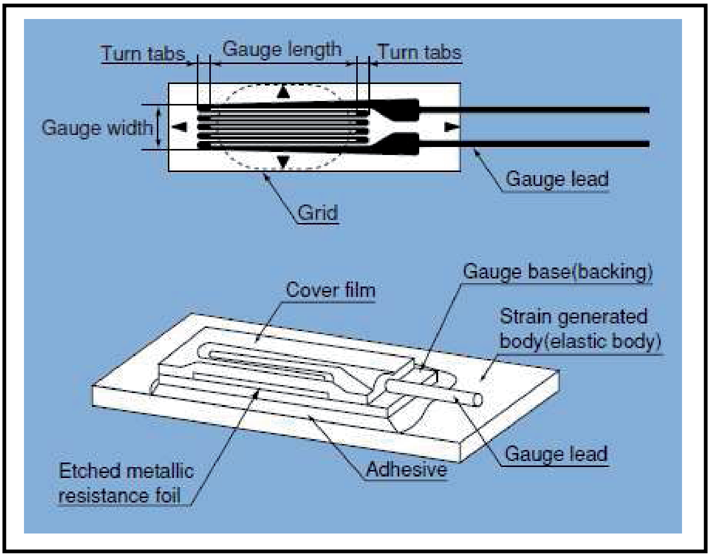

Figure 3-13 Strain gauge configuration, (TML strain gauges manual)

3.7.2 Strain Gauge Measurements

When strain is generated in a test specimen and a strain gauge is attached, the strain is relayed via the gauge base (electrical insulation) to the resistance wire or foil in the gauge. As a result, the fine wire or foil experiences a variation in electrical resistance the variation is exactly proportional to the strain as:

$$\varepsilon = \frac{\Delta L}{L} = \frac{\Delta R / R}{R} \quad \text{...3-1}$$

where,

ε : Strain measured. R : Gauge resistance. ΔR : Resistance change due to strain.

Normally, this resistance change is very small and requires a Wheatstone bridge circuit to convert it to voltage output as shown in Fig. 3-14.

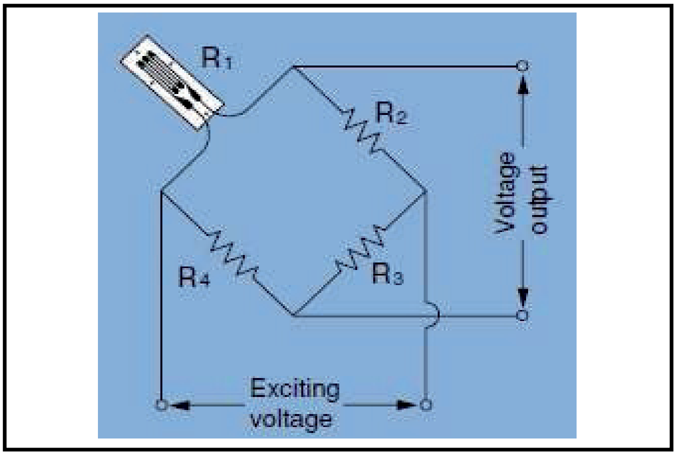

Figure 3-14 Strain gauge circuit**,** TML strain gauges manual

The voltage output of a bridge circuit is given as follows:

$$e = \frac{R_1R_3 - R_2R_4}{(R_1 + R_2)(R_3 + R_4)}E \qquad \text{...3-2}$$

where,

e : Voltage output. E: Input voltage. R_1: Gauge resistance.

$R_2 \sim R_4$: Fixed resistance

Assuming the value R is such that $R=R_1=R_2=R_3=R_4$, the active gauge resistance varies to $R+\Delta R$ due to strain. Thus, the output voltage Δe (variation) due to the strain is given as follows.

$$\Delta e = \frac{\Delta R}{4R + 2\Delta R}E \qquad \text{...3-3}$$

when $\Delta R << R$.

$$\Delta e = \frac{\Delta R}{4R} E = \frac{E}{4} K\varepsilon \quad \ldots 3\text{-}4$$

where, K = Gauge factor as shown on package.

The strain gauge is connected a strainmeter, which provides the Wheatstone bridge circuit and existing input voltage. The strain (ε) is measured on a digital or analog display.

A strain gage manufactured by TML Company was used in the present research. The gauge type is QFLA-2, gauge length is 2 mm while the width is 1.5 mm, the backing length and width of gauge are 6.5 and 3.0 mm respectively. The nominal gauge resistance is 120±0.3Ω, and the gauge factor is approximately 2.12.

Table 3-2 shows the properties of the used compatible coating material ***SB*** tape manufactured by the same company.

The compatible adhesive type ***CN*** (single component room-temperature-curing) manufactured by the same company was used. The properties of strain gauge adhesive are summarized in table 3-3.

Figure 3-15 shows the used TML strain gauges, ***SB*** tape, and compatible adhesive type ***CN*** .

Table 3-2 The properties of the strain gauge coating material ***SB*** tape

Material	Buthyl
Content per unit	10mm*3mm 5m Long/roll
Operational temperature	-30~+80°C
Curing conditions	Pressure sensitive
Purpose	Moisture-and water -proofing
Applications	3-mm thick tape-form coating very convenient usage

Table 3-3 The properties of the strain gauge adhesive

Type	Single component room-temperature-curing
Component	Cyanoacrylate
Applicable specimen	Plastic, Metal, Composite
Operational temperature	-196~ + 120°C
Curing temperature and time	Room temperature, 20 sec. – 1min (thumb pressure)
Applications	Single- component cement for strain gauges. The time required to bond the gauge is extremely short and handling is very easy. The thin bonding layer allows adhesion to plastic objects as well as metal. Curing time under normal conditions is 20~60 seconds

Figure 3-15 TML strain gauges, ***SB*** tape, and compatible adhesive type ***CN***

3.8 Datatronic 128-Channel Automatic Data Acquisition System

The 128-channel automatic data acquisition system has been designed and created to satisfy the requirements of all laboratories, and to considerably improve laboratory productivity and cost effectiveness. Data collection takes place completely automatic. A Windows based program with menu driven command selection is straightforward and easy to follow and does not require a skilled operator. The system can be used for: Oedometer (consolidation) tests, Direct and residual shear tests (cycle tests), Triaxial tests, Unconfined and uniaxial compression tests, CBR tests and Marshall tests. The appliance consists of a central unit with 32-bit processor. It has been created with an expandable structure and can be managed from a minimum of 16 different independent channels to a maximum of 128. In its standard supply the appliance is delivered with 16 channels, cable to RS232 connection. The expansion (optional) takes place through 16-channel internal analogue card. In the standard box it allows to store up to 64 channels. For more than 64 channels a “junction-box” is necessary which allows to store up to 64 additional channels for a total of 128 inputs for transducers. The high resolution and contrast (negative blue) wide display 320 × 240 LCD simultaneously visualizes 8 channels and by selection up to 128 channels. The device is capable of acquiring inputs from any type of transducer: Strain Gauge Bridge, LVDT (Linear Variable Differential Transformer) with optional adapter, Potentiometer. A continual live display of test diagrams is provided in addition to test data exportation with TXT files for consecutive processes, with Excel or other SW. A personalized printout of certificates and test diagrams is available. System configuration is facilitated by a 5 key membrane keyboard with encoder for rapid setting. The system allows memorization of every configuration and calibration. Data logging (from the PC using the Windows based program) is facilitated by user-friendly software included in the Datatronic package. The system allows setting for each channel the sampling type in linear form, square root form, logarithmic form and personalizable form, with frequencies from very fast (one second) to infinite, without reading limits (storage limits are linked to PC memory), with the possibility of delaying the start time. A password protects configuration and calibration. All data is saved on the RAM memory using battery backed data storage. This appliance contains an analogue / digital (24 bits) conversion device. Display type size can be chosen from engineering units for load, strain, volume variation, pressure and personalised units. Datatronic provides three auxiliary outputs for the excitation of the transducer supply

of 3Vdc, 5Vdc and 10Vdc transducers. A PGA regulation system allows a wide range of electric signals to be selected with an input of 20 mV to ± 2.5V (whether at half or full bridge). Power supply is: multivoltage from 90 to 264Vac 47-63Hz. Transducer input is from 0-20 mV to ± 2.5V set by the PGA Transducer excitation supply 3-5-10Vdc.
The dimensions of the unit are: 460 × 540 × 350 mm and Weight: 12 kg as shown in Fig. 3-16, (Fakhraldin, 2013).

3.9 Displacement Measurements

The vertical displacement of the footing was recorded using two dial gauges positioned at opposite sides of the footing at both sides. The capacity of each dial gauge is 50 mm. Every dial gauge is surrounded by a special clamp; the clamp is attached to a magnetic base through a sliding bar and the base in turn is attached to fixed bar. The dial gauges were calibrated by the Central Organization for Standardization and Quality Control, their sensitivity is 0.01 mm.

Figure 3-16 The Datatronic 128-Channel Automatic Data Acquisition System

3.10 Geogrids Types and Properties

Two types of geogrid were used in this study. Selection of these two types was according to the results of the study of Fakhraldin (2013) in which he pointed out that

among eleven geogrid types the **Netlon CE121 and Tensar SS2** geogrid have tensile strength and elastic modulus higher than that of other geogrids made by different manufactures. The typical properties of these two types are listed in Tables 3-4 and 3-5 respectively. Figure 3-17 shows the two types of the used geogrid.

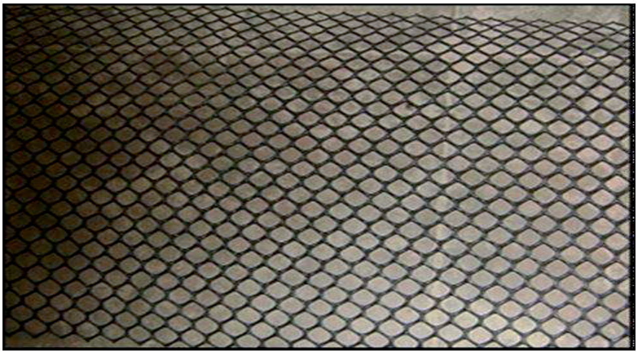

(a)

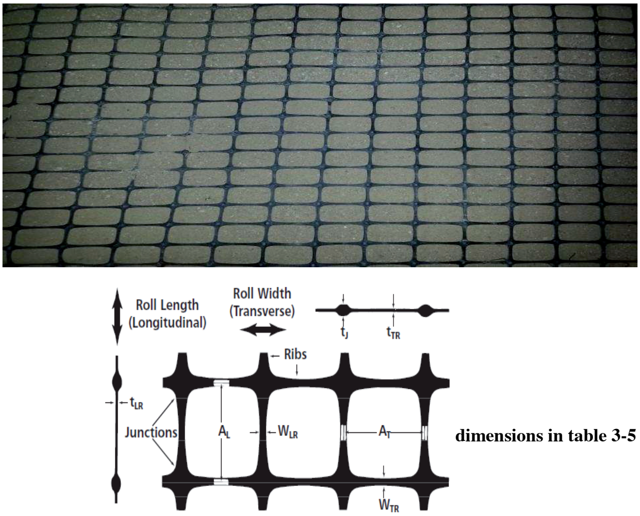

(b)

Figure 3-17 Types of used geogrids, (a) Netlon CE121 (b) Tensar SS2

Table 3-4 The typical properties of Netlon CE121 geogrid, (after Fakhraldin (2013)

Property	Units	Data
Polymer	-------	PP
Mesh type	-------	Diamond
Color	-------	Black
Packing	-------	Rolls
Unit weight	kg/m^2	0.74
Dimensions		
Aperture size (MD/XMD)	mm	6 × 8
Rib thickness	mm	1.6/1.45
Rib width	mm	2/2.75
Junction thickness	mm	2.75
Roll width	m	4
Roll length	m	50
The Mechanical Properties		
Peak Tensile Strength	kN/m	6.4
Elastic modules	GPa	0.39
Upper yield strength	MPa	5
Lower yield strength	MPa	5
Tensile strength	MPa	9
Non-proportional extension strength	MPa	6
Total extension strength	MPa	5
Fracture elongation	%	-99
Elongation at maximum load	%	6
Total elongation	%	11

Table 3-5 Typical properties of Tensar SS2, (after Fakhraldin (2013)

Property	Units	Data
Polymer	-------	PP
Minimum carbon Black	%	2
Roll width	m	4
Roll length	m	50
Unit weight	kg/m^2	0.29
Roll weight	kg	60
Dimensions		
A_L	mm	28
A_T	mm	40
W_{LR}	mm	3
W_{TR}	mm	3
t_J	mm	3.8
t_{LR}	mm	1.2
t_{TR}	mm	0.9
Rip shape	Rectangular with square edges	
The Mechanical Properties		
Peak Tensile Strength MD/XMD	kN/m	14.4/28.2
Elastic modules MD/XMD	GPa	0.57/0.99
Upper yield strength MD/XMD	MPa	1 /3
Lower yield strength MD/XMD	MPa	1/3
Tensile strength MD/XMD	MPa	24/30.7
Fracture percentage elongation MD/XMD	%	-98/-98
Percentage elongation at maximum load MD/XMD	%	3.5/2.9
Total percentage elongation MD/XMD	%	5/4.25

3.11 Research Program and Procedure

The program of the research is divided into two parts, the first is an experimental work while the second is a numerical work. The latter involves the comparison of numerical with experimental results and the economical comparison between the use of piles and geogrid within the limits of design. The program can be summarized as follows:

The experimental part

The first stage: It involves physical and chemical properties of the in-situ soil

a- Physical properties includes:

- Water content.
- Sieve analysis.
- Specific gravity.
- Maximum and minimum density.
- Porosity (n) against (Ø) relationship.

b- Chemical properties include:

- Gypsum content.
- SO_3 content.
- Total soluble salt content (T.S.S).

The second stage: It includes model tests on in-situ soil alone

a- Using strip footing on in-situ soil to find ultimate bearing capacity and stress-settlement relation.

b- Using rectangular footing on in-situ soil to find ultimate bearing capacity and stress-settlement relation.

c- Using plane strain pile test with the strip footing on in-situ soil to find ultimate pile capacity and load-settlement relation.

d- Using three square piles with the rectangular footing on in-situ soil to find ultimate piles capacity and load-settlement relation.

The third stage: It includes testing the reinforced soil model using strip and rectangular footings, the parametric studies include; surface model footing (D_f=0), u/B=0.25, h/B=0.375, N=3.

The testing procedure involves the following steps:

1- **Applying lubrication on both sides (the glass and plate each 600×1000 mm):**

The silicon grease and rubber membranes were used to lubricate the braced glass plate and also the opposite side. Lubrication system was used in the tests in order to minimize the effect of the side friction on the load measurements.

The silicon grease-latex membrane lubrication system is the established procedure to eliminate friction in geotechnical tests [(Rowe, 19964), Kirkpatrick and Yanikian (1975 and Al-Omari (1986)].

2- **Preparation of sand deposit in the test box:**

The sand was placed in the tank according to the raining technique, i.e. maintaining a dropping height of 800 mm in three layers, the thickness of each layers is 200 mm. After each test, the sand box should be completely emptied.

3- **Placing the reinforcement geogrid layers in the sand deposit:**

During the process of sand raining, the three reinforcement layers were placed. The upper layer was placed at depth below the foundation equal to **0.25B** (B is the width of footing) while the lowest layer was placed at depth equal to **B**. The spacing between individual layers is **0.375B**.

4- **Placing the footing on sand deposit:**

The type of footing was chosen (strip and rectangular) and placed over the sand deposit at the center line of box. The suitable knife–edge loading blades were fixed to the loading frame and made to touch the groove in the footing base.

5- **Placing the piled footings in contact with soil surface:**

To achieve plane strain condition for the piles under the strip footing, the plane strain model of pile was placed and attached to the strip footing. The piles under the rectangular footing were fixed to the footing. The suitable knife–edge loading blades are fixed to the loading frame and made to touch the groove in the two types of footing.

6- **Placing the piled footing with no soil contact with soil surface:**

a- **Without silicon rubber membrane lubrication**

To find the end bearing and skin resistance of piles separately, the procedure of point 5 above was repeated with a 5 cm distance between the free surface of

soil and the footings to eliminate the bearing pressure of footings such as the value of total capacity which comes only from the end bearing and skin friction.

b- **With silicone rubber membrane** To find the end bearing of pile, the procedure of point 6-a above was repeated using silicone grease and latex rubber membranes placed on all sides of pile to eliminate the skin friction of pile.

7- **Application of vertical load:**

A vertical load was applied through loading frame has a loading capacity of 2000 kN. A constant loading rate of 1 mm/min was employed in the entire testing program. The test was continued until approximately recording a continuous displacement of the footing under constant load. This load was read from a special gauge located near the loading frame, while the displacement of footing was read using two dial gauges of 0.01 mm sensitivity.

The fourth stage: It includes testing the reinforced sand model with the application of strain gauge measurements of strains occurring in the geogrid ribs. This stage involves the following steps:

I. **Preparing the rib surface**:

Any grease, scale, dust, paint, etc. is removed from the bonding area to provide a shiny surface. An abrasive paper is used to abrade an area slightly larger than the base of the strain gauge to be installed (the type of abrasive paper differs depending on the bonding surface material). The abraded surface is then cleaned with industrial tissue or cloth dampened with a small amount of solvent such as acetone. After surface preparation, the strain gauges are glued before the prepared surface generates an oxidizing membrane or is contaminated.

II. **Soldering the wires of strain gauges:**

This is a difficult step which requires a held care. After bonding the strain gauge to the rib of geogrid, the wires are laid on the ribs using an adhesive tape, and then soldering the wires by the caustic and lead materials.

III. **Coating the strain gauge surface:**

The ***SB*** must be cut from 5 to 10 mm long. The lead wire is lifted up and the ***SB*** tape is pressed onto the specimen surface under the lead. The lead wire is placed back down onto the ***SB*** tape. Enough attention is paid for coating on lead wire takeout because any moisture penetration through this point causes low insulation resistance. In order to ensure enough contact with the lead wire and the ***SB*** tape, twisted wire should be unbound. Parallel wire should be split into each core. Enough size was cut to cover the strain gauge and the area for taking out the lead wire.

The numerical part

The fifth stage: Analyzing the reinforced and unreinforced sand models using *PLAXIS 3D program* (finite element method).

The sixth stage: It includes comparison between the experimental and numerical results obtained from the *PLAXIS 3D program*.

The seventh stage: It involves an economical study to assess the positive and negative impact of using high strength geogrids instead of piles in order to enable the engineer in charge to make decisions in this aspect.

Figure 3-18 shows the flow chart of the experimental testing program.

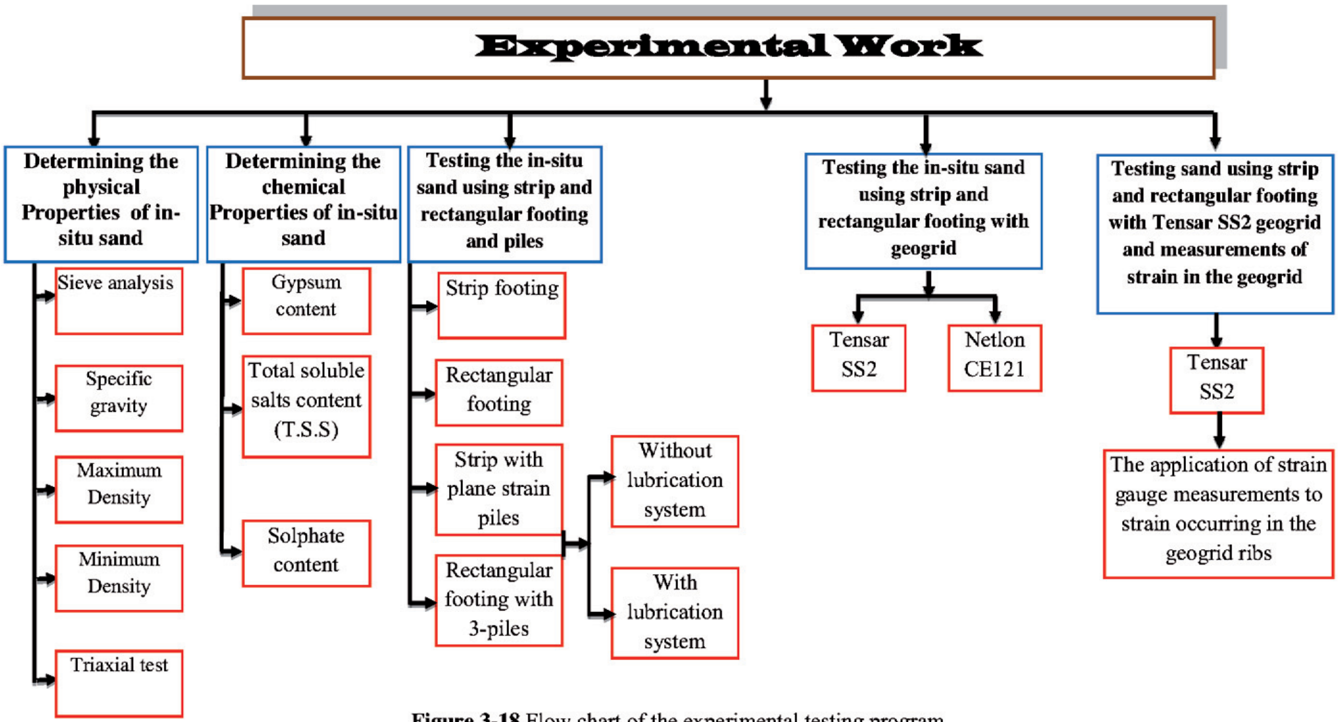

Figure 3-18 Flow chart of the experimental testing program

CHAPTER FOUR

PRESENTATION AND DISCUSSION OF EXPERIMENTAL RESULTS

4.1 Introduction

This chapter deals with the presentation and discussion of the results of the experimental work performed according to the test program described in chapter three. One of the main aims of this research is studying the ability of the use of geosynthetics (geogrid) instead of piles in the construction of foundation of interchange bridges in the middle of Iraq. The soil has been taken from the site to provide a reliable indication for the case study. Two types of footing were studied, strip and rectangular footing. The main experimental work is divided into four groups, they are bearing capacity model tests on the sand, tests using three layers for each type of geogrid for strip and rectangular footing, tests for studying the strain occurring in **Tensar SS2** geogrid and the fourth group is of piles capacity using the two types of footing. The comparison between the axial applied load on reinforced sand and the total capacity of piled-raft system was investigated as well as investigating the values of end bearing and skin friction of piles separately.

4.2 Unreinforced Soil Model Tests

Model tests were performed using strip and rectangular footings on unreinforced soil as shown in Fig. 4-1. The ultimate bearing capacity and load-settlement relation for strip and rectangular footings are shown in Fig. 4-2. The tests were performed using a rate of strain 1 mm/min for applying loading. The footing was placed on the upper free surface of soil. The value of bearing capacity for each footing is considered as a reference value to investigate the improvement of soil using the geogrid. From the relationship between bearing capacity and relative settlement (s/B %) of soil, it was found that the ultimate bearing capacity obtained for the strip and rectangular footings was 234.3 kPa and 123.2 kPa respectively. The relative settlement (s/B %) at the ultimate bearing capacity is 11.1% and 13.3% respectively. The point of ultimate bearing capacity was easily marked on the

load-settlement curve since the test was strain-controlled and the peak value was clearly visualized.

Figure 4-1 Model of strip and rectangular footing on unreinforced soil

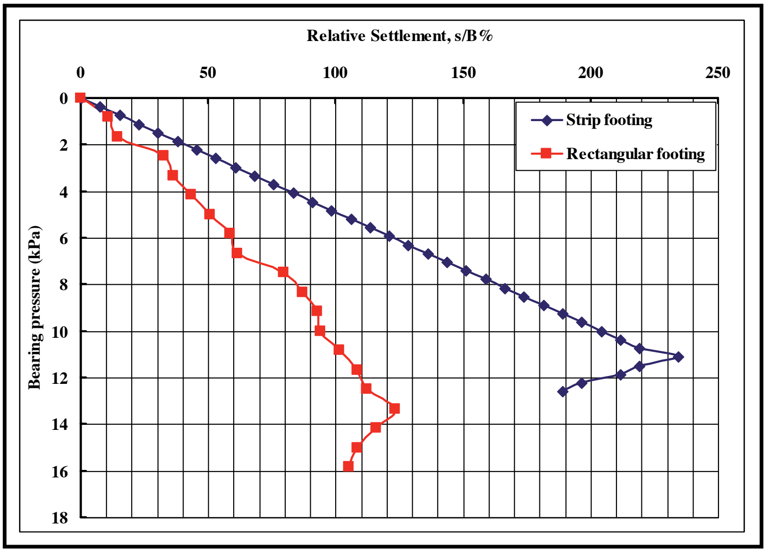

Figure 4-2 Bearing pressure versus relative settlement for strip and rectangular footings resting on unreinforced soil

4.3 Reinforced Sand Model Tests

A series of tests were conducted to study the effect of the footing types and geogrid stiffness on the bearing capacity of sand. Two types of geogrid reinforcement were studied using the two types of footing (strip and rectangular).

For all model test the depth of the top most reinforcement layer (u) was 0.25B where B is the footing width. This value of (u) is based on findings of other researchers as being the best to give higher bearing capacity, (Das et. al, 1993 and Fakhraldin, 2013). The number of geogrid layers was taken as three based on previous studies where three geogrid layers were found adequate to give a suitable improvement of bearing capacity, (El - Sawwaf, 2009). Fakhraldin (2013) noticed that the strain in the geogrid ribs almost vanished in the fourth and fifth layers. The distance between reinforcement layers (h) was 0.375 B and the depth of the lowest reinforcement layer was equal to the footing width (B) (Figs. 4-3 and 4-4).

Strip Footing:

The two types of geosynthetics represented by **Netlon CE121 and Tensar SS2** geogrids were used to study the behavior of the soil. Two tests were conducted on beds of reinforced sand using these two types of geogrids. The variable studied is the effect of geogrid stiffness on the bearing capacity of soil.

Figure 4-3 shows the geometry details for both the geogrid reinforcement and the strip footing considered in this investigation.

Rectangular Footing:

A rectangular footing was used with the dimension and geometry shown in Fig. 4-4 to investigate the bearing capacity of geogrid.

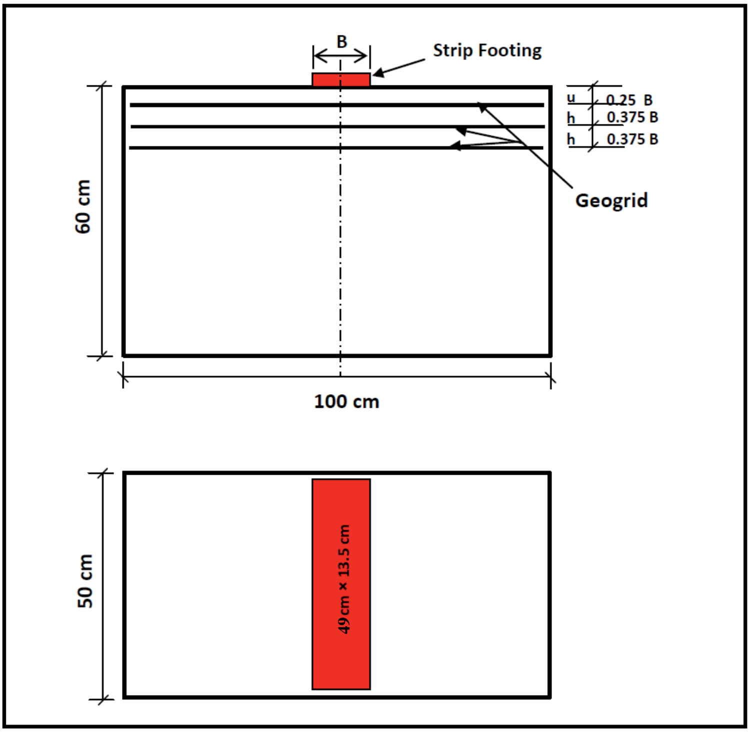

Figure 4-3 Geometry and top plan of the geogrid and strip footing model

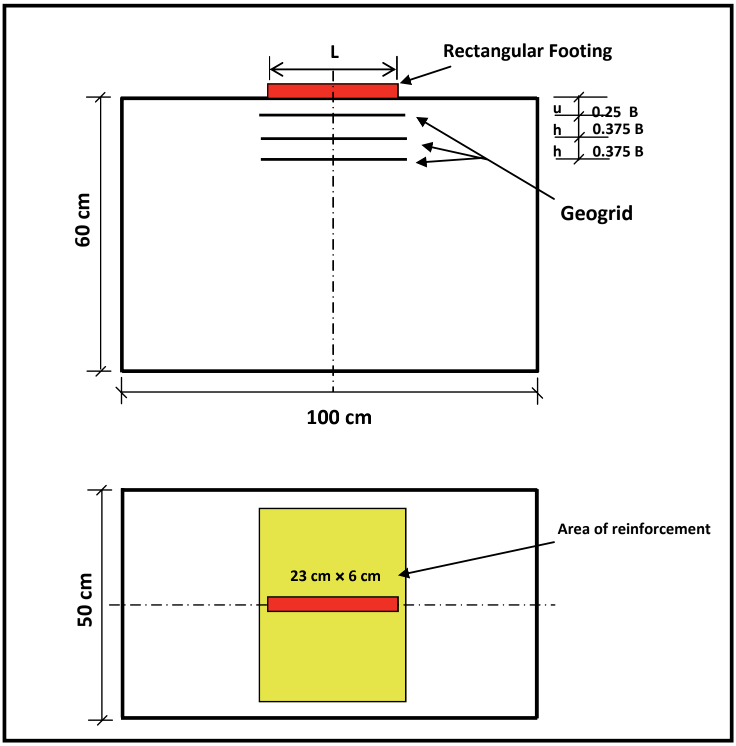

Figure 4-4 Geometry and top plan of the geogrid and rectangular footing model

4.4 Effect of Footing Type

Tests were conducted to study the effect of footing type on the ultimate bearing capacity using the two types of geogrids (Netlon CE121 and Tensar SS2) and two types of footings (Strip and Rectangular), (Fig. 4-5). The relation between the ultimate bearing capacity (q) and the relative settlement (s/B %) is plotted in Fig. 4-6 and Fig. 4-7 using both geogrids. The ultimate bearing capacity for the strip footing is higher than rectangular footing and the relative settlement smaller for strip than rectangular. Figure 4-7 shows yields similar trend of results but Tensar SS2 yields higher improvement. Figures 4-8 and 4-9 show the relation between the ultimate bearing capacity and relative settlement with

and without geogrid for the strip and rectangular footings respectively. From these figures it can be seen again that the Tensar SS2 type gives a higher improvement in bearing capacity than the Netlon CE121 using both types of footings. The bearing capacity ratio (BCR) is the ratio of bearing capacity using geogrid to the unreinforced bearing capacity. For the geogrid Netlon CE121, the BCR is 1.88 and 2.35 for strip and rectangular footings respectively. For Tensar SS2, the BCR is 2.5 and 2.9 for strip and rectangular footings respectively. This confirms the importance of the tensile strength of the geogrid material since the tensile strength of Tensar SS2 is 2 times higher than that of Netlon CE121. The results give indication to the selection of the type of geogrid to give a good improvement of soil. The main reason which makes BCR higher for the rectangular footing is that strain is allowed in the two directions of the horizontal plane which makes the grid function in two directions. The relative settlement of reinforced soil is smaller than that of unreinforced soil for the two type of footings.

Figure 4-5 Model with strip and rectangular footing on soil with geogrid

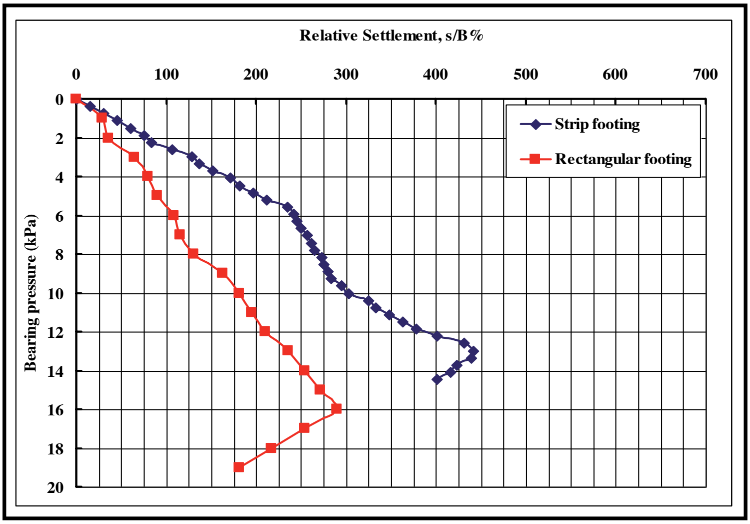

Figure 4-6 Bearing pressure versus relative settlement for two types of footings on reinforced soil using **Netlon CE121**

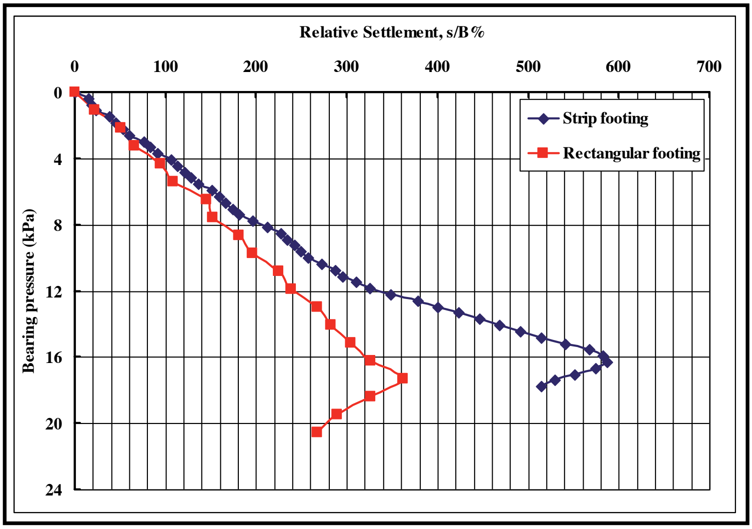

Figure 4-7 Bearing pressure versus relative settlement for two types of footings on reinforced soil using **Tensar SS2**

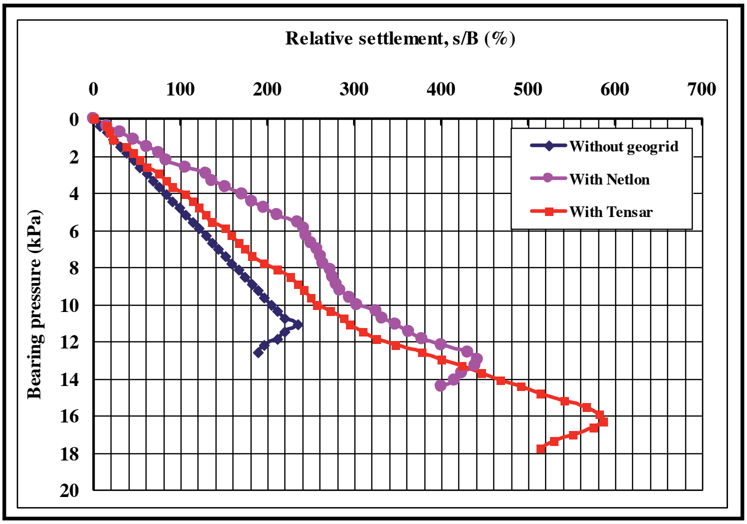

Figure 4-8 Bearing pressure versus relative settlement for strip footing with and without geogrid

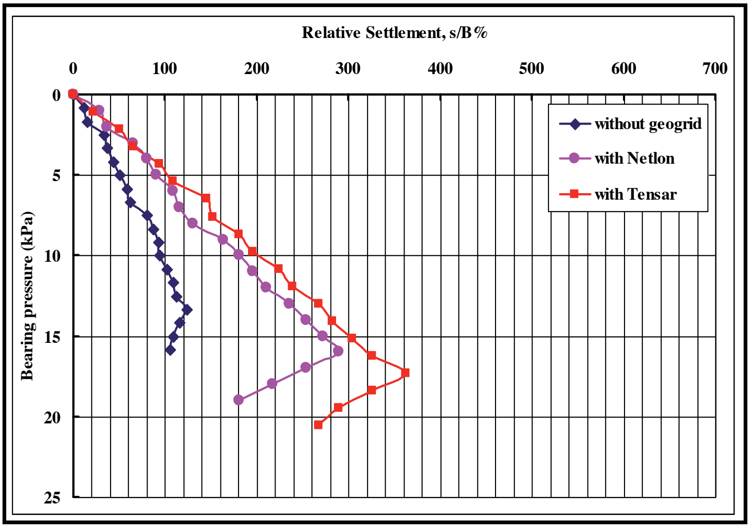

Figure 4-9 Bearing pressure versus relative settlement for rectangular footing with and without geogrid

4.5 Geogrid Strain and Elongation Measurements

On scrutiny of the nationally and internationally available literature, it appears that there is a little work on the straining mechanism occurring in the geogrid ribs during the application of foundation load in which the failure is progressive. The distribution of strains in the geogrid ribs is important to understand the enhancement mechanism of bearing capacity, to what extent there is a need for high stiffness/strength geogrids and at which stress level the soil-grid bond may break, (Fakhraldin, 2013).

In the next section the presentation of results will involve the strain occurring in the ribs of geogrid and its variation with horizontal distance of strain gauge from centerline of footing and position of reinforcement underneath the footing. The two types of footing models and **Tensar SS2** geogrid were used in these tests. Strains in the **Netlon CE121** geogrid have not been measured because there is not enough rib size to paste the strain gauges.

Three layers of geogrid (N=3) were embedded in the depth of (d) which is equal to the width of footing (B). The depth of first layer (u) was 0.25B from the base of footing, the leftover distance is divided into two layers, 0.375B for each layer.
TML strain gauges, the datatronic 128-channel automatic data acquisition system and strain gauge amplifier, as presented in chapter three, were used to measure the strain and elongation in the ribs of geogrid.

The strain gauges were fixed at center of geogrid rib using the compatible adhesive ***(CN)*** and coated using the suitable coating material ***(SB).*** The adhesive and coating materials are explained in chapter three. The strain gauge wires were soldered to available wires then the wires were connected to strain gauge amplifier which in turn was connected to the datatronic 128-channel automatic data acquisition system.

4.6 Calibration Methods

The datatronic 128-channel automatic data acquisition system reads the strain through an electric circuit as divisions. The calibration was presently performed using two

methods, these two methods were used by Fakhraldin (2013) in order to obtain high accuracy;

1- Calibration using a single rib geogrid:

A single rib of geogrid and the strain gauge was fixed on the middle of the rib and tested by the computer controlled electronic universal testing machine. The strain gauge was connected to strain gauge amplifier which by turn was connected to the datatronic 128-channel automatic data acquisition system. The computer controlled electronic universal testing machine records the strain against time, the datatronic acquisition system records the divisions against the same time. Accordingly a calibration between divisions and strains was carried out (Fig. 4-10) and the following equation was obtained with coefficient of determination R2 = 0.9689 as:

$$\varepsilon = 5 \times R \times 10^{-8} + 0.0002 \qquad \ldots 4\text{-}1$$

where R is the reading (divisions) of the data acquisition

2- Calibration using a steel cantilever:

The second method of calibration (used to calculate strain,) was performed using solid square steel bar connected by welding to steel I-section. This bar was connected with the steel I-section as a cantilever bar. The strain gauge was fixed on the steel square bar and connected to strain gauge amplifier which in turn was connected to the datatronic 128-channel automatic data acquisition system. The steel square bar contains hook to carry various load connected to the end of bar. Also a magnetic dial gauge (capacity 50 mm) was used to measure deflection, (Fakhraldin, 2013). By applying gradual weights the displacement was measured in various periods such as 0, 0.5, 1, 1.5, 2… 5 mm. For each displacement the readings are recorded and equation 4-2 (Hadee, 2011) is used to calculate strain (ε). Then the calibration between divisions (reading) and strain was carried out (Fig. 4-11) and represented in equation 4-3:

$$\varepsilon = \frac{3\delta h}{2L^2} \qquad \ldots 4\text{-}2$$

where

δ= the reading of dial gauge (displacement) in mm.

h= the height of cross section of steel square bar, (10.5 mm).

L= the distance from center of strain gauge to center of weight (472 mm).

Equation 4-3 is obtained from the second method of calibration and with coefficient of determination $R^2 = 0.9745$

$$\varepsilon = R \times 10^{-7} - 1 \times 10^{-7} \qquad \ldots 4\text{-}3$$

The applied strains taking place during the first method of calibration were high whereas they were low using the second calibration method. The actual strain in the ribs occurring during the bearing capacity test is expected to cover both ranges, (Fakhraldin, 2013).

The two sets of data from the two methods of calibration were merged and represented graphically and mathematically to find the relation between strains and readings, equation 4-4 was obtained with coefficient of determination $R^2 = 0.978$

$$\varepsilon = 6 \times R \times 10^{-8} + 8 \times 10^{-5}. \qquad \ldots 4\text{-}4$$

Equation 4-4 has been employed to calculate the strain in the geogrid ribs.

Figure 4-12 shows the adopted calibration that was obtained from the two methods.

For calculation of the elongation in the geogrid rib, Eq. 4-5 is used.

$$\Delta l = \varepsilon \times l \qquad \ldots 4\text{-}5$$

where

Δl = elongation in the rib (mm).

ε = strain occurred in the rib.

l= length of rib (mm).

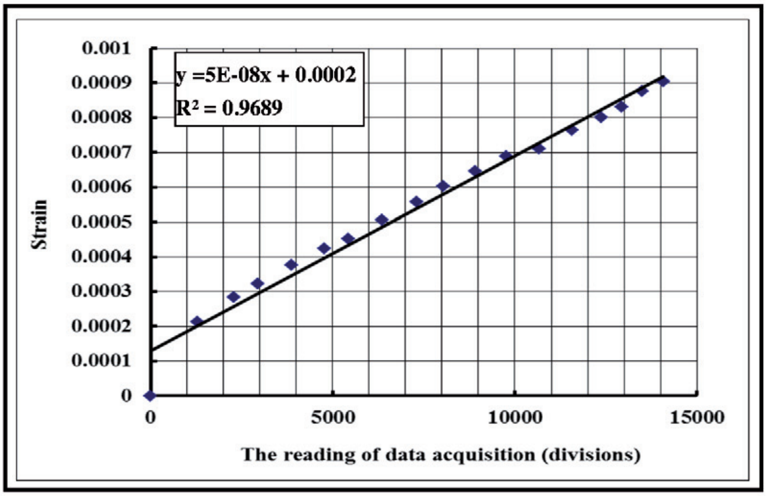

Figure 4-10 The calibration of strain occurring in the rib using the first method of calibration

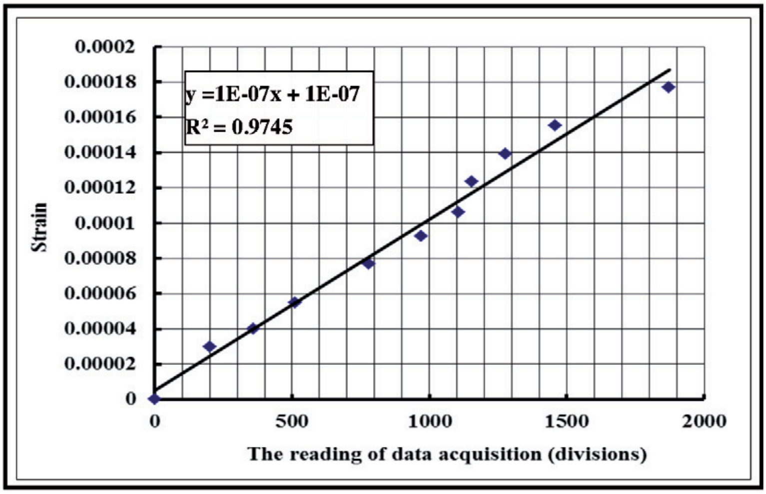

Figure 4-11 The calibration of strain occurring in the rib using the second method of calibration

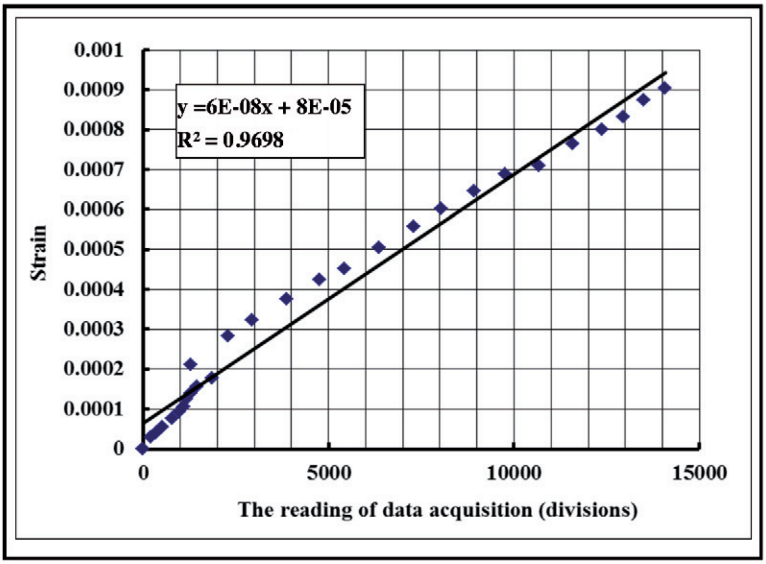

Figure 4-12: The calibration of strain occurring in the rib using the two method of calibration

4.7 Strains in Tensar SS2

The measurements of strain and elongation occurring in the ribs of geogrid were made for the two types of footings. The strip footing represents the case of plane strain condition. The study of strain and elongation in the ribs of geogrid was conducted for Tensar SS2 only.

4.7.1 Strip Footing

The strain gauges were distributed to cover one side of footing reinforcement because of the similarity. The strain gauges were pasted on the long rib only because of the higher strength and the plane strain condition as presented in chapter three. The long rib has tensile strength and modulus of elasticity higher than that of the short rib, therefore the transverse direction (XMD long rib) of Tensar SS2 was placed in the sand container in the

direction of lateral strain (long direction of sand container) during loading test in order to gain higher improvement. Fixing of strain gauges on the ribs of geogrid and the distribution of strain gauges are shown in Fig. 4-13. The laboratory model test is shown in Fig. 4-14.

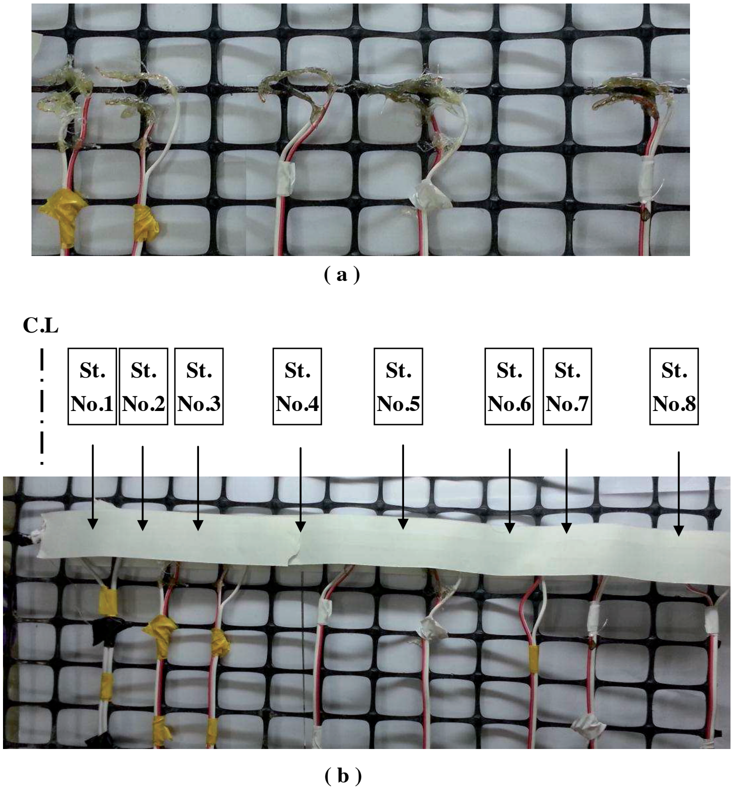

Figure 4-13 (a) Pasting operation. (b) The distribution of strain gauges in the strip footing

Table 4-1 shows the horizontal distances of the strain gauge from the center line of strip footing. The same distribution was repeated for the second and third layers. The centerline of the mesh of geogrid was coincides with the centerline of strip footing.

Table 4-1 Horizontal distances of the strain gauge from the center line of strip footing.

Strain gauge number	Distance of gauge (d) from the center of footing (mm)	Relative distance (d/B) of gauge from center of footing
1	40	0.29
2	80	0.59
3	120	0.89
4	200	1.48
5	280	2.07
6	400	2.96
7	440	3.26
8	480	3.6

The first reinforcement layer

Figures 4-15 and 4-16 respectively show the relationship between stress applied to the reinforced soil versus strain and elongation in the ribs of geogrid. From the figures it can be seen that the strain and elongation increase with increasing stress and nearly reach a constant value before reaching the ultimate bearing capacity. The results show also that the nearest the strain gauge to the footing centerline the higher, the strain and elongation in the ribs.

The second reinforcement layer

The relationships between the applied stress and strain occurring in the second layer of geogrid are shown in Fig. 4-17. The relationships are the same as for the first layer but with smaller values of strain. The strain gauge No. 1 gave a higher value of strain than the other gauges. The strain gradually decreases towards the edge. Figure 4-18 deals with the

applied stress-elongation relationships, the curves obviously have the same trend as that of strain.

The third reinforcement layer

The values of strain in the third layer are smaller than that of the above two layers, that can be seen from Figs 4-19 and 4-20. The obtained stress-strain relationships indicate that strain increases as the stress increase until reaching constant value before reaching the ultimate bearing capacity. The elongations in ribs exhibit the same behavior due to the intimate relation between them.

Figure 4-14 Strain measurements in Tensar SS2 geogrid for strip footing

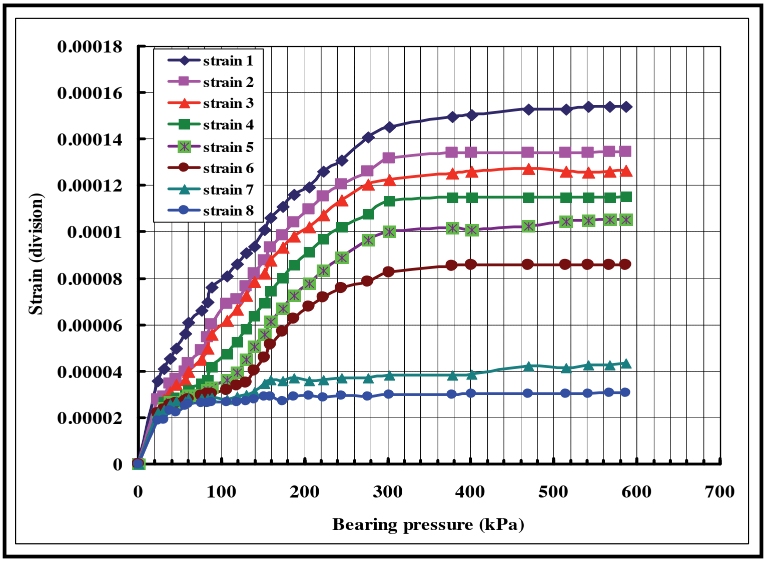

Figure 4-15 The relationship between strain in ribs of first geogrid layer (Tensar SS2) and applied stress to reinforced sand using strip footing

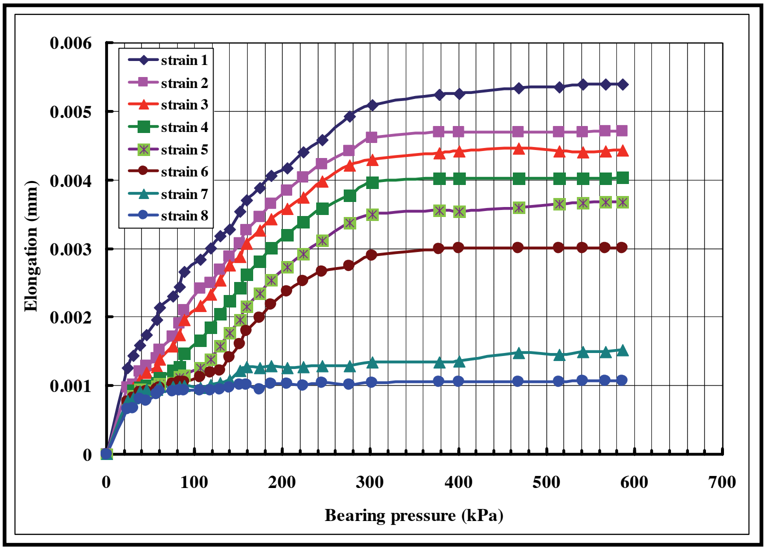

Figure 4-16 The relationship between elongation in ribs of first geogrid layer (Tensar SS2) and applied stress to reinforced sand using strip footing

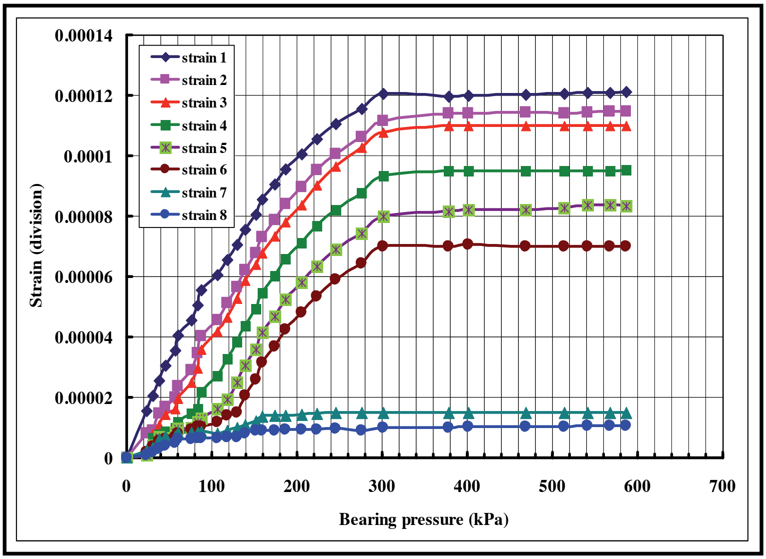

Figure 4-17 The relationship between strain in ribs of second geogrid layer (Tensar SS2) and applied stress to reinforced sand using strip footing

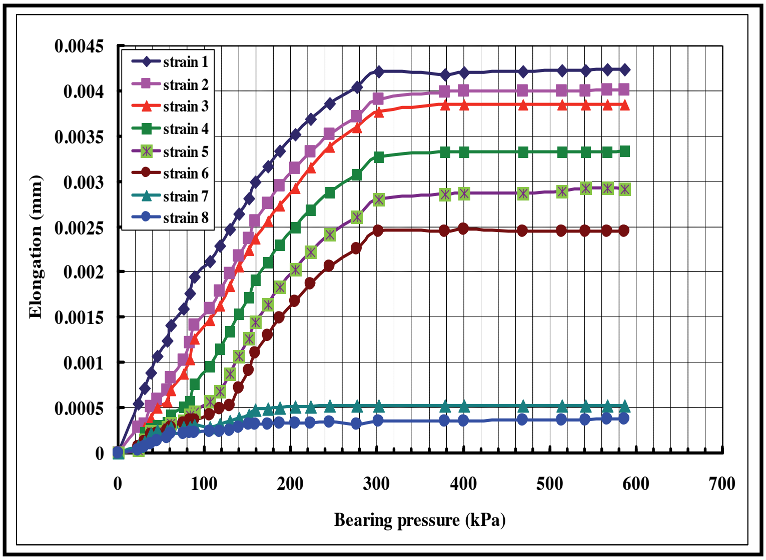

Figure 4-18 The relationship between elongation in ribs of second geogrid layer (Tensar SS2) and applied stress to reinforced sand using strip footing

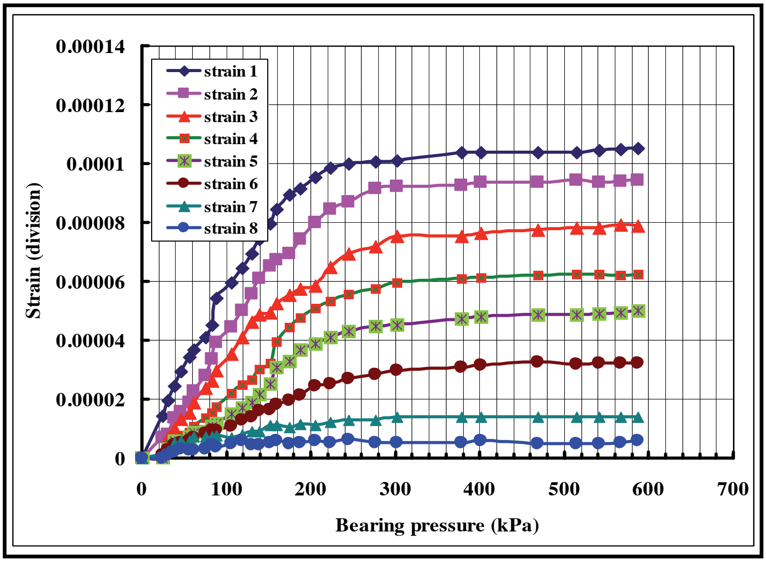

Figure 4-19 The relationship between strain in ribs of third geogrid layer (Tensar SS2) and applied stress to reinforced sand using strip footing

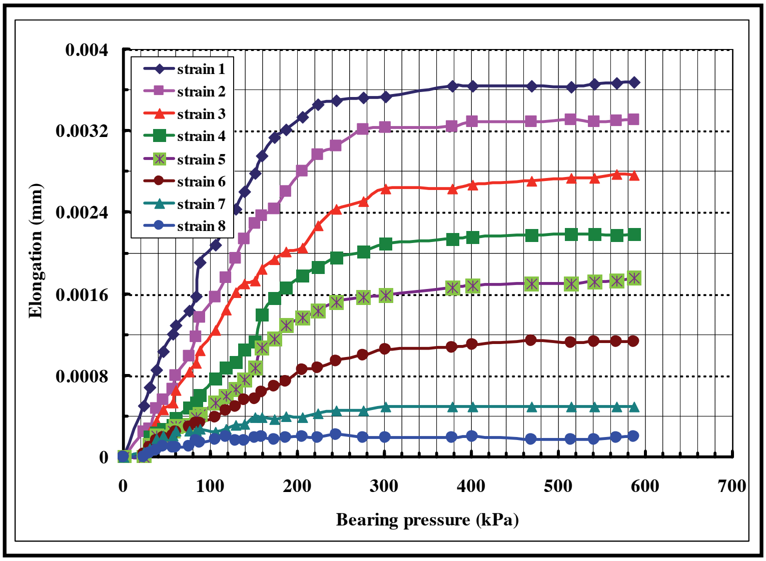

Figure 4-20 The relationship between elongation in ribs of third geogrid layer (Tensar SS2) and applied stress to reinforced sand using strip footing

Horizontal and vertical strain distribution

The horizontal distribution of strains on the ribs of geogrid are demonstrated in Figs. 4-21 and 4-22 respectively for three geogrid layers. The values shown in these figures are recorded at the ultimate bearing capacity.

Figure 4-21 demonstrates the relationship between the horizontal distance, relative distance, and strain. The relationship shows that the values of strain decrease when the strain gauge distance from the centerline of footing for each layer increases. The location of last strain gauge represents the value of 3.6B, which indicates the zone of the effective stresses.

Figure 4-22 shows the relationship between the horizontal distance, relative distance, and elongation in ribs of geogrid. The same behavior as in Fig. 4-21 is obviously found because of the linear relationship between the strain and elongation.

Figure 4-23 shows the relationship between the strain and the depth of strain gauges which are represented by the depth of geogrid mesh under the footing, relative depth and strain. The relationships are drawn for the values of strain at the ultimate bearing capacity. The strains decrease gently as the depth under footing increases.

Figure. 4-24 explains the relationship between elongation and depth, relative depth of strain gauges. The relationships demonstrate the values of elongation in each rib of geogrid. The elongation decreases as the depth increases. The elongations of ribs in the third layer to relatively small, that confirms the results of researchers which indicate that the three layers of geogrid down to B and the horizontal distance 3.6B from each side are the zone of effective soil stress in soil reinforced by geogrid, (Mohammed and Ilamparuthi, 2010).

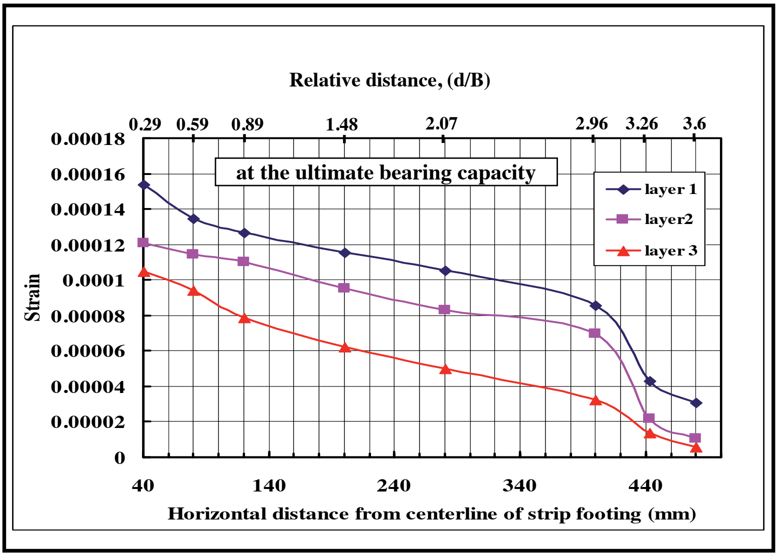

Figure 4-21 The relationship between strain and (relative distance, distance) in Tensar SS2 from the centerline of strip footing

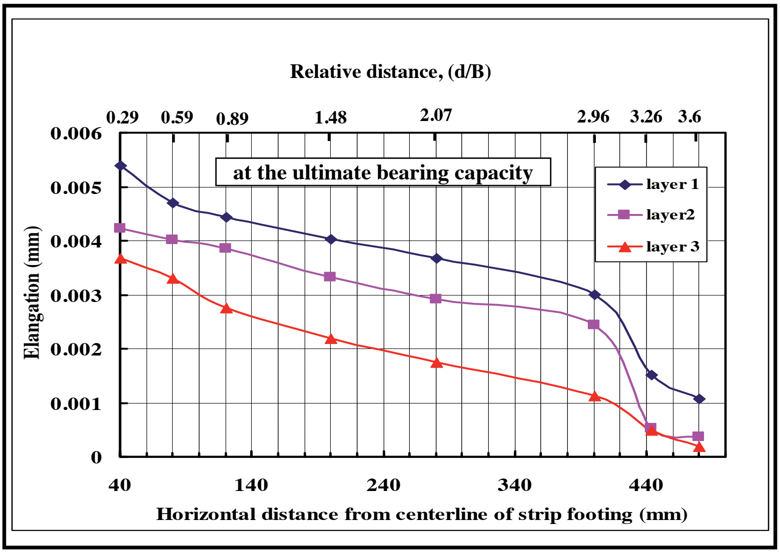

Figure 4-22 The relationship between elongation and (relative distance, distance) in Tensar SS2 from the centerline of strip footing

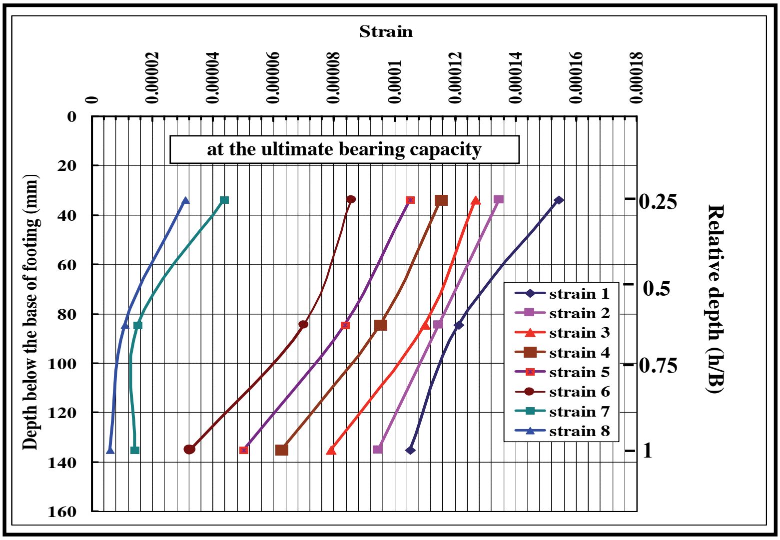

Figure 4-23 The relationship between strain and (relative depth, depth) below the base of strip footing

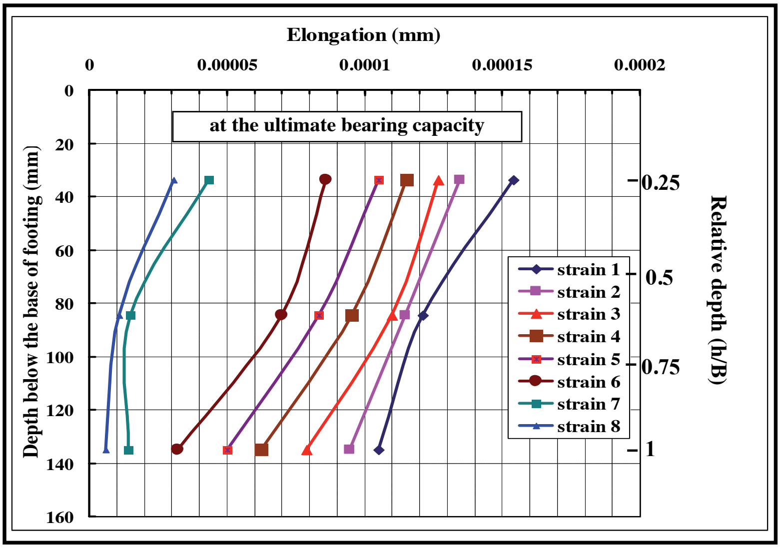

Figure 4-24 The relationship between strain and (relative depth, depth) below the base of strip footing

4.7.2 Rectangular Footing

The tests using the rectangular footing with geogrid were performed again to study the distribution of strain and elongation in ribs of mesh. Four strain gauges were pasted and distributed as shown in Fig. 4-25 and listed in table 4-2. The distances from the centerline of footing was chosen to represent the expected zone of stresses occurring during the loading. One side of footing was considered for the strain gauges because of similarity. As in the strip footing the long direction of ribs was chosen in the direction of lateral strain.

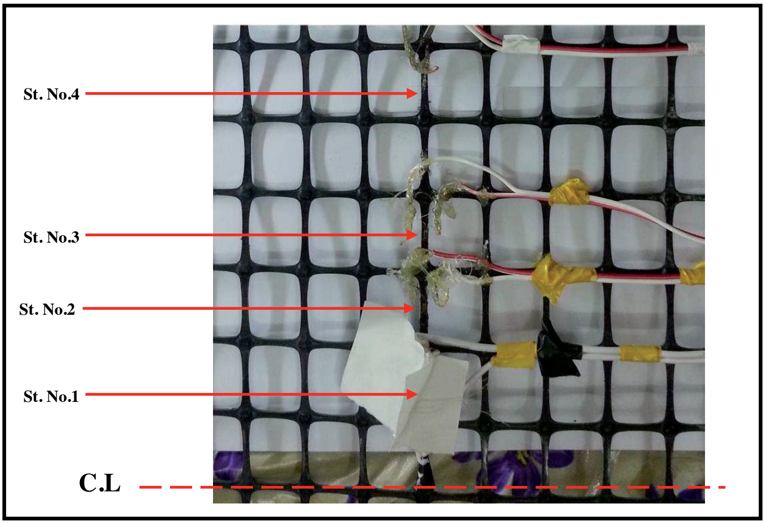

Figure 4-25 The distribution of strain gauges in the rectangular footing test

Table 4-2 shows the horizontal distances of the strain gauge from the center line of rectangular footing. The gauges were positioned along a straight line normal to the long side of the footing as it was the direction of higher strain.

Figure 4-26 shows the strain measurements model test for the Tensar SS2 under rectangular footing.

Table 4-2 Horizontal distances of the strain gauge from the center line of rectangular footing.

Strain gauge number	Distance of gauge (d) from the center of footing (mm)	Relative distance (d/B) of gauge from center of footing
1	60	1
2	100	1.67
3	140	2.33
4	220	3.6

Figure 4-26 Strain measurements in Tensar SS2 geogrid for rectangular footing

The first reinforcement layer

The relationships between stress applied to the reinforced soil versus strain and elongation in the ribs of geogrid are shown in Figs. 4-27 and 4-28. The relationship declares that the strain in the nearest gauges nearest to the footing center is higher than other gauges. The same behavior applies to the elongation because of the linear relation between the strain and elongation. These findings agree the finding of Chen, 2007 which was the distance of 3.6B from each side is almost the zone of stress concentration.

The second reinforcement layer

The relationships between the applied stress and strain occurring in the second layer of geogrid were shown in Fig. 4-29. The relationships are the same as for the first layer but the strains are smaller. The strain gauge No.1 has higher values of strain than other gauges. The strain gradually decreases towards the edge. Figure 4-30 illustrates the applied stress-elongation relationship, the curves obviously resemble that for strain.

The Third reinforcement layer

The values of strain in the third layer are smaller than these of the above two layers, that can be seen from Figs 4-31 and 4-32. The applied stress-strain relationship illustrates that the strain increases as the stress increases until reaching constant value before reaching the ultimate bearing capacity. The elongations in gauges exhibit the same behavior due to the intimate relation between them.

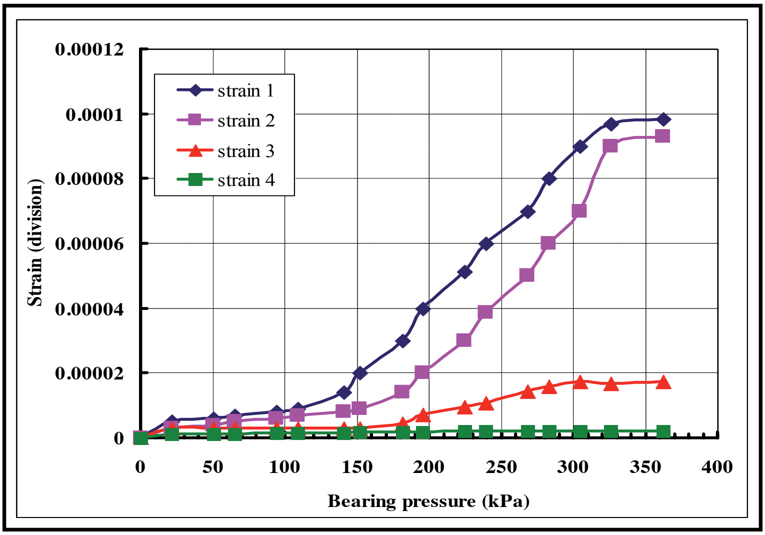

Figure 4-27 The relationship between strain in ribs of first geogrid layer (Tensar SS2) and applied stress to reinforced sand using rectangular footing

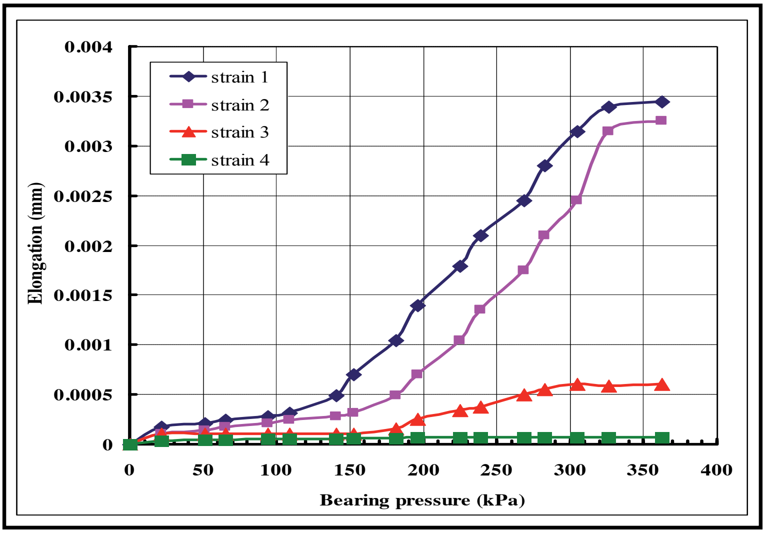

Figure 4-28 The relationship between elongation in ribs of first geogrid layer (Tensar SS2) and applied stress to reinforced sand using rectangular footing footing

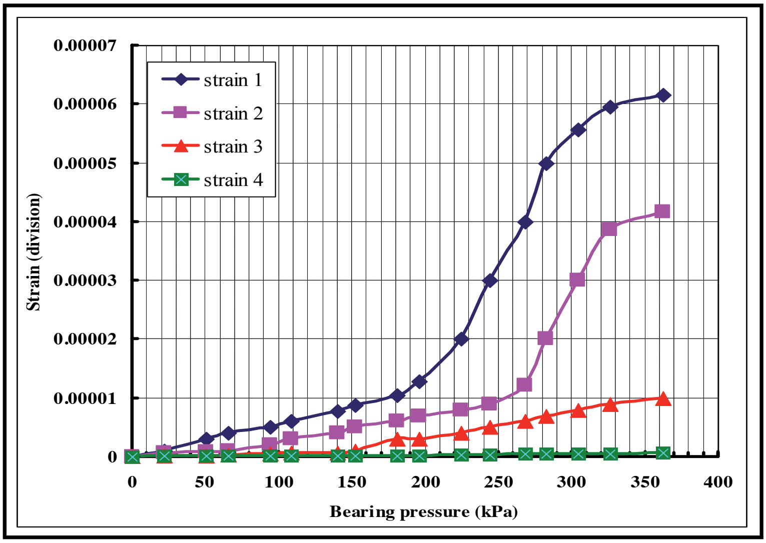

Figure 4-29 The relationship between strain in ribs of second geogrid layer (Tensar SS2) and applied stress to reinforced sand using rectangular footing footing

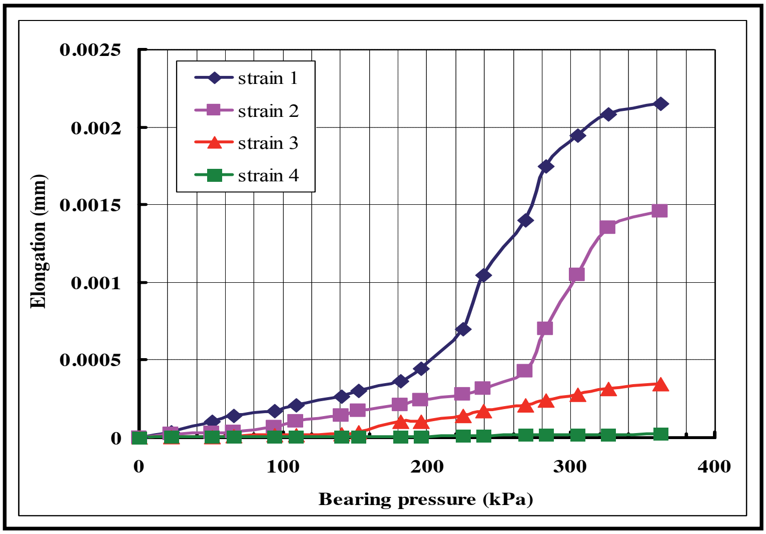

Figure 4-30 The relationship between elongation in ribs of second geogrid layer (Tensar SS2) and applied stress to reinforced sand using rectangular footing footing

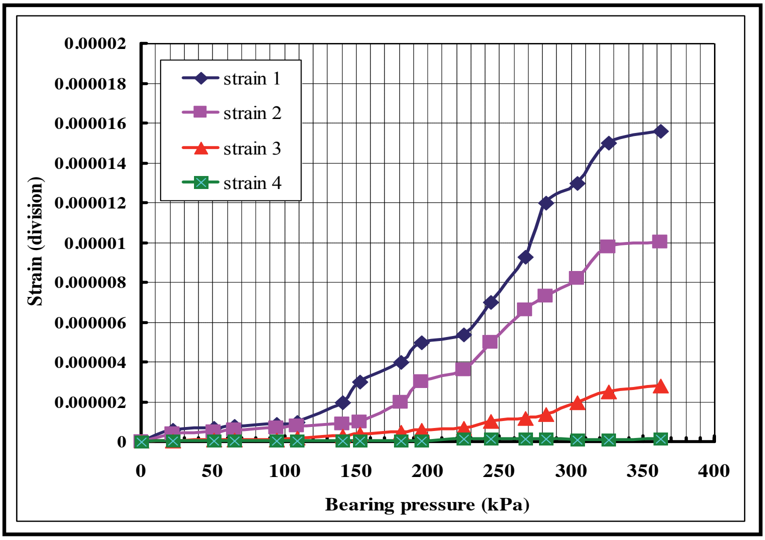

Figure 4-31 The relationship between strain in ribs of third geogrid layer (Tensar SS2) and applied stress to reinforced sand using rectangular footing footing

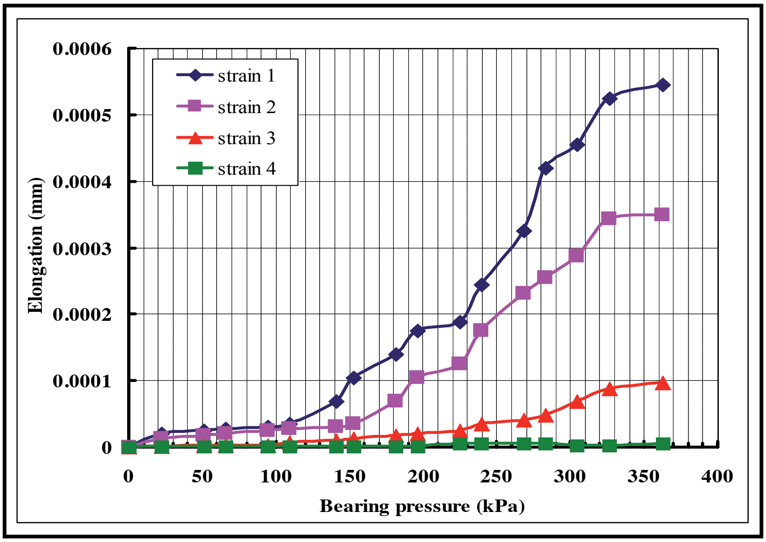

Figure 4-32 The relationship between elongation in ribs of third geogrid layer (Tensar SS2) and applied stress to reinforced sand using rectangular footing

Horizontal and vertical strain distribution

The horizontal distribution of strains occurring in strain gauges which are pasted on the ribs of geogrid are demonstrated in Figs. 4-33 and 4-34. The values shown in these figures are recorded at the ultimate bearing capacity.

Figure 4-33 demonstrates the relationship between the horizontal distance, relative distance, and strain. The relationship shows that the strain gently decreases up to a distance of 1.67B then rapidly dies out. The location of last strain gauge represents the value of 3.6B, which indicates the end of the zone of stress concentration.

Figure 4-34 presents the relationship between the horizontal distance, relative distance, and elongation in ribs of geogrid.

Figure 4-35 shows the vertical relationship between the depth of geogrid under the footing and strain. The relationships are drawn for the values of strain at the ultimate bearing capacity. The strain decreases as the depth under footing increases, the values of strain decrease to a small value for the third layer. Practically the depth B is that where the stress influence vanishes.

Figure 4-36 demonstrates the relationship between elongation and depth, relative depth of gauges. The elongation decreases as the depth increases. The elongation in the rib is very small in depth B.

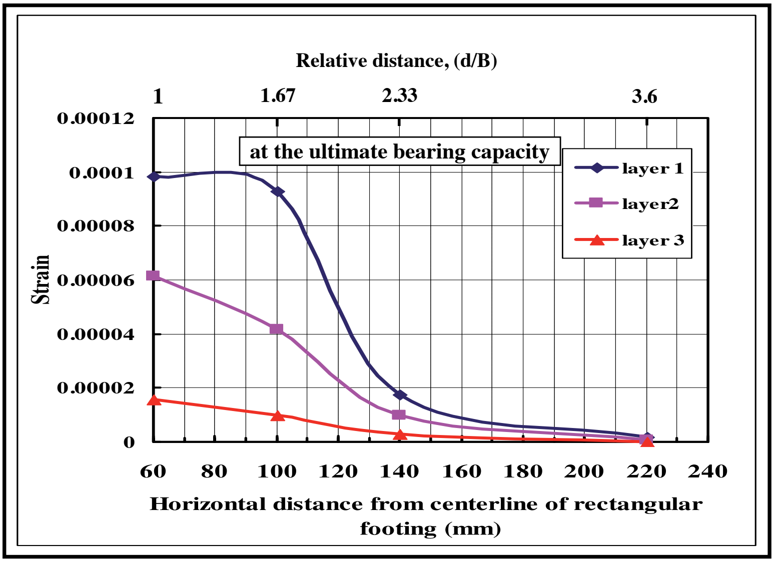

Figure 4-33 The relationship between strain and (relative distance, distance) from the centerline of rectangular footing

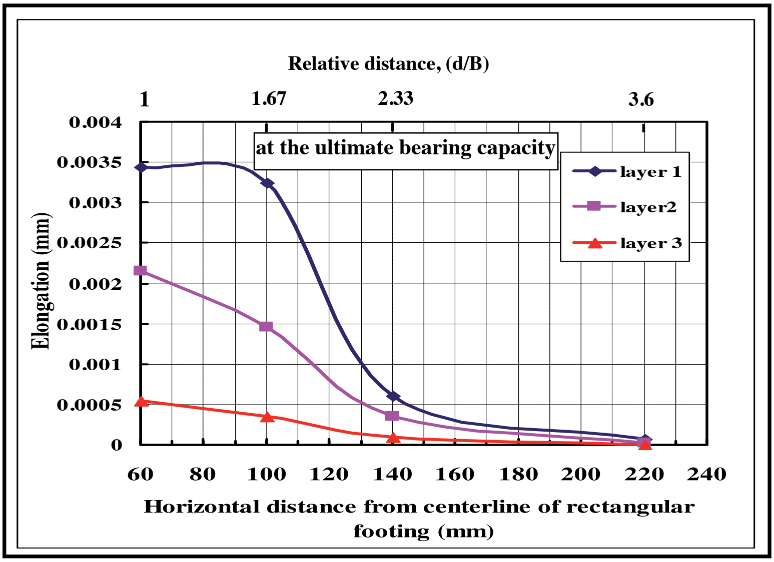

Figure 4-34 Relationship between elongation and (relative distance, distance) from the centerline of rectangular footing

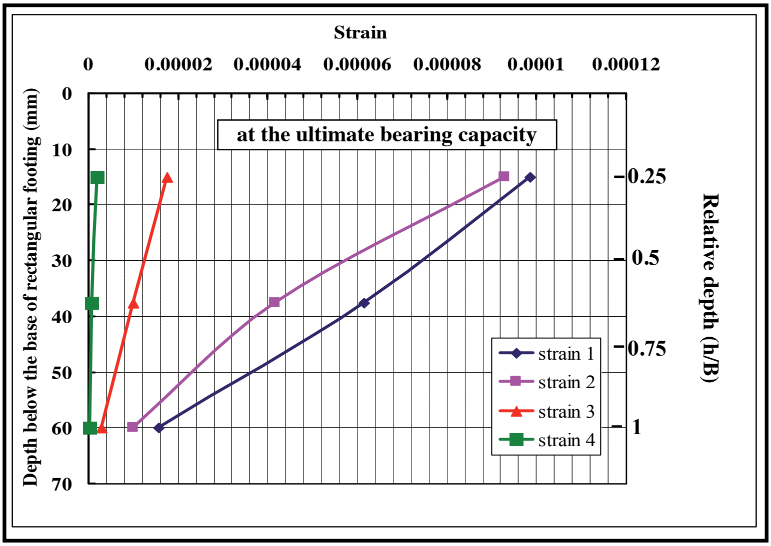

Figure 4-35 Relationship between strain and (relative depth, depth) below the base of rectangular footing

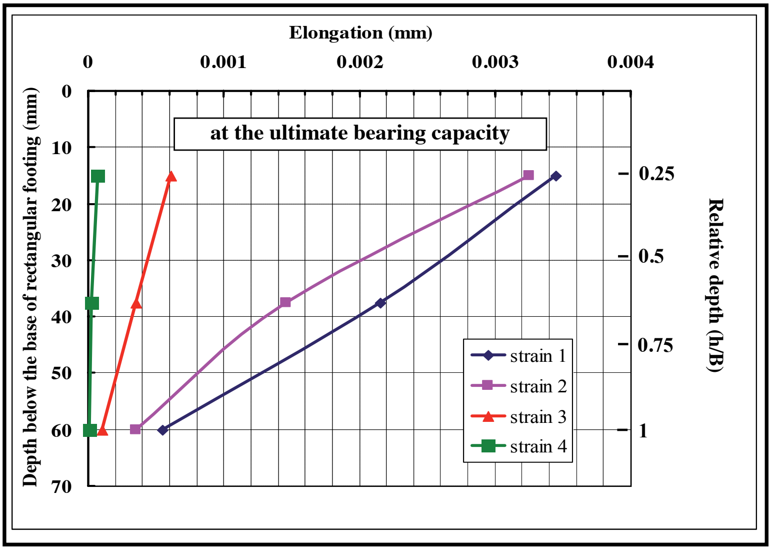

Figure 4-36 Relationship between elongation and (relative depth, depth) below the base of rectangular footing

4.8 Model Tests of Plane Strain Piles

4.8.1 Capacity of Plane Strain Piles under Strip Footing (Piled-Strip System)

The tests using piles under strip footing were performed to simulate the case study of the footing commonly used in the construction of interchange bridges all over the world generally and in Iraq especially. To achieve the plane strain principle in the analysis and design of piles, the piles model shown in Fig. 4-37 was made. The details fit of this model are discussed in chapter three. The pile was positioned under the strip footing in the test box, the load-settlement relation is shown in Fig. 4-38.

Figure 4-37 Plane strain piles model test under strip footing, (Piled-strip)

The settlement increases as the load increases until reaching the maximum capacity of piles-footing system. The maximum recorded load represents the piles capacity as well as the bearing capacity of the residual area of footing at the two sides of piles. This case simulates the case of the construction of interchange bridges.

Figure 4-39 shows a comparison between the results of loading the strip footing with geogrid, without geogrid and the piled-strip. The results clarify that the piled-strip capacity is higher than that of using of geogrids. The x-axis represents the load as a point load for footing and piled-strip not as pressure to integrate the values in comparisons. Total capacity of piled-strip system is higher than the improvement using geogrids because of the sharing of footing in resisting the loads. The improvement using piles reaches 4.4 which represents the ratio of total load using piled-strip system (68.2 kN) to the maximum axial load applied to unreinforced sand (15.5 kN) while these ratios are 1.88 and 2.5 for the improvement using Netlon CE121 and Tensar SS2 respectively. In the construction of bridges it is very important to take into account this case in which the pile cap rest on soil in the design of footings. In this case the footing can distribute the applied load and decrease the load on piles. The calculations of load shares will be discussed in chapter six.

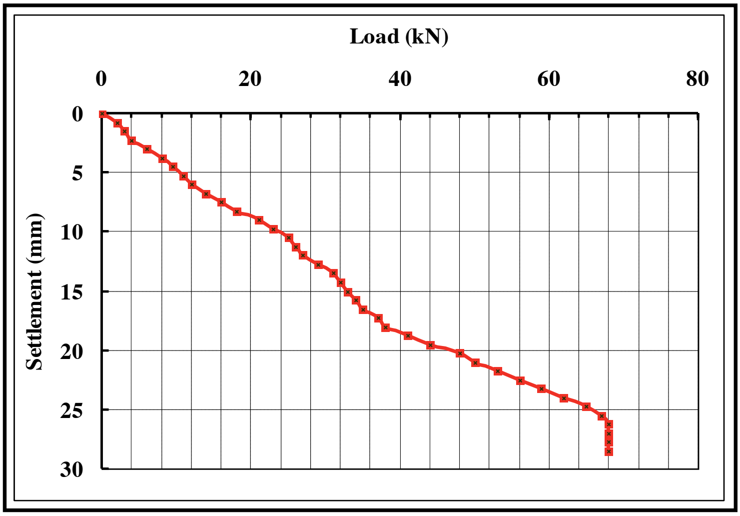

Figure 4-38 Load-Settlement relationship for piled-strip system

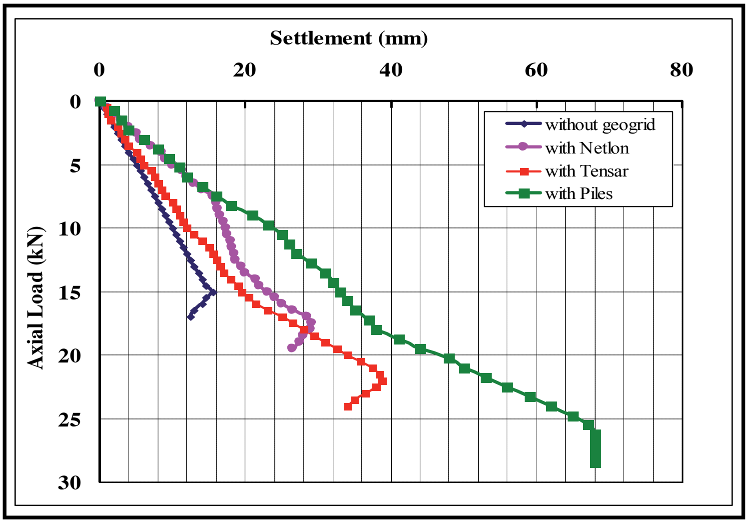

Figure 4-39 Comparison between the results of loading the strip footing with geogrid, without geogrid and the piled-strip system

4.8.2 Skin and End Bearing Piles Capacity

A load test was performed using the plane strain pile model with a gap between the strip and soil to obtain the capacity of piles only (skin and end bearing), (Fig. 4-40). The load-settlement curve for this case is demonstrated in Fig. 4-41. The relationship shows the same behavior of the piled-strip system with a smaller value of load and larger value of settlement because of the exclusion of the area of strip footing.

4.8.3 End Bearing Piles Capacity

This test was made to estimate the end bearing capacity of piles model only. To eliminate the skin friction, silicone grease-latex membrane was applied to the two sides of pile model. This method is successful in eliminating the friction between sand and pile surface. This technique was developed in the past to eliminate end friction in the triaxial specimen and then was used extensively in plane strain bearing capacity tests (Al-Omari, 1984).

Figure 4-40 Details about skin friction and end bearing for piled-strip model test

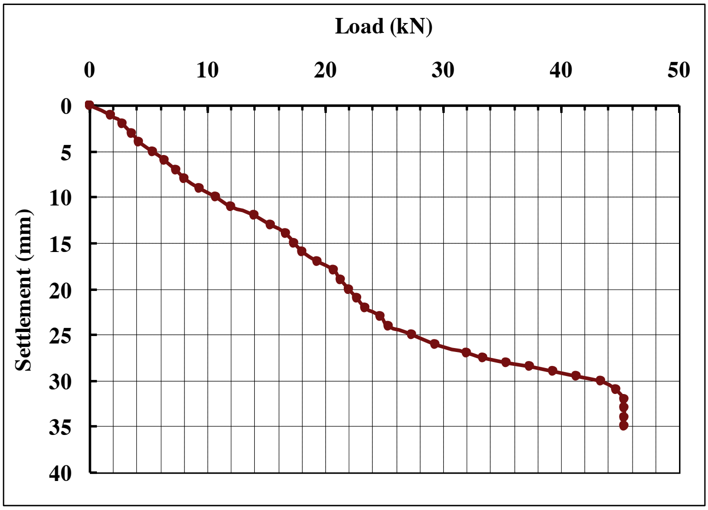

Figure 4-41 Load-Settlement relationship for skin and end bearing only

Figure 4-42 Details about end bearing piled-strip model test

4.8.4 Piled-Strip System Capacity Components

The piles capacity is a combination of end bearing and skin friction. The values of skin friction and end bearing capacity separately are investigated in this study. Figure 4-44 shows the details about skin friction, end bearing and piled-strip. The procedure for separating these values involves many stages as follows:-

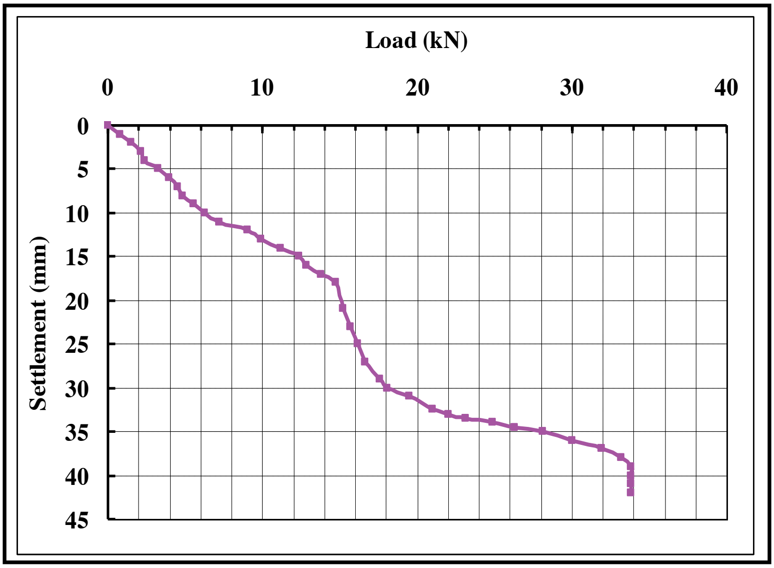

Figure 4-43 Load-Settlement relationship for end bearing only

1- Perform the test as a piled-strip system with strip in contact with soil. (Fig. 4-38)

2- Perform the test as in step 1 except that the strip placed is not in contact with soil using a suitable gap, (Fig. 4-41). From this step, the capacity of pile alone is measured.

3- Perform the tests in step 2 using a rubber membrane with silicon grease applied on the two sides of the piles model to eliminate the effect of friction between the sand and pile, the capacity of pile without friction was recorded, (Fig. 4-43).

4- The differences between the results obtained in steps 2 and 3 above yield the skin friction and end bearing capacity separately.

For example, the following data is taken to represent the calculations.

Pile-Footing system capacity = 68 kN (step 1 above)

Piles capacity (skin and bearing) = 45 kN (step 2 above)

Piles without skin (using lubrication) = 34 kN (step 3 above)

Then,

Skin friction = 45 – 34 = 11 kN (step 4 above)

Strip footing share = 68 – 45 = 23 kN = 33.8 % of total capacity.

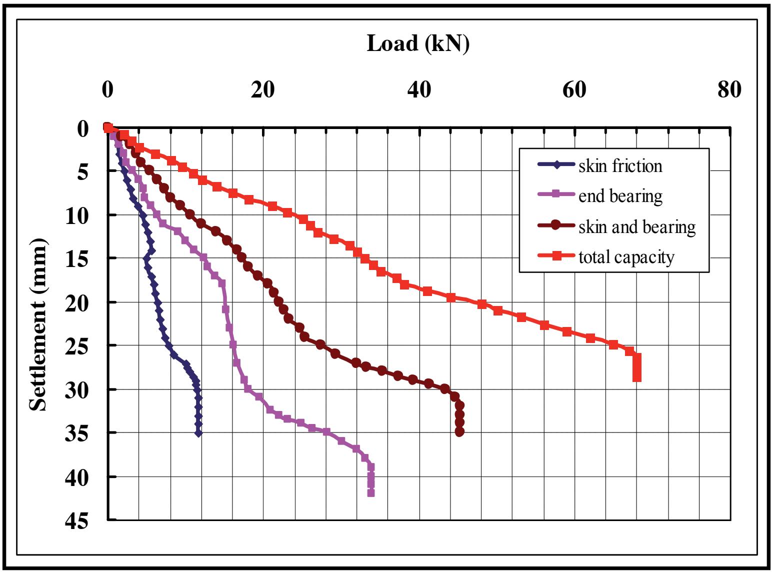

Figure 4-44 Details about skin friction and end bearing for piled-strip

4.9 Model Tests of Piled-Rectangular Footing

4.9.1 Full Capacity

The tests using piles under rectangular footing were performed using three single piles to make a group of piles as presented in chapter three. This case simulates a method in construction of interchange bridges. The rectangular piles model test is shown in Fig. 4-45. The piles were placed under the rectangular footing in the test box and the load-settlement relation is shown in Fig. 4-46.

Figure 4-45 Rectangular piles model test

The relationship shows that the settlement increases as the load increases until reaching the maximum capacity of pile-footing system. The maximum recorded load represents the piles capacity as well as the bearing capacity of the residual area of footing.

Figure 4-47 shows the comparison between the results of loading the rectangular footing without geogrid, with geogrid and piles. The results show that the pile option gives capacity higher than that of geogrid. The improvement ratio using piled-rectangular system reaches 2.6, this case is not a plane strain. The improvement marked a smaller improvement ratio than piled-strip system using plane strain condition. The improvement

ratio using the geogrid option is 2.35 and 2.9 using Netlon CE121 and Tensar SS2 respectively.

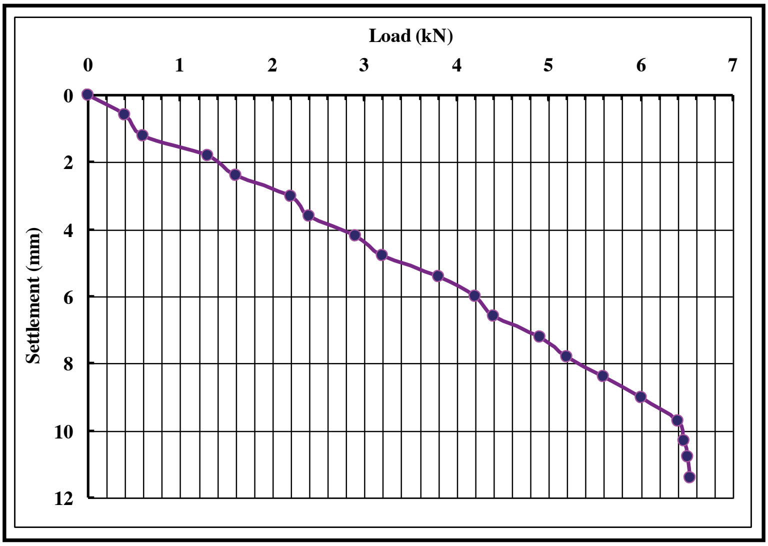

Figure 4-46 Load-Settlement relationship for piles under rectangular footing

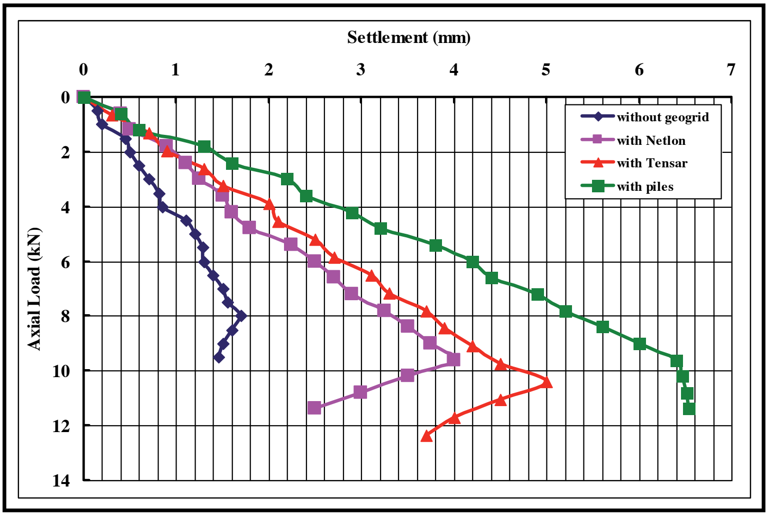

Figure 4-47 Comparison between the results of loading the rectangular footing without geogrid, with geogrid and with piles

4.9.2 Skin and End Bearing Piles Capacity

The test was performed using the rectangular piles under rectangular footing model with a gap between the footing and soil to obtain the capacity of piles only (skin and end bearing), (Fig. 4-48). The load-settlement curve for this case is demonstrated in Fig. 4-49. The relationship shows the same behavior of the piled-rectangular system with a smaller value.

4.9.3 End Bearing Piles Capacity

The test was conducted to estimate the end bearing capacity of rectangular piles model only. To eliminate the skin friction, rubber membranes were pasted on the four sides of piles model using silicon grease. As presented earlier this method is preferable to give the wall of piles model a high smoothness, then, the recorded capacity with a gap between footing and soil represents the end bearing piles capacity only. Figures 4-50 and 4-51 show the laboratory test and load-settlement relationship for this case.

Figure 4-48 Details of skin friction and end bearing for rectangular piles model test

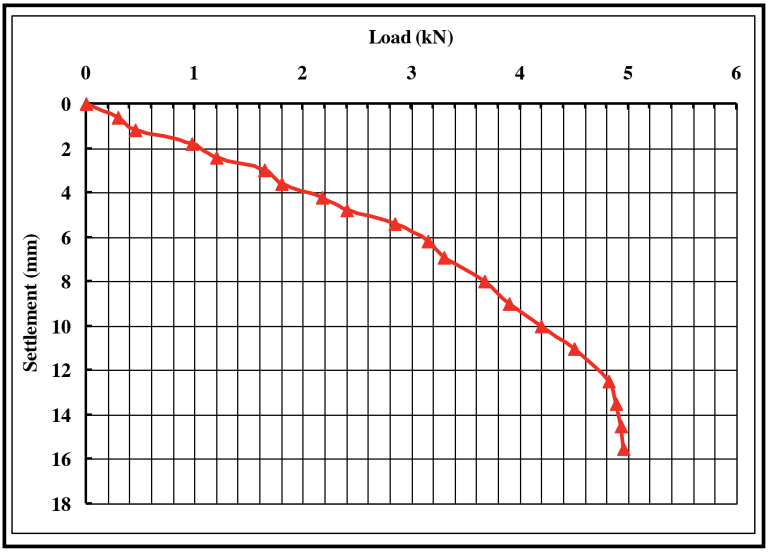

Figure 4-49 Load-Settlement relationship for skin and end bearing only of rectangular piles

4.9.4 Piled-Rectangular System Capacity Components

The same procedure of piled-strip system is repeated for the piled-rectangular. The values of skin friction and end bearing capacity are separated in this section. Figure 4-52 shows the details skin friction and end bearing for piles group under rectangular footing. The procedure for separating these values involves many stages as follows:-

1- Perform the test as a pile-footing system (rectangular on soil)

2- Perform the test as in step 1 except that the footing is placed using a suitable gap from the soil. From this step, the capacity of piles without footing was recorded.

3- Perform the test using rubber membranes with silicon grease applied to the four sides of each pile to eliminate the friction between the soil and piles. The capacity of piles without friction was recorded.

4- The difference between the values obtained in steps 2 and 3 above yields the skin friction and end bearing capacity separately.

For example, the following data was taken to represent the calculations.

Piles-Footing system capacity = 6.4 kN (step 1 above)

Piles capacity (skin and bearing) = 4.8 kN (step 2 above)

Piles without skin (using lubrication) = 3.5 kN (step 3 above)

Then,

Skin friction of piles = 4.8 – 3.5 = 1.3 kN (step 4 above)

Rectangular footing share = 6.4 – 4.8 = 1.6 kN = 25 % of total capacity.

Figure 4-50 Details of end bearing of rectangular piles model test

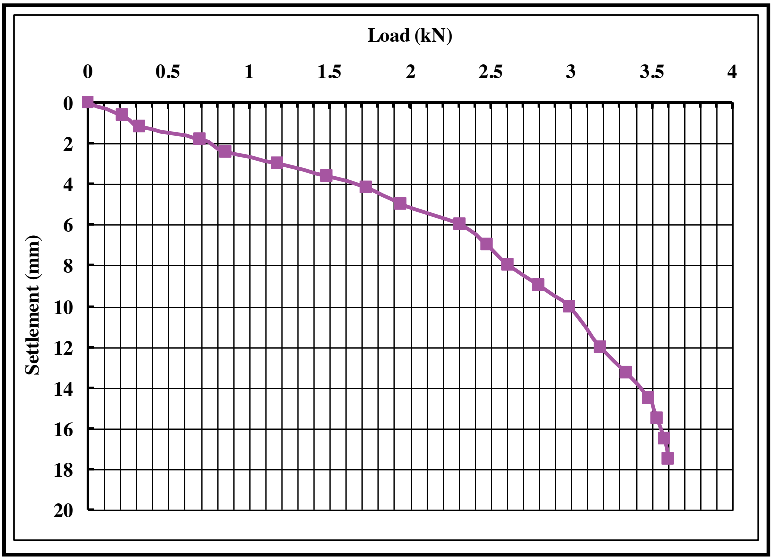

Figure 4-51 Details of end bearing only for piles under rectangular footing

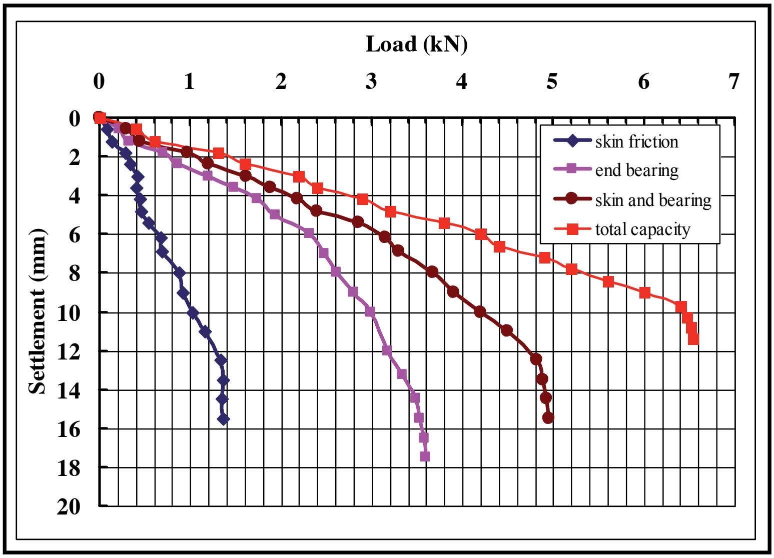

Figure 4-52 Details of skin friction and end bearing for piles under rectangular footing

CHAPTER FIVE

COMPARISON BETWEEN NUMERICAL RESULTS AND EXPERIMENTAL RESULTS

5.1 Introduction

In this chapter, the theoretical results of bearing capacity limit equilibrium methods of Terzaghi's, Meyerhof's, and Vesic's equations are compared with experimental footings. The finite element method results using 3D PLAXIS software are presented in this chapter. PLAXIS 3D FOUNDATION is a three-dimensional finite element program especially developed for the analysis of foundation structures, including off-shore foundations. It combines simple graphical input procedures, which allow the user to automatically generate complex finite element models, with advanced output facilities and robust calculation procedures. The program is designed such that a user can analyze complex constructions after only a few hours of training. The comparisons between numerical and experimental results are presented in this chapter too.

5.2 Theoretical Results

In this section, the bearing capacity of the two types of footing (strip and rectangular) and the capacity of two types of pile foundation (piled-strip and piled-rectangular) will be investigated. The approach used to estimate the bearing capacity of footings and piles will be the classical which is explained in most text books .

5.2.1 Bearing capacity

Bowles (1996) presented many equations to estimate the bearing capacity of footing. These equations are Terzaghi's, Meyerhof's, Hansen's and Vesic's. As Hansen's

and Meyerhof's equations are similar to the case of this study, Meyerhof's equation will be employed here.

5.2.1.1 Strip Footing

To estimate the bearing capacity of a strip footing, the value of angle of internal friction Ø° of the used soil as a plane strain value must be known. ***Bowles (1996)*** indicated that the plane strain Ø° can be concluded from the Triaxial Ø° as:

$Ø^{o}_{ps} = 1.1\ Ø^{o}_{Tr}$ (for $Ø^{o}_{Tr} \geq 30^{o}$)

$Ø^{o}_{Tr} = 40^{o}$ (as estimated in this study, chapter three)

Then,

Used $Ø = Ø^{o}_{ps} = 1.1 \times 40^{o} = 44^{o}$

1- Terzaghi's Equation:

$$q_{ult} = c\, N_c\, s_c + \bar{q}\, N_q + 0.5\, \gamma\, B\, N_\gamma\, s_\gamma \qquad \ldots 5\text{-}1$$

where

c = cohesion of soil under footing

N_c, N_q *and* N_γ = bearing capacity factors from the Terzaghi equations.

	strip	circular	square
s_c =	1.0	1.3	1.3
s_γ =	1.0	0.6	0.8

$\bar{q} = \gamma D_f$

γ = density of soil (similar above and under footing base).

D_f = depth of footing.

B = width of footing.

For this study the first and second terms are equal to zero because of the zero value of cohesion of used in-situ soil and the footing from the surface without surcharge ($D_f = 0$), then equation 5-1 becomes:

$$q_{ult} = 0.5\,\gamma\,B\,N_\gamma\,s_\gamma \qquad \text{...5-2}$$

($\gamma = 16.7\ kN/m^3$, $B = 0.135\ m$, $N_\gamma = 258.08$ for $Ø^o = 44^o$ and $s_\gamma = 1$) and with substitution in equation 5-2, **q_{ult} = 290.9 kPa.**

2- Meyerhof's Equation

$$q_{ult} = 0.5\,\gamma\,B\,N_\gamma\,s_\gamma\,d_\gamma \qquad \text{...5-3}$$

(the first and second terms of the equation are neglected).

$N_\gamma = 228.56$

$s_\gamma = 1$

$d_\gamma = 1$, substitution in the equation,

q_{ult} = 257.64 kPa.

3- Vesic equation

$$q_{ult} = 0.5\,\gamma\,B\,N_\gamma\,s_\gamma\,d_\gamma \qquad \text{...5-4}$$

(the first and second terms of the equation are neglected).

$d_\gamma = 1$ for all $Ø$

$N_\gamma = 238.9$ and $s_\gamma = 1$, substitution in the equation,

q_{ult} = 269.3 kPa.

5.2.1.2 Rectangular Footing

The same procedure can be repeated for the rectangular footing with $B = 0.06\ m$. The value of angle of internal friction Ø° can be used in the plane strain condition because L/B = 0.23/0.06 = 3.8 > 2 (Bowles, 1996).

1- Terzaghi's Equation:

(γ = 16.7 kN/m^3, B = 0.06 m, N_γ = 258.08 for Ø° = 44° and s_γ =1) and with substitution in equation 5-1 , **q_{ult} = 129.3 kPa.**

2- Meyerhof's Equation

(γ = 16.7 kN/m^3, B = 0.06 m, L = 0.23 m, N_γ = 228.56 for Ø° = 44°)

$s_\gamma = 1 + 0.1\ K_p(B/L)$

$K_p = tan^2(45 + Ø/2) = tan^2(45 + 44/2) = 5.55$

then,

$s_\gamma = 1 + 0.1 \times 5.55 \times (0.06/0.23) = 1.145$

d_γ= 1, substitution in the equation 5-2,

q_{ult} = 131.1 kPa.

3- Vesic equation

(γ = 16.7 kN/m^3, B = 0.06 m, L = 0.23 m, N_γ = 238.9 for Ø° = 44°)

s_γ=1- 0.4 (B/L) = 1 – 0.4 (0.06/0.23)=0.896.

substitution in the equation 5-3,

q_{ult} = 107.2 kPa.

5.2.2 Piles Capacity

5.2.2.1 Plane Strain Piles

As presented in chapter two, the plane strain principle is applied in this study to analyze the piled-strip. Due to complexity of this case in the calculation of piles capacity, the effect of footing is not included in the calculation of piles capacity. To calculate the capacity of piles, the following procedure can be followed:

$$Q_{ult} = Q_b + \sum Q_s \qquad \ldots 5\text{-}5$$

$$Q_b \leq Q_{b\,max}$$

$Q_{b\,max}$ for sand (c = 0) = (50 N_q tan Ø) A_b …5-6

$Q_{b\,max}$ for (c ≠ 0) = (c_b N_c + 50 N_q tan Ø) A_b …5-7

The total capacity of a single pile can be calculated by the following equation:

$Q_{ult\,(s.p)} = (c_b N_c + q N_q) A_b + \sum(\alpha c_s + \sigma_v K \tan \delta)A_s$ …5-8

For sandy soil c_b and c_s equals to zero.

q = soil pressure from the ground surface to the end of pile.

N_q = Using figure 5-1.

α term can be neglected for c = 0.

σ_v = vertical pressure of soil from the ground surface to the mid- height of pile within the layer.

A_b and A_s, are bearing area and skin friction area respectively.

Then, equation 5-8 can be written as:

$Q_{ult} = (q N_q) A_b + (\sigma_v K \tan \delta) A_s$ …5-9

$q = \gamma \times L = 16.7\ kN/m^3 \times 0.6\ m = 10.02\ kN/m^2$.

N_q = 380 (Figure 5-1, Ø = 44).

$A_b = 0.03\ m \times 0.48\ m = 0.0144\ m^2$.

$\sigma_v = 16.7\ kN/m^3 \times 0.3\ m = 5.01\ kN/m^2$.

k = (1- sin 44) = 0.305.

δ = Ø = 44º.

$A_s = (0.48\ m \times 0.6\ m) \times 2$ sides $= 0.576\ m^2$.

Then, substitution in equation 5-9:

$Q_{ult} = (10.02 \times 380)\ 0.0144 + (5.01 \times 0.305 \times \tan 44)\ 0.576$

Q_{ult} = 54.8 kN + 0.85 kN = 55.6 kN (for pile only from experimental Q_{ult} = 45 kN)

5.2.2.2 Rectangular Piles

The same procedure can be considered for the three rectangular piles which are used under rectangular footing. The same data above except A_b and A_s can be used as:

$A_b = 0.03\ m \times 0.03\ m \times 3\ piles = 0.0027\ m^2$.

$A_s = 4 \times 0.03\ m \times 0.4\ m \times 3\ piles = 0.144\ m^2$.

$q = \gamma \times L = 16.7\ kN/m^3 \times 0.4\ m = 6.68\ kN/m^2$.

$\sigma_v = 16.7\ kN/m^3 \times 0.2\ m = 3.34\ kN/m^2$.

Then,

$Q_{ult} = (6.68 \times 180)\ 0.0027 + (3.34 \times 0.357 \times \tan 40)\ 0.144$

Q_{ult} = 3.25 kN + 0.144 kN = 3.39 kN (for piles only from experimental Q_{ult} = 4.9 kN)

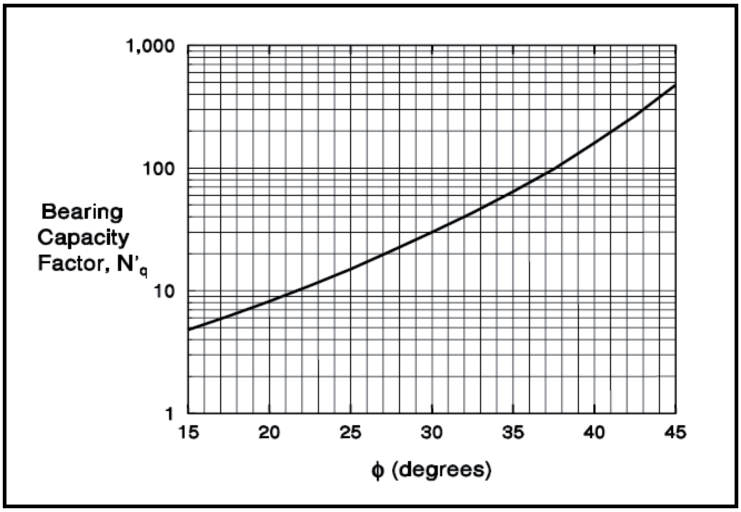

Figure 5-1 Bearing capacity factor N_q for piles, (FHWA, 2006a)

5.3 Numerical Investigation

5.3.1 3D PLAXIS Software

PLAXIS 3D is a finite element package intended for three-dimensional analysis of deformation and stability in geotechnical engineering. It is equipped with features to deal with various aspects of complex geotechnical structures and construction processes using robust and theoretically sound computational procedures.

With PLAXIS 3D, complex geometry of soil and structures can be defined in two different modes. These modes are specifically defined for Soil or Structural modeling. Independent solid models can automatically be intersected and meshed.

The staged constructions mode enables a realistic simulation of construction and excavation processes by activating and deactivating soil volume clusters and structural objects, application of loads, changing of water tables, etc. The output consists of a full suite of visualization tools to check details of the complex inner structure of a full 3D underground soil-structure model.

PLAXIS 3D is a user friendly 3d geotechnical program offering flexible and interoperable geometry, realistic simulation of construction stages, a robust and reliable calculation kernel, and comprehensive and detailed post-processing, (Available at http://www.plaxis.nl/plaxis3d/).

5.3.1.1 The Input Program

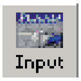

The above icon represents the Input program. This program consists of two different modes: *Model* and *Calculation*. The *Model* mode contains all facilities to create and to modify a geometry model and to generate a 2D and 3D finite element mesh. The *Calculation* mode contains all facilities to define calculation phases representing different stages of loading or construction, including the initial situation.

At the start of the Input program a dialog box appears in which a choice must be made between the selection of an existing project and the creation of a new project. When selecting New project the General settings window appears in which the basic model parameters of the new project can be set. When selecting *Existing project*, the dialog box

allows for a quick selection of one of the four most recent projects. If an existing project is to be selected that does not appear in the list, the option <<<*More files*>>> can be used (Fig. B-1, appendix B).

5.3.1.2 Starting The Program

It is assumed that the program has been installed correctly. It is advisable to create a separate directory in which data files are stored. The PLAXIS 3D FOUNDATION program can be started by selecting the *PLAXIS 3D FOUNDATION input* icon in the PLAXIS 3D FOUNDATION program group. The user is asked whether to define a new problem or to retrieve a previously defined project. If the latter option is chosen, the program lists four of the most recently used projects from which a direct choice can be made. Choosing the item "more files" that appears first in this list will give a file requester from which the user can choose any previously defined project for modification. The procedure of creating a model for each case will be presented in the next sections.

5.4 Strip Footing Modeling and Results

5.4.1 Unreinforced Soil

The modeling of a strip footing adopts the same dimensions of the laboratory model. Figure B-2 in appendix B shows the general setting of the model, the following steps will be followed to achieve the modeling:-

1- ***Creating the input***: Start the PLAXIS 3D FOUNDATION input program. A *Create/Open project* dialog box will appear in which an existing project can be selected or create a new one. Choose *New Project* and click the <OK> button. Now the *General settings* window appears, consisting of the two tab sheets *Project* and *Dimensions*, (Fig. B-2, appendix B).

2- ***General setting***: The first step in every analysis is to set the basic parameters of the finite element model. This is done in the General settings window. These settings include the description of the problem, the basic units and the size of the draw area.

To enter the appropriate settings for the raft foundation calculation the following steps may be employed;

- In the Project tab sheet, enter 'strip alone' in the Title box.
- The general box indicates a fixed gravity of 1.0 G, in the vertical direction downward (-Y). Also, the value of the acceleration of gravity (1.0 G) can be entered in the Earth gravity box. This should be kept to the default value of 9.8 m/s^2.
- In the γ_{water} box the unit weight of water can be entered. Keep this to the default value of 10 kN/m^3. Click the <Next> button below or click the Dimensions tab sheet.
- The dimensions tab sheet, keep the default units in the Units box (Unit of Length = m; Unit of Force = kN; Unit of Time = day).
- In the Geometry Dimensions box the size of the required draw area must be entered. When entering the upper and lower coordinate values of the geometry to be created, a small margin is automatically added so that the geometry will fit well within the draw area. Enter –0.5, 0.5, -0.25, 0.25 for X_{min}, X_{max}, Z_{min}, Z_{max} respectively.
- The *Grid* box contains the settings for the grid spacing. The grid provides a matrix of dots on the screen that can be used as reference points. It may also be used for snapping to regular points during the creation of a geometry. The distance between the dots is determined by the *Spacing* value. The spacing of snapping points can be further divided into smaller intervals by the *Number of intervals* value. Enter 0.25 for the spacing and 100 for the intervals.
- Click the <OK> button to confirm the settings. Now the draw area appears in which the geometry model can be drawn.

3- ***Work-planes:*** Work-planes are horizontal layers with different *y*-coordinates, at which the structural objects, loads and construction stages can be defined. Work-planes are needed at each level where a discontinuity in the geometry or the loading

occurs in the initial situation or in the construction process. They are defined in the *Work-planes* window. This window can be opened with the *Work-planes* button, found on the toolbar just left of the *Active Work-plane* combo-box, or from the *Work-planes* option in the *Geometry* menu. One work-plane has already been automatically created at *y* = 0.00. For this first project, we need to define two additional work-plane must be defined. To do this, follow these steps:

Open the *Work-planes* window by clicking the *Work-planes* button on the toolbar. A new window will appear, in which the automatically generated work-plane at *y* = 0 is shown. A vertical cross section is shown, indicating in red the currently selected *y*-coordinate.

- Click the <Add> button. A new work-plane is inserted at *y* = -0.6 m, below the current work-plane, (Fig. B-3, appendix B).
- Click the <OK> button to close the *Work-planes* window and return to the draw area.

4- ***Geometry of the case:*** To create the geometry of the strip footing, the strip can be drawn by moving the *geometry line* from the center point in *x* and *y* direction. Figure B-4 in appendix B shows the final geometry of the strip footing case.

5- ***Loads:*** The point load option can be selected to fix the load on the center of footing. The red point at the center of footing shown in Fig. B-4 in appendix B represents the point load acts on the footing.

6- ***Borehole:*** All information on the geometry in the vertical direction has been entered using work planes. Information on the soil layers and the water table is entered in a different way, using so called *Boreholes*. Boreholes are locations in the draw area at which the information on the location of soil layers and the water table is given. If multiple boreholes are defined, PLAXIS 3D FOUNDATION will automatically interpolate between the boreholes, and derive the position of the soil layers from the borehole information. Figure B-5 in appendix B shows the Borehole option and the required information about the water table which is neglected in the present case and the icons and tool box of the choosing materials of soil and footing.

Table 5-1 shows the properties of soil and the properties of the model of footing.

7- ***2D Mesh Generation:*** When the geometry model is complete and all borehole information has been entered, it is recommended to generate a 2D finite element before generating a full 3D mesh. PLAXIS 3D FOUNDATION allows for a fully automatic mesh generation procedure, in which the geometry is divided into volume elements and compatible structure elements , if applicable. The mesh generation takes full account of the position of lines and points in the geometry model, so that the exact position of layers, loads and structures is accounted for in the finite element mesh. The 2D mesh generation process is based on a robust triangulation principle that searches for optimized triangles and which results in an unstructured mesh.

Table 5-1 The properties of soil and the properties of the model of footing

Parameter	**Name**	**Value**	**Unit**
Material model	*Model*	Mohr-Coulomb	-
Type of material behavior	*Type*	Drained	-
Unit weight of soil above phreatic level	γ_{unsat}	16.7	kN/m^3
Unit weight of soil below phreatic level	γ_{sat}	16.7	kN/m^3
Young's modulus (constant)	E_{ref}	65500*	kN/m^2
Poisson's ratio	ν	0.3	-
Cohesion (constant)	c_{ref}	0.21**	kN/m^2
Friction angle	φ	44	degrees
Dilatancy angle	ψ	14***	degrees
Parameter	**Name**	**Footing Floor**	**Unit**
Type of behavior	Type	Linear	-
Thickness	d	0.01	m
Unit weight	γ	78	kN/m^3
Young's modulus	E	200	GPa
Shear modulus	G	8.33 10^7	kN/m^2
Poisson's ratio	ν	0.2	-

*(Bowles, 1996)
**PLAXIS can handle cohesionless sands (c = 0), but some options will not perform well. To avoid complications, nonexperienced users are advised to enter at least a small value (use c > 0.2 kPa).
*** $\psi \approx \varphi - 30°$ (Bolton, 1986).

Although unstructured meshes do not form regular patterns of elements, the numerical performance of these meshes is usually better than that of structured meshes with regular arrays of elements. In addition to the mesh generation itself, a transformation of the input data (properties, boundary conditions, material sets, etc.) from the geometry model (points, lines and clusters) to the finite element mesh (elements and nodes) is made, (Fig. B-6, appendix B).

8- ***3D Mesh Generation:*** After generation of the 2D mesh, the model must be extended to a fully 3D mesh. This can be done by clicking on the 3D mesh generation button or selecting the corresponding option from the *Mesh* menu. The information in vertical direction on layer boundaries, construction levels and changes in the geometry has already been entered, using work-planes and boreholes. No extra information is needed in order to generate the 3D mesh. The 3D mesh is created by connecting the corners of the 2D triangular elements to the corresponding points of the corresponding elements in the next work-plane. In this way a 3D mesh, composed of 15-noded wedge elements is formed. Where needed extra element levels are automatically introduced, so that the size of the elements in y-direction is about equal to the average element size defined for the 2D mesh. If multiple boreholes are used and not all layers are present in all boreholes, so-called degenerated elements will be introduced, to deal with the transition between the various layers (Fig. B-7, appendix B).

9- ***Performing Calculations:*** Once the mesh has been generated, the finite element model is complete. Before the actual calculation is started, the calculation stages have to be defined. The first of these will be the definition of initial conditions. Other stages can be the excavation and construction of the basement or the activation of loads. The definition of calculation stages, such as switching on and off parts of the geometry, assigning different material data sets to clusters or structural elements or changing the magnitude of loads, is done in the calculation mode of the Input program. Clicking the <Calculation> button will hide the geometry model toolbar and show the calculation toolbar. This toolbar, (Fig. B-8, appendix B), contains a calculation phases combo box and a number of buttons to

define calculation phases, perform the calculation and activate the *Output* program, in order to view the results. The calculation mode of the Input program is a separate mode where calculation phases are defined and calculations can be started. Clicking the *Phases* button will open the Phases window, (Fig. B-9, appendix B). This may be used to add and delete calculation phases, and to set the parameters for the calculation procedure. All defined calculation phases appear in the list at the lower part of the window.

Initial Conditions: Before starting the actual calculations the initial conditions must be generated. In general, the initial conditions comprise the initial geometry configuration and the initial stress state. The initial water conditions for the clay layer have been entered already in the *Borehole* window. These conditions are also taken into account to calculate the initial effective stress state.

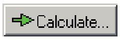

Click the *Calculation* button to switch to calculation mode.

The program proposes to save the model. Press <Yes> to do so and save the model under its predefined name (file name.PF3).

After clicking on the <Calculation> button, the calculation mode of the *Input* program becomes active and the calculation toolbar is shown. When a new project has been defined, a first calculation phase, named 'Initial phase', is automatically created and selected in the *Phase list* combo-box. All structural elements and loads that are present in the geometry are initially automatically switched off, only the soil clusters are initially active.

Except for performing the calculation to generate the initial conditions, no additional actions are needed for this example. However, before starting the calculations, two additional calculation phases will be added.

Defining Construction Stages: After the definition of the initial conditions, the construction of the foundation and the loading can be modelled. This will be done in two separate calculation phases, which need to be added. To do this, apply the following steps:

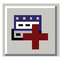

Click the *Next phase* button. This will add a new phase and open the *Phases* window and create a new calculation phase. This will be named <Phase 1> and automatically selected.

The *Parameters* tab sheet, (Fig. B-10, appendix B), contains the calculation control parameters. Change in the *Iterative procedure* box and keep the number of *Additional steps* to 1000. Make sure that *Reset displacements to zero* is checked, in order to reset the (unrealistic) deformations that will be generated during the calculation of the initial stresses in the *Initial phase*.

Double click the grey circle indicating the inactive point load at (0, 0). This will open a *Point load* window, where the magnitude and direction of the load can be entered. Enter load *y* = -3 kN (3 kN acting in the downward *y*-direction) and click <OK>. Make sure the load is activated, indicated by a blue arrow. If necessary, the load can be activated or deactivated by clicking once on the load (Fig. B-11, appendix B).

- Click the *Calculate* button. This will start the calculation process. All calculation phases that are marked for calculation, as indicated by a blue arrow (three phases in this case) will, in principle, be executed in the order controlled by the *Start from phase* parameter.
- During the execution of a calculation a window appears which gives information about the progress of the actual calculation phase, (Fig. B-12, appendix B). The information, which is continuously updated, shows amongst others the calculation progress, the current step number, the global error in the current iteration and the number of plastic points in the current calculation step.
- It will take several minutes to perform the calculation. When a calculation ends, the window is closed and focus is returned to the main window. Also, the *Phase list* is updated, showing a green tick mark to indicate that the calculation was finished successfully.

10- Viewing Output Results: Once the calculation has been completed, the results can be evaluated in the *Output* program. In the *Output* program the displacement and stresses in the full 3D model as well as in the individual work planes or structural elements can be viewed. The computational results are also available in tabular form. To view the results for the current analysis, follow these steps:

- Select the last calculation phase (Loading) in the *Phase list* combo box. Click the *Output* button to open the Output program. The Output program will by default show the 3D deformed mesh at the end of the selected calculation phase. The deformations are scaled to ensure that they are clearly visible.
- Select *Total displacements* from the *Deformations* menu. The plot shows the total displacements of all nodes as arrows, with an indication of their relative magnitude.
- The presentation of combo box in the toolbar currently reads *Arrows*. Select *Shadings* from this combo box. The plot shows color shadings of the total displacements. A legend is presented with the displacement values at the color boundaries.

Figure B-13 in appendix B shows samples of outputs of the case of strip footing on a soil without geogrid. In the next sections, the model of each case will be presented only to explain the case, because of the large number of plots and figures for all cases.

In return to the title of this section, the results of the outputs to draw the pressure-settlement relationship, the results saved in the table in 3D PLAXIS program will be used by taking the nearest values of displacement to the experimental results and the related pressure of numerical results to draw the relationship.

Figure 5-2 shows the comparison between the experimental and numerical results of the bearing pressure and relative settlement for the case of a strip footing on unreinforced soil. The ultimate bearing capacity obtained from the experimental test was 234.3 kPa and from PLAXIS it was 167.8 kPa which represents the last value of pressure on the curve. The procedure of running the program does not permit continuing after the failure, so, the last point on the curve of PLAXIS results represents the pressure at failure.. The agreement between the two results may be considered as reasonable in geotechnical problems. The ratio between ultimate bearing capacities obtained from PLAXIS to that obtained from experimental test is 71.6%.

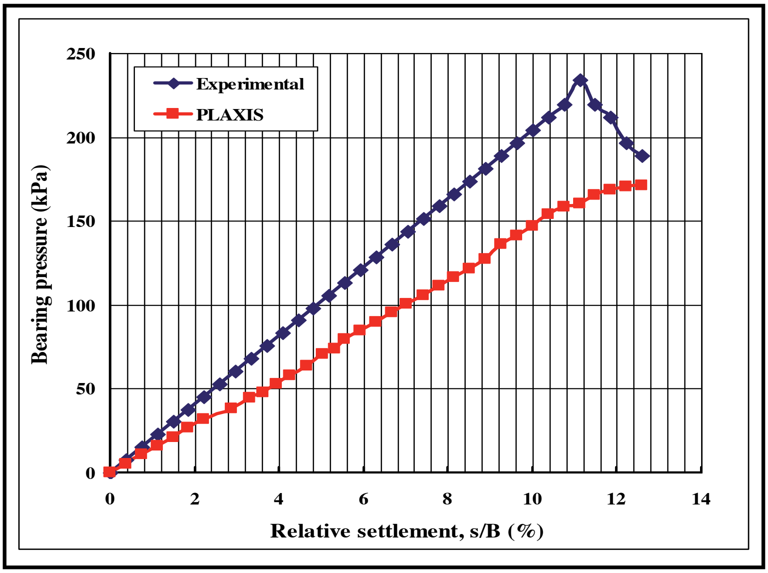

Figure 5-2 Bearing pressure versus relative settlement for strip footing resting on unreinforced sand

5.4.2 Reinforcing Soil Using Netlon CE121 Geogrid

Figure 5-3 shows the 3D PLAXIS model of the strip footing resting on reinforced soil with Netlon CE121 geogrid. Geogrid was modeled as a three layers of thin plates covered the area of model beneath the footing, the depth of each layer is same as of depth used in experimental investigations as 0.25B, 0.625B and B for first, second and third layer respectively. The properties of Netlon CE121 geogrid material are shown in table 5-2. The relationship between bearing capacity and relative settlement of sand using Netlon CE121 for experimental and Plaxis results is presented in Fig. 5-4. The experimental ultimate bearing capacities is 441.4 kPa while that obtained from PLAXIS is 363 kPa. The ratio of numerical to experimental ultimate bearing capacities is 82.2 %, the agreement can be considered as good between the two results.

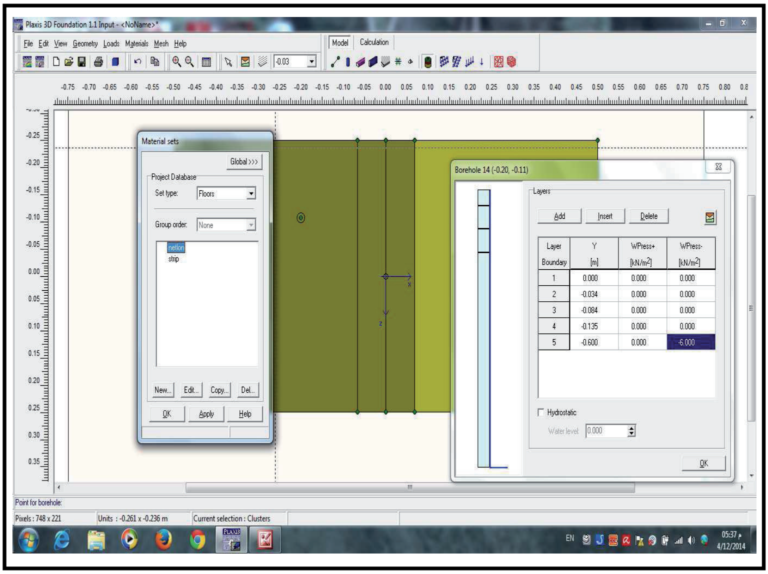

Figure 5-3 Borehole of the strip footing with Netlon CE121 geogrid case

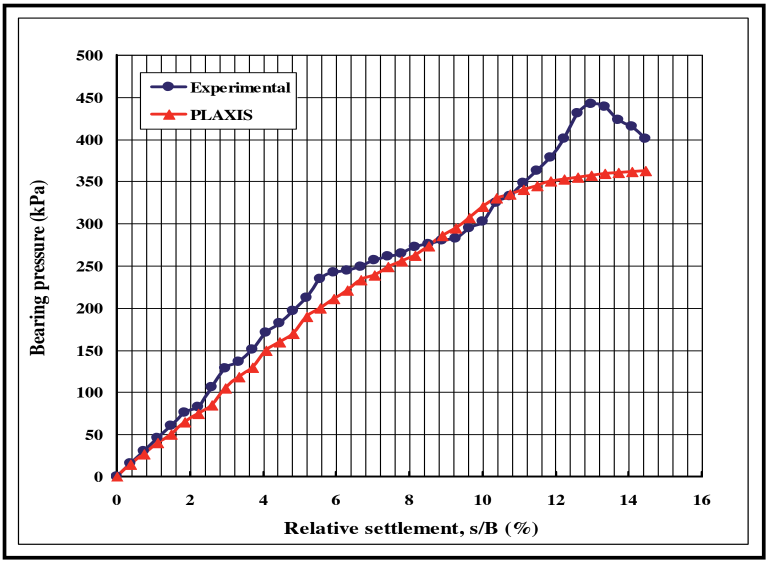

Figure 5-4 Bearing pressure versus relative settlement for strip footing with Netlon CE121 geogrid

5.4.3 Reinforcing Soil Using Tensar SS2 Geogrid

Figure 5-5 shows the 3D Plaxis model of the strip footing resting on reinforced soil with Tensar SS2 geogrid. The properties of Tensar SS2 material modeled in PLAXIS is shown in table 5-2. The relationship between bearing capacity and relative settlement of sand using Tensar SS2 for experimental and PLAXIS results is presented in Fig. 5-6. The experimental ultimate bearing capacities is 586.54 kPa while that obtained from PLAXIS is 460 kPa. The ratio of numerical to experimental ultimate bearing capacities is 78.4 %, the agreement can be considered good.

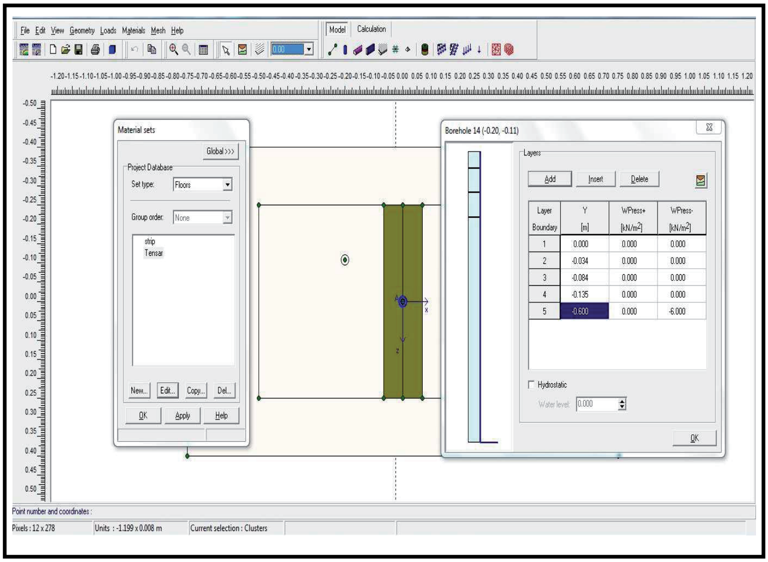

Figure 5-5 Borehole of the strip footing with Tensar SS2 geogrid case

Table 5-2 The properties of geogrids modeled in PLAXIS

	Parameter	Name	Footing	Unit
Netlon CE121	Type of behavior	Type	Linear	-
	Thickness	D	0.0016	m
	Weight	γ	7	kN/m^3
	Young's modulus	E	0.39	GPa
	Shear modulus	G	1.6×10^5	kN/m^2
	Poisson's ratio	N	0.2	-
Tensar SS2	**Parameter**	**Name**	**Footing**	**Unit**
	Type of behavior	Type	Linear	-
	Thickness	D	0.0015	m
	Weight	γ	7.4	kN/m^3
	Young's modulus	E	0.99	GPa
	Shear modulus	G	1.4×10^5	kN/m^2
	Poisson's ratio	N	0.2	-

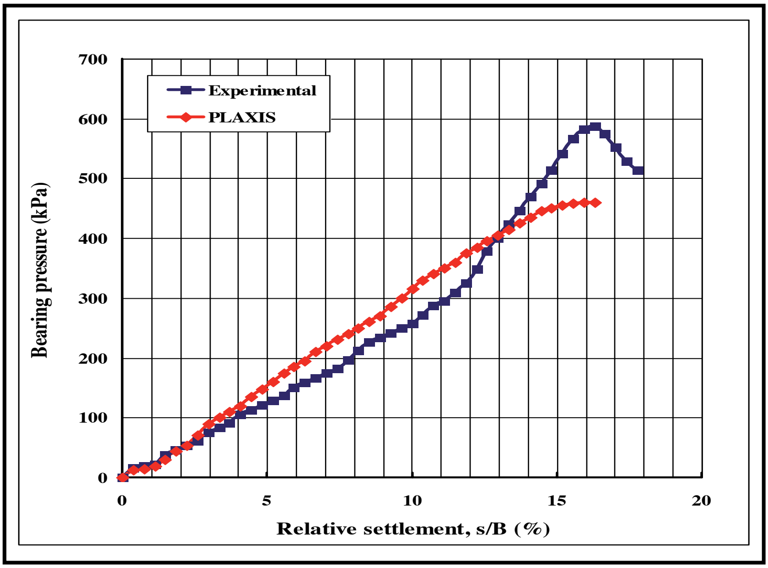

Figure 5-6 Bearing pressure versus relative settlement for strip footing with Tensar SS2 geogrid

5.5 Rectangular Footing Modeling and Results

5.5.1 Unreinforced Soil

Figure 5-7 shows the 3D PLAXIS model of the rectangular footing resting on unreinforced soil. This figure represents the model after generation of 3D mesh as presented in section 5.4.1. The relationship between bearing capacity and relative settlement of sand without geogrid for experimental and PLAXIS results is presented in Fig. 5-8. The experimental ultimate bearing capacities is 123.18 kPa, the numerical analysis by PLAXIS gives a value of 101 kPa. The ratio of numerical to experimental ultimate bearing capacities is 82 %, the agreement between the two results may be considered very good.

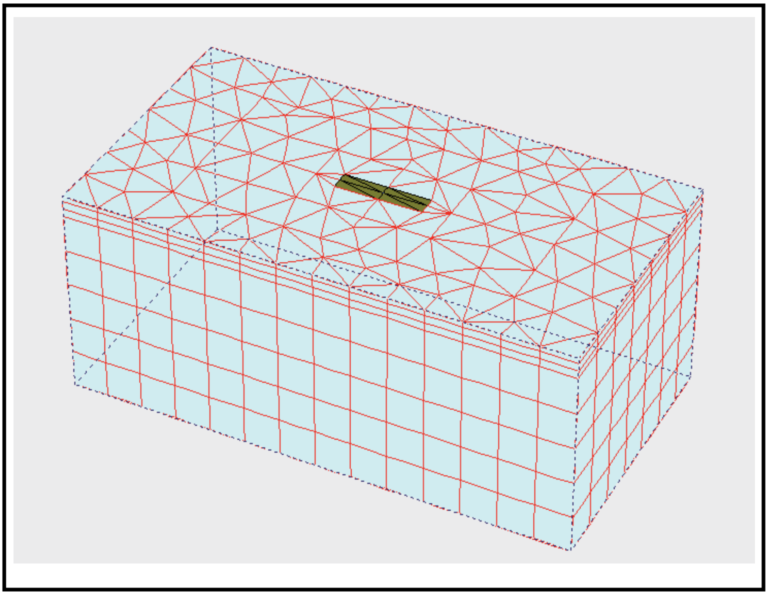

Figure 5-7 The geometry of the rectangular footing case on sand alone

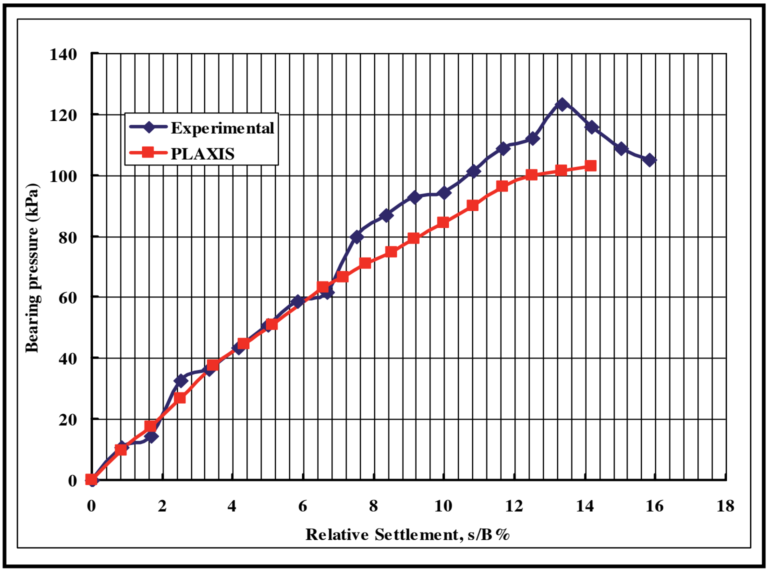

Figure 5-8 Bearing pressure versus relative settlement for rectangular footing resting on sand alone

5.5.2 Reinforcing Soil Using Netlon CE121 Geogrid

The borehole of the input parameters in 3D PLAXIS program is shown in Fig. 5-9, this borehole explains the layers of geogrid and the materials of footing and geogrid mesh. The properties of geogrid are the same as that in modeling of reinforced soil using strip and is shown in table 5-2. The relationship between bearing capacity and relative settlement of sand using Netlon CE 121 for experimental and PLAXIS results is shown in Fig. 5-10. The experimental ultimate bearing capacities is 289.85 kPa while that obtained from PLAXIS is 247 kPa. The ratio of numerical to experimental ultimate bearing capacities is 85.2 %, the agreement may be considered very good.

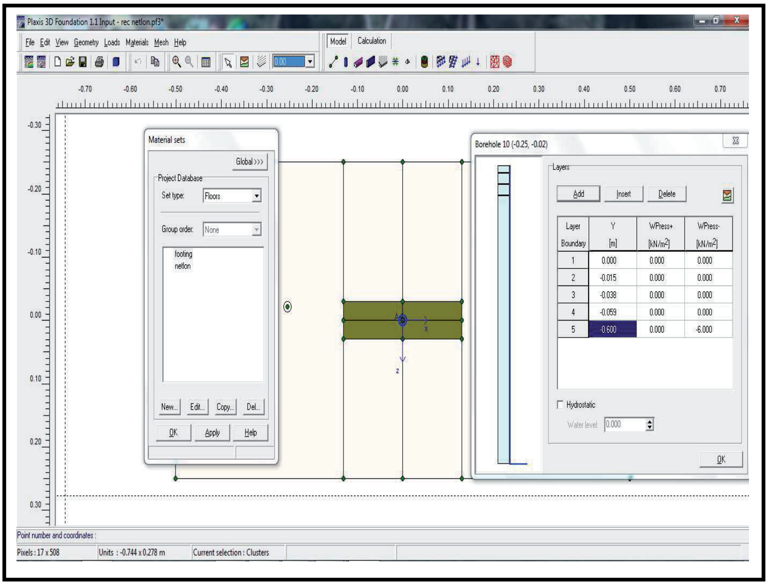

Figure 5-9 Borehole of the rectangular footing using Netlon CE121 geogrid case

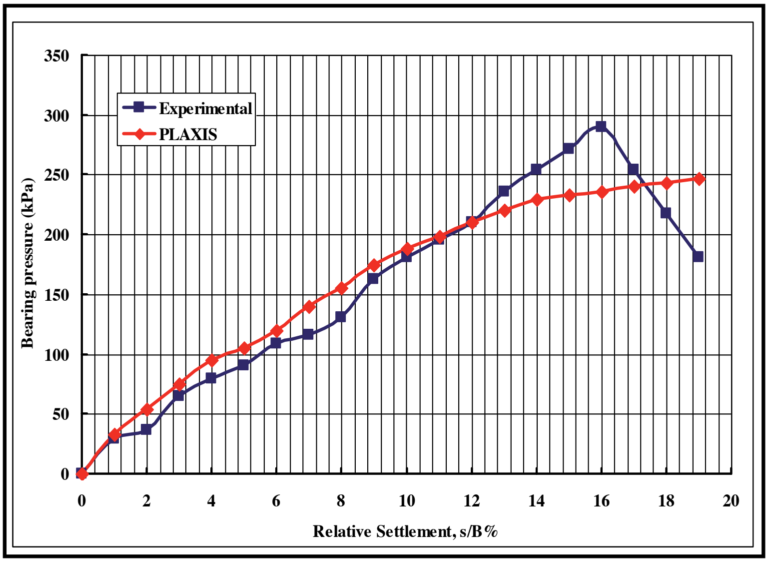

Figure 5-10 Bearing pressure versus relative settlement for rectangular footing with Netlon CE121 geogrid

5.5.3 Reinforcing Soil Using Tensar SS2 Geogrid

Figure 5-11 shows the final geometry for the case of rectangular footing on soil reinforced using Tensar SS2 geogrid represented by the borehole of the input parameters in 3D PLAXIS. This borehole explains the layers of geogrid and the materials of footing and mesh. Tensar SS2 is modeled as a thin plate as in strip with the same properties shown in table 5-2 The relationship between bearing capacity and relative settlement of sand using Tensar SS2 geogrid for experimental and PLAXIS results is shown Fig. 5-12. The experimental ultimate bearing capacities is 362.3 kPa while that obtained from PLAXIS is 300 kPa. The ratio of PLAXIS to experimental ultimate bearing capacities is 82.8 %, the agreement can be considered a very good.

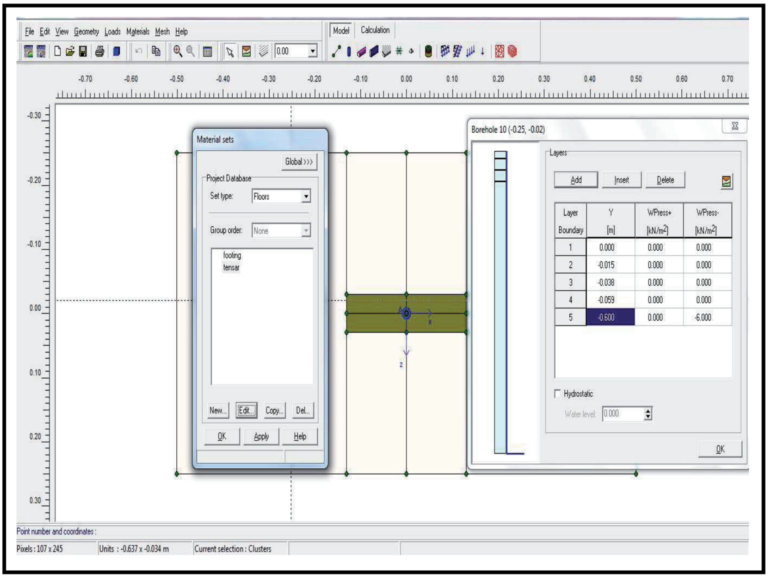

Figure 5-11 Borehole of the rectangular footing with Tensar SS2 geogrid case

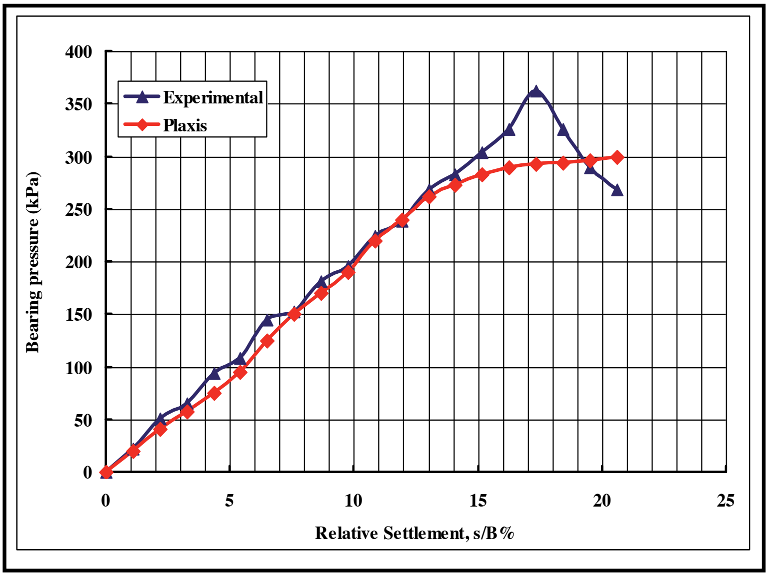

Figure 5-12 Bearing pressure versus relative settlement for rectangular footing on soil reinforced using Tensar SS2 geogrid

5.6 Plane Strain Piles Under Strip Footing (Piled-Strip) Modeling and Results

5.6.1 Piled-Strip System

To compare between the experimental and numerical results for the case of piled-strip system, the footing was modeled in PLAXIS resting on the surface of soil and above the upper end of pile as shown in Fig. 5-13. In PLAXIS, the plane strain piles cannot be modeled as in the laboratory, therefore, the case may be represented as a one row of bored piles with spacing center to center of three times of pile width. Load-Settlement relationship for experimental and numerical results is shown in Fig. 5-14, the results indicate a reasonable agreement since the maximum experimental capacity was 68 kN while that of PLAXIS was 50.8 kN with the difference being 74.7 %. The percentage of PLAXIS settlement to the experimental settlement at failure is 88.4 % that is 23 mm in PLAXIS and 26 mm experimentally.

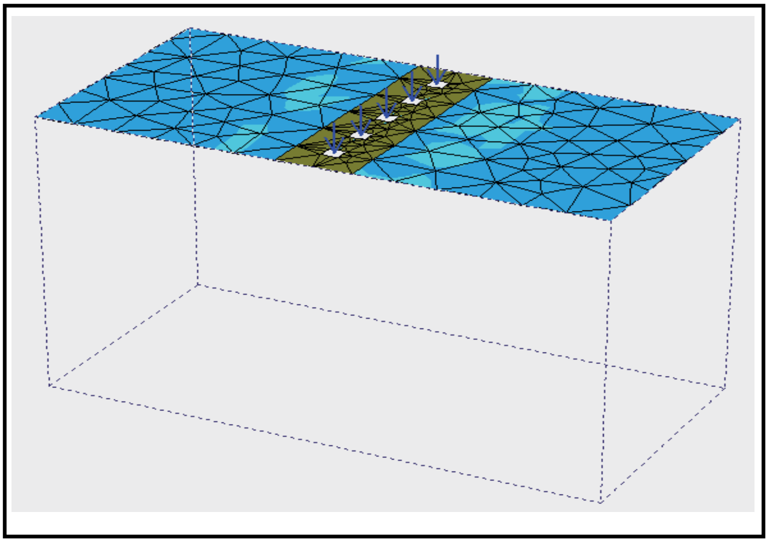

Figure 5-13 Final geometry of the piled-strip system

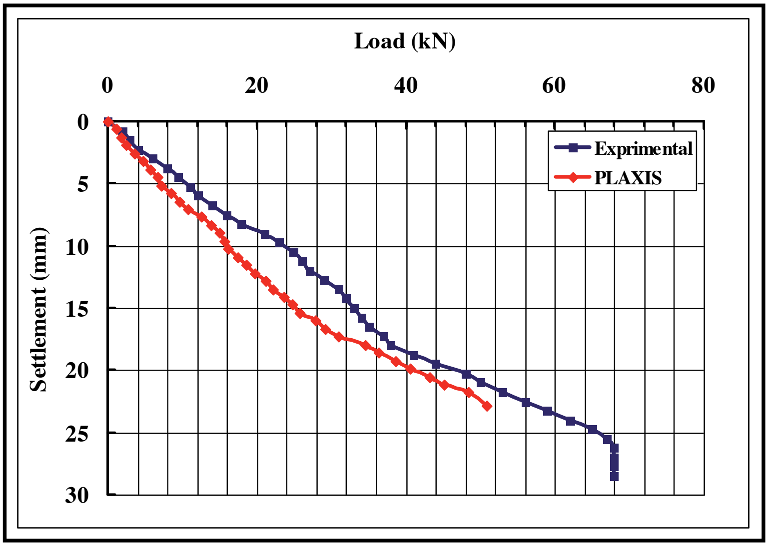

Figure 5-14 Load-Settlement relationship for pled-strip system

5.6.2 Skin and End Bearing Only

As presented in chapter four, the capacity of piles if we neglect the bearing area of footing is the Skin and Bearing case, the model of this case is shown in Fig. 5-15 while the load-settlement relation is given in Fig. 5-16. The results were reached after performing the calculations in PLAXIS for the capacity of piles due to skin friction and end bearing only is 37.1 kN, while the capacity for the same case of experimental work was 45.3 kN with the percentage difference being 81.9 %, this is acceptable for the problems in geotechnics. The value of final settlement in PLAXIS is 35 mm and from the experimental test was about 32 mm, that means the variation in the two values is 91.4 %,

5.6.3 End Bearing Only

Piles modeling in PLAXIS can be performed to calculate end bearing capacity only by choosing the option of Outside Interface, this option can be visualized clearly in Fig. 5-17, when the option is unmarked, the program neglects the skin friction resistance, and the results are given for end bearing only. Load-Settlement relationship from experimental and numerical results is shown in Fig. 5-18. The results indicate a good agreement because the experimental end bearing capacity was 33.8 kN while that of PLAXIS was 28 kN, the ratio of numerical to experimental capacity is 82.8%.

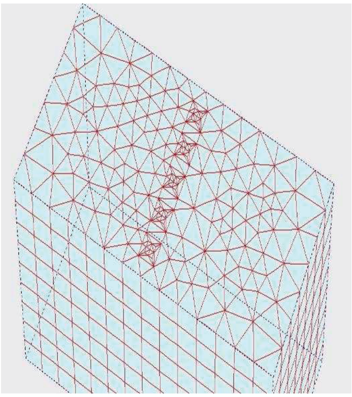

(a)

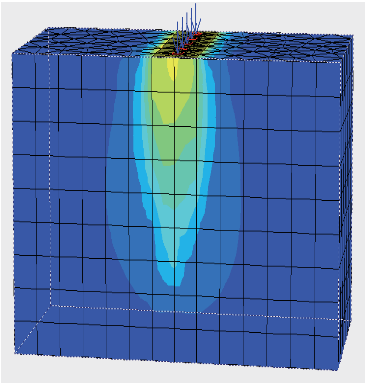

(b)

Figure 5-15 (a) 3D finite element mesh (b) Total displacement

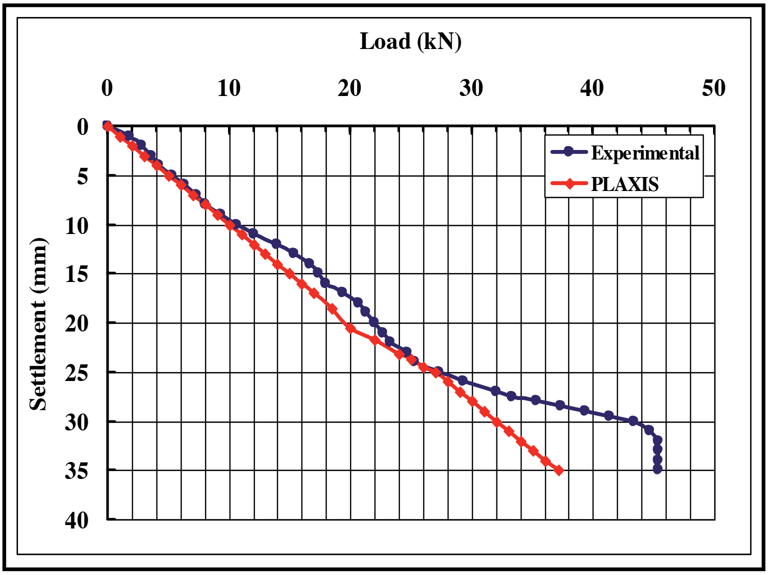

Figure 5-16 Load-Settlement relationship of skin and end bearing only for piled-strip system

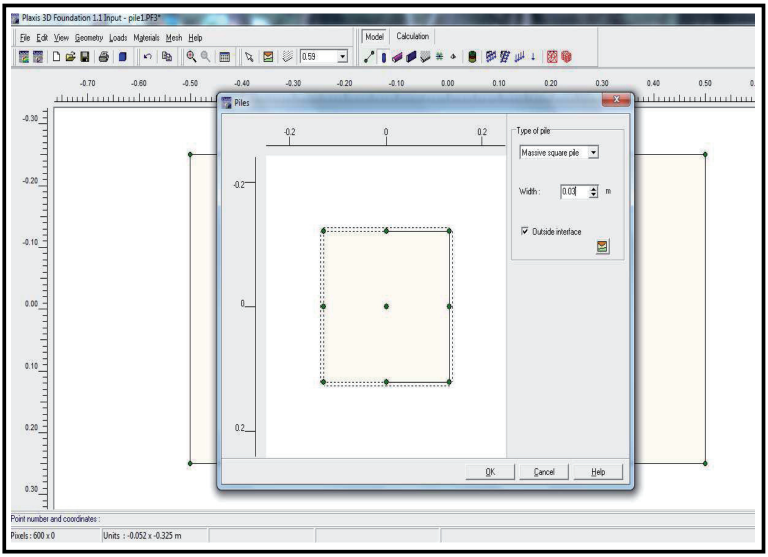

Figure 5-17 Option of elimination of skin friction of pile in PLAXIS

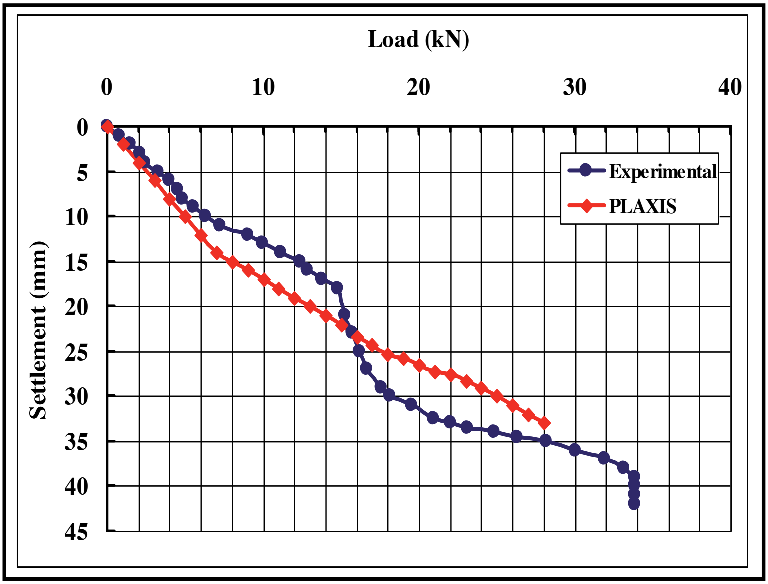

Figure 5-18 Load-Settlement relationship of end bearing only for piled-strip system

5.7 Piles Under Rectangular Footing (Piled-Rectangular) Modeling and Results

5.7.1 Piled-Rectangular System

PLAXIS used to model the case of three rectangular piles under the rectangular footing to study the behavior and load-settlement relationship and compare with the experimental work. Figure 5-19 shows the geometry of the related model in PLAXIS. The load-settlement relation from PLAXIS and experimental test is presented in Fig. 5-20. Total capacity of the system from PLAXIS is 5.5 kN and from experimental test is 6.5 kN, that means the ratio of two values is 84.6 %. The ratio of the numerical to experimental settlement at failure is 87.8 % for the values of settlement 9 mm and 10.3 mm respectively.

5.7.2 Skin and End Bearing Only

The geometry for the case of piles only was modeled as shown in Fig. 5-21. This model was performed to estimate the capacity of piles without footing which represent the case of skin friction and end bearing only. Load-Settlement relationship for this case is shown in Fig. 5-22, the values of capacity and settlement in PLAXIS model were smaller than the experimental values with a ratio of 80.6 % and 83.9 % respectively.

5.7.3 End Bearing Only

This section deals with the estimation of end bearing capacity of piles only. As mentioned in section 5.6.3, the skin friction of piles is eliminated by unmarking outside interface option . Figure. 5-23 shows the final geometry of this model. Load-Settlement curves from PLAXIS and experimental test are shown in Fig. 5-24. The values of end bearing capacity and settlement from PLAXIS were 3 kN and 15 mm respectively and from testing were 3.6 kN and 17.5 mm. The ratio between the two values were 83.3 % for capacity and 85.7 % for settlement, that can be considered acceptable.

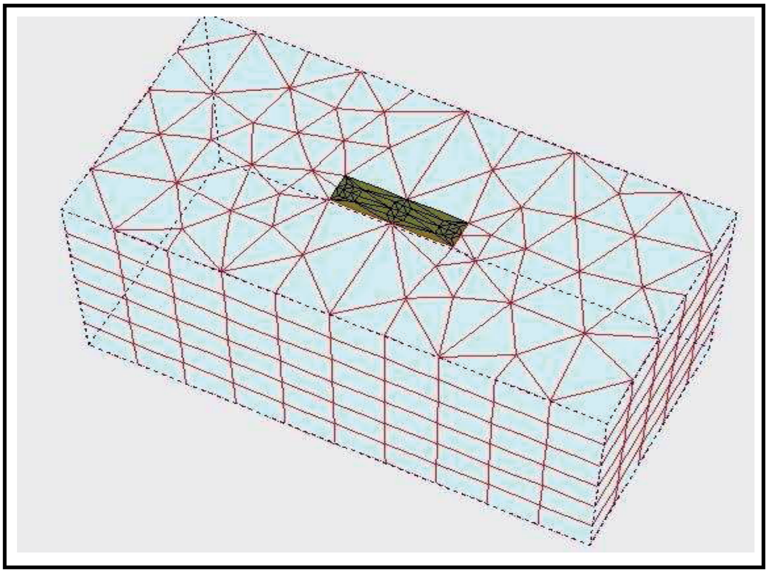

Figure 5-19 Final geometry of the piled-rectangular system

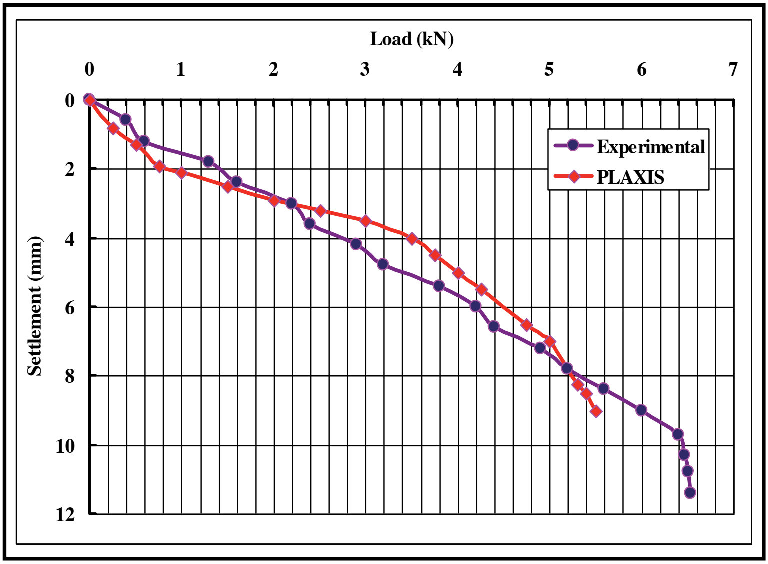

Figure 5-20 Load-Settlement relationship for piled-rectangular system

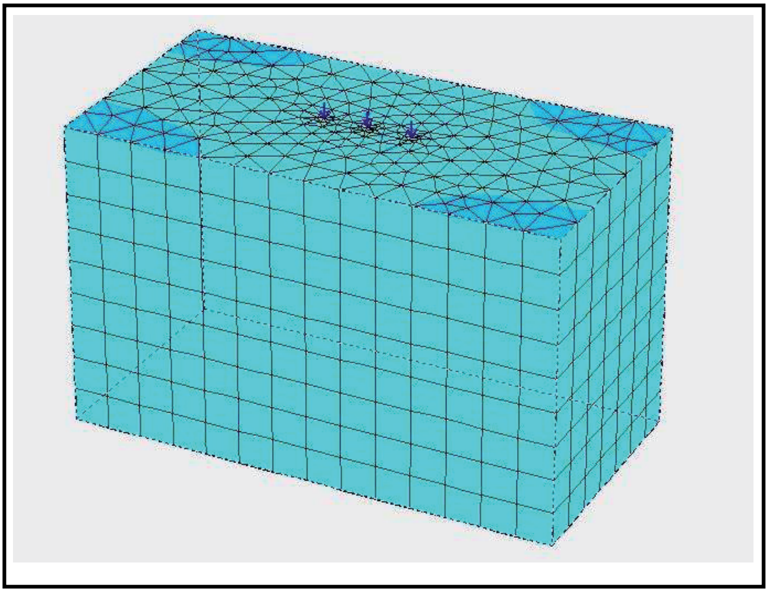

Figure 5-21 Final geometry of the rectangular piles without footing

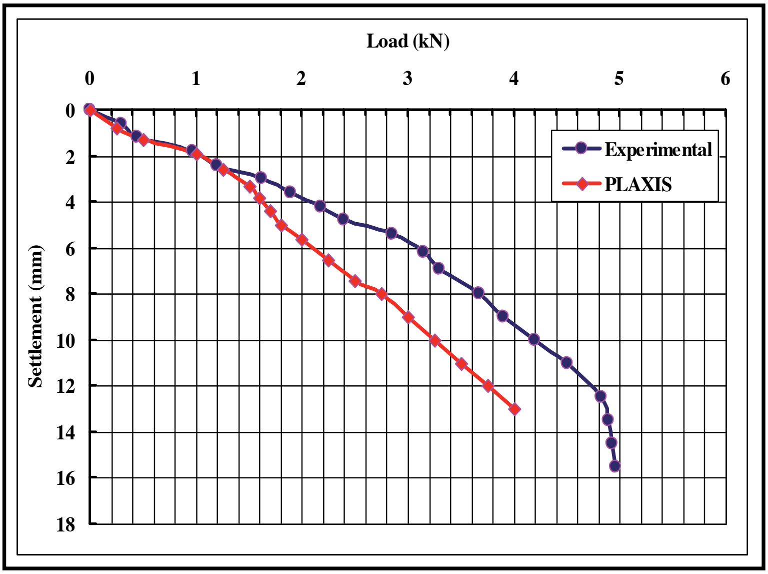

Figure 5-22 Load-Settlement relationship of skin and end bearing only for piled-rectangular system

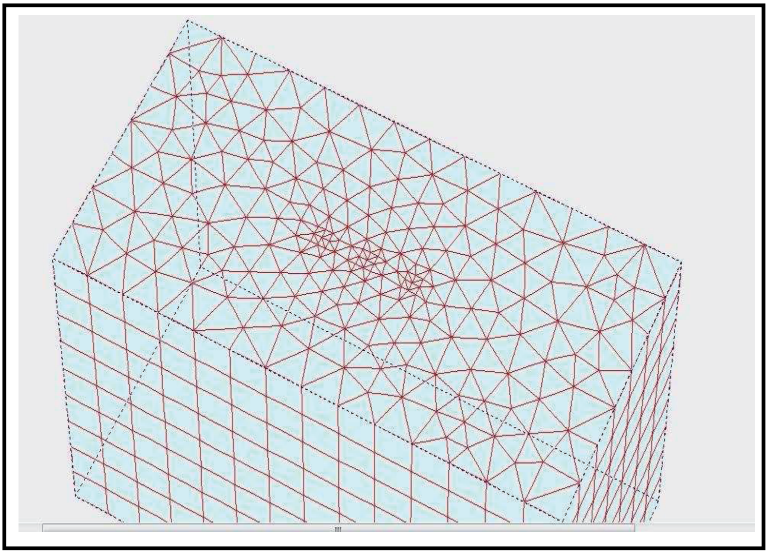

Figure 5-23 Option of elimination skin friction of pile in PLAXIS

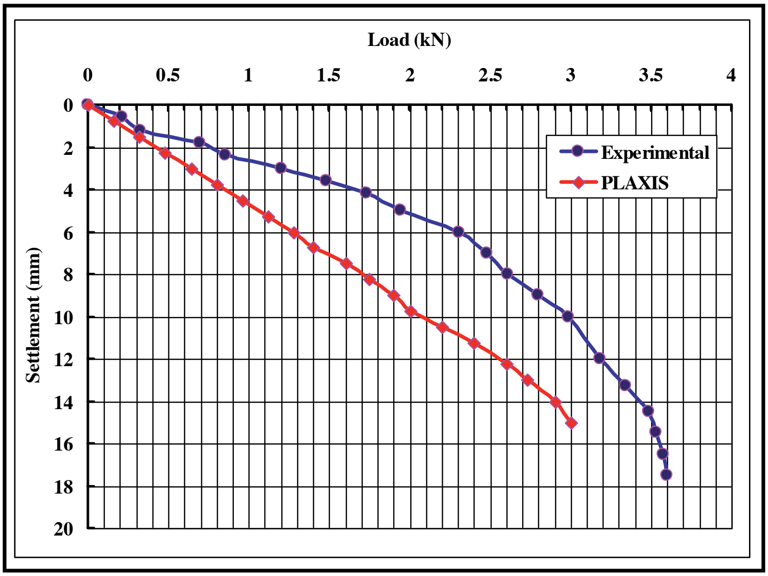

Figure 5-24 Load-Settlement relationship of end bearing only for piled-rectangular system

5.8 Load Sharing Between Piles and Footing

Foundations for heavy structures on weak soils are usually on piles and (or) pile-raft systems. These are also called basement raft supported piles or piled basements (Poulos, 2001; Tomlinson, 2008). When piles are founded on a compressible soil, the pile-raft system settles gradually resulting in a gradual buildup of pressure at the bottom of the raft. Thus, there is a gradual transfer of the total load to the raft and a reduction in the load is carried by the piles. The soil beneath the raft (located at a relatively shallow depth) is then compressed, causing a partial load transfer back to the piles. This is a continuous interaction process with the total load being shared by the raft and the piles.

Hence the piles must be designed to carry the full superstructure load initially, but the raft should be designed to carry a portion of the total load due to the subsequent load transfer process. To apportion these loads between the raft and the piles over a period of time is very difficult as it is a complex three-dimensional time-dependent problem. Several case studies carried out indicate varying load-sharing percentages. For example, the results

of the study conducted by Hooper (1973, 1979) for the load shared between raft and piles and the settlements are shown in Fig. 5-25. It can be seen from the figure that after the construction (40 months) piles and raft carried about 60% and 40% of the superstructure load. After that more loads got transferred to the piles from the raft and the percentages of total load shared by piles and raft became 66% and 34%, respectively.

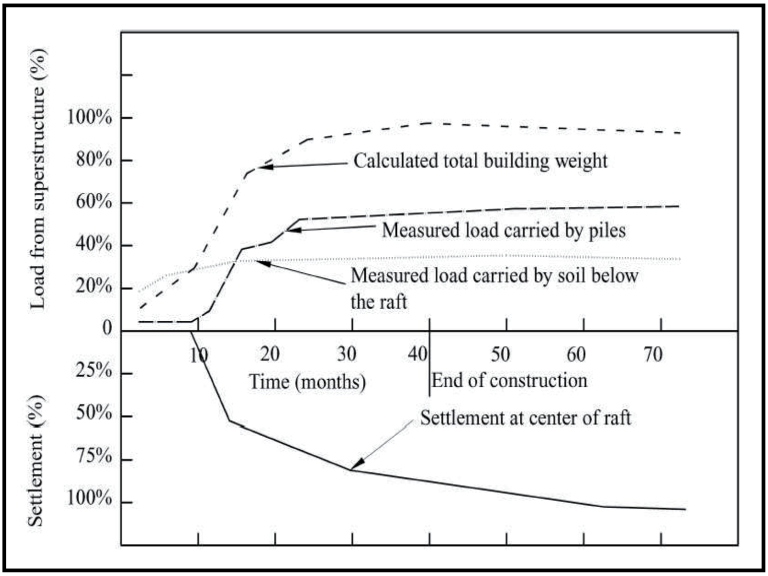

Figure 5-25 Load sharing between piles and raft, (after Hooper, 1973)

5.8.1 Load Sharing Between Piles and Footing From Experimental

The experimental results presented in chapter four show the values of piled-footing system capacity as well as the values of skin and friction only. Figure 4-44 shows the values of capacities for piled-strip system which is being 68 kN while it is 46 kN for skin and bearing only, these values give a load sharing between piles and strip footing of 66.2% for piles and 33.8% for strip footing.

Figure 4-52 shows the experimental results of piled-rectangular system capacities. Total capacity of the system is 6.4 kN and the capacity of skin and bearing only is 4.8 kN, that means the sharing between piles and rectangular footing is 75% for piles and 25% for rectangular footing.

The above sharing from experimental results have a good agreement with the study of Hooper (1973) and Sinha (2013) explained in chapter two.

5.8.2 Load Sharing Between Piles and Footing from PLAXIS

The numerical results presented in this chapter show the values of piled-footing system capacity and the values of skin and friction only. Figure 5-14 shows the value of capacity for piled-strip system from PLAXIS of 50.8 kN and Fig. 5-16 shows the value of skin and end bearing capacity only as 37.1 kN, these values give a load sharing between piles and strip footing of 73.1% for piles and 26.9% for strip footing.

Figures 5-20 and 5-22 show the PLAXIS results of piled-rectangular system and skin and bearing capacity only capacities. Total capacity of the system is 5.5 kN and the capacity of skin and end bearing only is 4 kN, that means the sharing between piles and rectangular footing from PLAXIS is 72.7% for piles and 27.3% for rectangular footing.

These sharing values from experimental and numerical results are in a good agreement with conventional knowledge presented in chapter two.

The results of sharing between piles and footings are summarized in Table 5-3.

5.9 Summary of Results

The experimental, theoretical and PLAXIS bearing capacity values are listed in table 5-4 to visualize the difference between them. The difference can be considered acceptable in the geotechnical studies due to the complicated behavior of soil and soil footing interaction.

Table 5-3 The results of sharing between piles and footings

Type of system	Type of results	Sharing of piles %	Sharing of footing %
Piled-strip	Experimental	66.2	33.8
	PLAXIS	73.1	26.9
Piled-rectangular	Experimental	75	25
	PLAXIS	72.7	27.3

5.10 Extrapolation of Results to Field Condition

It has been ascertained through the findings of this thesis that the use of high strength geogrid will significantly improve the bearing capacity of sand brought from the site of interchange bridges in Al-Najaf city although not to the same extent of the capacity of a pile group. It is intended in this section to check that the obtained allowable bearing capacity of reinforced sand in the field will exceed the applied pressure.

There is some evidence, from using small footings up to about 1 m for B, that the N_{γ} term does not increase the bearing capacity without bound, and for very large values of B, Vesic and De Beer suggest that the limiting value of q_{ult} approaches that of a deep foundation (Bowles, 1996), therefore Vesic's bearing capacity equation used to extrapolate the ultimate bearing capacity for the case study of intersection bridge is presented in appendix A. The pile cap represents the footing which is simulating the strip footing case in the experimental and theoretical work adopted in this chapter above. According to plans

of the project presented in appendix A the width of pile cap is 4 m which represents the case of strip footing, thus the Vesic's bearing capacity of case study according to (Bowels, 1996) can be written as follows:

$$q_{ult} = 0.5\ \gamma\ B\ N_{\gamma}\ s_{\gamma}\ d_{\gamma}\ r_{\gamma} \qquad \ldots 5\text{-}10$$

where r_{γ} = scaling factor = 0.92 for B = 4 m (Bowles, 1996)

So, the following equation may be used to extrapolate the ultimate bearing capacity to the field bearing capacity taking into account that the model tests were on dry sand while in the field it is usually assumed that the water table may rise up to the ground surface:

$\gamma_{d(used)}$ = 16.7 kN/m^3, e = 0.539, Gs = 2.62

$\gamma_{sat(used)}$ = [(2.62 + 1 × 0.539)/(1+0.539)] × 9.81 = 20.14 kN/m^3

$$\frac{(q_{ult})_{field}}{(q_{ult})_{laboratory}} = \frac{\gamma_{field}\ B_{field} \times r_{\gamma}}{\gamma_{laboratory} B_{lab}} \qquad \ldots 5\text{-}11$$

$$\frac{(q_{ult})_{field}}{234.3} = \frac{(20.14-9.81)\times 4\times 0.92}{16.7\times 0.135} \qquad \ldots 5\text{-}12$$

Then, $(q_{ult})_{field}$ = 3950 kN/m^2 …5-13

Thus, if the safety factor = 3,

$(q_{all})_{field}$ = 1317 kN/m^2 …5-14

The applied point load being transmitted from dead and live load of bridge is 41544 kN (appendix A), thus the applied pressure is [41544/(4×25)] = 415.44 kN/m^2.

According to the presented results in chapter four the ultimate bearing capacity of reinforced soil should be multiplied by BCR which is 1.88 for Netlon CE121 and 2.5 for Tensar SS2. However since the obtained allowable field bearing capacity of unreinforced sand has been found to be already higher than that of the applied load, the use of geogrids or piles will serve in the present bridge to increase the safety factor and it would eliminate the reluctance of the design engineer to using geogrids instead of piles to significantly save funds and time.

It should be recalled here that the engineer should not be surprised when noticing the very high value of the extrapolated ultimate field bearing capacity of sand given in eq. 5-13. The reasons are the high value of Ø, being slightly larger than 40º, and that in cohesionless soil the bearing capacity is almost proportional to the footing width. Bowles (1996) reported the result obtained by Muhs in Berlin of field bearing capacity of submerged sand. The relevant test parameters were B = 0.50 m and $Ø_{tr}$ = 42.7°. The measured ultimate bearing capacity was 1863 kN/m^2 while the corresponding theoretical values by Hansen and Meyerhof were 1902.5 and 2659 kN/m^2 respectively.

An important matter should be addressed here concerning the stress level. There are evidences that when the stress level exceeds 500-600 kN/m^2, crushing of sand particles takes place resulting in reducing the friction angle and hence the bearing capacity (Al-Omari, 1984). A discussion on this topic is available in Al-Omari (1988). Thereby, if the applied pressure exceeds the crushing stress the footing size should be increased whether the sand is reinforced or not, otherwise piled foundation should be relied upon. Piles spread the applied pressure around a larger soil bulk. Nevertheless a settlement analysis should also be implemented. Bowles (1996) addressed this point too and stated "some geotechnical consultants routinely limit the maximum allowable soil pressure to around 500 kPa in recommendations to client for design whether settlement is a factor or not".

Table 5-4 Summary of results

Type of footing	Experimental axial capacity of unreinforced sand (kN)	Experimental axial capacity of reinforced sand using Netlon (kN)	Experimental axial capacity of reinforced sand using Tensar (kN)	Experimental bearing capacity of unreinforced sand (kN/m²)	Experimental axial capacity of reinforced sand using Netlon (kN/m²)	Experimental axial capacity of reinforced sand using Tensar (kN/m²)	Theoretical bearing capacity (kN/m²)			PLAXIS axial capacity of unreinforced sand (kN)	PLAXIS axial capacity of reinforced sand using Netlon (kN)	PLAXIS bearing capacity of unreinforced sand using Tensar (kN)	PLAXIS bearing capacity of unreinforced sand (kN/m²)	PLAXIS axial capacity of reinforced sand using Netlon (kN/m²)	PLAXIS axial capacity of reinforced sand using Tensar (kN/m²)
							Terzaghi	Meyerhof	Vesic						
Strip	15.5	29.2	38.8	234.3	441.4	586.5	290.9	257.6	269.3	11.1	23.5	29.8	167.8	363	460
Rectangular	1.7	4	5	123.18	289.8	362.3	129.3	131.1	107.2	1.4	3.4	5.9	101	247	300
Piled-strip	68	-	-	-	-	-	45 kN			50.8	-	-	-	-	-
Piled-rectangular	6.4	-	-	-	-	-	3.39 kN			5.5	-	-	-	-	-

B_{strip} = 135 mm

$B_{rectangular}$ = 60 mm

CHAPTER SIX
ECONOMIC STUDY

6.1 Introduction

In all construction projects, engineers try to meet the project objectives with minimum cost. One of the important aims of this study is to investigate the feasibility of using geogrids in the foundation of interchange bridges in middle and south Iraq where most of the soil is sand. The bearing capacity of soil can be highly improved by reinforcing it with geogrids, so it can bear the applied load resulting from dead and live loads of bridges, without any need to use costly piles.

This chapter deals with an economic study of using geogrids in the foundation of interchange bridges instead of piles within the limits of applied loads prevailing in most of highway projects in Iraq and bearing capacities of reinforced soil of the most common type founded in the aforementioned region. Optimization technique is used to estimate the cost of construction of both types of footings (reinforced soil and piles). Comparison between the two cases is adopted to decide whether the use of geogrids is more economic than the use of piles within the range of applied load. The cost of construction is determined according to the prevailing local prices at the time of this study.

MATLAB optimization toolbox is used to formulate the optimization problems. It is a high-level language and interactive environment for numerical computation, visualization, and programming. Using MATLAB affords to the user analysis of data, developing algorithms, and creating models and applications. The language, tools, and built-in math functions enable researchers explore multiple approaches and reach a solution faster than with spreadsheets or traditional programming languages. MATLAB can be used for a range of applications, including signal processing and communications, image and video processing, control systems, test and measurement, computational finance, and computational biology (MATLAB manual, 2014). Constrained nonlinear minimization optimization technique is used to formulate the design problem of this study using the optimization tool in the package.

6.2 Calculations of Loads

The bridge design of thirty multi–level intersections in Al-Najaf , Karbala, and surroundings is reviewed in order to determine the limit of the most common applied loads. Related drawings of the design of the bridge of Northern Garage in Al-Najaf City are shown in appendix A as a representative case. The review of design and calculations reveals that the applied loads are within (10386 kN). This means that the total applied load on the pile cap is (41544 kN). The pile cap is considered to be rigid having four piles with 1.5 m diameter and 18 m length according to design.

6.3 Problem Statement

The problem is divided into two cases. Case one is to analyze the cost of construction using geogrids and case two is to analyze the cost of construction using piles, then optimization is carried out to get the optimal solution taking into account design constraints. Figure 6-1 shows the dimensions of the adopted unit case study.

6.3.1 Objective Function of the Reinforced Soil Case

The objective function represents the equation formulated to estimate cost. The case of reinforced soil is taken for a zone of 7.2B m × L m × h m (where h = B) according to the findings of chapter four. The input parameters are, total load on footing (P), submerged unit weight of in-situ soil as a worst case as presented in chapter five (section 5.10) (γ_b), angle of internal friction of in-situ soil (Ø), cost of geogrids (cg), cost of excavation (ce), cost of work (including laying of geogrids) (cw), cost of filling and compaction (cf), and safety factor (SF). The cost of the concrete footing itself is not included in the study because it is the same in both cases (reinforced soil and piles). The outputs of optimization are the optimum size of footing (L and B) and its cost.

The objective function of the total cost of footing construction is expressed as minimize:

$$F(x) = \text{cost of (geogrids + excavation + work + filling and compaction)} \qquad \ldots 6\text{-}1$$

For the sake of problem formulation, variables take the form of:

$$x_i = \{ x_1, x_2, x_3, \ldots\} \qquad \ldots 6\text{-}2$$

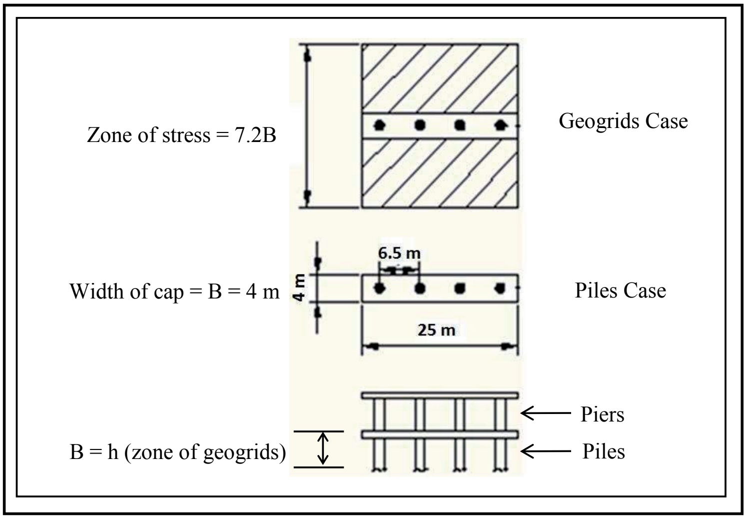

Figure 6-1 One design unit for the sake of cost comparison

In the case of the reinforced soil discussed here $x_1 = B, x_2 = L, \ x_3 = h$.

where,

B = width of footing in (m)

L = length of footing in (m)

h = depth of the end layer of geogrid in (m), (h = B, according to experimental results).

The objective function is formulated to yield the optimum size of footing and its cost in IQD (Iraqi Dinars) according to the aforementioned variables.

Then, the final expression of the objective function as written in MATLAB is:

$$F(x_i) = nl \times cg \times sz \times x_1 \times x_2 + ef \times ce \times (x_1)^2 \times x_2 + nl \times cw \times sz \times x_1 \times x_2 + ef \times sz \times cf \times (x_1)^2 \times x_2 \quad \ldots 6\text{-}3$$

where,

x_1 = width of footing in meters (B) or depth of the end layer of geogrid in meters (h = B).

x_2 =: L = length of footing in meters.

nl = number of geogrid layers (as presented in chapter four).

cg = cost of geogrids IQD/m^2.

sz = stress zone in both sides of the footing (as presented in chapter four = 7.2B).

ef = expansion factor for excavation and filling (for field purposes, the excavation usually required to excavate is a bit larger than geogrids zone).

ce = cost of excavation IQD/m^3.

cw = cost of work for one layer IQD/m^2.

cf = cost of filling and compaction IQD/m^3.

6.3.2 Constraints of the Reinforced Soil Case

The constraints of both cases cover both types of failure that design should account for, soil failure and structural failure. Soil failure must meet both main criteria of general bearing capacity and settlement limitation, while structural failure must meet shear and flexural strength. Therefore, constraints are formulated as follows:

i- The allowable soil pressure (q_{all}) must be greater than or equal to the maximum applied pressure (q_{max}):

$$q_{all} \geq q_{max} \qquad \ldots 6\text{-}4$$

or;

$$q_{ult} / SF \geq q_{max} \qquad \ldots 6\text{-}5$$

where the ultimate bearing capacity (q_{ult}) can be calculated using Hansen's equation as follows (Bowles 1996):

$$q_{ult} = cN_c s_c d_c + qN_q d_q + 0.5\gamma BN_\gamma s_\gamma d_\gamma \qquad \ldots 6\text{-}6$$

For the footing resting on the surface and the soil type is sand (c = 0), the equation of bearing capacity will be:

$$q_{ult} = 0.5\gamma BN_\gamma s_\gamma d_\gamma \qquad \ldots 6\text{-}7$$

where:

$$Nq = e^{\pi \tan Ø} \tan^2(45+Ø/2) \qquad \ldots 6\text{-}8$$

$$N_\gamma = 1.5(N_q-1) \tan Ø \qquad \ldots 6\text{-}9$$

$$s_\gamma = 1-0.4\ B/L \qquad ..6\text{-}10$$

$$d_\gamma = 1$$

The maximum applied pressure can be calculated from the basic principle as:

$$q_{max} = \frac{P}{BL} \qquad \text{…6-11}$$

$$q_{all} = \frac{q_{ult}}{SF} \qquad \text{6-12}$$

The value of bearing capacity of sand must be improved with BCR value calculated from experimental work (chapter four), BCR for Netlon CE121 equals to (1.88) and for Tensar SS2 equals to (2.5). Since the ratio of breadth to length of the footing is slightly larger than 6, the case may be approximated as plane strain and the BCR values obtained in chapter four are taken from the strip footing case.

Thus, the constraint can be written as:

$$g_1=-0.5\times\gamma\times x_1\times(1.5\times(Nq-1)\times\tan(\text{Ø}\times\pi/180))\times(1-0.4\times(x_1/x_2))\times BCR\times x_1\times x_2+SF\times P \qquad \text{…6-13}$$

ii-The immediate settlement of the footing must not exceed a permissible limit. To satisfy this limitation the equation of subgrade reaction is used:

$$s_i = w_t/\ k_s = (P/BL)/\ k_s \qquad \text{…6-14}$$

Where k_s= modulus of subgrade reaction (kN/m^3).

$$k_s = 120 * q_{all} \quad \text{(Bowles, 1996)} \qquad \text{…6-15}$$

Thus,

$$s_i = \frac{P/BL}{120(q_{ult}/SF)} \qquad \text{…6-16}$$

If the permissible $s_i = 0.025$ m then,

$$\frac{P/BL}{120(q_{ult}/SF)} \leq 0.025 \qquad \text{…6-17}$$

$$3*q_{ult}\,(BL) \geq SF \times P \qquad \text{…6-18}$$

$-3 \times q_{ult} \times (BL) + SF \times P \leq 0$ …6-19

Thus, the constraint can be written as:

$g_2 = -3(0.5\times\gamma\times x_1\times(1.5\times(Nq-1)\times\tan(\text{Ø}\times\pi/180))\times(1-0.4\times(x_1/x_2))\times BCR\times x_1\times x_2+SF\times P)$ …6-20

where,

γ = submerged unit weight of sand = (20.14 – 9.81) = 10.3 kN/m^3 (section 5.10, chapter five), (submerged unit weight is used as a worst case).

Nq = as above.

(Ø) = angle of internal friction of soil.

BCR = bearing capacity ratio.

SF = safety factor.

P = total axial load.

The program is required to restrict the lower and upper limits of x_i. For practical purposes the dimensions of footing must enclose the area of piers, therefore, the lower and upper limits of x_i (L and B) must be fixed in the optimization tool box in MATLAB (Fig. B-14, appendix B). The lower and upper limits of the dimensions of footing are used to represent a minimum required dimensions of a pile cap as 4 m width and 25 m length.

thus,

The optimization problem of reinforced soil case has the form:

Minimize:

$\mathbf{F(x_i) = nl\times cg\times sz\times x_1\times x_2+ef\times ce\times (x_1)^2\times x_2+nl\times cw\times sz\times x_1\times x_2+ef\times sz\times cf\times(x_1)^2\times x_2}$ …6-21

subject to

$\mathbf{-0.5\times\gamma\times x_1\times(1.5\times(Nq-1)\times\tan(\text{Ø}\times\pi/180))\times(1-0.4\times(x_1/x_2))\times BCR\times x_1\times x_2+SF\times P \leq 0}$ …6-22

$\mathbf{-3(0.5\times\gamma\times x_1\times(1.5\times(Nq-1)\times\tan(\text{Ø}\times\pi/180))\times(1-0.4\times(x_1/x_2))\times BCR\times x_1\times x_2+SF\times P) \leq 0}$ …6-23

$$\mathbf{4 \leq x_1 \leq 5 \quad \text{and} \quad 25 \leq x_2 \leq 30}$$

After running the program using constrained nonlinear minimization analysis, the optimum dimensions (B and L) and the minimum cost of construction of the reinforced soil at the zone of one row of piers is obtained. Table 6-1 shows the optimum cost dimensions determined by the program that makes the reinforced soil under footing safe in the sense of

bearing capacity and allowable settlement to bear the applied load from the super-structure of the bridge.

Figure B-14 in appendix B shows the objective function, constraints and the tool box of inputs and outputs in MATLAB.

Table 6-1 Inputs and outputs of cost optimization analyses of the reinforced soil case

<table>
<tr><th colspan="3">Inputs</th><th colspan="3">Outputs</th></tr>
<tr><th>item</th><th>unit</th><th>value</th><th>item</th><th>unit</th><th>value</th></tr>
<tr><td>P</td><td>kN</td><td>41544</td><td rowspan="3">B</td><td rowspan="3">m</td><td rowspan="3">4</td></tr>
<tr><td>Geogrids layers</td><td>No.</td><td>3</td></tr>
<tr><td rowspan="2">BCR</td><td>For Netlon</td><td>1.88</td></tr>
<tr><td>For Tensar</td><td>2.5</td><td rowspan="3">L</td><td rowspan="3">m</td><td rowspan="3">25</td></tr>
<tr><td>(cost of geogrid), cg</td><td>IQD/m^2</td><td>10000.000</td></tr>
<tr><td>(cost of excavation), ce</td><td>IQD/m^3</td><td>1000.000</td></tr>
<tr><td>(cost of work), cw</td><td>IQD/m^2</td><td>2000.000</td><td rowspan="5">Cost</td><td rowspan="5">IQD/row</td><td rowspan="5">29,856,000.000 Twenty nine millions and eight hundred fifty six thousands IQD</td></tr>
<tr><td>(cost of filling and compaction), cf</td><td>IQD/m^3</td><td>1000.000</td></tr>
<tr><td>(submerged unit weight of soil), γ_b</td><td>kN/m^3</td><td>10.3</td></tr>
<tr><td>(Plane strain angle of internal friction), Ø°</td><td>degrees</td><td>44</td></tr>
<tr><td>(safety factor), SF</td><td>---</td><td>3</td></tr>
</table>

6.3.3 The Objective Function of the Piles Case

In this case, one row of piles (Fig. 6-1) is considered to estimate the cost of construction. The construction cost of piles is almost divided into three items; cost of work (cwp), cost of concrete (cc), and cost of steel reinforcement (cs). The cost of work is measured per one meter of pile, the cost of concrete is per one cubic meter, and the cost of reinforcement is per ton. The cost of the piles cap is excluded as in the case of reinforced

soil. Other input parameters are total load on footing (Pp), submerged unit weight of soil (γ_b) as above, angle of internal friction (Ø) and safety factor (SF). The outputs of running the MATLAB are the optimum size of pile (diameter and length) and its cost.

The objective function is expressed in the form of the total cost of the construction of one row of piles as minimize:

F(x) = cost of (work + concrete + steel reinforcement) …6-24

For the sake of problem formulation, variables take the form of:

$x_i = \{ x_1, x_2, \ldots\}$ …6-25

in which; $x_1 = D_p$ and $x_2 = L_p$

The final expression of the objective function:

$f(x_i)=np\times cwp\times x_2+np\times cc\times\pi/4\times(x_1)^2\times x_2+0.01\times7.8\times np\times cs\times\pi/4\times(x_1)^2\times x_2$ 6-26

where,

$x_1 = D_p$ = diameter of pile in (m)

$x_2 = L_p$ = length of pile in (m)

$\gamma_{steel} = 7.8$ ton/m^3

np = number of piles,

and the minimum steel area is equal to (ρ_{min} × cross sectional area of pile) where (ρ_{min} = 0.01) (Bowles, 1996).

cwp = cost of work IQD/m for D_p = (1 – 1.5) m.

cc = cost of concrete IQD/m^3.

cs = cost of steel reinforcement IQD/ton. (γ_{steel} = 7.8 ton/m^3).

Steel area = 0.01 × cross sectional area of pile according to Bowles (1996).

SFp = safety factor for piles.

6.3.4 Constraints of the Piles Case

As mentioned before the total applied load on each pile is found to be 10386 kN which is a very important constraint. This maximum applied load to each pile should not exceed the allowable capacity of pile. Failure due to end bearing and skin friction is taken into account in the formulation of constraints. The piles are considered a bored pile as they are constructed in the field.

The ultimate capacity of a single pile is determined according to many well-known formulas presented in most text books. The American Petroleum Institute (API) provides design recommendations for axially loaded piles in the (API RP 2A) publication titled *''Recommended Practice for Planning, Designing, and Constructing Fixed Offshore Platforms''* (API 1993). It is worth being adopted here because the API recommendations are based on a large database of axial pile load tests that is continually evaluated and updated (Pelletier, et al., 1993), the procedure is as follows;

$Q_{ult} = Q_b + \sum Q_s$ …6-27

$Q_b \leq Q_{b\ max}$ …6-28

$Q_{b\ max}$ for sand (c=0) = $(50\ N_q \tan Ø)\ A_b$ …6-29

$Q_{b\ max}$ for $(c \neq 0) = (c_b\ N_c\ + 50\ N_q \tan Ø)\ A_b$ …6-30

$Q_{ult} = (\ c_b\ N_c + q\ N_q\ )\ A_b\ + \sum(\ \alpha\ c_s + \sigma_v\ K \tan \delta\ )A_s$ …6-31

For c = 0, one layer of soil according to the site investigation of site (Fig. A-4, appendix A), the formula becomes:

$Q_{ult} = q\ N_q\ A_b + (\ \sigma_v\ k \tan \delta\ )A_s$ …6-32

where:

$q = \gamma_b \times Lp$ …6-33

N_q = Fig. 6-2. For Triaxial $Ø = 40°$, $N_q = 160$

A_b = cross sectional area of pile.

$\sigma_v = \gamma_b \times (Lp/2)$ …6-34

$k = (1\text{-}\sin Ø)$ …6-35

$\delta = Ø$ (concrete contacts with soil directly)

A_s = surface area of pile.

Therefore, the capacity formula is be written as:

$Q_{ult} = \gamma_b \times Lp \times N_q \times \pi\ (Dp)^2/4 + (\gamma_b \times (Lp/2) \times (1\text{-}\sin Ø) \tan \delta \times \pi \times Dp \times Lp$ …6-36

which represents the ultimate capacity of a single pile. This capacity must be multiplied by 4 to suit the case study of four piles in one row.

The constraint is formulated as:

$Q_{ult\,(s.p)} \geq (Q_{max} \times SFp)$ …6-37

Thus, the constraint is written as:

$g1=-1\times share\times np\times (\gamma\times x_2/2\times Nq\times \pi/4\times (x_1)^2\times K\times (\tan(Ø\times\pi/180)) \times\pi\times x_1 \times x_2)+Pp\times SFp$ …6-38

where,

share = 33.8% (sharing ratio of footing presented in table 5-3 of chapter five, this ratio must be added to the pile capacity to simulate the actual case of construction, that means the capacity must be multiplied by 1.338 to give the piled-strip system capacity.

np = number of piles = 4.

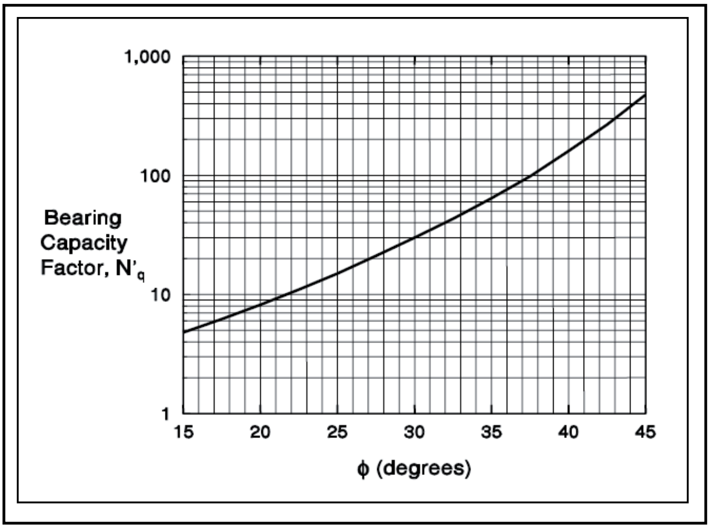

Figure 6-2 Chart for estimating bearing capacity factor N'q (FHWA, 2006).

γ = submerged unit weight of used sand = 10.3 kN/m^3, (submerged unit weight is used as a worst case because of the presence of water table at a depth about 2 m).

Nq = bearing capacity factor of pile (from Fig. 6-2).

Ø = angle of internal friction of soil, (used in MATLAB).

SFp = safety factor for piles.

Pp = total axial load on piled-strip system.

To compare between both cases (reinforced soil and piled-strip system), the size of pile (diameter and length) is used stated in the design plans of the project (Dp = 1.5 m and Lp = 18 m). The price of construction is considered according to the prevailing local prices at the time of this study.

thus,

The optimization problem of piles case has the form:

Minimize:

$$\mathbf{F(x_i) = np\times cwp\times x_2+np\times cc\times \pi/4\times(x_1)^2\times x_2+0.01\times 7.8\times np\times cs\times \pi/4\times(x_1)^2\times x_2} \quad \ldots 6\text{-}39$$

subject to

$$\mathbf{-1\times share\times np\times (\gamma\times x_2/2\times Nq\times \pi/4\times (x_1)^2\times K\times (\tan(\O\times \pi/180)) \times\pi\times x_1 \times x_2)+Pp\times SFp \leq 0} \quad \ldots 6\text{-}40$$

$$\mathbf{1.5 \leq x_1 \leq 2 \quad \text{and} \quad 18 \leq x_2 \leq 25}$$

After running the program, the optimum Dp and Lp and the minimum cost of one row of piles are obtained. The optimum values of Dp and Lp which are required to ensure piles are safe in the sense of capacity are shown in table 6-2. Figure B-15 in appendix B shows the objective function, constraints and the window of inputs and outputs of this case in MATLAB .

6.4 Discussion

For the case study adopted in this research, it is clear that the use of geogrids in the construction of interchange bridges on sandy soil is more economic than using piles within the limits of design loads adopted in the region, the angle of internal friction is higher than 40 degrees. The saving in cost is found to be as much as (54%) in analyzed case study. Consultants usually overdesign which is a traditional approach, pleading with low quality performance of labor, materials and engineering control. For soil reinforcement by geogrids, which is a new approach in the Iraqi construction industry, consultants awareness is very much higher.

Table 6-2 Inputs and outputs of cost optimization analyses of pile case

Inputs			Outputs		
item	unit	value	item	unit	value
Pp	kN	41544	Dp	m	1.5
(cost of work), cwp	IQD/m	500000.000			
(cost of concrete), cc	IQD/m^3	150000.000	Lp	m	18
(cost of reinforcement), cs	IQD/ton	1000000.000			
(submerged unit weight of soil), γ_b	kN/m^3	10.3	Cost	ID/row	65,009,466.000 Sixty five millions and nine thousands and four hundred sixty six IQD
(Triaxial angle of internal friction), Øº	degrees	40			
(safety factor), SFp	-	4			

6.5 Parametric Study

A parametric study of the optimum cost of construction is investigated for a wide range of loads and angles of internal friction of soil to explore more representative cases. In order to study the effect of angle of internal friction on the cost, a set of different loads on footing (varying from 20000 to 60000) is analyzed. Figures (6-3) and (6-4) show the relationship between (Øº) and the cost of Netlon and Tensar geogrid cases respectively. It is clear that the cost tends towards a constant value when (Øº) increases. For the wide range of loads, the cost of reinforced soil by Netlon and Tensar geogrids tends towards a constant value after (Ø = 35º) and (Ø = 32º) respectively. This is because Tensar geogrid has a higher BCR than of Netlon geogrid. For the same range of loads, the cost of piles with dimensions of (Dp = 1.5 m) and (Lp = 18 m) decreases gradually after (Ø = 20º) then remain constant when the value of (Ø) exceeds (25º), as shown in Fig. 6-5.

Figures (6-6), (6-7), (6-8), (6-9), and (6-10) illustrate a comparison between costs of different cases showing whether using geogrids or piles foundation is more economic. The analyses cover relationships between load and cost for values of (Ø = 20º, 25º, 30º, 35º and 40º).

Figure (6-6) shows the relationship between load and cost for (Ø = 20º), the cost increases when the applied load increase for Netlon CE121, Tensar SS2, and piled-strip cases.

Figure (6-7) shows the relationship between load and cost for (Ø = 25º), the cost of the piled-strip is constant for the same range of loads because the value of (Nq) is high enough and the capacity of the dimensions of piles are sufficient to resist the adopted range of loads.

Figures (6-8), (6-9), and (6-10) indicate that using geogrids foundation is much more economical than piles for the load range of (20000 kN) to (60000 kN) when Ø is 30º - 40º . This finding comes in line with the established knowledge that the more the fines in soil the less the effectiveness of reinforcement. Since physically, less Ø for the same relative density refers to more fines especially when it is (15%) finer than (0.075 mm) as required by AASHTO specifications and FHWA guidelines, (Charlie and Clark, 2013). The saving in cost increases rapidly when the value of (Ø) increases, especially when it became higher than (25º). The type of geogrids does not affect the cost because of the high bearing capacity of sand, especially when the value of (Ø) is higher than (30º).

6.6 Summary

The aim of this economic analysis is to emphasize the feasibility of using geogrids instead of piles in the foundation of bridges, resting on sandy soil. According to the costs listed in tables (6-1) and (6-2), and the behavior of cost shown in Figs. (6-3) to (6-10), it can be concluded that geogrids in the foundation of multi-level highway intersections bridges is significantly more economical than piles within the range of applied loads, allowable bearing capacities, and settlement covered by this study.

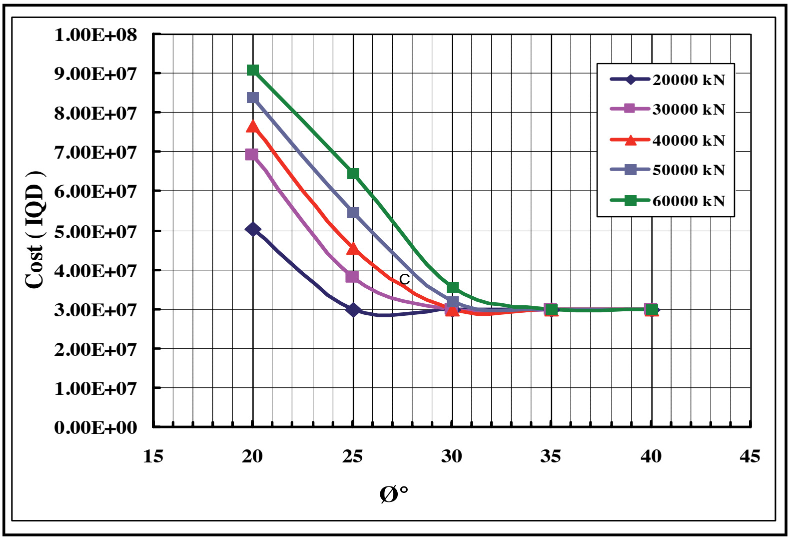

Figure 6-3 Relationship between Ø° and cost of Netlon CE121 geogrid

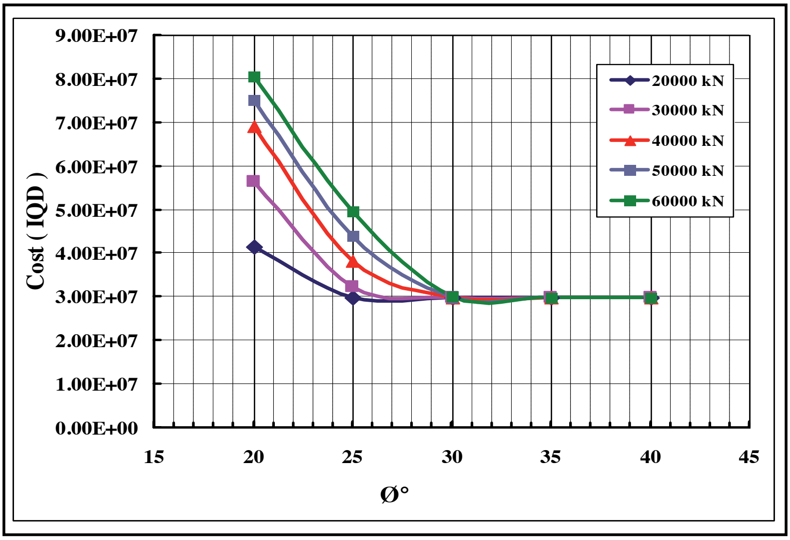

Figure 6-4 Relationship between Ø° and cost of Tensar SS2 geogrid

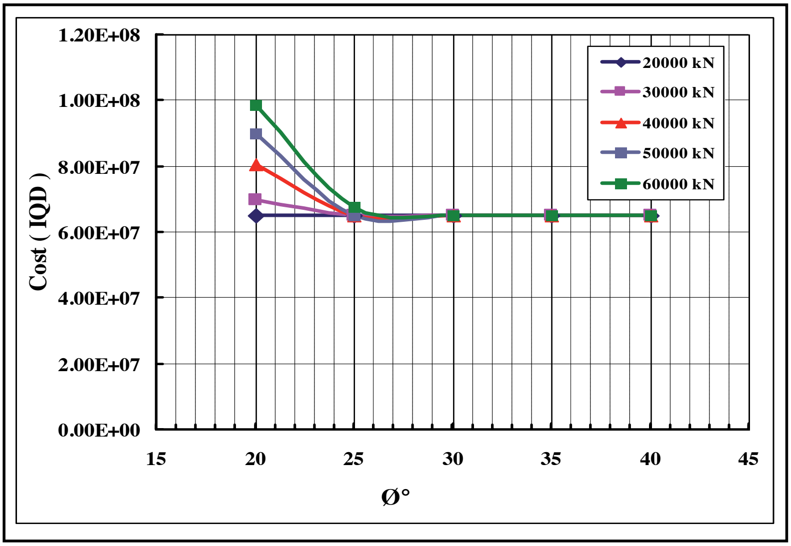

Figure 6-5 Relationship between Ø° and cost of piles

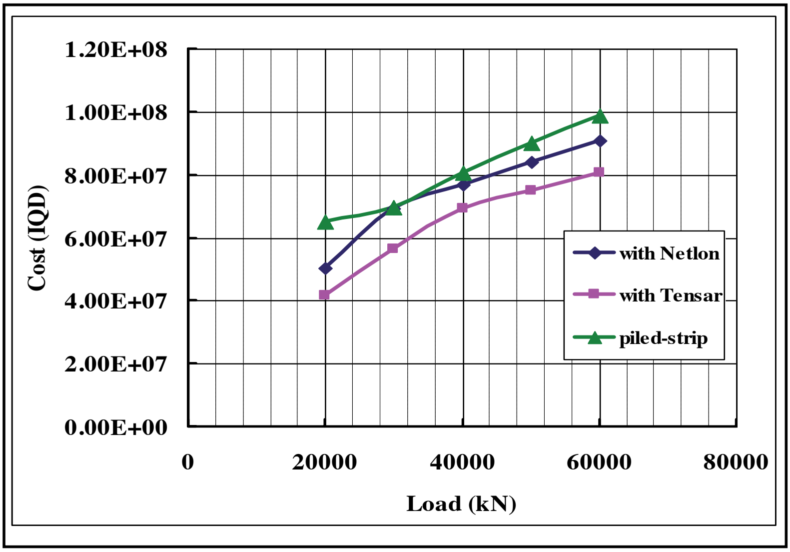

Figure 6-6 Relationship between load and cost of Ø = 20°

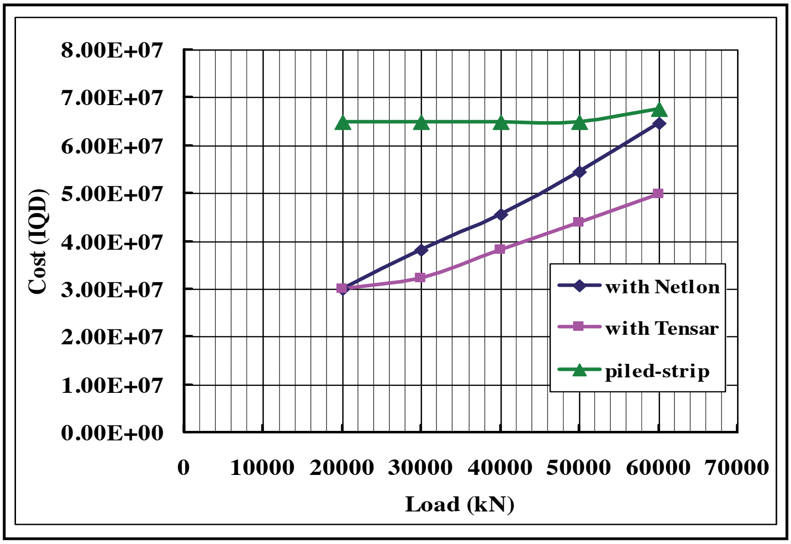

Figure 6-7 Relationship between load and cost of Ø = 25°

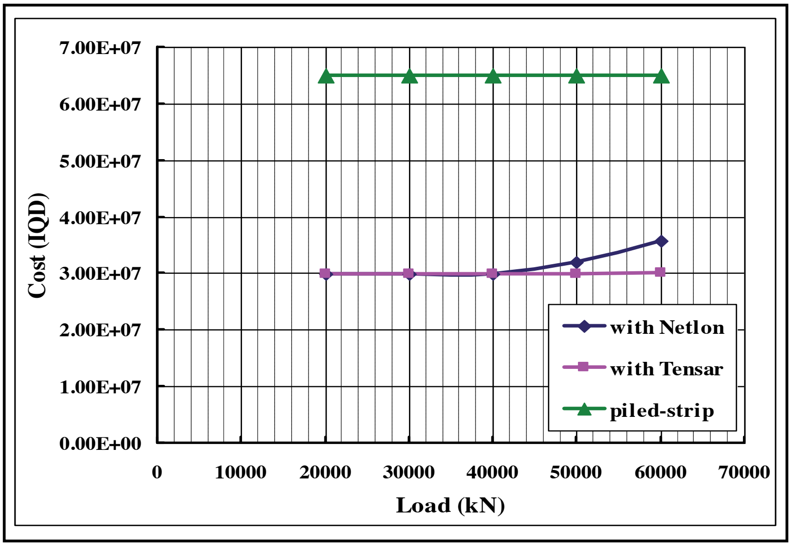

Figure 6-8 Relationship between load and cost of Ø = 30°

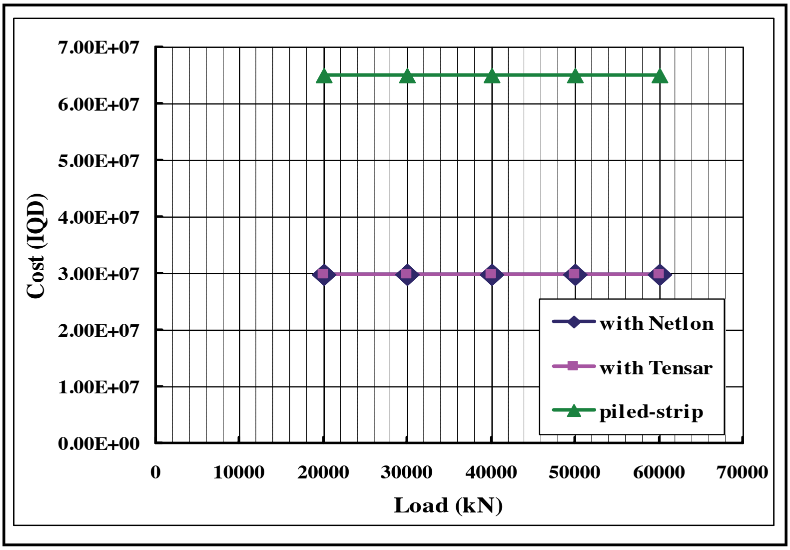

Figure 6-9 Relationship between load and cost of Ø = 35º

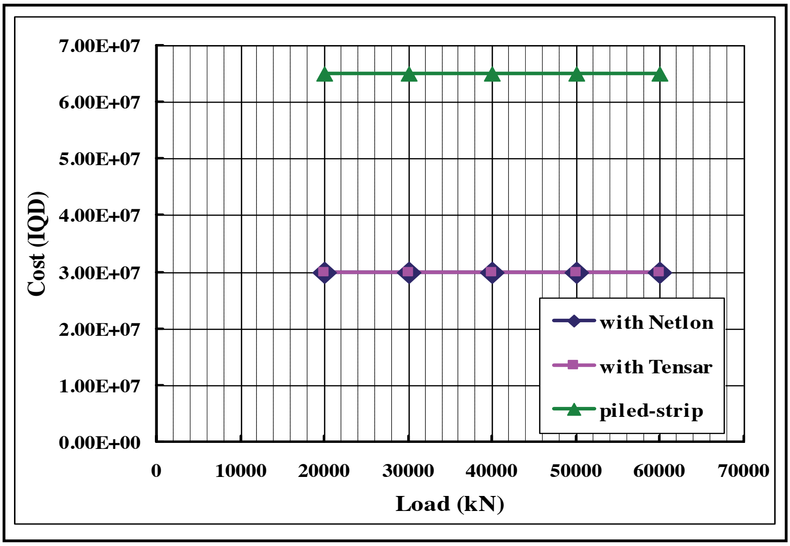

Figure 6-10 Relationship between load and cost of Ø = 40º

CHAPTER SEVEN

CONCLUSIONS AND RECOMMENDAIONS FOR FUTURE WORK

7.1 Conclusions from Experimental Work

7.1.1 Unreinforced and Reinforced Sand Model

The following conclusions are drawn based on the experimental study:

1- The shape of footing has an influence on the ultimate bearing capacity of unreinforced and reinforced sand. The bearing capacity of strip footing is higher than that of rectangular footing.

2- The reinforced to unreinforced bearing capacity ratio (BCR) for strip footing is 1.88 for Netlon CE121 and 2.5 for Tensar SS2.

3- The reinforced to unreinforced bearing capacity ratio (BCR) for rectangular footing is 2.35 for Netlon CE121 and 2.9 for Tensar SS2.

4- The Tensar SS2 geogrid has clearly caused the maximum enhancement in bearing capacity because its stiffness is higher than that of Netlon CE121. Therefore it recommended to use Tensar SS2 whenever the case need to bear higher loads.

5- The relative settlement of reinforced sand is smaller than that of unreinforced sand, the improvement in settlement of reinforced sand for strip footing amounts to 26.1% and 49.5% for Netlon CE121 and Tensar SS2 respectively. for rectangular footing the improvement in settlement amounts to 43.6% and 54.9% for Netlon CE121 and Tensar SS2 respectively.

7.1.2 The Geogrid Straining Mechanism

1- The horizontal distance from centerline of footing and the vertical depth underneath footing base has a very significant effect on the strains and elongations occurring in the geogrid ribs.

2- Strain and elongation increase with increasing stress and nearly reach a constant value just before reaching the ultimate bearing capacity. The results show also that

the nearest the strain gauge to the footing centerline the higher the strain and elongation in the strain gauge.

3- The values of strain and elongation decrease when the strain gauge distance from the centerline of footing for each layer increases. The distance of 3.6B indicates the approximate boundary of the zone of stress influence. This dimension of the stress zone offers an important indication of the required geogrids area for economic consideration.
4- The strain and elongation decrease as the depth under footing increase. The values of strain decrease to a small value for the third layer. Practically the depth B is that where the stress influence vanishes.
5- The maximum strain occurring in the ribs of Tensar SS2 geogrid is 0.000154 and 0.0000984 for strip and rectangular footing respectively.

7.1.3 Piled-Footings Systems

1- The piled-strip system gives an improvement in a total capacity reaching 438% greater than strip footing only and 232%, 175% greater than using Netlon CE121 and Tensar SS2 respectively.
2- The piled-rectangular system gives an improvement in a total capacity reaching 260% greater than rectangular footing only and 162%, 130% compared with that of using Netlon CE121 and Tensar SS2 respectively.
3- The components of group piles capacity involve 75.6% for end bearing and 24.4% for skin friction using plane strain piles model with strip footing.
4- Using rectangular piles with rectangular footing indicates that the end bearing resistance share is 73% and 27% for skin friction.

7.2 Comparisons of Experimental, Theoretical and Numerical Results

7.2.1 Bearing Capacity of Footings

1- Good agreement is obtained between experimental results and bearing capacity theories. For strip footing on unreinforced sand, the percentage of bearing capacity obtained from the experimental model and that obtained from Terzaghi, Meyerhof,

and Vesic equations are 80.5%, 90.9% and 87% respectively. For rectangular footing the agreement is 95.3%, 93.9% and 115% for the three equations respectively.

2- Good agreement is obtained between experimental and numerical results using PLAXIS 3D program for sand alone. The ratios of bearing capacity obtained from PLAXIS 3D program to experimental bearing capacity is 71.6%, 82% for strip and rectangular footings respectively

3- Good agreement is obtained between experimental and numerical results using PLAXIS 3D program for reinforced sand. For strip footing using Netlon CE121and Tensar SS2 geogrids, the percentage of bearing capacity obtained from PLAXIS 3D program to the experimental bearing capacity is 82.2% and 78.4% respectively. For rectangular footing the ratio is 85.2% and 82.8% for the two types of geogrids respectively.

7.2.2 Piled-Footings System

1- In SP sandy soil, the share of end bearing is 75.7% as a component of the pile capacity, while the share of skin friction is 24.3% using plane strain piles model with strip footing. In piled-rectangular system the share of end bearing is 72.9% as a component of the pile capacity, while the share of skin friction is 27.1%

2- Good agreement is obtained between experimental and numerical results using PLAXIS 3D program for piled-footings system. For piled-strip system, the ratio of total capacity obtained from PLAXIS 3D program to the experimental results is 74.7%. For piled-rectangular, the percentage of total capacity obtained from PLAXIS 3D program to the experimental results is 83.3%.

3- For skin friction and end bearing component capacity, the results shows a good agreement. The ratio of skin friction and end bearing results obtained from PLAXIS 3D program to the experimental work is 81.9% for piled-strip system and 80.6% for piled-rectangular system.

4- Good agreement is obtained for end bearing component capacity between experimental and numerical results using PLAXIS 3D program. The percentage of results obtained from PLAXIS 3D program to the experimental work is 83.3% for piled-strip system and 80.6% for piled-rectangular system.

7.3 Load Sharing Between Piles and Footing From Experimental and PLAXIS 3D Program

1- The capacity sharing of piles and footing is 66.2% for piles and 33.8% for footing in piled-strip system model in SP sandy soil. The sharing of piles and footing become 75% for piles and 25% for footing in the case of piled-rectangular system model.
2- In PLAXIS 3D program sharing between piles and footing is 73.1% for piles and 26.9% for footing in piled-strip system model, for piled-rectangular system model the sharing between piles and footing is 72.7% for piles and 27.3% for footing.

7.4 Economic Study

Optimization technique is used to estimate the field cost of construction of both types of constructions (reinforced soil and piles). Comparison between the two cases is adopted to decide in case that the use of geogrids is more economic than the use of piles within the range of applied load. The cost of construction is considered according to the prevailing regional prices at the period of this study. MATLAB package is used to formulate the optimization problems. The results indicate that:

1- The use of geogrids in the construction of interchange bridges on sandy soil is more economical than piles within the limits of design loads adopted in Iraq.
2- The type of geogrids does not affect the cost because of the high bearing capacity of sand, especially when the value of (Ø) is higher than (30º).
3- Savings when using geogrid reinforced soil reaches up to 54% of the construction cost compared to the piles foundation system for sandy soil having Øº higher than 25º.
4- The saving in cost increases rapidly when the value of (Ø) increases, especially when it becomes higher than (25º).
5- The overstated design of pile dimensions of the case study adopted in this research makes the cost of construction very high and makes the use of geogrids much more economical for the value of Øº larger 30º.

7.5 Recommendations for Future Work

It is recommended that future work should conduct:

1- Conduct laboratory tests using high stress level on reinforced sand to check dilatancy effects and the failure criterion.
2- Conduct laboratory tests for reinforced earth subjected to lateral loads.
3- Conduct field tests using the geogrid reinforced earth systems in conjunction with sophisticated instrumentation.
4- Conduct settlement analysis for unreinforced sand, reinforced sand and piles.
5- A study the advantage of using geosynthetics or fine geomesh to confine the zone of sand reinforced using geogrids.
6- Instrumenting few piles and caps being implemented in the construction of bridges.

REFERENCES

Alamshahi, S. and Hataf, N., (2009), "Bearing Capacity of Strip Footings on Sand Slopes Reinforced with Geogrid and Grid-Anchor", Journal of Geotextiles and Geomembranes, 27, pp. 217–226.

Al-Ani, T.M., (2008), "Reliability Based Design of Piled Raft Foundation", M.Sc. Thesis, University of Technology, Baghdad, Iraq.

Alawaji, H. A., (2005), "Creep and Rate of Loading Effects on Geogrid Reinforced Sand", Journal of Geotechnical and Geological Engineering, 23, pp. 583–600.

Al-Jebouri, J. M. (1986), "Bearing Capacity of Footing on Reinforced Sand", M.Sc. Thesis, University of Baghdad, Iraq.

Al-Omari, R.R., (1984), "Strip Foundation on A Sand layer overlying A Rigid Stratum", Ph.D. Thesis, Strathclyde University, Scotland, UK.

Al-Omari, R. R., Al-Dobaissi, H. H. and Al-wadood, B. A., (1987), "Inextensible Geomesh Included in Sand and Clay", Prediction and Performance in Geotechnical Engineering/Calgary/17-19 June, pp. 155-160.

Al-Omari, R. R., Mahmood, A. K. and Hamodi, F. J., (1988), "Dilatancy and Failure of Reinforced Sand", International Geotechnical Symposium on Theory and Practice of Earth Reinforcement/ Fukuoka Japan/ 5-7 October pp. 57-62.

Al-Omari, R.R., Nazhat, Y. N. and Dobaissi, H. H., (1995), "Effect of Stiffness and Amount of Reinforcement on Strength of Sand", Journal of Engineering Geology, No. 28, pp. 363-367.

AL-Sinaidi, A. R. and, Ali, A. H., (2006) "Improvement in Bearing Capacity of Soil by Geogrid - an Experimental Approach", IAEG 2006, paper No.240.

API (American Petroleum Institute), (1993), "Recommended Practice for Planning, Designing and Constructing Fixed Offshore Platforms – Load and Resistance Factor Design", API Recommended practice 2A-LRFD, 1st edition.

ASTM D422-63, 2007, "Standard Test Method for Particle Size-Analysis of Soils".

ASTM D792, 2007, "Standard Test Methods for Density and Specific Gravity (Relative Density) of Plastics by Displacement".

ASTM D854-05, 2007, "Standard Test Method for Specific Gravity of Soil Solids by Water Pycnometer".

ASTM D1388-96, 2007, "Standard Test Method for Stiffness of Fabrics".

ASTM D1505-03, 2007, "Standard Test Method for Density of Plastics by the Density-Gradient Technique".

ASTM D1777-96, 2007, "Standard Test Method for Thickness of Textile Materials".

ASTM D4253-2007, "Standard Test Method for Maximum Index Density and Unit Weight of Soils Using a Vibratory Table".

ASTM D4254-2007, "Standard Test Method for Minimum Index Density and Unit Weight of Soils and Calculation of Relative Density".

ASTM D6637-01-2007, "Standard Test Method for Determining Tensile Properties of Geogrids by the Single or Multi-Rib Tensile Method".

Bowles, J. E., (1996), "Foundation Analysis and Design", 5th Edition, McGraw-Hill Book Company.

BS 812, (1988) and ICS 91.100.15 71.080.01 19.020, manual 895/2003, "Testing Aggregates", Part 118, Method for Determination of Sulphate Content.

Chen, Q., (2007), "An Experimental Study on Characteristics and Behavior of Reinforced Soil Foundation", Ph.D. Thesis, University of Louisiana State, USA.

Das, B. M., (1999), "Shallow Foundation", Library of Congress in Publication.

Das, B. M., Omar, M. T., Puri, V. K. and Yen, S. C., (1993), "Ultimate Bearing Capacity of Shallow Foundation on Sand with Geogrid Reinforcement", Journal of Cand., 30, pp.545-549.

Day Robert W., (2006), "Foundation Engineering Handbook", Design and Construction with the 2006 international building code, McGraw-Hill Book Company.

El-Sawwaf, M., (2009), "Experimental and Numerical Study of Eccentrically Loaded Strip Footings Resting on Reinforced Sand", Journal of Geotechnical and Geoenvironmental Engineering, ASCE, October, pp.1509-1518.

Fakhraldin M. K., (2013), "Properties Measurements and Applications of some Geogrids in Sand", PhD Thesis, Alnahrain University.

Fannin, R. J., (1986), "Geogrid Reinforced of Granular Layers on Soft Clays A Study at Model and Full Scale", PhD. Thesis, University of Oxford, UK.

FHWA (U.S. Department of Transportation, Federal Highway Administration), (2006), "Soils and Foundations", Reference Manual – Volume II.

Gandhi, S.R. and Maharaj, D.K., (1996), "Analysis of Piled Raft Foundation", Bombay, India, Sixth International Conference and Exhibition on Piling and Deep Foundations.

Gassler, G. and Gudehus, G., (1981), "Soil Nailing-Some Aspects a New Technique", Proc. 10th Int. Conference. SMFE, Stockholm.

Geo-Institute Committee on Shallow Foundations, (2004), "Bering Capacity and settlement of Shallow foundations reinforced Soil", A Bibliography of the Technical Literature.

Hadi, N. H., (2010), Private Communications. Assistant Professor, Mechanical Engineering Department, College of Engineering, University of Baghdad.

Hain, S.J. and Lee, I.K., (1978), "The Analysis of Flexible Raft-Pile Systems", Geotechnique Vol. 28, No. 1, pp. 65-83.

Haripal, P. K., Behera, R. N and C R Patra, C. R., (2008), "Behavior of Surface Strip Footing on Geogrid Reinforced Sand Bed", the 12th International Conference of International Association for Computer Methods and Advances in Geomechanics (IACMAG), 1-6 October, Goa, India.

Head, K. H., (1984), "Manual of Soil Laboratory Testing", British Library Cataloguing in Publication Data.

Holm, G and Olsson C., (1993), "Pile foundation", The Swedish Building Centre and the Swedish Geotechnical Institute , Stockholm

Hooper, J.A., (1973), "Observations on the Behavior of a Piled-Raft Foundation on London Clay", Proceeding of Institution of Civil Engineers, Vol.55, No.2, pp. 855-877.

Kumar, S. V. and Llamparuthi, K., (2009), "Response of Footing on Sand Slopes", Indian Geotechnical Society Chennai Chpter.

Kuwabara, F. (1989), "An Elastic Analysis for Piled Raft Foundations in a Homogeneous Soil", Soils and Foundations, vol.29, No.1, pp.82-92.

Latha, G. M. and Somwanshi, A., (2009), "Effect of Reinforcement form on the Bearing Capacity of Square Footings on Sand", Journal of Geotextiles and Geomembranes 27, pp. 409–422.

Liu, W. and Novak, (1991), "Soil – Pile – Cap Static Interaction Analysis by Finite and Infinite Elements", Canadian Geotechnical Journal, Vol.28, pp.771-783.

Leng, J., (2002), "Characteristics and Behavior of Geogrid-Reinforced Aggregate under Cyclic Load", Ph.D. Thesis, University of North Carolina state, USA.

Liang F. Y., Chen L. Z., and Shi X. G. (2003), "Numerical Analysis of Composite Piled Raft with Cushion subjected to Vertical Load", Computers and Geotechnics, pp. 443-453.

Lovisa, J., Shukla, S. K. and Sivakugan, N., (2010), “Behaviour of Prestressed Geotextile-Reinforced Sand Bed Supporting A Loaded Circular Footing”, Journal Geotextiles and Geomembranes, 28, pp. 23–32.

MATLAB Manual, (2014), “MATLAB R2014a 8.3.0.532 Win 32 Software”, License Number 271828, February 11, 2014.

Maubeuge K. von, NAUE GmbH & Co. KG, Espelkamp-Fiestel, (2008), “ Reinforcement of Base Courses with Geogrids - Related Issues”, The First Pan American Geosynthetics Conference & Exhibition, 2-5 March 2008, Cancun, Mexico.

Mohammed Wajeeh and Ilamparuthi T.P. K., (2010), “Performance of Footing on Sand Bed With and Without Reinforcement”, Indian Geotechnical Conference16-18 December.

Naeini Seyed Abolhasan, Hosseinzade Mohammad, (2014) “Evaluation of Bearing Capacity of Vertically Loaded Strip Piled-Raft Embedded in Soft Clay”, World Academy of Science, Engineering and Technology International Journal of Civil, Architectural, Structural and Construction Engineering Vol:8 No:1, 2014.

Nakai, S., Mano, H., Kato, H., Ishida, R., (2004), “Effect of Pile/Raft Connection Condition on the Dynamic Behavior of Piled Raft Foundation”, 11th International Conference on Soil Dynamics and Earthquake Engineering and the 3rd International Conference on Earthquake Geotechnical Engineering Proceedings, Volume 2. Vol. 2, pp. 821-828.

Oyegbile B. O., (2011), “ Parametric Studies on the Behaviour of Reinforced Soil Retaining Walls under Static and Dynamic Loadings”, MSc. Thesis, The National Technical University, Postgraduate school of civil engineering.

Palmeira, E. M., (1987), “The Study of Soil-Reinforcement Interaction by Means of Large Scale Laboratory Test”, Ph.D. Thesis, Oxford University, Britain.

Patra C. R., Das B. M. and Atalar C., (2009), “Bearing |Capacity of Embedded Strip Foundation on Geogrid-Reinforced Sand”, Technical note.

Pedley, M. J., (1990), “The Performance of Soil Reinforcement in Bending and Shear”, Ph.D. Thesis, Oxford University, Britain.

Pelletier, J.H., Murff, J. D., A. C., (1993),“Historical Development and Assessment of the Current API Design Method for Axially Loaded piles", In Proc. Offshore Technology Center, Houston, TX, OTC paper 7157, pp. 253-282.

Phanikumar, B. R., Prasad, R. and Singh, A., (2009), “Compressive Load Response of Geogrid-Reinforced Fine, Medium and Coarse Sands”, Journal of Geotextiles and Geomembranes, 27, pp.183–186.

Poulos, H. G., (2001), “Methods of Analysis of Piled Raft Foundations”, a report prepared on Behalf of Technical Committee TC18 on piled foundations, website, www.issmge.org.

Prakoso W.A. and Kulhawy F.H. (2001), “Contribution to Piled Raft Foundation Design”, Journal of Geotechnical and Geoenvironmental Engineering, vol. 127, No. 1, ASCE, pp. 17-24

Research development and technology, (2001), “Performance Test for Geosynthetics Reinforced Soil Including Effect of Preloading”, Federal Highway Administration.

Reul, O., (2005), “Interplay Between in Situ – Measurements and Numerical Modeling in the Design of Foundations and Deep Excavations”, Proceeding 9th International Symposium on Numerical Models in Geomechanics, Ottawa, Rotterdam: Balkema.

Ryltenius, Andre. (2011) “FEM Modelling of Piled Raft Foundations in Two and Three Dimensions”. Master’s Dissertation. Geotechnical Engineering, Lund University.

Shin E. C. and Das B. M., (2000), “Experimental Study of Bearing capacity of a Strip Foundation on Geogrid-Reinforced sand”, Journal of Geosynthetics International, Vol. 7, No. 1, pp.59-71.

Shinde, A. L. and Mandal, J. N., (2007), “Behavior of Reinforced Soil Retaining Wall with Limited Fill Zone”, Journal of Geotechnical and Geology Engineering, 25, pp. 657–672.

Sinha Anup, (2013), “3-D Modeling of piled Raft Foundation”, PhD. Thesis, The Department of Building, Civil and Environmental Engineering, Concordia University, Canada.

Small, J.C. and Zhang, H.H., (2000), “Piled Raft Foundations Subjected to General Loadings”, Developments in Theory Geomechanics, Ed. D.W. Smith, & J.P. Carter, Balkema, Rotterdam, pp. 431-444.

Sulaiman, R. M., (1991), “Interference between Adjacent Footings on Reinforced Earth”, M.Sc. Thesis, University of Mosul, Iraq.

Tafreshi, S. N. M. and Dawson, A. R., (2010), “Comparison of Bearing Capacity of A Strip Footing on Sand with Geocell and with Planar Forms of Geotextile Reinforcement”, Journal of Geotextiles and Geomembranes, 28, pp. 72–84.

Tan Y.C. and Chow C.M, (2004), “Design of piled raft foundation on soft ground, GSMIEM Forum”, The roles of Engineering geology & geotechnical engineering in construction works, Department of Geology, University of Malaysia.

Terzaghi, K., (1943), “Theoretical Soil Mechanics”, John Wily and Sons, NewYork.

The Reinforced Earth Company, 12001 Sunrise Valley Drive, Ste 400, Reston, VA 20191, website http://www.reinforcedearth.com/locations-contacts.html.
Tomlinson Michael and John Woodward, (2008),“Pile Design and Construction Practice”, Fifth Edition, Tailor and Francis Group, London and New York.

U.S. Army Corps of Engineers (1991), "Design of Pile Foundations", Engineer Manual, 1110-2-2906.

Wikipedia, The free encyclopedia, (2014), "Geosynthetics", website http://en.wikipedia.org/wiki/Geosynthetics.

Yamashita, K., Kakurai, M. and Yamada, T., (1994), "Investigation of a Piled Raft Foundation on Stiff Clay", XIII International Conference on Soil Mechanics and Foundation Engineering, New Delhi, India, pp. 543-546.

Yu Bao, (2003), "Three-Dimensional Nonlinear FEM Analysis of Vertically loaded Piled Raft", Term Project Report, ASEN 5367 Advanced Finite Element Method.

Zhang, M. X., Javad, A. A. and Min, X., (2006), "Triaxial Tests of Sand Reinforced with 3D Inclusions", Journal of Geotextiles and Geomembranes, 24, pp. 201–209.

Zhou, H. and Wen, X., (2008), "Model Studies on Geogrid- or Geocell-reinforced Sand Cushion on Soft Soil", Journal of Geotextiles and Geomembranes 26, pp. 231–238.

APPENDIX A

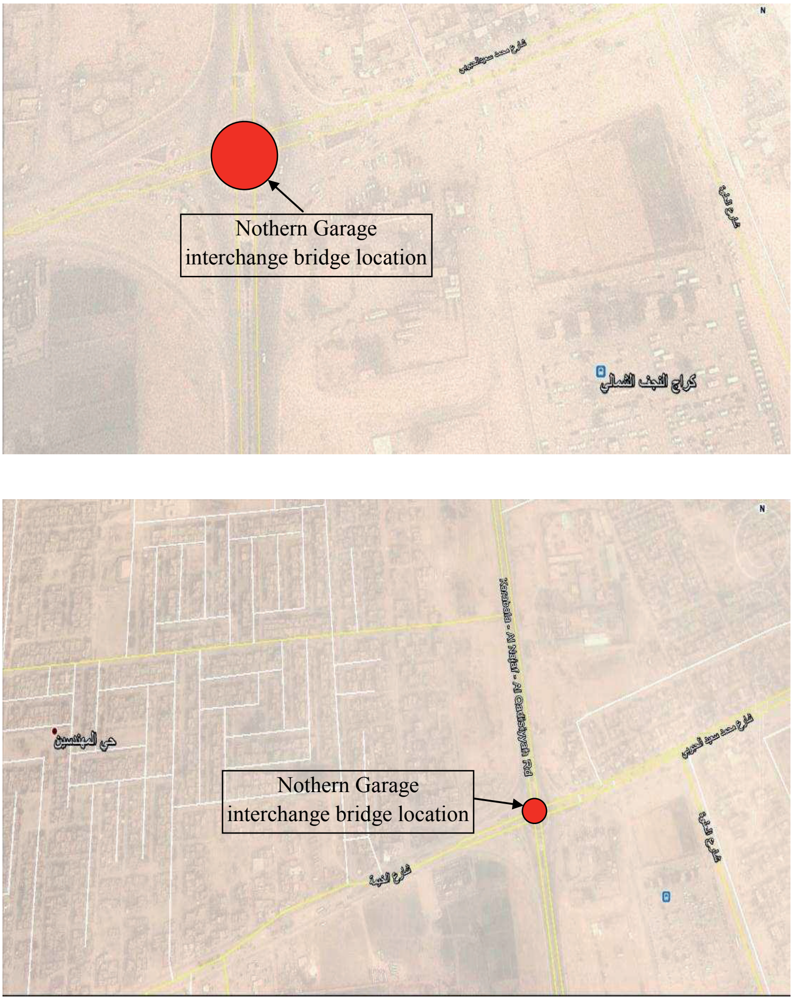

Figure A-1 Location of the Nothern Garage interchange bridge in Al-Najaf city

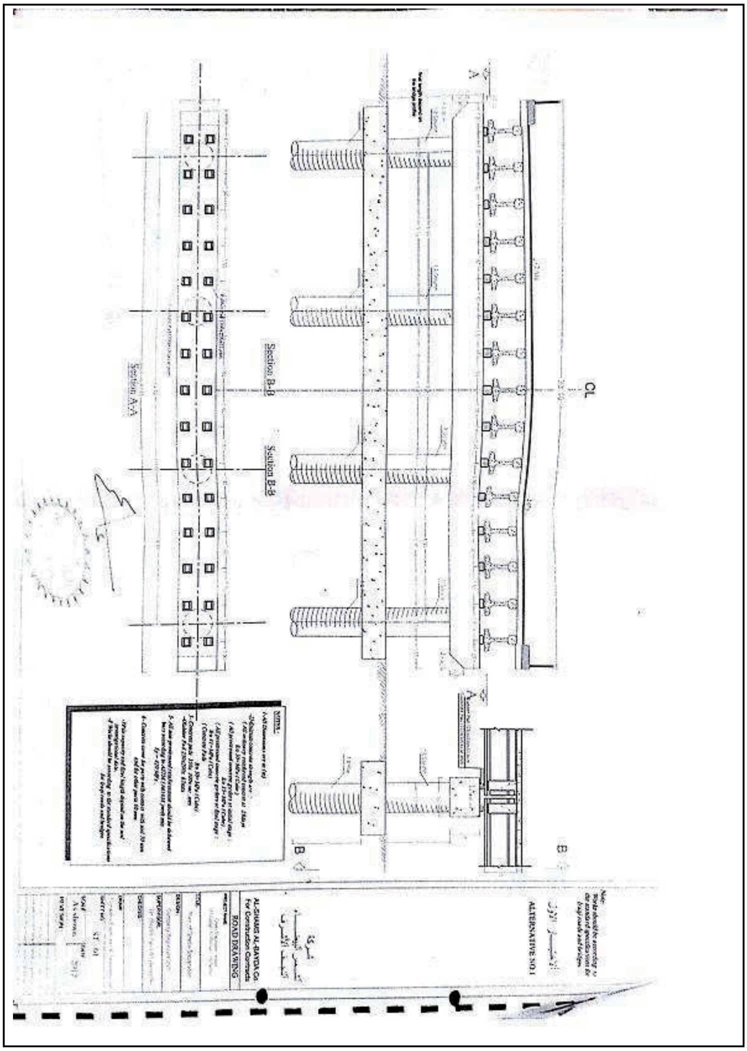

Figure A-2 Plan of grade separation of bridge

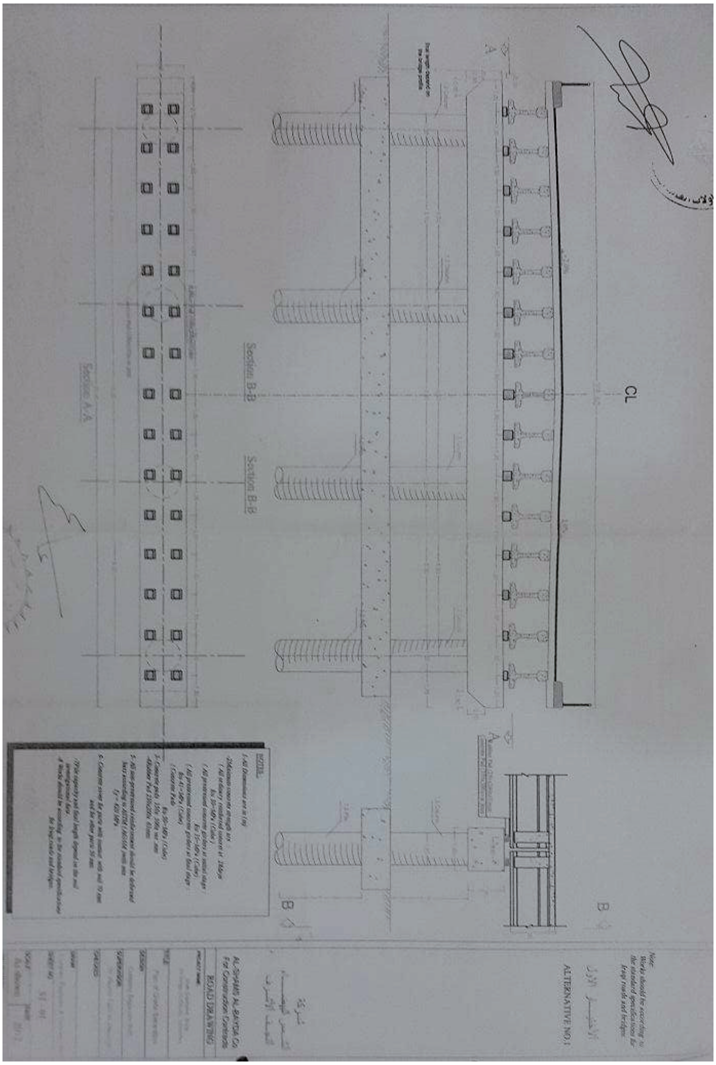

Figure A-3 Row of piers and piles

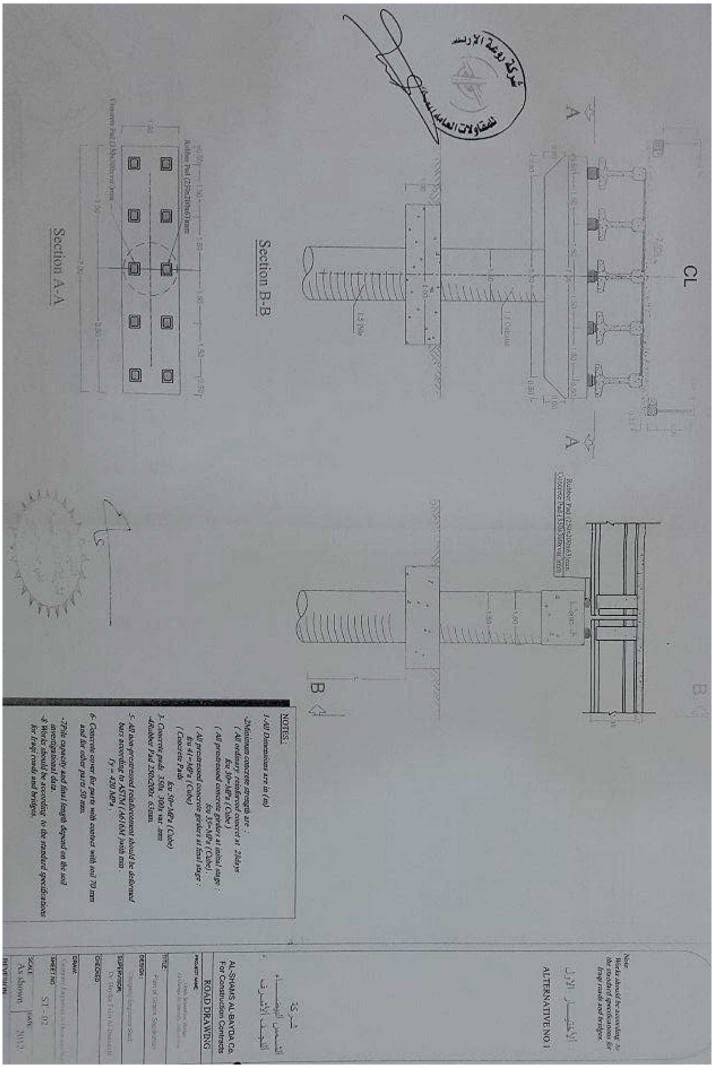

Figure A-4 Section of piled-strip system of bridge

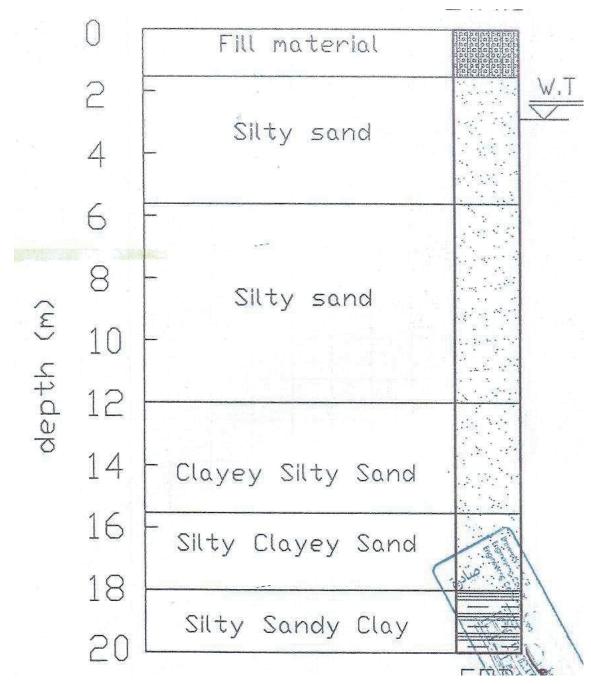

Figure A-5 Section in site soil of project

Calculation of Loads

Given data:

Typical span = 23.5 m (6 lanes)

Spacing of girders = 1.5 m

No. of girders = 15

Deck overlap = 1.2 m

All piles constructed with diameter = 1.5 m as presented in the tender of contracting. (Table A-1, as presented in contracting documents).

Carriage way = 14 spacing @ 1.5 m = 21 m

Total span = 8 spans @ 23 m = 184 m

Beam type = prestressed concrete girder of height = 1.35 m

Weight of beam = 230 kN

Weight of beam per length = (230/25) = 9.2 kN

(Fig. A-6)

Calculate dead load per span

- **Slab = 0.2 × 25 × 23.4 × 25 = 2925 kN**
- **Sidewalk = 2 × 1.2 × o.3 × 23.4 × 25 = 421.2 kN**
- **Surface = 0.08 × 22 × 21 × 25 = 924 kN**
- **Diaphram = 3 × 0.3 × 1.2 × 1.25 × 23.4 = 31.59 kN**
- **Beam (girder) = 15 × 230 = 3150 kN**

Then,

Total dead load = 7751.8 kN per span

Live load per span (Iraqi Standard)

No. of lanes = 6 , lane width = 3 m

1) **U.D.L = 32.2 kN/m of lane**

Modified U.D.L = 32.2 × (3/3.05) = 31.67 kN/m of lanes

U.D.L = 2 × 31.67 v 25 + (2/3) × 31.67 × 25 = 2106 kN

KEL = 2 × 40.18 × 3 + (2/3) × 40.18 × 3 = 301.35 kN

Sidewalk = 3.78 × 2 × 1.2 × 25 = 226.8 kN

Then,

Total live load = 2634.15 kN per span

2) **Military loading**

Two tracks 90 tons tanks = 900 kN

2 × 900 = 1800 kN

I = 0.32 from table for impact factor

I/2 = 0.16

(L.L + I) = 1.16 × 1800 = 2088 kN

3) **Apply load to span configuration for max. effect: apply at joint for max. reaction.**

18.43 × 17.38 = 320.31

18.43 × (17.38+1.58) = 355.9

27.66 × (19.51 + 3.66) = 640.9

13.83 × 14.51 = 200.7

Then,

Total load = (1517.8)/25 → 60.4 + 27.66 = 88.37 tons × 2 = 176.74 tons

= 1767.4 kN

R = (L.L× I) = 1.32 × 1767.4 = 2333 kN

SW = 226.8 kn

Then,

Total load = 2559.8 kN < 2634 kN

Load on pier

Max. L.L = 2634 kN

D.L = 7751.8 kN

Then,

<u>Total load = 10386 kN per pier.</u>

Table A-1 Part of contracting tender of case study

2,520,000,000	60,000,000	42	عدد	تجهيز المواد و المعدات اللازمة لصب ركائز خرسانية مسلحة باستعمال السمنت المقاوم للأملاح صنف C30 بقطر 1.5 متر وحسب المخططات و التصاميم الإنشائية شاملا السعر حديد التسليح و كافة متطلبات العمل من الحفريات اللازمة والاسناد وحسب المواصفات العامة للطرق و الجسور و توجيهات المهندس المشرف.	7
2,660,000,000	1,400,000	1900	م³	صب خرسانة مسلحة لاسس الجدران والAbutment والapproach slab صنف C30 وحسب المخططات الانشائية والمواصفات العامة للطرق والجسور.	8
1,200,000,000	1,500,000	800	م³	تجهيز مواد وصب خرسانة مسلحة للجدران الاستنادية باستعمال السمنت المقاوم للاملاح صنف C30 مع استخدام الفلانكوت من الداخل وحسب المواصفات العامة للطرق والجسور.	9
130,000,000	1,300,000	100	م³	تجهيز المواد و المعدات اللازمة لصب خرسانة مسلحة للأعمدة صنف C30 حسب المخططات و التصاميم الإنشائية وحسب المخططات الانشائية والمواصفات العامة للطرق والجسور.	10
494,000,000	1,300,000	380	م³	تجهيز المواد و المعدات اللازمة لصب خرسانة مسلحة لقبعة الاعمدة CROSS BEAM صنف C30 وحسب المخططات و التصاميم الإنشائية شاملا السعر حديد التسليح و كافة متطلبات العمل.	11
380,000,000	1,250,000	304	عدد	تجهيز و نصب مساند ارتكاز مطاطية حسب المواصفات الفنية مع صب قواعدها الخرسانية المسلحة بخرسانة صنف C50 بموجب المخططات الانشائية.	12
4,480,000,000	35,000,000	128	عدد	تجهيز و نصب روافد من الخرسانة المسلحة المسبقة الصب وباطوال مختلفة حسب المخططات و التصاميم الانشائية شاملا السعر كل ما يلزم لتنفيذ العمل بموجب المواصفات العامة للطرق و الجسور و توجيهات المهندس المشرف.	13
1,500,000,000	1,000,000	1500	م³	تجهيز المواد و المعدات اللازمة لصب خرسانة مسلحة لسطح الجسروالمماشي والدايفرامات وكافة المقاطع الخرسانية الاخرى المتعلقة بسطح الجسر صنف C30 وحسب المخططات و التصاميم الانشائية شاملا السعر كل ما يلزم لتنفيذ العمل بموجب المخططات الانشائية.	14

Page 2 of 4

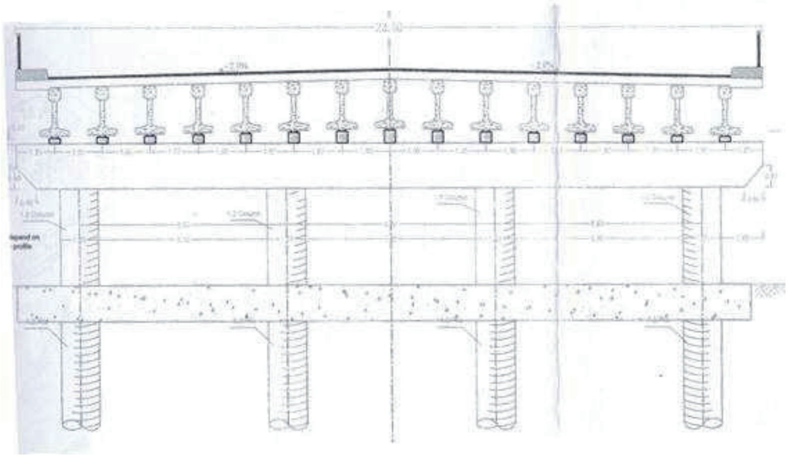

Figure A-6 Cross section of Bridge

APPENDIX B

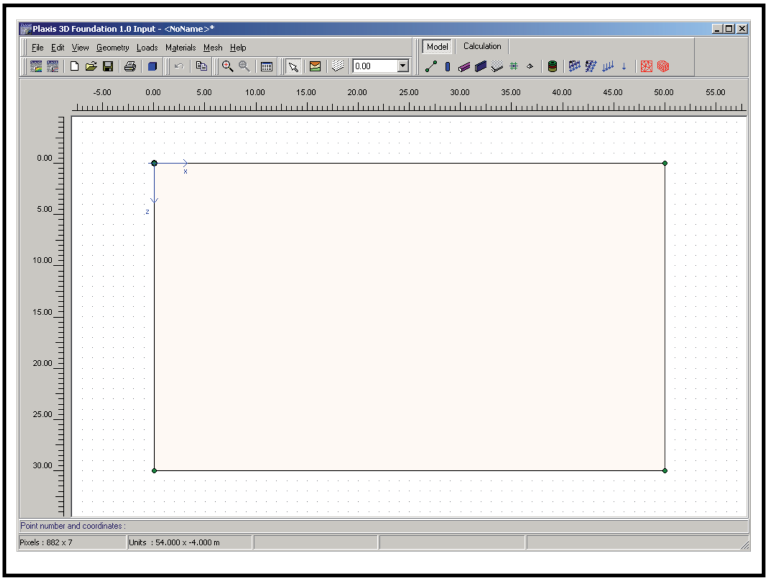

Figure B-1 Main window of the input program (Model mode)

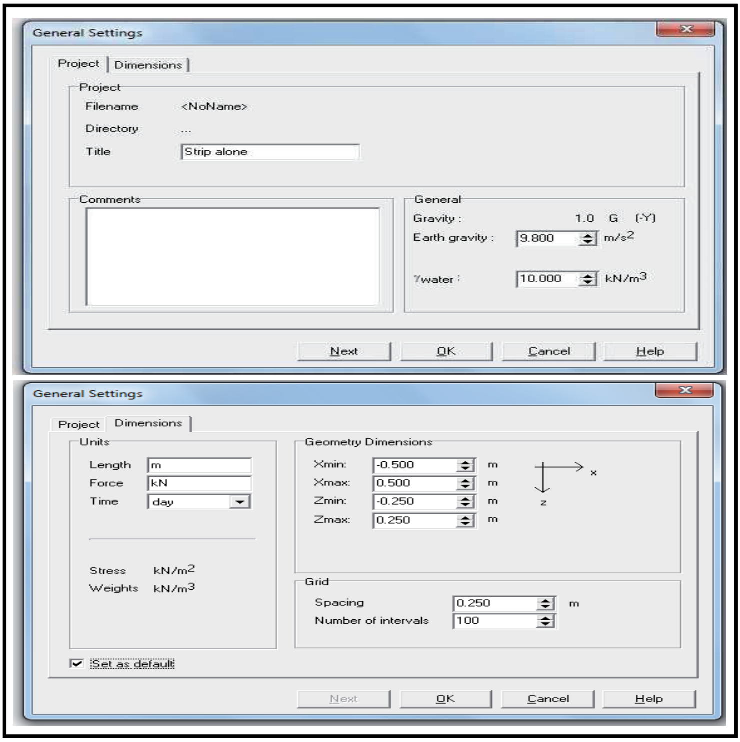

Figure B-2 Project and dimensions tabs sheet of the general settings window

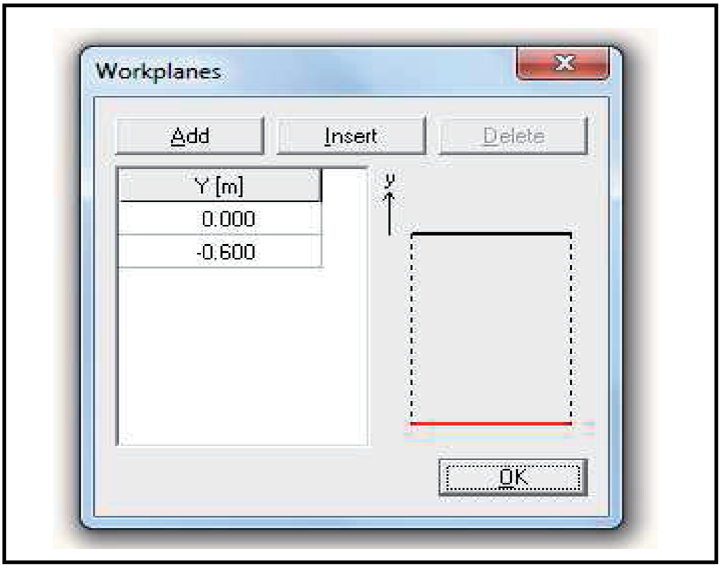

Figure B-3 Work-planes window

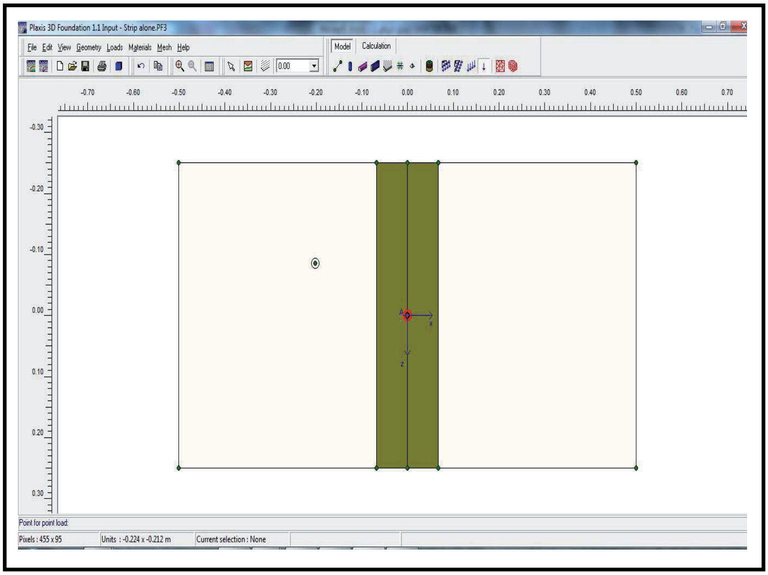

Figure B-4 Final geometry of the strip footing case

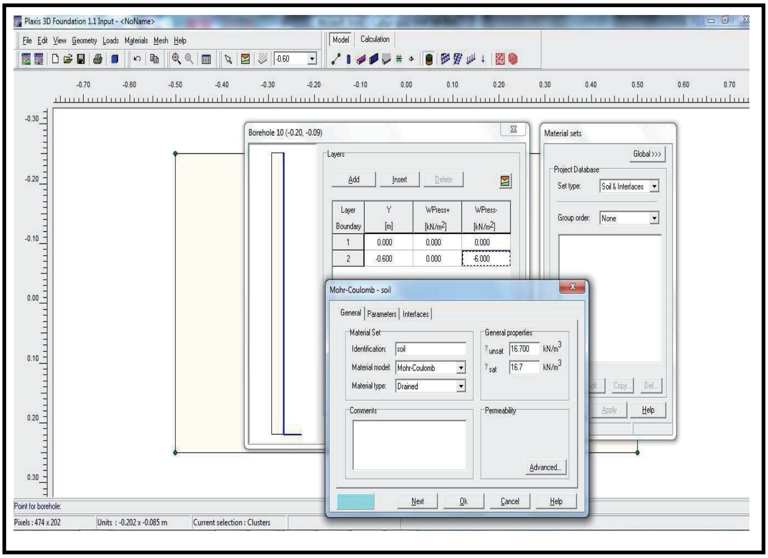

Figure B-5 Borehole of the strip footing case

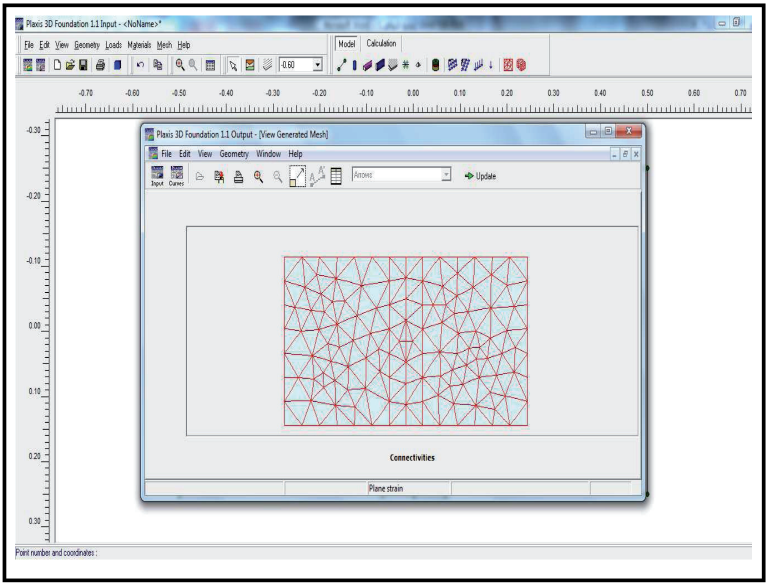

Figure B-6 2D finite element mesh of the geometry

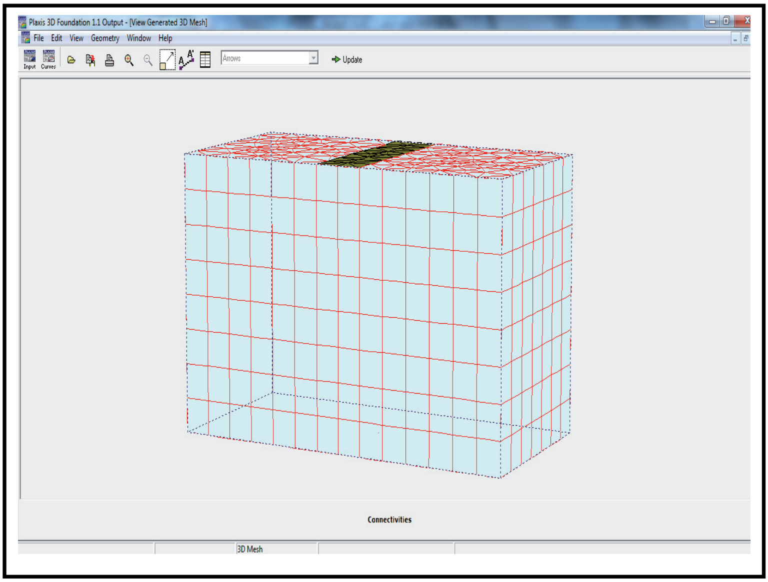

Figure B-7 Generated 3D mesh in the output window

Figure B-8 The calculations toolbar

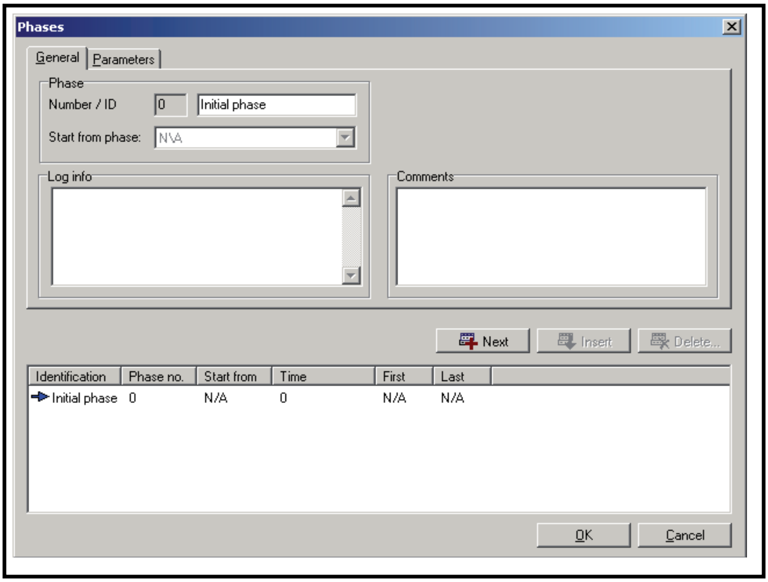

Figure B-9 The phases window with the general tab sheet

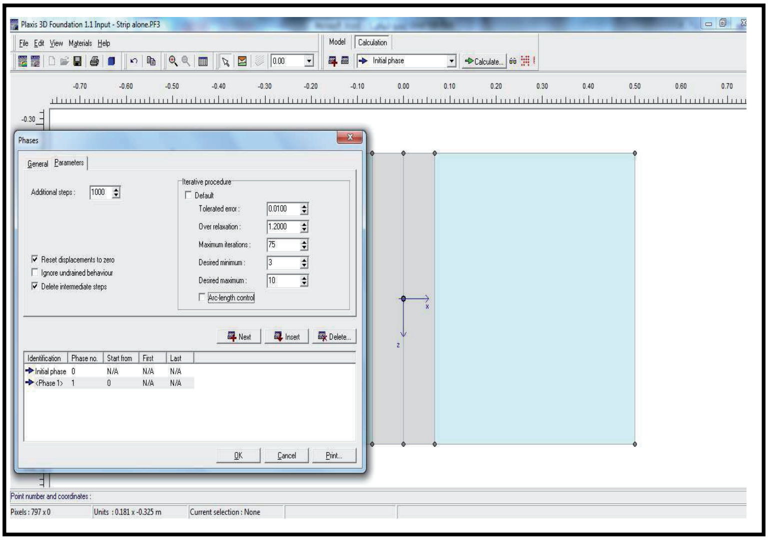

Figure B-10 The parameters tab sheet of the phases window

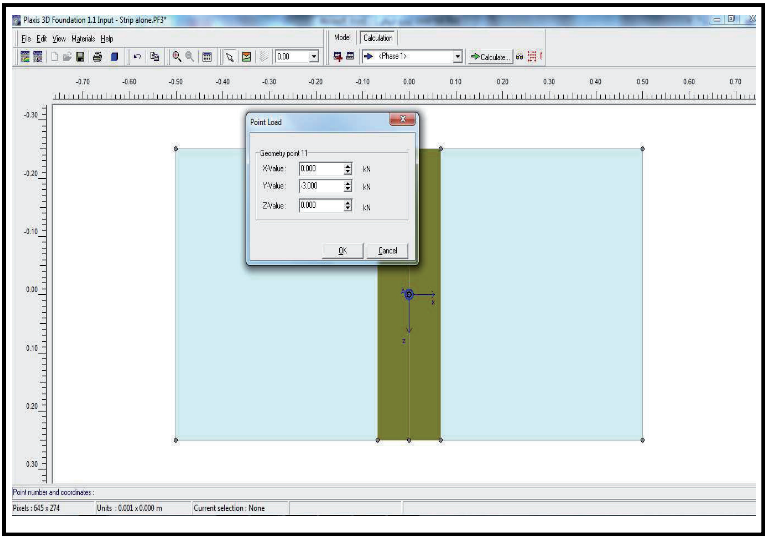

Figure B-11 Setting the magnitude of load for phases

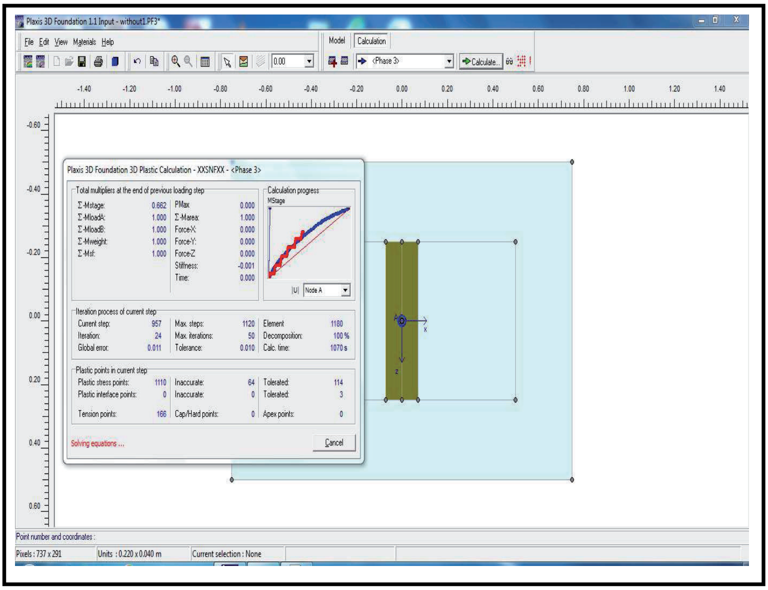

Figure B-12 The calculations information window

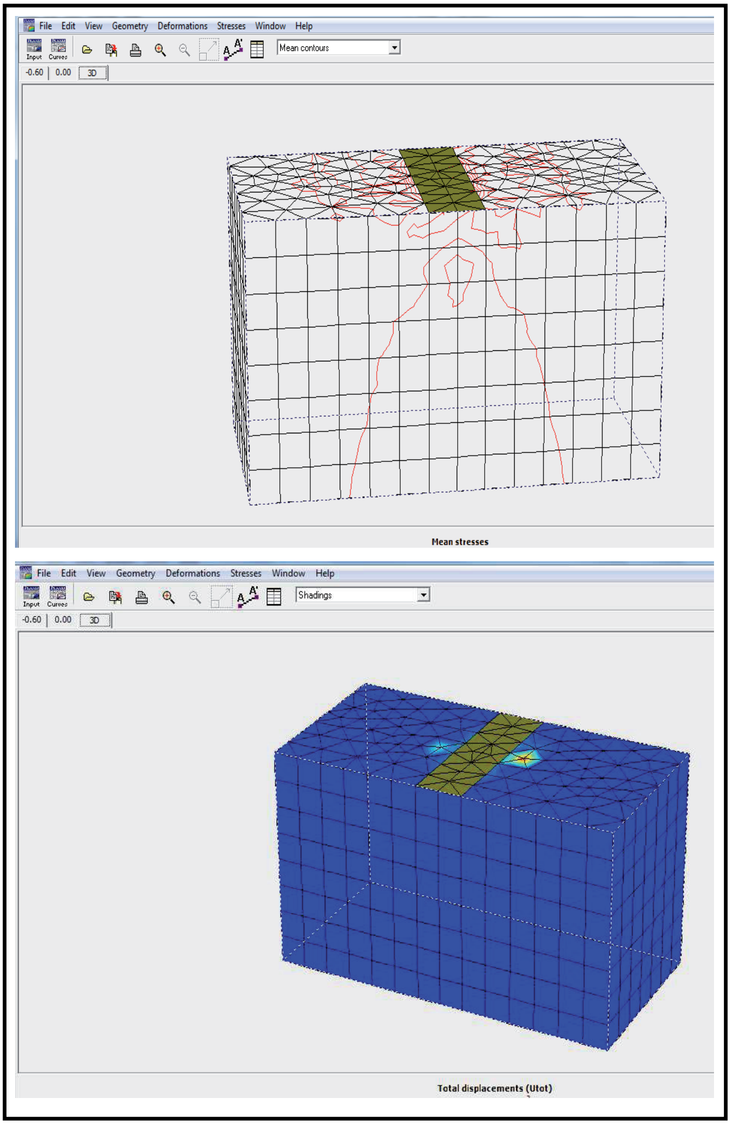

Figure B-13 Samples of Outputs

```
function F=COST(x)
cg=10000;
ce=1000;
cw=2000;
cf=1000;
nl=3;
sz=7.2;
ef=1.2;
F=nl*cg*sz*x(1)*x(2)+ef*ce*x(1)^2*x(2)+nl*cw*sz*x(1)*x(2)+ef*sz*cf*x(1)^2*x(2);
end
```

```
function [c,ceq]=CONSCOST(x)
gama=10.33;
fai=44;
Nq=(exp(pi*tan(fai*pi/180)))*(tan((45+fai/2)*pi/180))^2;
BCR=2.5;
SF=3;
P=41544;
g1=-0.5*gama*x(1)*(1.5*(Nq-1)*tan(fai*pi/180))*(1-0.4*x(1)/x(2))*BCR*x(1)*x(2)+SF*P;
g2=-3*(0.5*gama*x(1)*(1.5*(Nq-1)*tan(fai*pi/180))*(1-0.4*x(1)/x(2))*BCR*x(1)*x(2))+SF*P;
c=[g1 g2]
ceq=[];
end
```

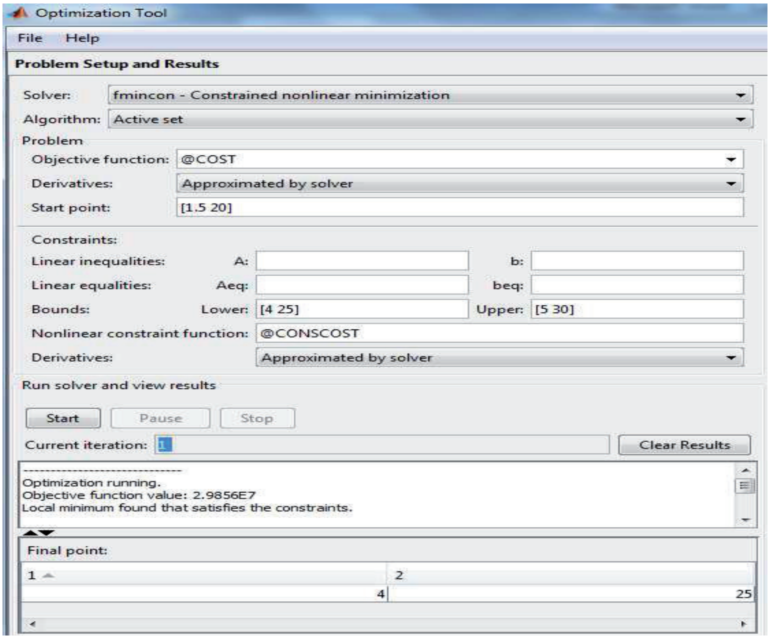

Figure B-14 Formulation and running the optimization of reinforced soil case in MATLAB

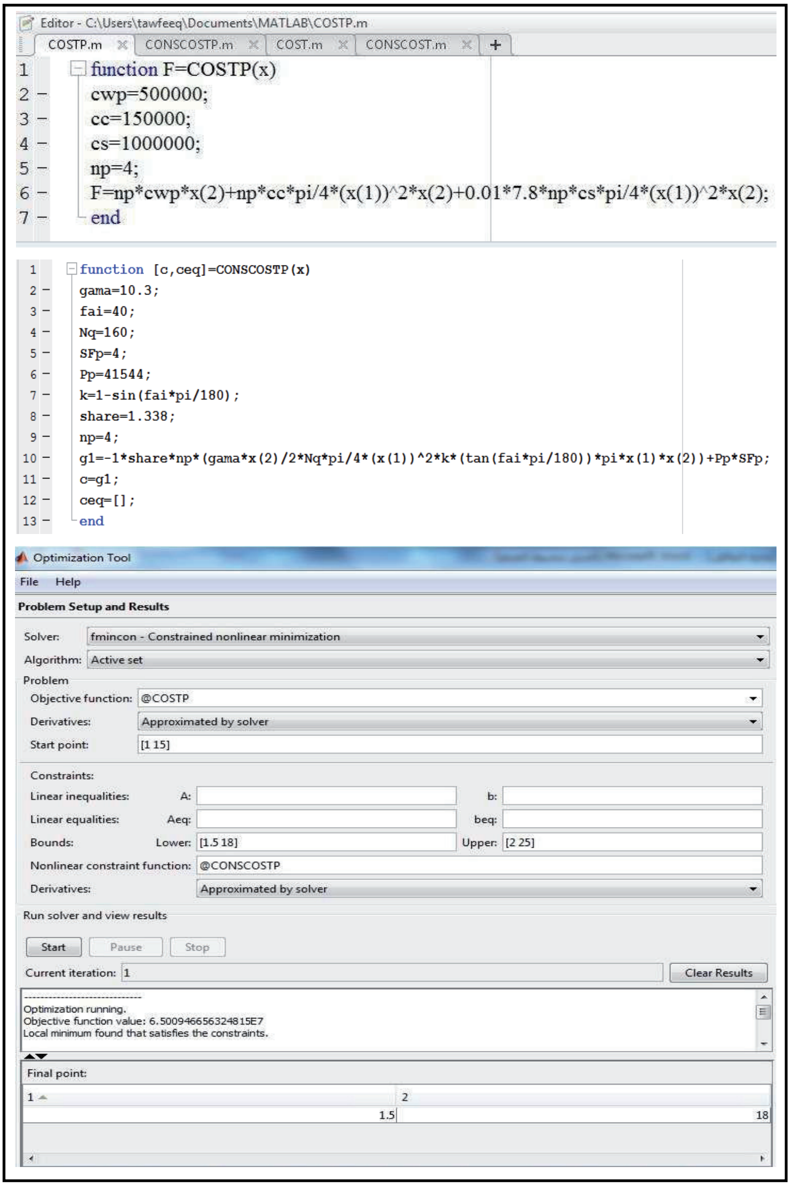

Figure B-15 Formulation and running the optimization of piles in MATLAB

PAPERS

1) Tawfek Sheer Ali, Raid R. Al-Omary, Zeyad S. M. Kaled, (2014). "**Behavior of Geogrids under Strip Footing Resting on Sandy Soil**", Asian Academic Research Journal of Multidisciplinary (AARJMD), Volume 1, Issue 24, August 2014, pp. 591-609.

2) Tawfek Sheer Ali, Raid R. Al-Omary, Zeyad S. M. Kaled, (2014). "**Behavior and Load Sharing of Piled-Strip System in Sandy Soil**", International Journal of Scientific and Engineering Research (IJSER), Volume 5, Issue8, August 2014 Edition (ISSN 2229-5518), pp. 1028-1034.

3) Accepted paper in the **15th Asian Regional Conference on Soil Mechanics and Geotechnical Engineering (15ARC) which will be held from 9 to 12 November 2015 in Fukuoka, Japan.**

   Raid R. Al-Omary, Zeyad S. M. Kaled, Tawfek Sheer Ali, (2014). "**Strain Behavior of Geogrids Reinforcing Sand under a Rectangular Footing**".

4) Zeyad S. M. Kaled, Raid R. Al-Omary, Tawfek Sheer Ali, (2014). "**Cost Optimization of Using geogrids VS Piles in the Foundation of Interchange Bridges**", International Journal of Civil Engineering and Technology (IJCIET), Volume 5, Issue 11, November 2014, pp. 181-191.

AARJMD VOLUME 1 ISSUE 24 (AUGUST 2014) ISSN : 2319 - 2801

A Peer Reviewed International Journal of Asian Academic Research Associates

AARJMD
ASIAN ACADEMIC RESEARCH JOURNAL OF MULTIDISCIPLINARY

BEHAVIOR OF GEOGRIDS UNDER STRIP FOOTING RESTING ON SANDY SOIL

TAWFEK SHEER ALI[1]; RAID R. AL-OMARY[2]; ZEYAD S. M. KHALED[3]

[1]Assistant Lecturer, Department of Civil Engineering, College of Engineering, Kufa University, Najaf, Iraq, PhD researcher in Alnahrain University, Baghdad, Iraq,
[2]Professor of Geotechnical Engineering, Department of Civil Engineering, College of Engineering, Alnahrain University, Baghdad, Iraq,
[3]Assistant Professor of Construction Management, Department of Civil Engineering, College of Engineering, Alnahrain University, Baghdad, Iraq,

Abstract

A study of the behavior of two types of geogrids used to reinforce sandy soil under strip footings. Three layers of Netlon CE121 and Tensar SS2 geogrid were used. A series of a laboratory tests were performed to compare the estimate a bearing capacity of sand with and without using geogrids. The aim of the study is to measure the strain and elongation occurring in the ribs of Tensar SS2 geogrid only. TML strain gauges and other required accessories are used for this purpose. The soil is loaded with a rate of loadings 1 mm/s in order to simulate a static loading case with relative density of sand as 71.8 % using raining technique. It is found that the use of geogrids gives a bearing capacity with geogrid to bearing capacity without geogrid (BCR) of 1.9 and 2.5 for Netlon CE121 and Tensar SS2 respectively. The results founded also that the strain and elongation decrease gradually when the depth under footing increases as well as the distance from the centerline of footing. The strain in geogrid ribs approaches zero at a depth of about the width of footing (B) and a distance of about 3.6B from the centerline of footing. The strain and elongation have vanished in the third layer located at depth B beneath the footing.

Keywords : sandy soil, bearing capacity, Tensar SS2 geogrid, Netlon CE121 geogrid, strain and elongation of geogrid.

International Journal of Scientific & Engineering Research, Volume 5, Issue 8,August-2014 1028
ISSN 2229-5518

Behavior and Load Sharing of Piled-Strip System in Sandy Soil

Tawfek Sheer Ali 1, Raid R. Al-Omary 2 and Zeyad S. M. Khaled3
1Assistant Lecturer, Department of Civil Engineering, College of Engineering, Kufa University, Najaf, Iraq, PhD researcher in Alnahrain University, Baghdad, Iraq, tawfeeq76@gmail.com, tawfeeq76@yahoomail.com.
2Professor of Geotechnical Engineering, Department of Civil Engineering, College of Engineering, Alnahrain University, Baghdad, Iraq, tosharaid@yahoo.com.
3Assistant Professor of Construction Management, Department of Civil Engineering, College of Engineering, Alnahrain University, Baghdad, Iraq, zeyadsmkhalid@yahoo.com.

Abstract— Probably the most common type of deep foundations is the pile foundation. Piles are defined as relatively long, slender, column-like members. The piles is constructed with a pile cap in most of work of buildings and bridges. The piles in this case are considered carry the load alone and the cap only distribute the load on piles, this system is called piled-raft foundation. The aim of this paper is study the behavior of piled-strip system under a rate of loadings of 1 mm/s as a static loading and presents the sharing between footing and piles in. The sand container is manufactured to contain the soil using inside dimensions of 1 m long, 0.5 m width and 0.6 m depth. The box consists of four steel side frames and a steel base frame which are connected to each other by bolting and welding to form the box frames of the model. Strip footing model is manufactured to represents the pile cap of which encloses the piles under the columns load. The model was made of steel plates welded to transform the load using two v-shaped grooves to house the knife – edge loading blades. To achieve a plane strain condition the dimensions of footing are chosen to have 0.49 m length, 0.135 m width, and 0.2 m height. To achieve the plane strain piles conditions of piles footing, the steel frame with the dimensions of 0.49 m length, 0.4 m depth, and 0.03 m thickness is enfolded by 1 mm aluminum plate. Abrasive papers were glued to give the required roughness to simulate the piles in site. An experimental tests shows that the two capacities of pile, end bearing capacity and skin friction resistance sharing with 75.6% and 24.4% of piles capacity respectively. The results show also that the settlement is smaller for piled-strip system than the piles alone. The results also show that the sharing of footing in capacity with a 33.8% and the piles with 66.2%.

Index Terms— Deep foundation, Piled-raft, Piled-strip, Sharing between piles and footing.

IJSER

---

1 Introduction

Foundations for heavy structures on weak soils are usually on piles and (or) pile-raft systems. These are also called basement raft supported piles or piled basements [1], [2]. When piles are founded on a compressible soil, the pile-raft system settles gradually resulting in a gradual buildup of pressure at the bottom of the raft. Thus, there is a gradual transfer of the total load to the raft and a reduction in the load carried by the piles. The soil beneath the raft (located at a relatively shallow depth) is then compressed, causing a partial load transfer back to the piles. This is a continuous interaction process with the total load being shared by the raft and the piles.

Hooper [3] examined the behavior of piled raft foundation supporting a tower block incentral London. The study was made on the building constructed on piled raft foundation of area 618 m2 with 51 bored concrete piles of length 25 m and
diameter 0.91 m. during several years, the field measurements were taken. The analysis was carried out assuming uniformly distributed load on the raft. The instruments used for measurement of pile load, contact pressure and settlement were pile load cell, earth pressure cell and level. The average settlement of the building measured was 18 mm. Based on the field measurements the estimated proportions of load taken by piles and the raft at the end of construction were 60 % and 40 %. It was found that the long term effect of consolidation is to increase the load carried by piles and to decrease raft contact pressure.

Hain and Lee [4] developed an analysis to predict the behavior of a raft-pile foundation system. The analysis considers the system as flexible elastic plate supported on a group of compressible friction piles, and the supporting soil is represented as an elastic homogeneous or nonhomogeneous material. In the analysis, they suggested that the behavior of the piled raft would depend on the relative flexibility of the raft and the relative stiffness of the pile to the soil. Four different interactions between the piles, raft and soil were introduced and thoroughly considered in the analysis. In addition, a 'load cut-off' procedure was introduced to account for the development of the ultimate load capacities of the piles.

Yamashita et al. [5] analyzed a five story building on piled raft foundation of size 24m × 23m with 20 piles of length 16 m and diameter 0.75 m. The results of field observations during construction and analytical study of the same building have been compared. At the time of completion of the building, the settlement measured was 10 to 20 mm and the load shared by piles was 49 %. Analytical simulation of the settlement behavior of the building is presented taking into account the interaction between piles,

Gmail

Tawfeeq Amir <tawfeeq76@gmail.com>

Fw: Notification of your abstract for ISSMGE-15ARC Fukuoka Japan

tawfeeq amer <tawfeeq76@yahoo.com> Mon, Nov 3, 2014 at 11:09 AM
Reply-To: tawfeeq amer <tawfeeq76@yahoo.com>
To: Tawfeeq Amir <tawfeeq76@gmail.com>

On Friday, October 31, 2014 9:31 PM, Raid R. Al-Omari <tosharaid@yahoo.com> wrote:

On Thursday, October 30, 2014 3:09 AM, Yoichi Watabe <watabe@ipc.pari.go.jp> wrote:

30 Oct 2014

Ref: IGS-04

Dear Sir/Madam

Thank you for submitting an abstract for the 15th Asian Regional Conference on Soil Mechanics and Geotechnical Engineering (15ARC) which will be held from 9 to 12 November 2015 in Fukuoka, Japan.

On behalf of the organizing committee, we are pleased to inform you that your abstract detailed below has been accepted by the scientific committee of 15ARC. We now invite you to submit a full paper to be involved in the conference proceedings. A template for the full paper will be sent to you later. Also, please check our website.
http://www.15arc.org/

Abstract number: IGS-04
Title:
STRAIN BEHAVIOR OF GEOGRIDS REINFORCING SAND UNDER A RECTANGULAR FOOTING
Authors:
Raid R. Al-Omari
Zeyad S. M. Khaled
Tawfek Sheer Ali

INTERNATIONAL JOURNAL OF CIVIL ENGINEERING AND TECHNOLOGY (IJCIET)

ISSN 0976 – 6308 (Print)
ISSN 0976 – 6316(Online)
Volume 5, Issue 11, November (2014), pp. 181-191
© IAEME: www.iaeme.com/Ijciet.asp
Journal Impact Factor (2014): 7.9290 (Calculated by GISI)
www.jifactor.com

IJCIET

©IAEME

COST OPTIMIZATION OF USING GEOGRIDS VS PILES IN THE FOUNDATION OF INTERCHANGE BRIDGES

Zeyad S. M. Khaled[1], Raid R. Al-Omari[2], Tawfek Sheer Ali[3]

[1]Assistant Professor, College of Engineering, Al-Nahrain University, Baghdad, Iraq
[2]Professor, College of Engineering, Al-Nahrain University, Baghdad, Iraq
[3]Assistant Lecturer, College of Engineering, Kufa University, Najaf, Iraq

ABSTRACT

The use of soil reinforcement has become widely adopted due to successive development of different types of geosynthetics. Although soil reinforcement had gained wide acceptance in other countries, Iraq is still hesitated to adopt the system. This paper is an economic study to investigate the feasibility of using geogrids in the foundation of interchange bridges, resting on sandy soils, instead of piles. The design restrictions are imposed as design constraints in the analysis of both cases (geogrids and piles). Choice of the design parameters are made in a way that fit local circumstances in middle and south Iraq considering common safety factors. Three layers of two types of geogrids are analyzed namely Netlon CE121 and Tensar SS2. MATLAB package program is used for optimization. The constraints and the objective function are designed to optimize one unit block of foundation (under one piles cap). Tables of optimal costs and figures showing cost behavior for different combinations of loads and angles of internal friction of soil are presented. It has been found that reinforced soil is considered as cost-effective solution which is much more economical than piles. Based on a typical design commonly used on local scale, cost saving appear to reach (54%).

Keywords: Bearing Capacity, Geosynthetics, Netlon CE121 and Tensar SS2 Geogrids, Optimal Cost Design, Optimization, Sandy Soil.

1. INTRODUCTION

This paper is an economic study of using geogrids in the foundation of highway multi-level intersection bridges instead of piles. The study is limited to the range of applied loads prevailing in most of highway projects in middle and south Iraq and the bearing capacity of reinforced soil of the most common type founded in the aforementioned area where most of the soil is sand. MATLAB is used as an optimization technique in order to find the optimum cost of construction of both types of

الخلاصة

يشهد استخدام مشبكات تسليح التربة (Geogrids) نمواً مضطرداً كجزء من تطبيقات تعزيز التربة اصطناعياً (Geosynthetics)، ولكنها ليست من الأنسجة المحاكة أو غير المحاكة أو الظفيرية، وإنما هي لدائن مصنعة على هيئة مشبكات ذات أضلع طولية وعرضية تضم فيما بينها فتحات واسعة.

يهدف هذا البحث إلى دراسة إمكانية وجدوى استعمال مشبكات تسليح التربة عوضاً عن الركائز في أسس مجسرات التقاطعات التي تنشأ على ترب رملية، ودراسة تصرف هذه المشبكات تحت الأسس الشريطية والمستطيلة.

إذ أجريت سلسلة من الفحوصات المختبرية لمقارنة قابلية تحمل التربة المسلحة بهذه المشبكات مع قابليتها قبل تسليحها، باستعمال نوعين من المشبكات هما (Nelton CE121) و(Tensar SS2)، زيادة على قياس الانفعال والاستطالة الحاصلين في أضلع المشبكات باستعمال مقاييس (TML) وملحقات متوافقة معها.

كما أجريت فحوصات مختبرية مستقلة لأسس شريطية وأخرى مستطيلة ترتكز على ركائز، باستعمال نموذج ركيزة الانفعال المستوي (Plane strain) في فحص الأسس الشريطية، ونموذج ذي ثلاث ركائز مربعة المقطع في فحص الأسس المستطيلة، وتم حساب تحمل نهايات الركائز والاحتكاك السطحي، وحساب تقاسم الحمل بين الركائز وقواعد الأسس.

لقد وجد بأن استعمال المشبكات في تسليح التربة تحت الأسس الشريطية يولد قابلية على تحمل الأحمال أعلى بنسبة (BCR) تعادل (1.9) و(2.5) مرة بقدر قابلية التربة غير المسلحة ولنوعي المشبكات (Nelton CE121) و(Tensar SS2) على التوالي، وان نسبة (BCR) تصبح (2.35) و(2.9) لنوعي المشبكات المذكورين آنفاً عند استعمالهما تحت الأسس المستطيلة. وأظهرت نتائج الفحوصات أن انفعال واستطالة أضلع المشبكات يقلان تدريجياً كلما زاد عمق الطبقة وكلما ابتعدنا عن خط مركز الأسس.

كما وجد عند استخدام نموذج الركيزة ذات الانفعال المستوي تحت الأسس الشريطية، بأن المساهمة في التحمل تتوزع بنسبة (75.7٪) على نهاية الركيزة و(24.3٪) على الاحتكاك السطحي. بينما تتوزع المساهمة في التحمل بنسبة (72.9٪) على نهاية الركيزة و(27.1٪) على الاحتكاك السطحي عند استخدام النموذج ذي الركائز المربعة الثلاث تحت الأسس المستطيلة، وذلك لاختلاف تناسب طول الركيزة إلى مساحة نهايتها. وأظهرت النتائج أيضاً بأن الحمل يتوزع بنسبة (66.2٪) للركائز و(33.8٪) لقاعدة الأساس نفسه إذا كان شريطياً، وبنسبة (75٪) للركائز و(25٪) لقاعدة الأساس نفسه إذا كان مستطيلاً. ثم تم إجراء التحليل النظري باستعمال برنامج (PLAXIS) لأجل التحقق من النتائج المستحصلة مختبرياً لقابلية التحمل.

وبالإضافة إلى ما تقدم، فقد أجريت دراسة اقتصادية باستعمال برنامج (MATLAB) تم فيها صياغة حالة دراسية بطريقة الأمثلية لأجل التحري عن الجدوى الاقتصادية لاستخدام مشبكات تسليح التربة بدلاً من الركائز في أسس مجسرات التقاطعات. وقد توصلت الدراسة إلى أن استعمال المشبكات يؤدي إلى خفض التكاليف بنسبة تصل إلى (54٪) ضمن حدود الأحمال وخصائص التربة المعتمدة في الدراسة.

شكر وتقدير

قبل أي شيء أشكر الله ربي الرحيم العطوف الرحمن الجليل العلي عن نقص الأوصاف الذي مكنني من انجاز وإكمال هذا البحث.

أعرب عن امتناني وشكري وتقديري الكبير للسادة المشرفين الاستاذ الدكتور رائد رمزي العمري والاستاذ المساعد الدكتور زياد سليمان محمد خالد لما أبدوه من نصائح ثمينة وتوجيه تقني وتشجيع مستمر وصبر رائع في مراجعة أطروحتي ووضعها في أحسن صيغة.

كذلك أقدم شكري وتقديري للدكتور حاتم عبد الرحمن رشيد، رئيس قسم الهندسة المدنية/كلية الهندسة/جامعة النهرين و إلى كل الموظفين لدعمهم المتواصل طيلة فترة الدراسة.

شكري واعتزازي الخاص الى الدكتور ليث خالد الحديثي و الدكتور نبيل حسن هادي والدكتور مصطفى سلمان شبر و الدكتور ليث جواد عزيز للمساعدة الكبيرة التي قدموها لي.

أود كذلك أن أقدم الشكر الى عائلتي لدعمهم الكبير لي أثناء فترة هذا العمل.

شكر وتقدير الى هيئة اعمار النجف الاشرف متمثلة برئيسها المهندس حيدر الميالي لتقديمهم العون والمساعدة في انجاز العمل.

الامتنان ايضا الى الدكتور محمد كاظم فخر الدين لما ابداه من مساعدة مستمرة طيلة فترة العمل.

أعرب عن تقديري لكل شخص ساعدني في انجاز الاطروحة وبالخصوص الدكتور حيدر الخضري والاستاذ نبراس علي الصحاف و الدكتور عباس طالب الهدابي والاستاذ أسعد محمد باقر والأستاذ أحمد الكاتب و الاستاذ حيدر علي عبد الحسين والدكتور عدي محمد عباس و الاستاذ فاضل عبد العباس والمهندسة حنان عبد عباس و المهندسة ابتهال يوسف عبد.

توفيق عامر جواد شبر علي

نيسان – 2015

وزارة التعليم العالي و البحث العلمي

جامعة النهرين/ كلية الهندسة

قسم الهندسة المدنية

مقارنة بين التربة المسلحة بالمشبكات والركائز في أسس المجسرات

توفيق عامر جواد شيرعلي

بكالوريوس(هندسة مدنية, 1998)

ماجستير(هندسة جيوتكنيكية, 2001)

رجب 1436

نيسان 2015

I want morebooks!

Buy your books fast and straightforward online - at one of the world's fastest growing online book stores! Environmentally sound due to Print-on-Demand technologies.

Buy your books online at

www.get-morebooks.com

Kaufen Sie Ihre Bücher schnell und unkompliziert online – auf einer der am schnellsten wachsenden Buchhandelsplattformen weltweit!
Dank Print-On-Demand umwelt- und ressourcenschonend produziert.

Bücher schneller online kaufen

www.morebooks.de

OmniScriptum Marketing DEU GmbH
Bahnhofstr. 28
D - 66111 Saarbrücken
Telefax: +49 681 93 81 567-9

info@omniscriptum.com
www.omniscriptum.com

OMNIScriptum